



2007

FUNCTIONAL PROPERTIES OF L-GLUTAMATE REGULATION IN ANESTHETIZED AND FREELY MOVING MICE

Kevin N. Hascup
University of Kentucky

[Right click to open a feedback form in a new tab to let us know how this document benefits you.](#)

Recommended Citation

Hascup, Kevin N., "FUNCTIONAL PROPERTIES OF L-GLUTAMATE REGULATION IN ANESTHETIZED AND FREELY MOVING MICE" (2007). *Theses and Dissertations--Neuroscience*. 16.
https://uknowledge.uky.edu/neurobio_etds/16

This Doctoral Dissertation is brought to you for free and open access by the Neuroscience at UKnowledge. It has been accepted for inclusion in Theses and Dissertations--Neuroscience by an authorized administrator of UKnowledge. For more information, please contact UKnowledge@lsv.uky.edu.

STUDENT AGREEMENT:

I represent that my thesis or dissertation and abstract are my original work. Proper attribution has been given to all outside sources. I understand that I am solely responsible for obtaining any needed copyright permissions. I have obtained needed written permission statement(s) from the owner(s) of each third-party copyrighted matter to be included in my work, allowing electronic distribution (if such use is not permitted by the fair use doctrine) which will be submitted to UKnowledge as Additional File.

I hereby grant to The University of Kentucky and its agents the irrevocable, non-exclusive, and royalty-free license to archive and make accessible my work in whole or in part in all forms of media, now or hereafter known. I agree that the document mentioned above may be made available immediately for worldwide access unless an embargo applies.

I retain all other ownership rights to the copyright of my work. I also retain the right to use in future works (such as articles or books) all or part of my work. I understand that I am free to register the copyright to my work.

REVIEW, APPROVAL AND ACCEPTANCE

The document mentioned above has been reviewed and accepted by the student's advisor, on behalf of the advisory committee, and by the Director of Graduate Studies (DGS), on behalf of the program; we verify that this is the final, approved version of the student's thesis including all changes required by the advisory committee. The undersigned agree to abide by the statements above.

Kevin N. Hascup, Student

Dr. Greg Gerhardt, Major Professor

Dr. Jane Joseph, Director of Graduate Studies

ABSTRACT OF DISSERTATION

Kevin Nicholas Hascup

The Graduate School
University of Kentucky

2007

FUNCTIONAL PROPERTIES OF L-GLUTAMATE REGULATION IN
ANESTHETIZED AND FREELY MOVING MICE

ABSTRACT OF DISSERTATION

A dissertation submitted in partial fulfillment of the
requirements for the degree of Doctor of Philosophy in the
College of Medicine
at the University of Kentucky

By
Kevin Nicholas Hascup

Lexington, Kentucky

Director: Dr. Greg Gerhardt, Professor of Anatomy and Neurobiology

Lexington, Kentucky

2007

Copyright © Kevin Nicholas Hascup 2007

ABSTRACT OF DISSERTATION

FUNCTIONAL PROPERTIES OF L-GLUTAMATE REGULATION IN ANESTHETIZED AND FREELY MOVING MICE

L-glutamate (Glu) is the predominant excitatory neurotransmitter in the mammalian central nervous system with involvement encompassing learning and memory, cognition, plasticity, and motor movement. Dysregulation of the glutamatergic system is implicated in several neurological disorders including Parkinson's disease, Alzheimer's disease, Huntington's disease and amyotrophic lateral sclerosis. The mechanisms underlying these neurological disorders are not clear, but evidence suggests that abnormal Glu neurotransmission plays a role. Elevated levels of Glu in the synaptic cleft overstimulate the N-methyl-D-aspartate receptor leading to excitotoxicity, which causes neuronal loss in chronic neurological diseases. What is less understood is the source for the elevated Glu levels. One hypothesis involves alterations in either activity or concentration of Glu metabolizing enzymes. To study this, two transgenic mouse models were developed that increase levels of Glu pyruvate transaminase (GPT), responsible for Glu degradation, and Glu dehydrogenase (GLUD1), responsible for Glu synthesis. Our laboratory is interested in studying stimulus-evoked Glu release and re-uptake dynamics in these mice using an enzyme-based multisite microelectrode array (MEA) capable of subsecond measurements with low detection limits. Our main finding indicates that GLUD1 mice have increased release of Glu. The GLUD1 mice show spontaneous motor neuron degeneration of the hind limbs that could be correlated to an excitotoxic effect from the increased release of Glu. We wanted to study these GLUD1, motor deficient mice without the affects of anesthesia. First, we needed to modify the current MEAs for use in the awake, freely moving mouse. In these studies we measured resting Glu levels as well as MEA viability with local application of 1 mM Glu in both the striatum and prefrontal cortex of C57BL/6 mice. No change in MEA sensitivity for Glu was observed on days 3 through 7 post-implantation. Resting Glu levels are examined in the striatum of the freely moving mouse by locally applying an uptake inhibitor or a sodium-channel blocker. Our studies indicate the resting Glu levels are partially neuronally derived and not from reversal of the high-affinity transporters. This

characterization has laid the foundation to study behavioral alterations of Glu in the GLUD1 mice.

Keywords: Amperometry, Microelectrode, Sensor, Neurotransmitter, Neurodegeneration

Kevin Nicholas Hascup

10/04/07

FUNCTIONAL PROPERTIES OF L-GLUTAMATE REGULATION IN
ANESTHETIZED AND FREELY MOVING MICE

By

Kevin Nicholas Hascup

Greg A. Gerhardt
Director of Dissertation

Jane Joseph
Director of Graduate Studies

10/04/07

RULES FOR THE USE OF DISSERTATIONS

Unpublished dissertations submitted for the Doctor's degree and deposited in the University of Kentucky Library are as a rule open for inspection, but are to be used only with due regard to the rights of the authors. Bibliographical references may be noted, but quotations or summaries of parts may be published only with the permission of the author, and with the usual scholarly acknowledgments.

Extensive copying or publication of the dissertation in whole or in part also requires the consent of the Dean of the Graduate School of the University of Kentucky.

A library that borrows this dissertation for use by its patrons is expected to secure the signature of each user.

Name

Date

DISSERTATION

Kevin Nicholas Hascup

The Graduate School

University of Kentucky

2007

FUNCTIONAL PROPERTIES OF L-GLUTAMATE REGULATION IN
ANESTHETIZED AND FREELY MOVING MICE

DISSERTATION

A dissertation submitted in partial fulfillment of the
requirements for the degree of Doctor of Philosophy
in the College of Medicine
at the University of Kentucky

By
Kevin Nicholas Hascup

Lexington, Kentucky

Director: Dr. Greg A. Gerhardt, Professor of Anatomy and Neurobiology

Lexington, Kentucky

2007

Copyright © Kevin Nicholas Hascup

Dedicated to my wife, Erin Rutherford Hascup, and my parents, Richard and
Christine Hascup.

ACKNOWLEDGEMENTS

It is difficult to put into words my gratitude towards those who helped me along the road to this prestigious endeavour. First and foremost, I would like to thank my parents, Richard and Christine Hascup. If it were not for their emotional and financial support throughout my collegiate career, I would have been able to reach this point. They taught me the value of hardwork, discipline, and to never stop chasing my dreams. I hope to be as good of a parent to my children that my parents were to me.

Next, I would like to thank my mentor, Greg A. Gerhardt. It is truly unique to study under an individual that is performing cutting edge research while taking the time to teach his students how to survive in such a difficult profession. I deeply appreciate his loyalty and support especially during moments when I made life difficult for myself. I look forward to continuing our friendship and scientific endeavours throughout the upcoming years in Stockholm and wherever the winds may carry me.

What has made our laboratory great over the years is the willingness of the senior graduate students to take the time to teach the incoming graduate students. Those that guided my graduate career path include Keith Day, Matt Joyce, and Justin Nickell. With their help and support I learned how to properly use our technology, design appropriate experiments, and critically interpret my data. I wish them continued success in their medical as well as academic careers.

I would also like to thank the rest of the members of our laboratory including Pete Huettl, François Pomerleau, and Robin Lindsay. They have helped in numerous ways from system development to ordering critical laboratory supplies. Without their help this laboratory would undoubtedly grind to a halt. In addition to the senior laboratory members, fellow graduate students and post-docs have helped make my days in the laboratory more interesting, while helping me achieve academic and scientific success. These members include Garretson

Epperly, Josh Fuqua, Jason Hinzman, Maeghan Littrell, Martin Lundblad, Jorge Quintero, Michelle Stephens, Pooja Talauliker, Theresa Thomas Currier, and Catherine Werner. In particular I also want to thank several undergraduate laboratory members including Amanda Chism and Thomas Schlierf. Both of these students made my life dramatically easier in the lab by simply coating microelectrodes or preparing solutions. I wish them continued success in the pursuit of their medical careers.

My fellow IBSers including Laurie Davis, Mary Bosserman, Yuri Klyachkin, Ravi Subramanian, Missy Smith, and Rich Singiser. We suffered together that first year and it's great to see everyone achieving their dreams. I wish everyone the best in their future pursuits.

Finally, but most importantly, I want to thank my laboratory sweetheart, and now my wife, Erin Rutherford Hascup. She has helped me in so many ways it is impossible to describe. By challenging my thinking and reasoning she has helped me better understand and interpret my data. Her love and support has helped me overcome the largest obstacles and climb out of the darkest pits. I will always love her with all of my heart.

Table of Contents

ACKNOWLEDGEMENTS.....	iii
List of Tables.....	vii
List of Figures.....	viii
Chapter One: Introduction.....	1
Intracranial Electrode Applications.....	1
An Overview of L-Glutamate Neurotransmission in the Mammalian Central Nervous System.....	2
Excitotoxicity.....	9
L-Glutamate Metabolism.....	11
Glutamate Pyruvate Transaminase.....	14
Glutamate Dehydrogenase.....	14
Techniques for Measuring L-glutamate: Microdialysis.....	17
Techniques for Measuring L-glutamate: Amperometric Detection with Microelectrode Arrays.....	20
Mouse Models.....	21
Thesis Outline.....	22
Chapter Two: Materials and Methods.....	25
Principles of <i>In Vivo</i> Electrochemistry.....	25
Microelectrode Array Fabrication.....	26
Potentiostat.....	32
Microelectrode Array Cleaning Procedures.....	32
Exclusion Layers.....	34
Nafion [®] Exclusion Layer.....	35
1,3-phenylenediamine.....	36
Enzyme Layer Coatings.....	38
L-Glutamate Oxidase.....	41
L-Glutamate Oxidase Coating Procedure.....	41
Calibration Preparation.....	43
Calibration Procedure.....	44
Microelectrode Array Calibration Criteria.....	45
Glass Micropipettes.....	47
Ag/AgCl Reference Electrode.....	50
MEA Preparation for Awake, Freely Moving Mice.....	51
Freely Moving Recording Apparatus.....	53
Chronic Implantation Procedure.....	55
Self-Referencing.....	57
Signal Analysis.....	61
Development of Mouse Lines.....	65
Chapter Three: Glutamate Dynamics in Glutamate Dehydrogenase C57BL/6 and BALB/C Transgenic Mice.....	66
Introduction.....	66
Methods.....	68
Results.....	71
Discussion.....	90

Chapter Four: Glutamate Dynamics in Glutamate Pyruvate Transaminase Transgenic and Knockout C57BL/6 Mice	100
Introduction.....	100
Methods	102
Results	104
Discussion	122
Chapter Five: Understanding L-Glutamate Dynamics in the Awake, Freely Moving C57BL/6 Mouse.....	127
Introduction.....	127
Methods	130
Results	131
Discussion	145
Chapter Six: Conclusion	152
Introduction.....	152
Alzheimer’s Disease	152
Amyotrophic Lateral Sclerosis.....	154
Epilepsy	155
Huntington’s Disease.....	156
Parkinsons Disease	157
Final Notes	157
Appendix A: L-Glutamate Dynamics in Male Glutamate Pyruvate Transaminase Knock Out Mice.....	159
Introduction.....	159
Methods	160
Results	161
Discussion	171
Appendix B: Understanding L-Glutamate Dynamics in the Awake, Freely Moving BALB/C Mouse Model.	173
Introduction.....	173
Methods	173
Results	175
Discussion	175
Appendix C: Development of a Self-Referencing Microelectrode Array for Detection of Hydrogen Peroxide	181
Introduction.....	181
Materials and Methods	184
Results	186
Discussion	194
References	200
VITA	229

List of Tables

Table 1.1: Ionotropic Glutamate Receptors	5
Table 1.1: (continued).....	6
Table 1.2: Metabotropic Glutamate Receptors	8
Table 2.1: Enzymes Capable of Producing a Reporter Molecule	39
Table 2.1: (continued).....	40
Table 3.1: Amperometric Glu Current with Increasing Buffer Concentration of α -Ketoglutarate	74
Table 3.2: Microarray Comparison of Transgenic to WT GLUD1 C57BL/6 Mice	91
Table 5.1: Local Application and Resting Glu Measures on Days 3 through 7 Post-Implantation.....	135
Table 5.2: Clearance Kinetics of Exogenously Applied 1 mM Glu	139
Table 5.3: Comparison of Resting Glu Levels in the Str of C57BL/6 Mice.....	149

List of Figures

Figure 1.1: Glutamate Synapse Schematic	4
Figure 1.2: The Glutamate-Glutamine Cycle Revisited.....	13
Figure 1.3: Glutamate Metabolic Pathways	15
Figure 2.1: Ceramic Wafer	28
Figure 2.2: Microelectrode Array Fabrication Process.....	30
Figure 2.3: Microelectrode Array Photographs	31
Figure 2.4: FAST 16 Mark II Potentiostat Diagram.....	33
Figure 2.5: Calibration Results From Nafion [®] and mPD Coated MEAs	46
Figure 2.6: Positioning of the Glass Micropipette	49
Figure 2.7: Awake, Freely Moving MEA Preparation	52
Figure 2.8: Diagram of the Freely Moving Recording Chamber.....	54
Figure 2.9: MEA Implantation Surgery.....	56
Figure 2.10: Nafion [®] and mPD Self-Referencing MEA Schematic	59
Figure 2.11: Screen Capture of an <i>In Vivo</i> Glu Response on a Self-Referencing MEA.....	60
Figure 2.12: Example of Self-Referencing Subtraction.....	62
Figure 2.13: Analysis Parameters.....	64
Figure 3.1: Western Blot Analysis of Exogenous GLUD1	70
Figure 3.2: Reproducibility of Glu Signals From 70 mM KCl Depolarization.....	72
Figure 3.3: Effects of α -Ketoglutarate on MEA Sensitivity	73
Figure 3.4: 70 mM KCl-Evoked Glu Release Traces in the C57BL/6 Mouse.....	75
Figure 3.5: Stimulus-Evoked Glu Release in C57BL/6 GLUD1 Transgenic Mice	77
Figure 3.6: Stimulus-Evoked Glu Release Depth Profile in the C57BL/6 Mouse.....	78
Figure 3.7: Stimulus-Evoked Glu Uptake in the C57BL/6 Mouse Groups.....	79
Figure 3.8: Clearance of Exogenously Applied 5 mM Glu	80
Figure 3.9: 70 mM KCl-Evoked Glu Release Traces in the BALB/C Mouse.....	82
Figure 3.10: Stimulus-Evoked Glu Release in BALB/C GLUD1 Transgenic Mice	83
Figure 3.11: Stimulus-Evoked Glu Release Depth Profile in the BALB/C Transgenic Mice	84
Figure 3.12: Stimulus-Evoked Glu Uptake in the BALB/C Mouse Groups.....	85
Figure 3.13: Clearance of Exogenously Applied 5 mM Glu in BALB/C Mice	87
Figure 3.14: Resting Glu Levels in the BALB/C GLUD1 Transgenic Mice	88
Figure 3.15: Endogenous GLUD1 Expression Correlates with Stimulus-Evoked Glu Release.....	89
Figure 3.16: C57BL/6 GLUD1 Transgenic Mouse Motor Cortex Histology	95
Figure 3.17: C57BL/6 GLUD1 Transgenic Mouse Spinal Cord Histopathology	96
Figure 3.18: Proposed Excitotoxic Mechanism for GLUD1 C57BL/6 Mice	98
Figure 4.1: Reproducibility of Glu Signals from 70 mM KCl Depolarization	105
Figure 4.2: 70 mM KCl-Evoked Glu Release Traces in the GPT Transgenic Mice	106

Figure 4.3: Stimulus-Evoked Glu Release in GPT Transgenic Mice.....	107
Figure 4.4: Stimulus-Evoked Glu Release Depth Profile in the GPT Transgenic Mouse.....	108
Figure 4.5: Stimulus-Evoked Glu Uptake in the GPT Transgenic Mouse Groups	110
Figure 4.6: Stimulus-Evoked Glu Uptake Depth Profile in the GPT Transgenic Mouse.....	111
Figure 4.7: 5 mM Glu Clearance in the GPT Transgenic Mouse Groups	112
Figure 4.8: Exogenously Applied 5 mM Glu Clearance Depth Analysis	113
Figure 4.9: 70 mM KCl-Evoked Glu Release Traces in the Female GPT KO Mice	115
Figure 4.10: Stimulus-Evoked Glu Release in the Female GPT KO Mice	116
Figure 4.11: Stimulus-Evoked Glu Release Depth Profile in the Female GPT KO Mice.....	117
Figure 4.12: Stimulus-Evoked Glu Uptake in the Female GPT KO Mice	119
Figure 4.13: 5 mM Glu Clearance in the Female GPT KO Mice.....	120
Figure 4.14: 5 mM Glu Clearance Depth Profile in the Female GPT KO Mice	121
Figure 4.15: Resting Glu Levels in the Female GPT KO Mice.....	123
Figure 5.1: Representative Glu Traces After Local Application of 1 mM Glu... ..	132
Figure 5.2: Local Application of Glu in the PFC and Str	133
Figure 5.3: Representative Traces of Glu Clearance in the Str and PFC	136
Figure 5.4: Clearance Rate of Locally Applied 1 mM Glu	137
Figure 5.5: t_{80} of Locally Applied 1 mM Glu	138
Figure 5.6: Resting Glu Levels in the Str and PFC.....	141
Figure 5.7: Local Application of 100 μ M THA	142
Figure 5.8: Local Application of 1 μ M TTX.....	143
Figure 5.9: Fox Urine Affects Resting Glu Levels	144
Figure A.1: Stimulus-Evoked Glu Release in the Male GPT KO Mice	162
Figure A.2: Stimulus-Evoked Glu Release Depth Profile in the Male GPT KO Mice.....	163
Figure A.3: Stimulus-Evoked Glu Uptake in the Male GPT KO Mouse Groups.....	165
Figure A.4: Stimulus-evoked Glu Uptake Depth Profile in the Male GPT KO Mice	166
Figure A.5: 5 mM Glu Clearance in the Male GPT KO Mouse Groups.....	168
Figure A.6: 5 mM Glu Clearance Depth Profile in the Male GPT KO Mice	169
Figure A.7: Resting Glu Levels in the Male GPT KO Mice	170
Figure B.1: Representative Glu Traces From Local Application of 1 mM Glu.. ..	176
Figure B.2: Local Application and Resting Glu Levels in the PFC of BALB/C Mice	177
Figure B.3: Local Application of CPG in the PFC of BALB/C Mice	178
Figure C.1: Mitochondrial Electron Transport Chain.....	183
Figure C.2: Calibration Trace of a Catalase MEA.....	187
Figure C.3: Local Application of 100 μ M H ₂ O ₂	188
Figure C.4: Potential Change for H ₂ O ₂ Determination.....	190
Figure C.5: Increasing Volume of Locally Applied 100 μ M H ₂ O ₂	191

Figure C.6: Calibration of a Glutamate Oxidase and Catalase Coated MEA... 193
Figure C.7: Amperometric Traces of H₂O₂ Produced from Mitochondria
Preparations 195

Chapter One: Introduction

Intracranial Electrode Applications

The idea behind merging technology with the human brain for improving quality of life is not a new concept. In fact, the first documented human cortical stimulation was conducted over a century ago (Barthlow, 1874). When human stereotactic devices were developed in the later 1940s, neurosurgeons were able to investigate the effects of stimulating deeper brain structures (Spiegel et al., 1947). The concept of treating neurological disorders with chronic stimulation emerged in the 1960's, but this was used mainly to pinpoint surgical lesions (Perlmutter and Mink, 2006). Stereotaxic thalatomy and pallidotomy were popular neurosurgical techniques for treating disabling tremor until levodopa therapy emerged in the 1970s. Unfortunately, researchers discovered that prolonged levodopa therapy resulted in drug related complications for advancing the very symptoms the drug was intended to treat. At this same time, it was discovered that chronic stimulation could be used for treating pain (Hosobuchi *et al.*, 1973), movement disorders, or epilepsy (Cooper, 1973). In an effort to find alternative therapies for levodopa, pacemaker technology was merged with chronically implanted deep brain electrodes for long-term deep brain stimulation (DBS) (Benabid, et al., 1991, 1996). Researchers discovered that a high-frequency electrical current can have the same effects as a lesion without the need for destroying brain tissue. Since this time, DBS has been used to treat a variety of neurological disorders including essential tremor, Parkinson disease (PD), dystonias, tourette syndrome, pain, and obsessive compulsive disorder (Perlmutter and Mink, 2006). Technology has emerged to not only treat patients with electrical stimulation, but rather create brain-machine interfaces (BMIs) that can translate the electrical activity of neuronal populations and perform the desired motor movement. This would essentially return motor control to severely disabled patients suffering from amyotrophic lateral sclerosis (ALS), spinal cord injury, stroke, cerebral palsy, and amputees (Lebedev and Nicolelis, 2006).

Clearly, intracranial electrode applications such as DBS and BMI hold a great deal of promise but much more research is needed to fully understand how these devices effect chemical signaling within and between neuronal subregions. Neuroscientists have become interested in coupling these techniques with the ability to monitor specific neurotransmitters. Since neurotransmitters such as dopamine (DA), L-glutamate (Glu), γ -aminobutyric acid (GABA), and acetylcholine (to name a few) are the key chemicals for neuronal signaling (Cooper, Bloom, and Roth, 2003) techniques have developed to better understand their role in neuronal communication. The most widely used technique for studying neurotransmitters, microdialysis, has several limitations as discussed below. Our laboratory has spent the past 15 years developing an enzyme-based microelectrode array (MEA) that is capable of recording specific neurochemicals. These devices have been routinely used in rats, mice, and monkeys (both anesthetized and freely moving) to better understand the glutamatergic system in relation to various neurological disorders including, but not limited to, PD and epilepsy. The goal is to move this technology into the operating room, either by itself or coupled with DBS and BMI, to further enhance the quality of life for patients suffering from movement disorders.

An Overview of L-Glutamate Neurotransmission in the Mammalian Central Nervous System

Glu is the predominant excitatory neurotransmitter in the mammalian central nervous system (CNS) existing in all main afferent fibers ascending to the brain cortex and in excitatory nerves (Boksha, 2004). Glu is involved in most aspects of normal brain function including cognition, memory and learning, plasticity, and motor movement. As a neurotransmitter, Glu is found in glutamatergic neurons, which are defined by the presence of vesicular glutamate transporters (VGLUT). This protein is responsible for loading Glu into synaptic vesicles through a proton-dependent electrochemical gradient across the vesicle membrane that is created by a vacuolar-type ATPase (Takamori, 2006). When these vesicles dock with the pre-synaptic plasma membrane and release Glu into

the synaptic cleft there are two different classes of receptors that Glu can activate; (a) ionotropic and (b) metabotropic. Their localizations are shown in figure 1.1.

Ionotropic Glu receptors (iGluRs) contain three major types, all named after the agonists that were originally used to selectively activate them; N-methyl-D-aspartate (NMDA), α -amino-3-hydroxy-5-methyl-4-isoazolepropionic acid (AMPA), and 2-carboxy-3-carboxymethyl-4-isopropenylpyrrolidine (Kainate; KA). Table 1.1 outlines some of the agonists and antagonist for NMDA, AMPA, and KA receptors. All three iGluRs are ligand-gated ion channels that are predominantly associated with modulating postsynaptic excitability and plasticity (Kew and Kemp, 2005; Swanson *et al.*, 2005). They are also found pre-synaptically to modulate the release of Glu and other neurotransmitters (Engelman and MacDermott, 2004; Galvan *et al.*, 2006). AMPA and KA receptors are believed to be responsible for fast, excitatory neurotransmission (Greene and Greenamyre, 1996). Upon Glu binding, both AMPA and KA receptors change conformation to allow sodium influx into the post-synaptic neuron and depolarize the membrane. The NMDA receptor is unique in that it binds two ligands (Glu and the coagonist glycine) as well as being a voltage-sensitive ion channel. At resting membrane potential, the ion channel is blocked by extracellular magnesium which prevents calcium influx irregardless of agonist binding. Since this blockade is voltage-dependent, post-synaptic depolarization facilitates NMDA receptor activation. Upon Glu binding to AMPA or KA receptors, sodium enters the post-synaptic neuron leading to membrane depolarization. This removes the magnesium block found in the NMDA channel. Upon Glu and glycine binding to the NMDA receptor, the pore opens allowing an influx of calcium (Swanson *et al.*, 2005; Gardoni and Di Luca, 2006). This mechanism for receptor activation underlies the fundamental physiological function of learning and memory; however, it is also the means by which excitotoxicity occurs; in both acute and chronic neurodegeneration (Albin and Greenamyre, 1992; Beal, 1992; Greene and Greenamyre, 1996).

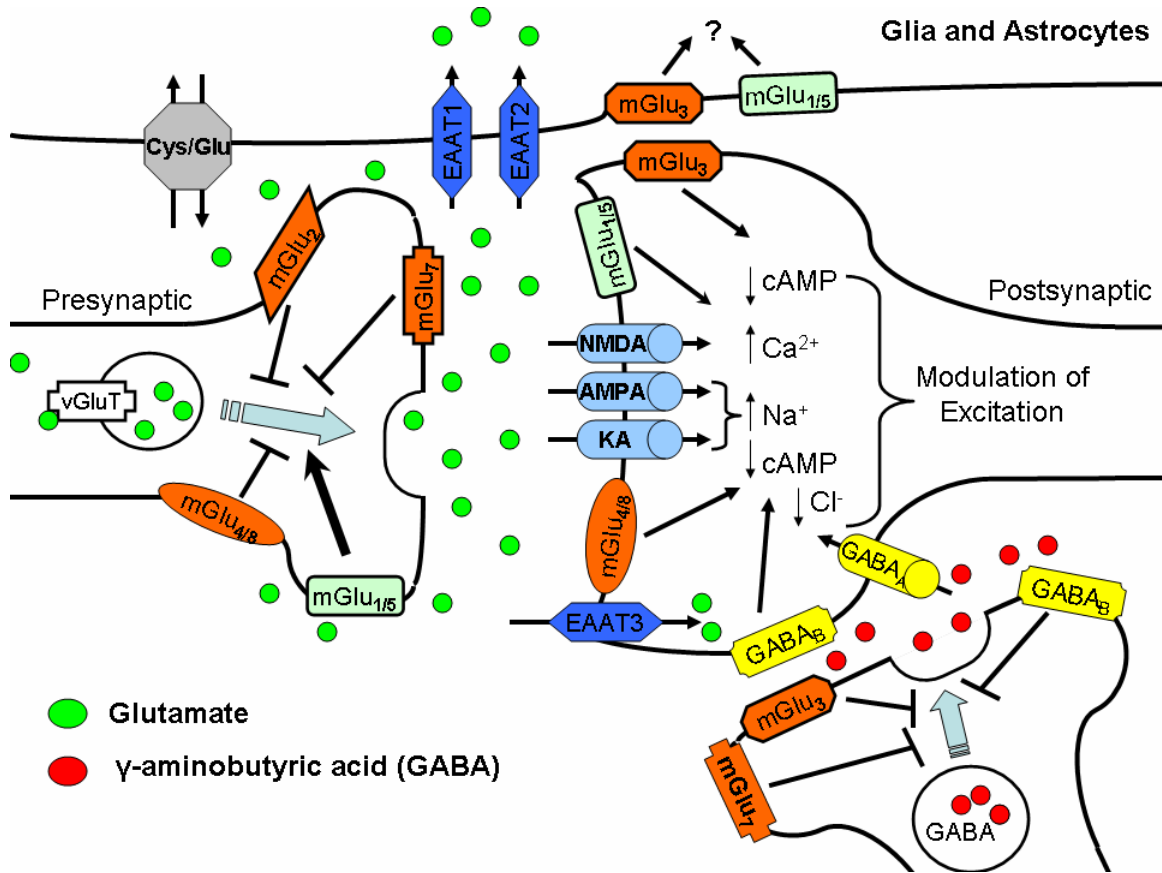


Figure 1.1: Glutamate Synapse Schematic

Schematic representation of a typical glutamatergic synapse. Glu is loaded into vesicle by vGluTs and upon depolarization, the vesicles fuse and release the neurotransmitter into the synaptic cleft. Once in the synaptic cleft, Glu can induce downstream signaling by postsynaptic neurons through mGluRs and iGluRs. Sodium-dependent, high-affinity transporters located on both glia and neurons are responsible for uptake of Glu with the majority of Glu transported into glia and astrocytes. Gamma aminobutyric acid (GABA) neurons can also be regulated by mGluR Groups II and III, which can affect downstream glutamatergic signaling. Adapted from Schoepp *et al.*, 2001.

Table 1.1: Ionotropic Glutamate Receptors

	Ionotropic Receptors (iGluRs)		
	NMDA	AMPA	Kainate
Receptor Subunits	NR1, NR2A, NR2B NR2C, NR2D NR3A, NR3B	GluR1, GluR2, GluR3, GluR4	GluR5, GluR6 GluR7, KA-1 KA-2
Signal Transduction	Ca ²⁺ , Na ⁺	Na ⁺ (Ca ²⁺)	Na ⁺ (Ca ²⁺)
Agonists	NMDA, Quinolinate Homocysteate	AMPA, ACPA L-Quisqualic acid	Kainic Acid, ATPA SYM2081 LY339434
Allosteric Potentiators	Glycine, D-Serine D-Cycloserine, Spermine, Spermidine	CX516, CX546, CX614 Cyclothiazide, IDRA-21, PEPA, LY404187 LY392098, LY503430	Concanavillin A
Antagonists	CGS 19755, PEAQX PPDA, D-AP5	NBQX, YM872 ZK200775	LY382884, UBP296
Allosteric Antagonists	Dizocilpine, Ifenprodil Memantine, Ro 25-698 (+)-CP-101,606 Ro 63-1908 Benzimidazole Benzamidines	GYKI 52466 (R)-LY303070 (R)-LY300164 CP-465,022 CP-526,427	NS3763
Channel Blockers	Phencyclidine Dizocilpine, Ketamine	Jorospider toxin	N/A

(*R,S*)-2-amino-3-(3-carboxy-5-methyl-4-isoxazolyl)propionic acid (**ACPA**); 5-*tert*-butyl-4-isoxazolepropionic acid (**ATPA**); (2*S*,4*R*) 4-methyl glutamic acid (**SYM2081**); (2*S*,4*R*,6*E*)-2-amino-4-carboxy-7-(2-naphthyl)hept-6-enoic acid (**LY339434**); (±)-*cis*-4-phosphonomethyl-2-piperidine carboxylic acid (**CGS 19755**); (2*S*^{*},3*R*^{*})-1-(phenanthrene-2-carbonyl)piperazine-2,3-dicarboxylic acid (**PPDA**); (*R*)-2-amino-5-phosphonopentanoate (D-AP5); 2,3-dihydroxy-6-nitro-7-sulfamoyl-benzo(*F*)quinoxaline (**NBQX**); [2,3-dioxo-7-(1*H*-imidazol-1-yl)-6-nitro-1,2,3,4-tetrahydro-1-quinoxaliny]-acetic acid (**YM872**); [1,2,3,4-tetrahydro-7-morpholinyl-2,3-dioxo-6-(trifluoromethyl)quinoxalin-1-yl] methylphosphonate (**ZK200775**); (3*S*,4*aR*,6*S*,8*aR*)-6-(4-carboxyphenyl)methyl-1,2,3,4,4*a*,5,6,7,8,8*a*-decahydroxyisoquinoline-3-carboxylate (**LY382884**); (*R,S*)-3-(2-carboxybenzyl)willardiine (**UBP296**); 5-carboxyl-2,4-di-benzamido-benzoic acid (**NS3763**); (*R*-(*R*^{*},*S*^{*})-α-(4-hydroxyphenyl)-β -methyl-4-(phenylmethyl)-1-piperidine propanol (**Ro 25-6981**); 1-[2-(4-hydroxy-phenoxy)-ethyl]-4-(4-methyl-benzyl)-piperidin-4-ol (**Ro 63-1908/Co 101244/PD 174494**); 1-(4-aminophenyl)-4-methyl-7,8-methylenedioxy-5*H*-2,3-benzodiazepine (GYKI 52466); (*R*)-1-(4-aminophenyl)-4-methyl-7,8-methylenedioxy-4,5-dihydro-3-methylcarbonyl-2,3-benzodiazepine (**GYKI 53784/LY303070**); (*R*)-7-acetyl-5-(4-aminophenyl)-

Table 1.1: (continued)

8,9-dihydro-8-methyl-7*H*-1,3-dioxolo(4,5-*h*) (2,3) benzodiazepine (**GYKI 53773/LY300164**); 3-(2-Chloro-phenyl)-2-[2-(6-diethylaminomethyl-pyridin-2-yl)-vinyl]-6-fluoro-3*H*-quinazolin-4-one (**CP-465,022**); 2-{2-[3-(2-Chloro-phenyl)-6-fluoro-4-oxo-3,4-dihydro-quinazolin-2-yl]-vinyl}-nicotinonitrile (**CP-526,427**); 1-(quinoxalin-6-ylcarbonyl)-piperidine (**CX516**); 5-carboxyl-2,4-dibenzoamido-benzoic acid, (**NS3763**) 1-(1,4-benzothiadiazine 1,1-dioxide (**CX546**); 2*H*,3*H*,6*aH*-pyrrolidino[2",1"-3'2']1,3-oxazino[6'5'-5,4]benzo[e]1,4-dioxan-10-one (**CX614**); 7-chloro-3-methyl-3,4-dihydro-2*H*-1,2,4-benzothiadiazine 1,1-dioxide (**IDRA-21**); (4-[2-(phenylsulphonylamino)ethylthio]-2,6-difluorophenoxyacetamide (**PEPA**); (*R,S*)-*N*-2-(4-(3-thienyl)phenyl)propyl-2-propanesulfonamide (**LY392098**); *N*-2-[4-(4-cyanophenyl)phenyl]propyl 2-propanesulfonamide (**LY404187**); (*R*)-4-[1-fluoro-1-methyl-2-(propane-2-sulphonylamino)-ethyl]-biphenyl-4-carboxylic acid methylamide (**LY503430**)

Metabotropic Glu receptors (mGluRs) are G-protein coupled receptors that regulate Glu release and modify postsynaptic excitability to Glu, high-affinity Glu transporters, and vGluTs (Swanson *et al.*, 2005). Since mGluRs rely on second messenger responses, they are generally slower than iGluRs. These receptors contain seven alpha-helical transmembrane domains with a ligand binding site located on the extracellular N-terminus (Kew and Kemp, 2005). mGluRs are classified into three groups. Group I (mGlu₁ and mGlu₅) are excitatory receptors localized on glial and post-synaptic, glutamatergic neurons. Group II (mGlu₂ and mGlu₃) receptors are inhibitory. mGlu₂ is located primarily on pre-synaptic glutamatergic terminals, while mGlu₃ is expressed on both glial and pre- and post-synaptic glutamatergic neurons. Finally, Group III (mGlu₄, mGlu₆, mGlu₇ and mGlu₈) are also inhibitory receptors, but they are not as specific for glutamatergic neurons. mGlu₄ and mGlu₇ receptors are located both pre- and post-synaptically on both glutamatergic and other neurotransmitter synapses. mGlu₈ is localized primarily on pre-synaptic glutamatergic and other neurotransmitter terminals, while mGlu₆ expression is only confirmed on retinal cells. (Refer to Table 1.2 for further information regarding mGluRs).

Proper activation of Glu receptors requires that extracellular concentrations of Glu be kept low for a high signal-to-noise ratio in synaptic transmission, thus allowing for stimulation with low levels of neurotransmitter release. No extracellular enzymes for Glu metabolism have been identified, so Glu clearance from the extracellular space is achieved by means of sodium-dependent, high-affinity transporters located primarily on glial cells. These transporters are more commonly known as excitatory amino acid transporters (EAATs). The uptake process is electrogenic and is therefore stimulated by a negative membrane potential, which is maintained by the sodium/potassium adenosine triphosphatase (Na⁺/K⁺ ATPase). Sodium is required for Glu binding while potassium is required for net transport of Glu through the EAATs. To be precise, for every 1 molecule of Glu transported into the cell, 3 sodium ions and 1 hydrogen ion are cotransported, while one potassium ion is transported out of the cell (Takahashi *et al.*, 1997; Danbolt, 2001; Kanai and Hediger, 2004; Grewer

Table 1.2: Metabotropic Glutamate Receptors

	Receptor	G-Protein	Glutamatergic Localization and Functions	Agonist	Antagonist
Group I	mGluR1	Gq; increase PLC	Post-synaptic; activation enhances excitability	DHPG ACPD quisqualate	LY393675 LY367385
	mGluR5		Post-synaptic; also found in glia; indicated in synaptic plasticity	DHPG quisqualate CHPG	MPEP
Group II	mGluR2	Go; decrease AC	Pre-synaptic; linked to LTD	DCG-IV APDC ACPD LY354740 LY379268	EGLU LY404039 LY341495
	mGluR3		Pre- and post-synaptic; found on glia where it is linked to neurotrophin release		
Group III	mGluR4	Go; Gi decrease AC	Pre- and post-synaptic; linked to motor learning	L-SOP ACPT-1 L-AP4	MSOP MAP4 CPPG
	mGluR6		Expression localized to retinal tissue	L-SOP L-AP4	MSOP MAP4
	mGluR7		Pre- and post-synaptic; autoreceptor		
	mGluR8		Pre-synaptic; regulation of lateral perforant path	L-SOP L-AP4 DCPG	

3,5-dihydroxyphenylglycine, **DHPG**; (1*S*,3*S*)-1-aminocyclopentane-1,3-dicarboxylic acid, **ACPD**; 2-(*S*)-amino-2-(3-*cis*-carboxycyclobutyl)-3-(9*H*-thioxanthen-9-yl) propionic acid, **LY393675**; [(+)-2-methyl-4-carboxyphenylglycine], **LY367385**; (*RS*)-2-chloro-5-hydroxyphenylglycine, **CHPG**; 2-methyl-6-(phenylethyl)pyridine, **MPEP**; (2*S*, 2'*R*,3'*R*)-2-(2',3'-dicarboxycyclopropyl)glycine, **DCG-IV**; 2*R*,4*R*-4-aminopyrrolidine-2,4-dicarboxylic acid, **APDC**; (1*S*,2*S*,5*R*,6*S*)-2-aminobicyclo[3.1.0]hexane-2,6-dicarboxylate monohydrate, **LY354740**; (-)-2-oxa-4-aminobicyclo[3.1.0]hexane-4,6-dicarboxylate, **LY379268**; (*S*)- α -ethylglutamic acid, **EGLU**; (-)-(1*R*,4*S*,5*S*,6*S*)-4-amino-2-sulfonylbicyclo[3.1.0]hexane-4,6-dicarboxylic acid, **LY404039**; L(+)-2-amino-4-phosphonobutyric acid, **LY341495**; *S*-serine-O-phosphate, **L-SOP**; (1*S*,3*R*,4*S*)-1-aminocyclopentane-1,3,4-tricarboxylic acid, **ACPT-1**; L(+)-2-amino-4-phosphonobutyric acid, **L-AP4**, (*RS*)- α -methylserine-O-phosphate, **MSOP**; (*S*)-2-amino-2-methyl-4-phosphonobutanoic acid/ α -methyl, **MAP4**; (*RS*)-4-phosphonophenyl glycine, **CPPG**; (*S*)-3,4-dicarboxyphenylglycine, **DCPG**

and Rauen, 2005). To date, five Glu transporters have been cloned and numbered EAAT1-5. EAAT1 (Glu-Aspartate Transporter (GLAST) in rodents) and EAAT2 (Glu Transporter (GLT-1) in rodents) are responsible for the majority of Glu uptake in the mammalian CNS and both are located exclusively on glial cells. Glu transporters differ in brain localization; EAAT1 predominates in the cerebellum, while EAAT2 is the major Glu transporter of the forebrain. EAAT3 (Excitatory Amino Acid Carrier (EAAC1) in rodents) is expressed in the lowest concentration compared to the others and thought to account for a small percentage of Glu uptake. It has a wide expression throughout the mammalian brain, located primarily on neurons. EAAT4 is found in Purkinje cells of the cerebellar molecular layer, while EAAT5 is found in the retina. For a comprehensive review on Glu transporters, refer to Danbolt, 2001.

Excitotoxicity

While Glu normally functions as a neurotransmitter; excessive stimulation of Glu receptors can cause neuronal degeneration by a mechanism termed excitotoxicity (Olney, 1978). Olney and colleagues defined this process as “a phenomenon whereby the excitatory action of Glu and related excitatory amino acids becomes transformed into a neuropathological process that can rapidly kill CNS neurons.” Excitotoxic cell death involves prolonged depolarization of neurons, changes in intracellular calcium concentrations, and the activation of enzymatic and nuclear mechanisms of cell death (Doble, 1999). In the classical model of excitotoxicity, post-synaptic depolarization is initiated by activation of AMPA receptors and voltage-dependent sodium channels, leading to sodium entry and further depolarization. To maintain ionic equilibrium, chloride ions enter the cell along with water that is following the osmotic gradient. Entry of water causes osmotic swelling of the cell, but the process is reversible and therefore is not the final mechanism of excitotoxicity (Choi, 1987). Instead, the calcium-dependent part of the cascade seems essential for toxicity and cellular death. Depolarization of the membrane by sodium leads to opening of voltage-sensitive calcium channels as well as removal of the magnesium block on the

NMDA receptor. These are the two primary sources for calcium entry into the cell. This appears to be the irreversible step and the ability of the neuron to survive this calcium influx may depend on intracellular organelles, such as the mitochondria or endoplasmic reticulum, to buffer the influx of calcium (Doble, 1999). If the neuron is unable to buffer the large quantities of calcium entering the cell, calcium can overstimulate proteases, protein kinases, and nitric oxide synthetases. This leads to production of free radicals or apoptotic mechanisms and eventually cell death (Nicholls and Budd 2000; Sattler and Tymianski, 2000).

During the time course of excitotoxicity, the extracellular concentrations of Glu rise for three main reasons. First, influx of calcium leads to vesicular release of Glu from pre-synaptic neurons. Second, more Glu is being released into the extracellular space due to cell lysis. Finally, since Glu transport is electrogenic, membrane depolarization can slow down or even reverse these transporters keeping Glu in the extracellular space for prolonged periods of time (Doble, 1999). This increase in extracellular Glu can diffuse to nearby neurons, thus propagating and amplifying cell death.

The above process is most commonly seen in stroke, ischemia, and traumatic brain injury and referred to as acute excitotoxicity. Evidence exists for a slower, indirect form of excitotoxicity involved with chronic neurodegenerative diseases. In this form of excitotoxicity, mitochondria become damaged leading to energy impairment and subsequent decrease in intracellular ATP levels (Beal, 1992; Greene and Greenamyre, 1996; Doble, 1999). As ATP levels decrease, the Na^+/K^+ ATPase, responsible for maintaining the resting membrane potential slows down leading to depolarization. This can relieve the magnesium block on NMDA channels as well as open voltage-gated calcium channels. With the magnesium block removed, the NMDA receptor is more susceptible to activation by ambient or even slightly elevated levels of extracellular Glu (Beal, 1992; Greene and Greenamyre, 1996; Doble, 1999). Over prolonged periods of time (years) this process becomes similar to what is seen in acute excitotoxicity. For this reason, it has been postulated that slow, indirect excitotoxicity is partly responsible for the neuronal loss seen in several neurodegenerative disorders

including amyotrophic lateral sclerosis (ALS). ALS is characterized by progressive muscular weakness leading to paralysis and eventual death due to respiratory failure (Williams and Windebank, 1991). This neurodegenerative disease has the largest body of evidence supporting excitotoxicity contributes to the progression of symptoms (Doble, 1999). Several studies have suggested that there is a defect in Glu metabolism (Heath and Shaw, 2002; Rao and Weiss, 2004) causing elevated levels of the neurotransmitter Glu in the cerebrospinal fluid (Rothstein *et al.*, 1990; Shaw *et al.*, 1995; Spreux-Varoquaux *et al.*, 2002) of ALS patients compared to control patients. The failure to properly metabolize Glu may result in raised extracellular Glu levels that overtime could contribute to excitotoxic and motorneuron degeneration described above.

L-Glutamate Metabolism

Metabolic compartmentation in the brain was first demonstrated by Lajtha and colleagues (1959) when they injected [^{14}C] Glu into the rat brain and found that glutamine was the predominant molecule containing the isotope. They interpreted this data as glutamine was formed exclusively from a “small” pool of Glu that rapidly accumulates Glu and synthesizes glutamine (Hertz, 2004). Computer simulation studies over the next decade by Van den Berg and Garfinkel (1971) showed the flow of Glu from a “large” compartment where it was degraded to glutamine in a “small” compartment and an identical flow of glutamine in the opposite direction. This process became known as the Glutamate-glutamine cycle (Benjamin and Quastel, 1975). But, it wasn’t until the selective localization of glutamine synthetase that the “small” pool was determined to be astrocytes (Norenberg and Martinez-Hernandez, 1979). Since glutamine synthetase is absent in neurons, this meant all neuronal constituents constitute the “large compartment.”

Today, the Glutamate-glutamine cycle is a well understood mechanism. Upon depolarization and vesicular release of Glu, it is taken up into astrocytes by high affinity transporters (Danbolt, 2001). Once in the astrocytes, Glu is aminated into glutamine by glutamine synthetase that is localized only in

astrocytes. Glutamine is not neurotoxic and therefore it can be safely transported out of the astrocytes through System N located on astroglial cells. In the extracellular space, glutamine is transported into neurons through System A (Bak *et al.*, 2006). When returned to the neuron, glutamine is converted back into Glu by phosphate-activated glutaminase (PAG), which is located on the inner mitochondrial membrane (Kvamme *et al.*, 2000). The Glu formed is returned to the cytosol and subsequently packaged into vesicles for future neurotransmitter signaling.

Since neurons are incapable of net synthesis of Glu from glucose (Waagepetersen *et al.*, 2005), the Glutamate-glutamine cycle was previously thought to provide neurons with all the Glu necessary for neurotransmitter signaling. Because of this theory, the Glutamate-glutamine cycle was originally thought to operate in a stoichiometric one-to-one ratio. For every Glu released, one glutamine was transported into neurons to replenish the neurotransmitter pool of Glu. However, recent evidence suggests this process is oversimplified and other enzymes must be responsible for replenishing the neurotransmitter pool of Glu (Fonnum, 1993; Peng *et al.*, 1993; Broman *et al.*, 2000; Waagepetersen *et al.*, 2000; Danbolt, 2001; Waagepetersen *et al.*, 2005). It is now known that Glu is metabolically closely related to the tricarboxylic acid (TCA) cycle (Waagepetersen *et al.*, 2005). For example, when Glu is transported into astrocytes, it can be metabolized into glutamine by glutamine synthetase or transaminated into α -ketoglutarate. Alpha-ketoglutarate can then enter the TCA cycle where it is eventually metabolized into malate, and malate can be decarboxylated into pyruvate and reduced to lactate. Lactate can be transported out of astrocytes and into neurons by monocarboxylate transporters (Gladden, 2004; Pierre and Pellerin, 2005). Once in the neurons, lactate can be oxidized to pyruvate and either re-enter the TCA cycle or it can be transaminated back into Glu for neurotransmitter packaging and signaling. (Please refer to Figure 1.2). This example highlights one of the many possible fates of Glu and is used to show the complicated competition for Glu between cellular energy demands and neurotransmitter signaling. Furthermore, Hassel and Bråthe (2000)

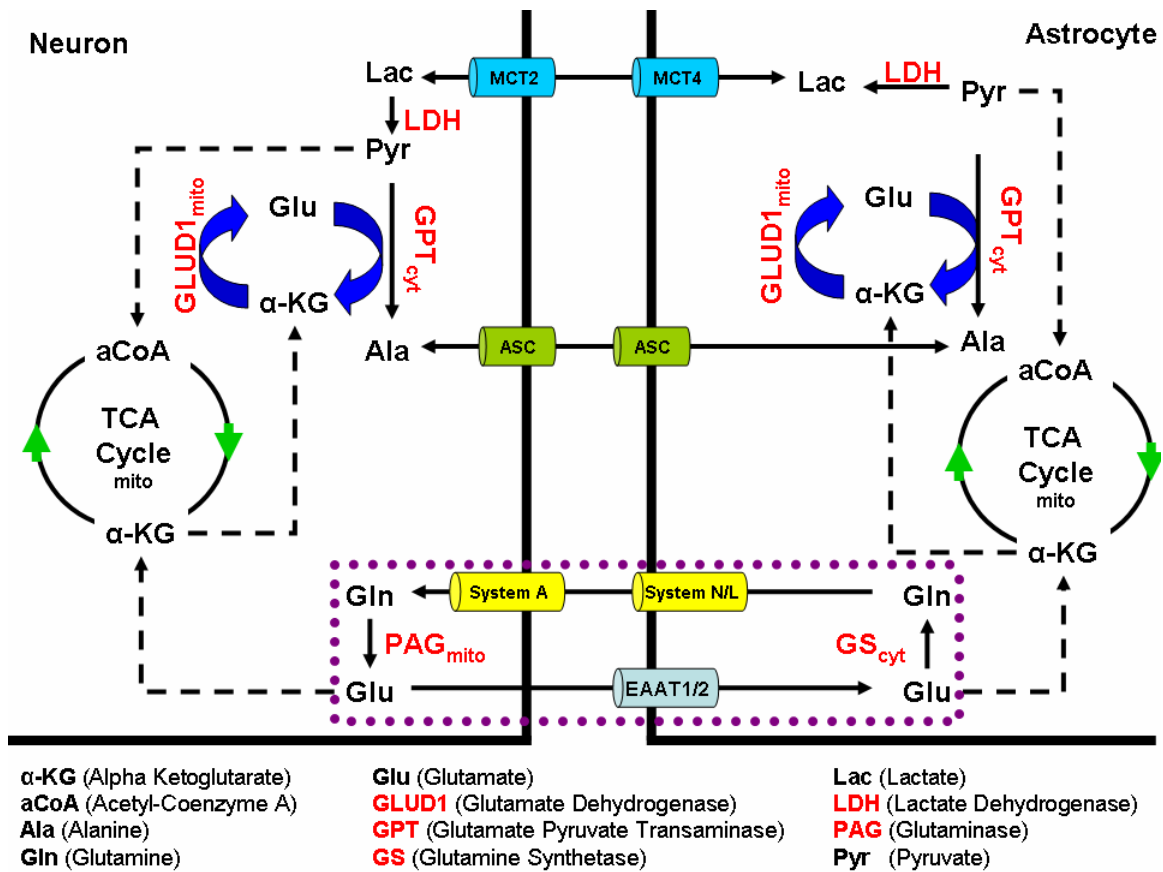


Figure 1.2: The Glutamate-Glutamine Cycle Revisited

Schematic representation of Glu synthesis between astrocytes and neurons. The classic Glu/glutamine cycle is highlighted in the purple, dashed box. All enzymes are shown in RED, while dashed arrows indicate multiple metabolic steps that are not shown due to size limitations. The terms “mito” and “cyt” indicate either mitochondrial or cytoplasmic localization, respectively. Figure modified from Waagepetersen *et al.*, 2000.

demonstrated that it is possible to obtain Glu formation independent of glutamine. This implies that enzymes other than PAG and glutamine synthetase are responsible for *de novo* synthesis or degradation of Glu. Two such Glu metabolizing enzymes found in neurons are glutamate pyruvate transaminase (GPT) and glutamate dehydrogenase (GLUD1).

Glutamate Pyruvate Transaminase

GPT exists as a dimer with a molecular mass of approximately 100 kDa in most species (Saier and Jenkins, 1967). The enzyme catalyzes a reversible transaminase reaction using pyruvate as a co-substrate to form alanine and α -ketoglutarate (Figure 1.3A). Biochemical studies show GPT activity in both the cytosol and mitochondria of astrocytes and neurons (Balazs and Haslam, 1965; Erecińska *et al.*, 1994), but the greatest activity is found in astrocytes of the cerebral cortex (Westergaard *et al.*, 1993). It is debated throughout the literature whether GPT favors Glu degradation (Saier Jr. and Jenkins, 1967; Ruščák *et al.*, 1982; Erecińska *et al.*, 1994) or synthesis (Peng *et al.*, 1991, 1993; Schousboe *et al.*, 2003). This process most likely depends on the amount of substrates/products available. However, Matthews and colleagues (2000, 2003) demonstrated that GPT is an active Glu degrading enzyme that acts as an effective neuroprotectant in cell culture models of exogenous and endogenous Glu excitotoxicity. Unfortunately, GPT does not exist in the extracellular space and, due to its large size, is unable to cross the blood-brain barrier. This makes it an unsuitable candidate for excitotoxicity therapeutics; nevertheless these studies demonstrate the propensity for GPT to metabolize Glu.

Glutamate Dehydrogenase

Similar to GPT, GLUD1 catalyzes a reversible reaction; however, this reaction favors Glu formation from ammonia and α -ketoglutarate, using NAD(P)⁺ as co-factors as shown in figure 1.3B (Yudkoff *et al.*, 1991; Kanamori and Ross, 1995; Bak *et al.*, 2006). GLUD1 is composed of six identical subunits, each with a molecular mass of 56 kDa (Mastorodemos *et al.*, 2005). Biochemical and

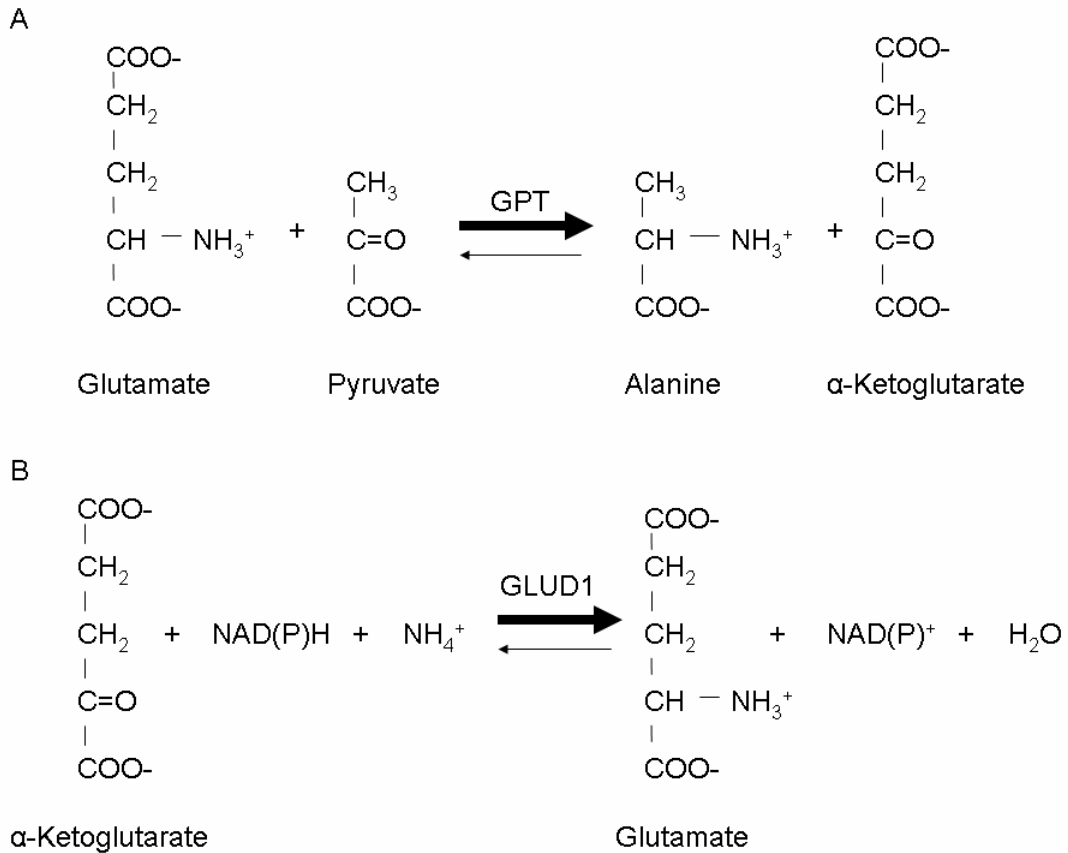


Figure 1.3: Glutamate Metabolic Pathways

A) Glu metabolism by Glutamate Pyruvate Transaminase. B) Glu synthesis by Glutamate Dehydrogenase.

histochemical studies show GLUD1 is localized to the inner mitochondrial membrane of neurons (Toledano *et al.*, 1979; Rothe *et al.*, 1990; McKenna *et al.*, 2000), while immunohistochemical studies show astrocytic localization (Kaneko *et al.*, 1987). This suggests that GLUD1 is ubiquitously expressed in mitochondria throughout the mammalian brain (Madl *et al.*, 1988). Recently, however, two isoforms of Glu dehydrogenase (GLUD1 and GLUD2 have been identified in humans and primates (Burki and Kaessmann, 2004), which may account for the discrepancies in localization. GLUD1 is considered a housekeeping gene ubiquitously expressed throughout mammals while GLUD2 is a brain-specific isotype found in primates and humans (Plaitakis and Zaganas, 2001; Burki and Kaessmann, 2004; Mastorodemos *et al.*, 2005; Kanavouras *et al.*, 2007). Burki and Kaessmann (2004) demonstrated that GLUD2 formed by retroposition of GLUD1 to the X chromosome in primates 23 million years ago and may be indicative of higher thought processes. In humans, these two isoforms are homologous differing in only 16 amino acids (Kanavouras *et al.*, 2007). Because the retroposition occurred in primates, rodents only have the GLUD1 copy.

GLUD1 is thought to be controlled by cellular energy demands since it is allosterically stimulated by ADP and inhibited by ATP (Smith, 1979; Plaitakis and Zaganas, 2001). This indicates that the activity of the enzyme can operate in the direction of oxidative deamination when cellular supplies of ATP are low. By converting Glu to α -ketoglutarate the mitochondria is provided with essential reducing equivalents, through NAD(P)H, for synthesis of ATP. In addition, the α -ketoglutarate formed can be metabolized in the TCA cycle for further production of ATP. This has been supported by studies examining pancreatic beta cells and modulation of GLUD1 to regulate insulin release (Gylfe, 1976; Stanley *et al.*, 1998).

Several studies examining post-mortem CNS tissue have determined that increases in GLUD1 activity are associated with several different neurological disorders. Malessa and colleagues (1991) found that GLUD1 activity was

significantly increased in the ventral white matter and in the dorsal horn of the spinal cord in ALS patients compared to control. It is well documented that Glu levels are increased in the CSF of ALS patients (Rothstein *et al.*, 1990; Doble, 1999; Heath and Shaw, 2002; Spreux-Varoquaux *et al.*, 2002). Since the GLUD1 reaction favors Glu formation, this finding by Malessa and colleagues, suggests a causative relation for the increased levels of Glu. These CSF Glu levels may be high enough to cause excitotoxicity and damage the lower motor neurons—a hallmark of ALS. Burbaeva and colleagues (2005) determined that GLUD1 was increased in brain tissue homogenate from the prefrontal cortex (PFC) of Alzheimer's disease (AD) patients compared to control patients. Additionally, the same group (Burbaeva *et al.*, 2003, 2007) determined that GLUD1 activity was increased in the PFC of schizophrenic patients compared to control patients. In both studies this group concludes that alterations in Glu metabolizing enzymes may be responsible for changes in the extracellular concentration of Glu. The results of all of these independent studies strongly suggests that increased GLUD1 activity is involved in three different neurological disease states.

Techniques for Measuring L-glutamate: Microdialysis

Microdialysis is a technique that utilizes semipermeable membranes to restrict the diffusion of extracellular molecules or neurotransmitters along their concentration gradients. (Ungerstedt, 1984; Di Chiara *et al.*, 1996). A microdialysis probe consists of a cylindrical dialysis membrane with inlet and outlet tubes. These probes have a diameter of 150-400 μm with an average length of 1-4 mm (Kennedy *et al.*, 2002). Dialysis probes are stereotaxically compatible and therefore have been used in both anesthetized and awake animal models. Once implanted, dialysate samples are collected every 5 to 20 minutes and experiments can last from hours up to 3 or 4 days (Westerink, 1995). Collected fractions are generally analyzed using analytical chemistry techniques. High performance liquid chromatography coupled with electrochemical or fluorescence detection is often used due to their sensitivity

and ability to handle small sample sizes ($< 10 \mu\text{l}$) (Westerink, 1995). The high sensitivity of the analytical techniques allows for detection of low concentration of analytes in the femtomolar range (Kennedy *et al.*, 2002). Another advantage of microdialysis is the ability to measure multiple analytes simultaneously thus allowing the researcher to study several neurotransmitter systems at once. Despite how commonplace the technique has become in the laboratory, there are several large disadvantages that make microdialysis unsuitable for measuring Glu.

Due to the high-affinity transporters, Glu neurotransmission lasts on the order of milliseconds to seconds (Kinney *et al.*, 1997). Since dialysate samples are collected over minutes, Glu release and re-uptake is often missed or grouped together into larger pools within the samples, which makes it exceptionally difficult to study behavioral paradigms. Recent advances in the collection and analyzing methods have increased the time resolution into the range of seconds. Lada and colleagues (1997) showed that using capillary electrophoresis coupled with laser-induced fluorescence detection resulted in sample collection every 12 seconds. That same year, Tucci and colleagues (1997) demonstrated a similar method with samples collected every 6 seconds. However, the fastest collection time published was by Rossell and colleagues (2003) that demonstrated a 1-second collection method. For these methods, dialysate samples are collected in a tube and this tube is cut into specific lengths corresponding to the desired collection time (Kennedy *et al.*, 2002). This is a controversial method because diffusion through the tubing (band broadening) can affect concentration values in different time intervals, if the tubing is not cut immediately (Rossell *et al.*, 2003). Also, the flow rates and dead volume can drastically change the temporal response, which suggests band broadening is responsible for a sluggish response to analyte in the fractions collected (Lada *et al.*, 1997). In this paper, Lada goes onto explain that band broadening within the dialysis probe or tubing prevents this method from achieving faster than a 10 second temporal response. This brings into question the validity of the Rossell study claiming 1 second response times.

The large size of the microdialysis probe causes substantial short- and long-term trauma, which is evidenced by histological, physiological, and biochemical changes in nearby CNS tissue (Bungay *et al.*, 2003). During the first hours after implantation the blood-brain barrier is disrupted, blood flow to the tissue surrounding the probe is decreased and release of neurotransmitters is altered (Westerink, 1995). Positron emission tomography (PET) imaging has revealed that glucose metabolism is drastically and irreversibly altered by chronic implantation of a microdialysis cannula/probe (Schiffer *et al.*, 2006). Three days after implantation a glial barrier is observed and may account for probe blockage (Benveniste and Diemer, 1987). This glial barrier is markedly increased if nonfunctional microdialysis probes are removed and functional probes are reinserted in an attempt to continue freely moving studies within the same animal (Georgieva *et al.*, 1992). Clapp-Lilly and colleagues (1999) demonstrated that ultrastructural damage occurs up to 1.4 mm away from a microdialysis probe implant site. In addition, perfusion and removal of material by the probe may produce concentration gradients that can further damage tissue up to several millimeters away from the implant site (Bungay *et al.*, 1990). The implantation damage caused by microdialysis probes has drastic effects on local neurotransmitter dynamics. Carbon fiber microelectrodes coupled with voltammetric techniques were used to demonstrate that evoked dopamine release is attenuated up to 220-250 μm from the microdialysis probe implant site (Yang *et al.*, 1998; Borland *et al.*, 2005). If this probe-induced trauma along with glial barrier formation is not taken into account for microdialysis analysis, the estimation of extracellular concentrations and clearance of neurotransmitters such as DA and Glu can be underestimated (Lu *et al.*, 1998; Yang *et al.*, 1998; Bungay *et al.*, 2003). Furthermore, Frumberg and colleagues (2007) demonstrated that rats implanted with microdialysis probes performed significantly worse in object recognition tasks despite no change in locomotor activity. These studies demonstrate the excessive damage caused by a dialysis probe as well as question the physiological validity of dialysis samples.

Finally, previous microdialysis studies indicate that resting Glu levels are virtually tetrodotoxin (TTX) and calcium-independent (Timmerman and Westerink, 1997). This does not fulfill the classical criteria for exocytotic release thus raising doubt as to the vesicular origin of Glu. Several laboratories have also demonstrated that increases in neurotransmitters due to stress are largely TTX-independent as well. These studies indicate that physiological release of Glu, whether it be resting or stimulated, is from non-neuronal sources such as reversal of the high-affinity transporters (Kanai and Hediger, 2004). However, little data supports this hypothesis. Instead, since Glu released from neuronal pools is rapidly cleared and has limited diffusion, it has been hypothesized that microdialysis fails to reliably sample synaptic pools of Glu (Drew *et al.*, 2004). Drew and colleagues claim that the current microdialysis probes sample from too large of an area to reliably measure changes close to the synapse. For this reason, the relevance of using microdialysis to study Glu neurotransmission is uncertain.

Techniques for Measuring L-glutamate: Amperometric Detection with Microelectrode Arrays

The poor temporal and spatial resolution as well as the severe damage on CNS tissue due to implantation has warranted more reliable techniques that are less invasive for the study of Glu. Within the past decade several groups have developed Glu selective microelectrodes to address the above inconsistencies with microdialysis studies on glutamatergic physiology (Hu *et al.*, 1994; Rahman *et al.*, 2005) and some studies utilizing these microelectrodes have shown that Glu is TTX-dependent (Kulagina *et al.*, 1999; Day *et al.*, 2006; Oldenziel *et al.*, 2006). Our laboratory has developed an enzyme-based multisite microelectrode array (MEA) that uses amperometric recording techniques with subsecond measurements (Burmeister *et al.*, 2000; Burmeister and Gerhardt, 2001; Burmeister *et al.*, 2002; Nickell, *et al.*, 2004; Day *et al.*, 2006; Nickell *et al.*, 2007). These MEAs have 4 platinum (Pt) recording sites each measuring 333 X 15 μm , and because of the small size, the MEAs have been shown to cause minimal

damage to surrounding CNS tissue and are viable for at least one week post-implantation (Rutherford *et al.*, 2007). Furthermore, through a specific coating technique that is referred to as self-referencing, our laboratory is able to selectively measure resting Glu levels and consistently demonstrate that resting Glu levels are TTX-sensitive (Day *et al.*, 2006). For a thorough explanation regarding the MEAs and self-referencing, please refer to Chapter Two: Materials and Methods.

Mouse Models

The mouse model has many advantages as an experimental animal model. They have a unique adaptation and ability to survive inbreeding (Joyner and Sedivy, 2000), they have a short generation turnover and low maintenance cost for breeding, housing, and drug administration (Cryan and Holmes 2005; Jacobson and Cryan, 2007). More importantly, mouse and humans share close metabolic and anatomical similarities. Genes between the two species are greater than 99% conserved (Consortium, 2002). This provides the researcher with a model system to study human diseases including diabetes, cancer, immunological, and neurological disorders.

Inbred mice strains offer several additional advantages to those already mentioned including genetic and phenotypic uniformity. This uniformity reduces the number of animals needed for experiments, because variability is limited to extragenetic or varying controllable environmental factors. In particular, the inbred mouse is a valuable tool for studying the aforementioned human diseases. Since inbred strains trace back to a common ancestor, they are considered isogenic and homozygous at all loci. (Beck *et al.*, 2002), which indicates that differences between mouse strains as well as genetically modified mice and wildtype (WT) littermates is a function of the change in genotype (Crabbe *et al.*, 2002; Lesch, 2004; Festing, 2004).

Thesis Outline

The present studies address the use of these MEAs to study Glu dynamics in both anesthetized and awake, freely moving mice. For our anesthetized studies, we studied the importance of GPT and GLUD1 on the neurotransmitter pool of Glu. Since no specific modulators for either of these enzymes exist, we used transgenic mouse models that were developed at the University of Kansas by Dr. Elias K. Michaelis's group. The remainder of the work addresses the adaptation and validation of the MEAs for use in awake, freely moving mice. It serves to develop and characterize a new technique as well as expand upon the current knowledge regarding resting Glu levels in the freely moving mouse. The long-term goal is to incorporate the freely moving technology with the GPT and GLUD1 transgenic mouse models, so we can determine if altering Glu metabolizing enzymes has any effect on behavior.

In Chapter Three, we investigated how upregulation of GLUD1 affects stimulus-evoked Glu release and uptake as well as exogenously applied Glu in the striatum (Str) of two inbred mouse strains: C57BL/6 and BALB/C. We examined two different mouse strains due to histochemical data acquired at the University of Kansas that revealed C57BL/6 mice have endogenously higher levels of GLUD1 protein compared to BALB/C mice. Local application of 70 mM KCl resulted in a significant increase in Glu release in both strains of GLUD1 transgenic mice compared to WT littermates. Furthermore, uptake of 70 mM KCl-evoked Glu release as well as clearance of 5 mM Glu was similar for the GLUD1 transgenic mice compared to WT littermates in both mouse strains. At 16 months of age, the C57BL/6 GLUD1 transgenic mice developed lower limb atrophy that resulted in severe gait disorders and righting problems. Histological data conducted at the University of Kansas revealed severe atrophy of Betz cells within the motor cortex and atrophy of lower motor neurons in the spinal cord. To our knowledge, this is the first animal model that displays a late onset neurodegeneration, similar to what is observed in patients suffering from ALS.

In Chapter Four we examined how upregulation as well as knockout (KO) of the GPT gene affects Glu neurotransmission in C57BL/6 mice. Similar to

studies in Chapter Three, we investigated stimulus-evoked Glu release and uptake as well as clearance of exogenously applied Glu in the Str. In the GPT transgenic mice, we did not observe any differences in stimulus-evoked Glu release, but did observe significantly slower uptake dynamics of both stimulus-evoked Glu and exogenously applied Glu. In the GPT KO mice, homozygous mice released significantly more Glu compared to WT littermates. We also observed that GPT homozygous KO mice cleared exogenously applied Glu slower compared to WT. Despite these differences, we have not observed any noticeable phenotypic or behavioral alterations due to upregulation or KO of the GPT gene.

In Chapter Five we wanted to study the GLUD1 motor deficient mice in an awake, freely moving mouse model. Before we could do this, we had to develop and characterize our current freely moving technology for a mouse model. We adapted our current technology for freely moving rats to make the recording apparatus smaller and lighter weight for recordings in the awake mouse. Using our self-referencing MEAs that were selective for Glu measures, we reliably measured Glu for 7 days post-implantation in both the Str and PFC of the C57BL/6 mouse. Through an attached guide cannula we locally applied a solution of 1 mM Glu and saw no loss in MEA sensitivity on days 3 through 7 post-implantation. However, we did observe changes in both uptake rate and time for 80 percent of the Glu signal decay (t_{80}) over days. Uptake rate became slower, while the t_{80} 's became longer over days in both the Str and PFC. With our self-referencing MEAs we were able to measure resting Glu levels in both brain areas and found that the Str had elevated resting Glu levels compared to the PFC. Through the attached guide cannula we locally applied DL-*threo*- β -hydroxyaspartate (THA), a non-selective Glu transport blocker and tetrodotoxin (TTX), a potent sodium-channel blocker to pharmacologically alter resting Glu levels. We found that local application of THA increased resting Glu levels since the uptake was blocked, while TTX decreased resting Glu levels because neuronal depolarization and subsequent vesicular release of Glu was prevented. These two studies indicate that the source of resting Glu levels in the Str is at

least partially neuronally derived and not from reversal of the high-affinity transporters. Finally, we measured Glu changes due to a stressor. Introduction of a fox urine soaked cotton ball into the recording chamber resulted in an increase in Glu levels throughout the duration of the stressor. Glu levels returned to baseline 15 minutes after the stressor was removed. The ability to monitor Glu without anesthesia allowed us to study Glu dynamics for at least 7 days post-implantation. When we couple this finding with our changes in Glu from a stressor such as fox urine we can design behavioral paradigms to better understand physiological release and uptake of Glu and apply this technique to better understand the role of Glu metabolizing enzymes on the neurotransmitter pool of Glu

Copyright © Kevin Nicholas Hascup

Chapter Two: Materials and Methods

Principles of *In Vivo* Electrochemistry

In vivo electrochemistry utilizes microelectrodes that were implanted into the mammalian CNS providing a means to record chemical signaling of neurons. The microelectrode's recording surface, or working electrode (normally an inert metal such as Pt or carbon, could oxidize or reduce compounds of interest. A potential was applied versus a reference electrode, normally a Ag/AgCl reference electrode that was in ionic contact with the working microelectrode. Low noise headstages, which include potentiostats, apply this potential and were computer-controlled with multiple inputs to simultaneously record from several microelectrodes or several recording surfaces on a single MEA. If the potential at the microelectrode surface was sufficient, molecules directly at the recording surface of the working electrode were either oxidized or reduced depending upon their intrinsic electrochemical properties. Oxidized molecules donate one or more electrons to the recording surface while reduced molecules receive electrons from the recording surface. The currents generated from those Faradaic reactions were linear with respect to concentration of the electroactive molecule(s) in the tissue surrounding the microelectrode. This basic principle allows for *in vitro* calibration methods for *in vivo* studies.

One of the simplest electrochemical techniques was amperometry and involves the measurement of current at a constant fixed potential. The current was continuously monitored, thus, events were measured as quickly as ≤ 1 ms. Since the voltage was applied continuously to the working electrode, the non-Faradaic background current recorded from the microelectrode was low and allowed for sensitive measurements of electrochemically active molecules.

Several neurochemicals reside in the extracellular space of the CNS that were electrochemically active on Pt recording surfaces at low or high oxidation potentials including ascorbic acid (AA), dopamine (DA), norepinephrine (NE), serotonin (5-HT), 5-hydroxyindoleacetic acid (5-HIAA), homovanillic acid (HVA), nitric oxide (NO), uric acid, and 3,4-dihydroxyphenylacetic acid (DOPAC). In

addition, enzymes were applied to the recording surface to produce an electrochemically active reporter molecule, such as hydrogen peroxide (H_2O_2), to allow measurements of molecules that were not inherently electrochemically active. When a potential of +0.7 V versus a Ag/AgCl reference was applied to the Pt recording sites, the newly formed H_2O_2 oxidizes and the resulting change in current from the transfer of electrons to the Pt recording surface was detected. While O_2 was required as a cofactor for oxidase enzymes, the oxidation of the reporter molecule, H_2O_2 , generates a portion of the O_2 for continued reactions. This did not, however, allow measures using oxidase enzymes in zero O_2 environments.

An important and often forgotten aspect of microelectrodes was that analytes from only a small area (microns) of tissue surrounding the recording surface were detected. This was useful for studying small or layered structures in the brain or the spinal cord. Additionally, microelectrodes with multiple recordings surfaces could be geometrically arranged to measure analyte concentrations from two or more distinct brain regions. Since microelectrodes coupled with amperometric techniques measured analytes of interest on rapid time scales (1-1000 ms), uptake and release kinetics of faster neurotransmitters, such as Glu, were easily studied.

Microelectrode Array Fabrication

Enzyme-based multisite MEAs were mass fabricated using photolithographic methods (*Methods and Materials in Microelectronic Technology*, 1984; *Wire Bond*, 1998; *Photolithography*, 2001). For a detailed account regarding MEA design and use, refer to Hascup *et al.*, 2006. An advantage of photolithography allowed routine production of reproducible recording surfaces as small as 5-10 μm . In addition multiple microelectrodes were patterned onto a single fabrication substrate (usually 2.5 cm x 2.5 cm) allowing for increased fabrication numbers at a decreased cost. Finally, photolithographic methods were used to manufacture numerous MEA designs

with multiple recordings sites in well-defined, highly reproducible, geometrical configurations.

Our multisite MEAs were constructed in conjunction with Thin Films Technology, Inc., (Buellton, California). Initially, MEA photographic masks were designed on a computer aided design program where arrays of 4-16 recording sites were arranged on templates. A 2.5 cm x 2.5 cm x 125 μm thick ceramic wafer (alumina, Al_2O_3 , Coors Ceramic, Coors Superstrate 996) served as a common substrate for the MEAs. Ceramic reduced the cross-talk from adjacent connecting lines. Additionally, ceramic was strong and rigid, which aided in precise stereotaxic placement into tissues with minimal flexing or breaking. The ceramic substrate was polished or lapped down to achieve MEAs as thin as 37.5 microns.

Following cleaning, photoresist was spun onto the ceramic wafer. To transfer the MEA image onto the wafer, collimated light was passed through a photomask of the MEA design, thus exposing the design onto the photoresist. Spaces for the recording sites, connecting lines and bonding pads were not exposed to light. Solvents were used to remove unexposed photoresist from the wafer. Many 1 cm long MEAs (34-64) were patterned onto the wafer simultaneously to facilitate production and increase the number of MEAs that were made from the ceramic substrate (figure 2.1). Patterning could also be performed on the reverse side of the ceramic wafer to increase recording site density for future generations of MEA designs.

Next, an adhesion layer of Titanium (Ti) was used to allow Pt adhere to the ceramic substrate. Ti (500 \AA thick) was sputtered onto the developed photoresist-covered-ceramic wafer. Following the adhesion layer, the active recording metal layer, Pt, for most of our work, was sputtered onto the substrate ($\sim 1.5 \mu\text{m}$ thick). Solvents were used to remove the developed photoresist and unwanted metals left on the recording pads, connecting lines, and connecting pads.

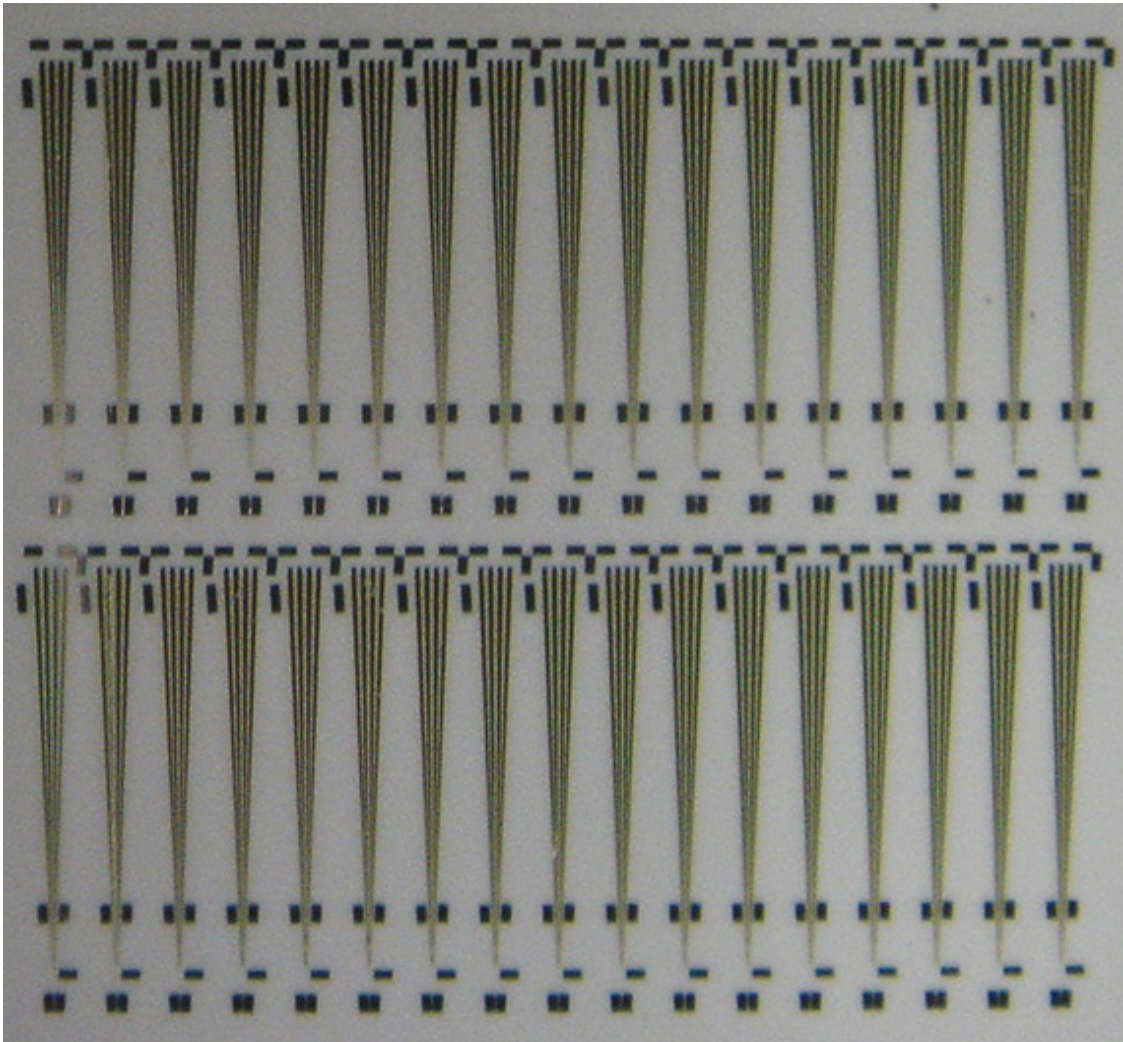


Figure 2.1: Ceramic Wafer

Photograph of a ceramic wafer containing 34 microelectrodes with Pt bonding pads, connecting lines and recording sites (not visible) were patterned onto the 2.5 cm x 2.5 cm, 125 μm thick substrate.

Once the Pt recording sites, connecting lines, and bonding pads were in place, the connecting lines were coated with an insulator using another photolithographic step. The connecting lines act as wires to connect the bonding pads to the recording sites and must be insulated from aqueous environments. To accomplish this, the MEAs were again coated with photoresist. A second photomask was used to define the areas where polyimide was placed. Polyimide acts as an insulator to define the recording site active area and the bonding pads as well as reducing the cross talk between the connecting lines. After the photoresist was developed, polyimide was spun onto the wafer (2-4 μm thick). Once the insulating layer was applied, only the recording sites and bonding pads were exposed. The photoresist and excess polyimide were removed and the remaining polyimide was cured at 200°C. The complete fabrication process is depicted in figure 2.2.

After the formation of the MEA on the ceramic wafer, a diamond saw was used to form or “cut out” the individual MEAs. A major advantage of the diamond saw was that it produced highly polished edges for reduced tissue damage during implantation. The ceramic wafer with Pt recording sites was attached to a printed circuit board (PCB) holder for easier handling and connection to recording equipment. To connect the ceramic wafer to the PCB holder, each bonding pad was wire bonded to an individual Pt recording site on the ceramic wafer. The tips were epoxied onto the paddle for stability and insulation of the wire bonds. Cutting and assembly was performed in conjunction with Hybrid Circuits, Inc., (Sunnyvale, CA). The PCB holder and fully constructed multisite MEA for anesthetized measurements are shown in figures 2.3A and 2.3B, respectively. Figure 2.3C is a version of the MEA for awake animal recordings.

Due to the flexibility of the fabrication process, our MEAs were manufactured with different recording site geometric configurations. An S2 MEA was used for both anesthetized and freely moving experiments. The ceramic tip of an S2 (figure 2.3D) has 4 Pt recording sites (333 μm X 15 μm) in a side-by-side configuration. This configuration allows for dual detection in a similar brain region.

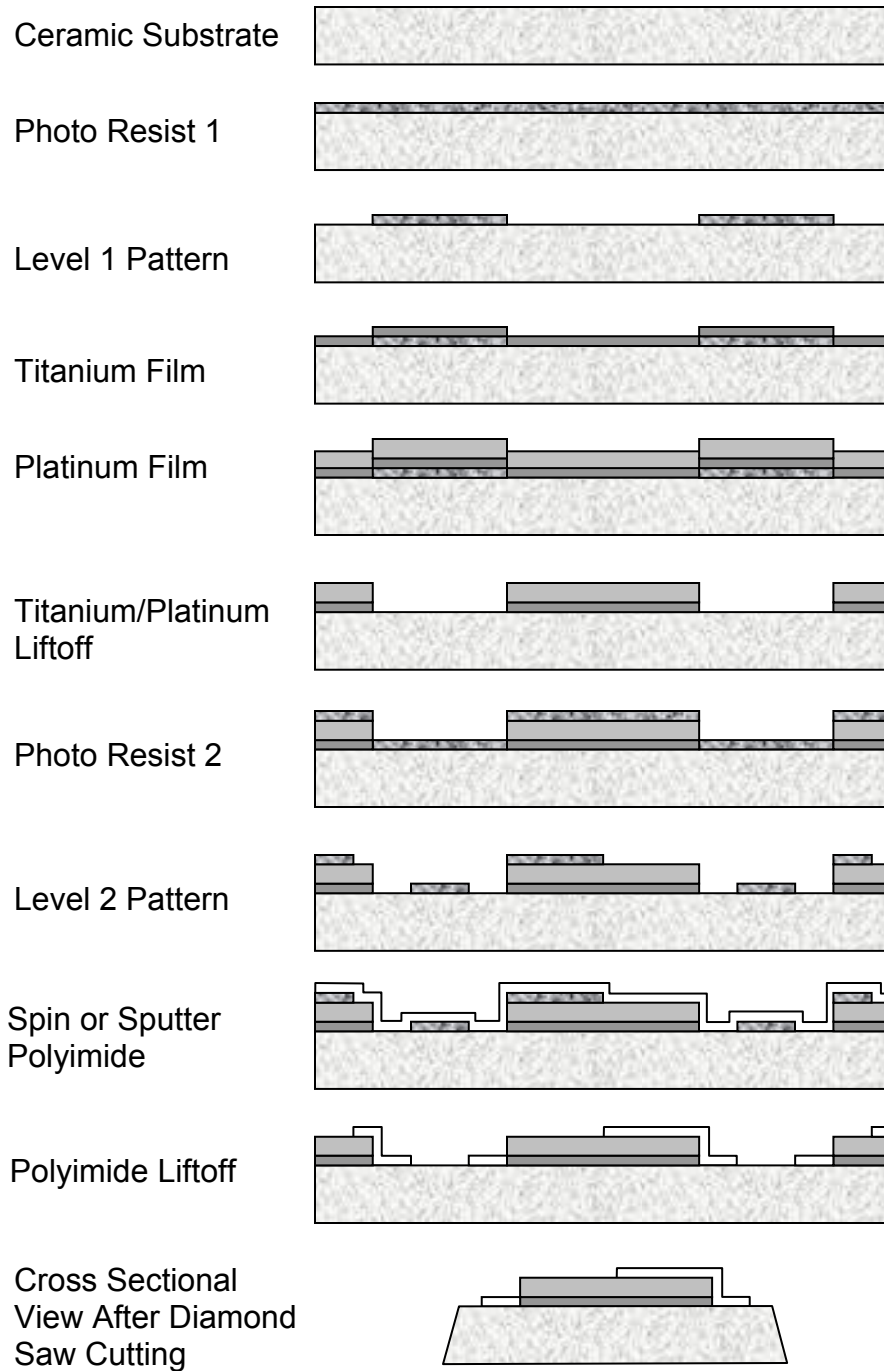


Figure 2.2: Microelectrode Array Fabrication Process

Schematic of the fabrication sequence for the ceramic wafers with Pt recording sites.

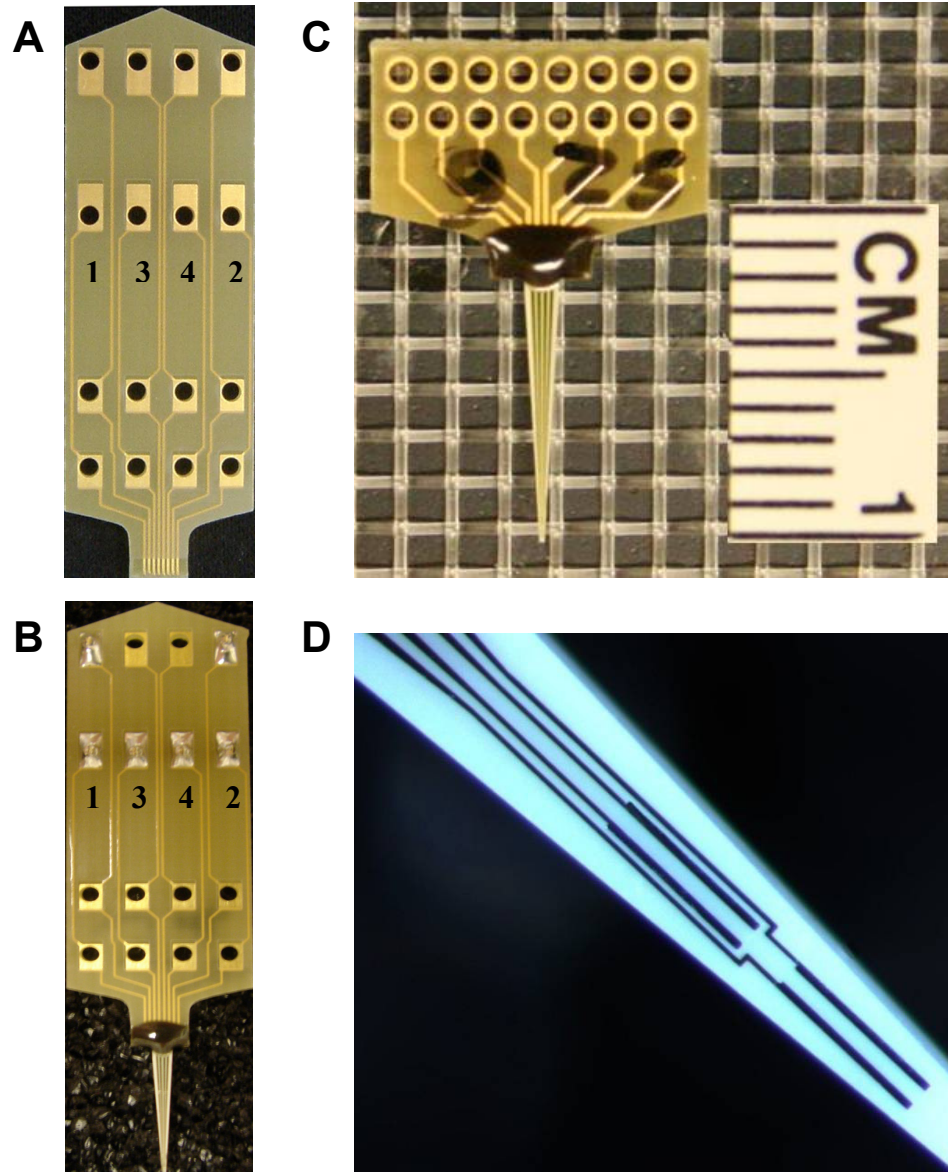


Figure 2.3: Microelectrode Array Photographs

Photograph of the MEA PCB with and without the attached ceramic tip. A.) Close-up view of the PCB. Numbers beneath the pin holes indicate the specific Pt recording site connection. B.) Fully assembled MEA. Black epoxy was used to insulate the wire bonding from the ceramic tip to the PCB as well as to provide stability. Pins were soldered into place for MEA attachment into a dual inline pin (DIP) socket. Pins placed in the upper left and right of the PCB provided added stability. C.) Fully assembled MEA for recordings in freely moving animals. D.) Photomicrograph of an S2 ceramic tip containing 4 Pt recording sites in a side-by-side configuration.

Potentiostat

Our headstage/potentiostat was referred to as the Fast Analytical Sensing Technology (FAST) 16 Mark II system (Quanteon L.L.C, Nicholasville, KY). The purpose of the potentiostat was to create a constant potential difference between the Ag/AgCl reference electrode and the MEA to force a non-spontaneous redox reaction to occur. The potentiostat held a constant potential at the reference electrode so that the applied potential at the working electrode was known. In other words, the potential applied at the working electrode was measured against the standard potential of the reference electrode. The FAST 16 Mark II system amplified and digitized the electrical current generated by oxidation or reduction reactions. For our Glu experiments, the amplification resulted in a gain scaling factor of 200 pA/V. Figure 2.4 shows an illustration of the flow of current through our FAST 16 Mark II recording system from a GluOx coated MEA.

Our Windows™ based FAST 16 Mark II system software created and recorded second-by-second (1 Hz), or faster data files. The software was written for eight simultaneous channel recordings, which could increase as the number of Pt recording sites increases in future generations of MEAs. The FAST 16 Mark II software displayed amperometric or chronoamperometric recordings at display rates of up to 40 Hz (nominal 1-10 Hz). Recorded files were exported to other Windows™ based applications, such as Excel™, for easier data processing; or processed directly through the data analysis software package on the FAST 16 Mark II system software. The low noise design and software oversampling allowed the FAST 16 Mark II recording system to be used for bench top experimentation without the need of a Faraday cage. However, greater performance was achieved with the use of a Faraday cage or appropriate shielding for most applications.

Microelectrode Array Cleaning Procedures

MEAs received from Hybrid Circuits underwent a cleaning procedure to remove any particulate matter or residue from the Pt recording sites that were deposited during the manufacturing process. New MEAs were placed into a

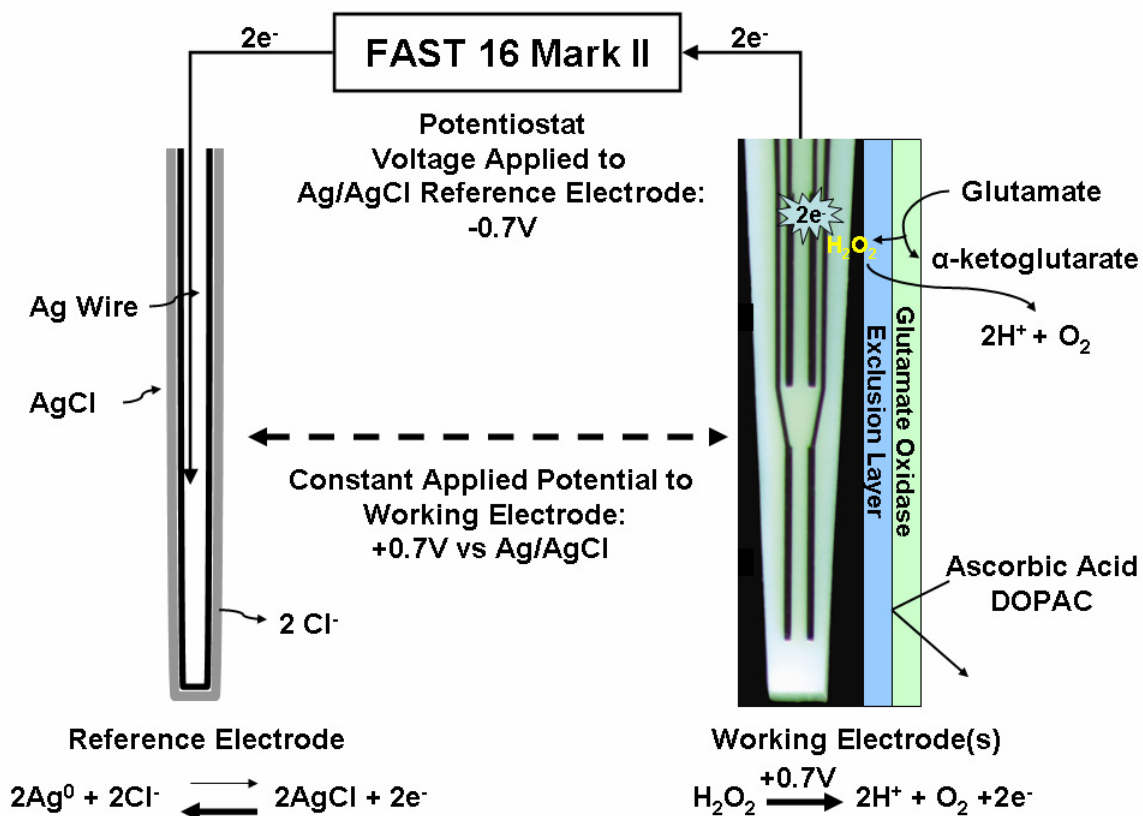


Figure 2.4: FAST 16 Mark II Potentiostat Diagram

The above diagram outlines the flow of electrons through our FAST 16 Mark II recording system. The potentiostat held a constant potential of -0.7 V to our Ag/AgCl reference electrode which created an applied potential of +0.7 V at our working electrode. In the case of an MEA coated with GluOx; when Glu came into contact with GluOx, it was metabolized into α -ketoglutarate and H_2O_2 . The H_2O_2 diffused through the exclusion layer that was used to repel interferences such as AA and DOPAC. When the H_2O_2 came into contact with a Pt recording surface at an applied potential of +0.7 V, it was oxidized and the transfer of two electrons to the Pt recording sites were detected on the recording system. To keep the reaction thermodynamically stable, the two electrons traveled to the Ag/AgCl reference electrode where two chloride ions were released. The half reactions are written beneath their respective reference and working electrodes.

stirred solution of Fisherbrand Citrisolv™ (Fisher Scientific, Catalog #22- 143-975) for five minutes followed by a five minute rinse in ddH₂O. After the chemical cleaning procedure, a thin film can develop on the Pt recording sites, so a Kimwipe® (Kimberly-Clark Professional) was delicately swiped across the tip of the MEAs to remove this film and any excess ddH₂O. MEAs were then dried for fifteen minutes in an oven at 105 – 115 °C prior to coating.

An advantage of these MEAs was the ability to reuse them for multiple experiments. Any applied enzyme layers (described below) need to be removed from the Pt recording surfaces. A slightly different cleaning procedure was employed for MEAs that were previously coated with an enzyme layer. The MEA tip was placed into a stirred solution of ddH₂O at 80°C to soften the protein matrix on the Pt recording sites. Following 30 minutes of soaking, the MEAs were cleaned as described in the preceding paragraph and tested for response to H₂O₂ to ensure good sensitivity of the Pt recording surfaces.

Exclusion Layers

Exclusion layer coatings were applied after successful cleaning of the MEAs and were used to alter their recording properties. Exclusion layers were applied to block or minimize undesirable electrochemically active compounds found in high concentrations in the CNS such as AA (250-500 μM) or DOPAC (25-40 μM). By blocking these undesired electrochemically active molecules from the Pt recording sites, the MEA had better selectivity for the analyte of interest. The planar geometry of the multisite MEAs often affected how materials adhered to the recording surfaces. Exclusion and enzyme layer coatings retarded compounds from diffusing to the MEA surface by creating a diffusion barrier, thus limiting the response time of the MEA. For this reason, coating parametrics were performed to determine optimal coating procedures for both exclusion layer and enzyme layer coatings.

Nafion[®] Exclusion Layer

Nafion[®], an anionic Teflon[®] derivative, is one of the most widely used methods for improving the selectivity of voltammetric recordings in CNS tissue. Historically, Nafion[®] is used on the surface of carbon fiber microelectrodes for the detection of catecholamines (Gerhardt *et al.*, 1984; Rice *et al.*, 1985; Rose *et al.*, 1985; Kuhr and Wightman, 1986; Rose *et al.*, 1986; Gerhardt and Hoffman, 2001). The negatively charged sulfonic acid groups substituted into the polymer matrix of Nafion[®] repelled anions from the Pt recording surfaces. If these anions were not blocked, they caused high background signals that interfered with reliable recordings. At the same time, the negatively charged sulfonic acid groups on Nafion[®] concentrated cationic species such as DA, NE and 5-HT. With the development of the multisite MEAs, Nafion[®] was a logical choice for an exclusion layer and was used reliably in our studies of Glu (Nickell, *et al.*, 2004; Day *et al.*, 2006; Nickell *et al.*, 2006; Rutherford *et al.*, 2007). However, since Nafion[®] attracted catecholamines to the Pt recording surface, which were oxidizable on Pt, other exclusion layers were used in CNS regions with high catecholamine levels except in the freely moving mouse studies. Only Nafion[®] coated MEAs were used for freely moving mouse studies due to its longevity *in vivo* compared to other exclusion layers.

Nafion[®] (5%, Sigma-Aldrich, Catalog #27,470-4) was aliquoted into a 1 mL brown glass vial. The MEA tip was then lowered half-way into the aliquot of Nafion[®] and then rotated in a circle five times lasting approximately one second per rotation. The tip was pulled straight out of the Nafion[®] solution. Next, MEAs were placed into an oven at 165-175°C for four minutes to allow the Nafion[®] layer to cure on the tip. In general, lower temperature curing produced thicker films compared to higher temperature curing (Gerhardt and Hoffman, 2001). Also, longer drying times at higher temperatures produced MEAs with lower responses to both AA and to analytes such as Glu. MEAs coated with excessive Nafion[®] showed little or no detectable response to electrochemically active molecules. MEAs not coated with enough Nafion[®] recorded high levels of background AA once inserted into the brain. After MEAs cured, they were allowed to cool to

room temperature for 30 minutes before enzyme coating. An important concept to remember was that once a prepared Nafion[®] coated MEA was placed into an aqueous solution (either a beaker or the brain) the tip must remain wet or at the very least, removed from solution for only a limited time. When Nafion[®] dried after soaking, it cracked allowing areas where interferents passed through and were oxidized on the Pt recording surfaces. If the Nafion[®] layer cracked, the MEA was no longer selective for the analyte being measured.

1,3-phenylenediamine

The organic molecule 1,3-phenylenediamine (mPD) was another chemical used to create an exclusion layer for Pt recording microelectrodes (Lowry *et al.*, 1998; McMahon and O'Neill, 2005; Kirwan *et al.*, 2007). A potential was applied to a solution of mPD causing mPD to electropolymerize on Pt recording surfaces. Historically, mPD or its derivate 1,2-phenylenediamine (oPD), was used on carbon fiber microelectrodes for selectivity and prevention of microelectrode fouling; a process where oxidizable molecules such as serotonin adhered to the carbon fiber surface thus preventing detection. Electropolymerized mPD selectivity was achieved by forming a size exclusion layer approximately 30 nm in thickness (Murphy, 1998; Kirwan *et al.*, 2007) that prevented larger molecules such as AA, DA, and DOPAC from reaching the recording surface. Smaller molecules, such as nitric oxide and H₂O₂, were still able to pass through the matrix (Friedeman *et al.*, 1996). Since H₂O₂ was a reporter molecule for oxidase enzymes, this made mPD an ideal exclusion layer for our enzyme-based multisite MEAs (Lowry *et al.*, 1998; Kirwan *et al.*, 2007).

The electropolymerizing procedure was completely different from Nafion[®] coating but had four distinct advantages. 1) The matrix formed by mPD blocked catecholamines such as DA, NE, and 5-HT from reaching the Pt recording sites. This helped make the MEA more selective for measuring the analyte of interest, Glu. 2) The mPD was electropolymerized onto the MEA after the MEA was coated with an enzyme layer. mPD electropolymerized through the enzyme layer and formed the matrix. Since mPD was electropolymerized after enzyme

coating, additional coatings of mPD could be applied to the MEA surface without cleaning the MEA. If the matrix degraded during an experiment, the MEA could be replated, recalibrated, and re-used to finish the experiment. 3) Because a potential must be applied for mPD coating, individual Pt recording sites could also be selectively coated with mPD. Removing the applied potential between a Pt recording site and the headstage prevented mPD from being electropolymerized onto that site. 4) Once mPD was successfully electropolymerized onto the Pt recording sites, the solution did not have to remain wet. Since mPD was hydrophilic (Murphy, 1998) our laboratory found that aqueous solutions slowly degraded the matrix over time, which made it unsuitable for chronic recordings in the freely moving mouse. The electropolymerization procedure is outlined below.

Our laboratory found that 1,3-phenylenediamine dihydrochloride, 99% (Sigma-Aldrich, Catalog# 235903-25g) worked best for electroplating and matrix formation on the Pt recording sites. First, a solution of 5 mM mPD was prepared in a degassed solution of 0.05 M phosphate buffered saline (PBS). Degassing was accomplished by bubbling nitrogen gas through the 0.05 M PBS solution for 20 minutes to remove oxygen before dissolving mPD. Once the 5 mM mPD was dissolved in the degassed 0.05 M PBS, the mPD solution was stored in a brown glass bottle to prevent oxidation from light. If the solution turned yellow, it had oxidized and did not electropolymerize on the MEA recording surface. Even with these storage methods, the 5 mM mPD solution oxidized after several hours so we recommended using the solution immediately. When the mPD solution was prepared, the MEA was connected to the FAST 16 Mark II recording system and approximately 40 mL of the 5 mM mPD was poured into a 50 mL beaker. The MEA tip was lowered half-way into the solution along with a glass, Ag/AgCl reference electrode (Bioanalytical Systems, Inc. RE-5B, Catalog #MF-2079). A fast-cyclic potential of +0.25 to +0.75 versus a Ag/AgCl reference electrode was applied for fifteen minutes to allow the mPD to electropolymerize onto the Pt recording sites. At fifteen minutes, the MEA tip was removed from the 5 mM

mPD solution, rinsed with ddH₂O, and stored at room temperature for 24 hours prior to calibration.

Enzyme Layer Coatings

Enzymes provided a means to convert a molecule that was not inherently electroactive, and thus not measurable, into a reporter molecule such as H₂O₂ that was oxidized at the Pt recording surfaces of the MEAs. The current measured from the oxidation of H₂O₂ generated during the enzymatic breakdown was directly proportional to the analyte concentration. Table 2.1 provides a list of available oxidase enzymes and their potential uses. Oxidase enzymes that our laboratory has used to measure neurochemicals are shown in **BOLD** and include L-glutamate oxidase (GluOx) (Burmeister and Gerhardt, 2001; Burmeister *et al.*, 2002; Pomerleau *et al.*, 2003; Nickell *et al.*, 2005; Day *et al.*, 2006; Rutherford *et al.*, 2007), choline oxidase (Burmeister *et al.*, 2004; Parikh *et al.*, 2005) L-lactate oxidase (Burmeister *et al.*, 2005) and L-glucose oxidase. Furthermore, acetylcholine esterase was used to measure acetylcholine (in conjunction with choline oxidase) and catalase was used to prevent H₂O₂ detection.

As previously mentioned, the O₂ dependence of oxidase enzyme-coated MEAs is also a concern. It is widely known that O₂ is required by the enzymes to measure the analyte, but a portion is returned to the tissue by the oxidation of H₂O₂ to O₂ and H⁺ at the MEA surfaces. In our experience oxidase enzyme-coated MEAs were relatively free from O₂ dependence over a useful range *in vivo* (Burmeister *et al.*, 2003), but certain applications, such as those during recordings of stroke episodes, require correction by use of an O₂ sensing microelectrode.

Immobilization of enzymes to the Pt recording surface helped stabilize the enzymes and made them active for longer periods of time. Our laboratory has immobilized several of the oxidase enzymes onto the Pt recording surfaces. While the general procedure remains the same for crosslinking the enzymes to the Pt recording sites, relative ratios of the enzyme to protein mixtures varies.

Table 2.1: Enzymes Capable of Producing a Reporter Molecule

<i>Enzyme</i>	<i>Substrate</i>	<i>Product</i>	<i>Measure</i>
Acetylcholinesterase	Acetylcholine	Choline, Acetic Acid	Choline with Choline oxidase
Alcohol oxidase	Alcohol, O₂	H₂O₂, Aldehyde	Alcohols
D-amino acid oxidase	D-amino acids, O ₂	H ₂ O ₂ , NH ₄ ⁺ , 2-oxo acid	D-amino acids
L-amino acid oxidase	L-amino acids, O ₂	H ₂ O ₂ , NH ₄ ⁺ , 2-oxo acid	L-amino acids
Ascorbate oxidase	Ascorbate, O₂	Dehydroascorbate	Remove Ascorbate
Aspartate oxidase	Aspartate, O ₂	H ₂ O ₂ , NH ₄ ⁺ Oxaloacetate	Aspartate
Catalase	H₂O₂	O₂	H₂O₂
Cholesterol esterase	Cholesteryl oleate, or other Cholesterol ester, Taurocholate	Cholesterol, Oleic acid, or other corresponding ketone	Cholesterol ester with Cholesterol oxidase
Cholesterol Oxidase	Cholesterol, O ₂	H ₂ O ₂ 4-cholesten-3-one	Cholesterol
Choline Oxidase	Choline, O₂	H₂O₂, Betaine	Choline
Galactose oxidase	D-galactose, O ₂	H ₂ O ₂ D-galacto-hexodialose	Galactose
Glucose oxidase	Glucose, O₂	H₂O₂, Gluconic Acid	Glucose
L-glutamate oxidase	L-glutamate, O₂	H₂O₂, α-ketoglutarate	L-glutamate
GABAase	GABA α-ketoglutarate	NADPH, H⁺ L-glutamate	GABA with L-glutamate oxidase
Glutaminase	Glutamine	NH ₄ ⁺ , L-glutamate	Glutamine with L-glutamate oxidase
Glycerol kinase	Glycerol, ATP	Glycerol-3-phosphate, ADP	Glycerol with Glycerol-3-phosphate oxidase

Table 2.1: (continued)

<i>Enzyme</i>	<i>Substrate</i>	<i>Product</i>	<i>Measure</i>
Glycerol-3-phosphate oxidase	Glycerol-3-phosphate, O ₂	H ₂ O ₂ Dihydroxyacetone phosphate	Glycerol
Hexokinase	ATP, Glucose	Glucose-6-phosphate, ADP	ATP with L-glutamate oxidase
Horseradish peroxidase	H ₂ O ₂	H ₂ O, O ₂	Use as mediator for H ₂ O ₂ detection
Lactate oxidase	Lactate, O₂	H₂O₂, Pyruvate	Lactate
Lysine oxidase	Lysine, O ₂	H ₂ O ₂ , NH ₄ ⁺ 6-amino-2-oxohexanoic acid	Lysine
Pyruvate oxidase	Pyruvate, O ₂ , Phosphate	H ₂ O ₂ , CO ₂ , acetyl phosphate	Pyruvate
Sarcosine oxidase	Sarcosine, O ₂	H ₂ O ₂ , Glycine, Formaldehyde	Sarcosine
Xanthine oxidase	Xanthine, O ₂	H ₂ O ₂ , Uric acid	Xanthine

This table shows oxidase enzymes that can be immobilized onto the Pt recording surface of our MEA. The enzymes that were used to measure analytes of interest by our laboratory are in **BOLD** lettering.

Our laboratory focuses on GluOx for the detection of Glu dynamics in the mammalian CNS whose immobilization procedure is outlined in detail below.

L-Glutamate Oxidase

GluOx was purified from a wheat bran culture of *Streptomyces* sp. X-119-6 and metabolized Glu with co-substrates O₂ and H₂O to form α -ketoglutarate, H₂O₂, and ammonia (Kusakabe *et al.*, 1984). The enzyme had maximal specificity at physiological pH (7.4) and temperature (37°C) (Kusakabe *et al.*, 1983). GluOx is specific for the L-enantiomer of Glu with a K_M value of 0.21 mM and shows no activity for D-Glutamate nor did this enantiomer block enzyme activity (Kusakabe *et al.*, 1983). L-aspartate was also oxidized, but to a lesser extent (0.6%) and had a considerably higher K_M value of 29 mM (Kusakabe *et al.*, 1983). Our laboratory has shown that local application of 200 μ M L-aspartate *in vivo* does not elicit a response on the MEA (Pomerleau *et al.*, 2003). In addition, salt solutions such as potassium chloride, sodium chloride, nor calcium chloride do not have an effect on the relative activity of the enzyme (Kusakabe *et al.*, 1983). This was further verified when local application of 0.9% physiological saline, did not elicit a response on the MEA (Pomerleau *et al.*, 2003).

L-Glutamate Oxidase Coating Procedure

A stock solution of GluOx (Associates of Cape Cod, Seikagaku America, Catalog #100645-1) was prepared by adding 50 μ l of ddH₂O to the lyophilized, purified enzyme in a vial to make a final concentration of 1 UI/ μ l. All proteins and enzymes were brought to room temperature and 0.010 g of bovine serum albumin (BSA) Fraction V, 99% (Sigma-Aldrich, Catalog #A-3059) was dissolved in a 1.5 mL microcentrifuge tube containing 985 μ l ddH₂O by manual agitation. Once dissolved, 5 μ l of glutaraldehyde (Glut) solution, Grade I, 25% (Sigma-Aldrich Catalog #G-6257) was added to the BSA mixture and manually mixed by inversion five times. The solution was then set aside for five minutes until it turned a faint yellow color. Glut crosslinked proteins that adhered to the MEA

surface when cured. The BSA served as a matrix to protect the oxidase enzyme activity during immobilization. Next, 9 μl of the BSA/Glut mixture was removed and added to a 300 μl microcentrifuge tube and to this 1 μl of the GluOx stock solution (1 U/ μl) was added and mixed by pipette agitation. This 10 μl solution had a final concentration of 1% BSA, 0.125% Glut, and approximately 1% GluOx. We have carried out an extensive series of parametric studies to determine this optimized stoichiometry for enzyme immobilization.

All enzymes were applied to the Pt recording sites by hand. Solutions were drawn up into a 10 μl Gastight[®] Hamilton microsyringe (Hamilton Co. Catalog #80065) and slowly dispensed to form a small droplet of solution at the tip of the microsyringe. Using a dissecting microscope (and a steady set of hands), the droplet was briefly applied to the Pt recording sites. The solution quickly dried, leaving behind a thin, translucent layer of enzyme that was visible underneath a dissecting microscope. Two additional coats of enzyme were applied in the same manner with one minute dry times in between each coat. This procedure was complete once a visible film remained following coating. The advantage of using multisite MEAs was that a pair of recording sites was coated with the enzyme mixture and the adjacent sites were coated with the inactive protein matrix (BSA and Glut) in the same manner as applying the enzyme mixture. Our laboratory referred to this technique as “self-referencing” (Burmeister and Gerhardt, 2002) and this approach had many advantages which are discussed in more detail in the section entitled ‘Self-Referencing.’

Once the enzyme and/or inactive protein matrix was applied, MEAs were stored at room temperature. Enzyme-coated MEAs must cure at room temperature for 48-72 hours prior to calibration and experimentation. Complete curing increased enzyme layer adhesion to the MEA surface. The enzyme/protein layers on “uncured MEAs” dissolved when placed in solution. A 48-72 hour curing time provided better sensitivity to Glu as well as increased the shelf-life of the MEAs. Optimal curing times varied depending on temperature, humidity, and enzyme. GluOx coated MEAs were optimal for at least three weeks..

Calibration

We often observed that the micro-fabricated MEAs have highly reproducible Pt recording surfaces. However, manufacturing procedures only investigated the geometric surface area of the MEAs. Since each Pt recording site on a MEA responded differently to H₂O₂ and therefore Glu, they must be calibrated *in vitro* prior to experimentation to determine standard curves. Thus, calibrations were used to equate a change in current from the oxidation of H₂O₂ to a proportional change in analyte concentration from the Glu generating the H₂O₂. A known concentration of analyte was added to 40 mL of 0.05 M PBS solution at 37°C to generate a current in picoamperes (pA) that was measured by the FAST 16 Mark II system. The FAST 16 Mark II system software recorded the current for each addition of analyte, created a calibration curve for each Pt recording site, and stored the slope (nA/μM) of this calibration. Also, known interferences such as AA were added during the calibration to test the selectivity of the recording sites to the analyte of interest versus interferences. When the experiment was performed, the calibration data was recalled and used to determine the concentration of analyte measured from the current during experiments *in vivo*.

Calibration Preparation

Nafion[®] coated MEA tips were soaked in a solution of 0.05 M PBS at 37°C for at least one hour prior to calibration. These MEAs can be placed in the PBS solution overnight for calibration the next morning. The soaking time allowed for better diffusion of analytes through the Nafion[®] layer as well as activation of the enzyme layer. The mPD coated MEAs, on the other hand, did not require long soaking times. The time period the MEA tip soaked in the calibration solution was sufficient for proper enzyme activation without additional soaking.

All stock solutions for Glu calibrations were prepared in ddH₂O and listed below:

- 1.) 20 mM AA (Ascorbic acid powder, Fisher Scientific, Catalog #A62)

- 2.) 20 mM L-glutamic acid sodium salt hydrate, minimum 99%
(Sigma-Aldrich, Catalog #G1626)
- 3.) 2 mM DA (3-Hydroxytyramine hydrochloride, Sigma-Aldrich,
Catalog #H-8502)
- 4.) 8.8 mM H₂O₂ (Rite Aid, 3% H₂O₂ Topical Solution)

Solutions were stored at 4°C. AA and H₂O₂ were made fresh daily since they oxidize in solution. Glu was made fresh on a weekly basis. DA was kept for a month providing the stock solution contained 0.01 M perchloric acid.

Calibration Procedure

Forty milliliters of 0.05 M PBS was measured out with a graduated cylinder and added to a 50 mL beaker. This beaker was placed in a recirculating water bath (Quanteon, L.L.C.) set at 37°C resting upon a battery operated, portable magnetic stir plate (Barnant Co., Model #700-0153). The calibration temperature was maintained at 37°C to activate GluOx for physiologically relevant temperatures. We used a battery operated stir plate to reduce potential AC (60 Hz) current that affected the recordings. A 10 x 3 mm stir bar was added to the 0.05 M PBS and the solution was slowly stirred to facilitate diffusion without forming a vortex in the solution. A glass Ag/AgCl reference electrode was placed in the buffer solution. Finally, the MEA tip was lowered halfway into the buffer solution.

After initial system settings were completed on the FAST 16 software, the FAST 16 Mark II recording system applied a potential of +0.7 V versus the Ag/AgCl reference to the MEA recording surfaces. Once calibration started, the current was allowed to reach a stable baseline (approximately 10-15 minutes, but occasionally longer). When a stable baseline was achieved, the baseline was marked. (When 'marking' a time point for an event, such as baseline, interferent, or analyte addition, was recorded by the FAST 16 Mark II software. A series of data points before the 'mark' were averaged and used in the calibration analysis). Next, 500 µl of 20 mM AA (interferent) was added for a final beaker concentration of 250 µM. When a new stable baseline was reached, the interferent was

marked. Next, three, 40 μl additions of 20 mM Glu were added for final buffer concentrations of 20, 40, and 60 μM Glu. Analyte marks were recorded after each addition to create the standard curve. After 3 additions of analyte, 40 μl of 2 mM DA (2 μM final beaker concentration) was added to the solution as a test substance and marked. Finally, 40 μl of 8.8 mM H_2O_2 (8.8 μM final beaker concentration) was added to the solution to confirm MEA sensitivity and the addition was marked. The test substances were used to check selectivity. The additions of test substances did not factor into calculating the standard curve for the analyte of interest. All chemicals used *in vivo* were tested *in vitro* to ensure that they were not electrochemically active on the Pt recording surface. It was important to know whether a chemical was electrochemically active *in vitro* prior to its local application near the Pt recording sites during experimentation. This guaranteed that *in vitro* or *in vivo* analyte concentration changes were from the analyte of interest rather than due to local application of drugs. Upon completion of the calibration, the program was stopped, the data were saved, and the MEA tip was removed from the buffer solution and stored appropriately. Nafion[®] coated MEAs were placed in 0.05 M PBS while mPD electroplated MEAs were kept dry. Graphs of typical self-referencing Glu calibrations with either Nafion[®] or mPD applied as exclusion layers are shown in figures 2.5A and 2.5B, respectively.

Microelectrode Array Calibration Criteria

During calibration, the FAST 16 Mark II recording software automatically calculated selectivity ratios for Glu over AA as well as the slope (MEA sensitivity for Glu), limit of detection (LOD), and linearity (R^2). What do all these numbers mean and how did one know if they have a satisfactory Glu MEA? A poor R^2 was rarely seen with good MEAs. Since the MEA fabrication procedure was highly reproducible, we have found that Glu responses were extremely linear and often resulted in linear regression curve fits with $R^2 \geq 0.99$.

Slope or sensitivity of the MEA referred to how well the MEA measured the change in Glu concentration. The number was used to equate a change

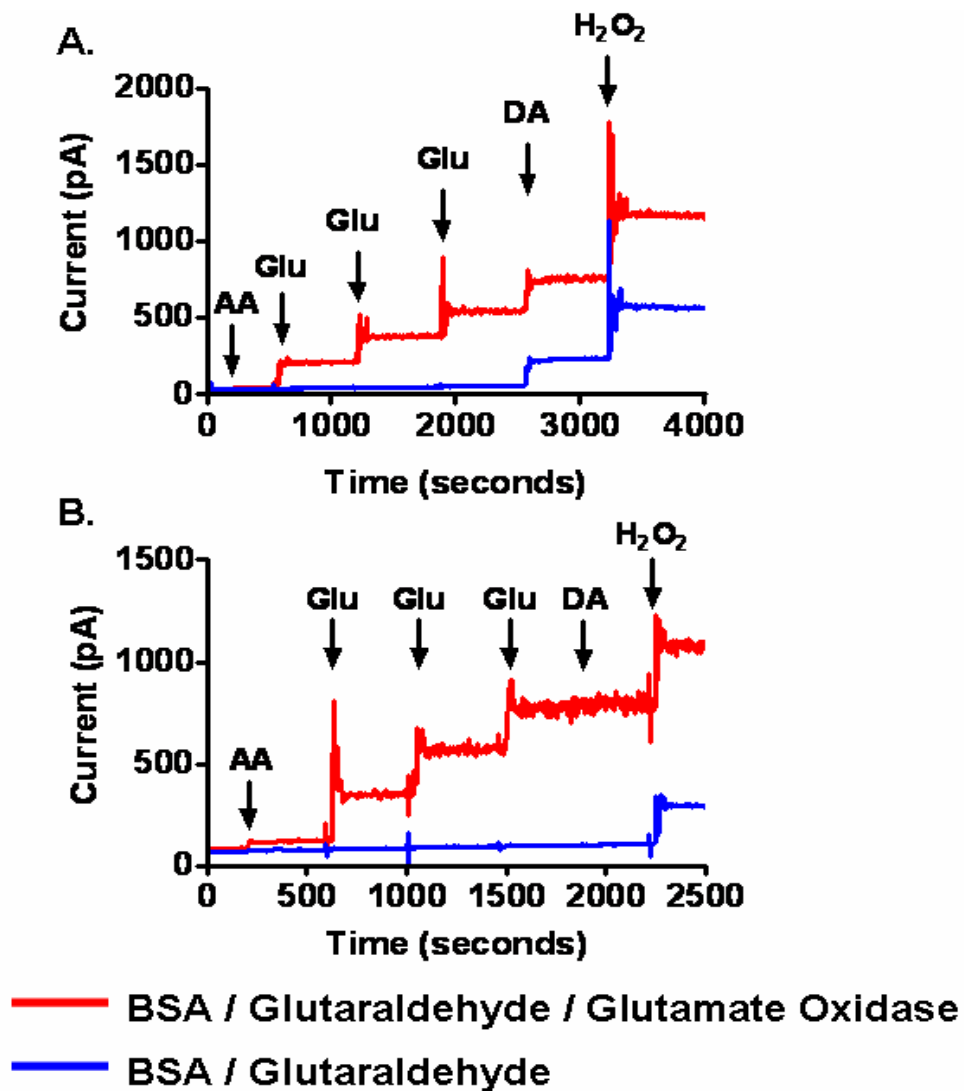


Figure 2.5: Calibration Results From Nafion[®] and mPD Coated MEAs

A) The calibration of a Nafion[®] coated Glu self-referencing MEA. During calibration, solutions were added to determine each recording site's sensitivity to Glu, selectivity for Glu over AA, lowest LOD, and responsiveness to other electroactive molecules (e.g. DA and H₂O₂). The enzyme-coated Glu recording site responded well to Glu and some electroactive molecules. The enzyme-free sentinel site did not respond to Glu but showed similar responses to the same electroactive molecules. Final concentrations of each addition: 250 μM AA, 20, 40, and 60 μM Glu, 2 μM DA, and 8.8 μM H₂O₂. B.) Calibration of an mPD coated Glu self-referencing MEA. All calibration concentrations were the same as previously described. Note how mPD excluded the DA response on both the GluOx and sentinel recording sites.

in current to a change in Glu concentration. The slope was also used to calculate LODs, which were the most important criteria for determining if a MEA was satisfactory for use. We use LODs to select MEAs because slopes were misleading. LOD was defined as the analyte concentration that yielded an MEA response that was equivalent to 3 times the background noise of the recording system. This was a conservative calculation of the lowest detectable change in analyte concentration that was not attributed to noise. Our MEA LODs range from 0.2 to 1.0 μM , depending on the recording enzyme composition and stability of the sites. Typically, for *in vivo* experiments MEAs with LODs $\leq 1 \mu\text{M}$ were used since this was smaller than the response expected.

Selectivity referred to the ratio of the MEAs sensitivity to Glu over the sensitivity to interferents such as AA. It was calculated by dividing the Glu slope by the AA slope. A MEA with a selectivity of 100:1 meant that a 100 μM concentration increase of AA resulted in an apparent 1 μM concentration increase in Glu. With a selectivity of 100:1, the MEA was 99% effective at blocking AA. Selectivity ratios of 100:1 or greater were ideal, but selectivity ratios of 20:1 were used and effective at blocking interferents since this ratio was not a linear correlation. In other words, a MEA with a selectivity of 50:1 was blocking approximately 98% of the AA while a MEA with a selectivity of 20:1 was still blocking approximately 95% of the AA signal.

Glass Micropipettes

After calibrations were completed, a glass micropipette was attached to the PCB holder so the tip of the glass micropipette rested among the 4 Pt recording sites. Through this glass micropipette, drug solutions were locally applied for pharmacological manipulations of the CNS. We used a vertical pipette puller (David Kopf Instruments, Model 700C, Catalog #730) to prepare single barrel (1 mm o.d., 0.58 mm i.d., A-M Systems, Inc., Catalog #601500) glass micropipettes. Using an upright stereomicroscope, the tip of the micropipette was bumped against a glass stir rod to create an internal diameter of 12-15 μm . Next, modeling clay was attached to the PCB holder. The glass

micropipette was attached to the modeling clay (used to hold the glass micropipette steady while it was positioned among the recording sites). Once the glass micropipette was properly positioned, it was held more firmly in place by applying melted Sticky Wax (Kerr Corporation, Catalog #00625) onto the PCB between the ceramic wafer and the modeling clay. The drying of the Sticky Wax repositioned the glass micropipette relative to its placement amongst and above the Pt recording sites. If necessary, the tip of a spatula was heated to help remodel the Sticky Wax and thus reposition the glass micropipette. Figure 2.6A shows a glass micropipette attached to the PCB with modeling clay and Sticky Wax. Figure 2.6B shows the tip of a glass micropipette positioned among the recording sites for an S2 MEA. The tip of the glass micropipette did not touch the ceramic surface. Rather it was positioned between 50-100 microns above the Pt recording sites (as shown in figure 2.6C). This distance allowed an optimal amount of CNS tissue between the glass micropipette and MEA when it was lowered into the brain. If the MEA was too close to the Pt recording sites, pressure ejection of fluid caused a dilution artifact *in vivo* (an actual decrease in analyte concentration due to the introduction of exogenous fluid in the area of the Pt recording site). If positioned too far, the rapid diffusion and uptake of Glu into glia limited its diffusion to the Pt recording sites on the MEA surface. For proper positioning of the glass micropipette among the Pt recording sites, the MEA was viewed at two angles underneath a dissecting microscope.

The glass micropipette was filled with solution using a 30-gauge, four inch long hypodermic needle (Popper and Sons, Inc., Standard Female Luer Hub, Catalog #7400). Glass micropipettes were always filled prior to implantation. First, drug solutions were drawn into a 1 mL tuberculin tip syringe (Beckton-Dickinson, and Co., Catalog #309602), which was then attached to the intake end of a μ Star 0.22 μ m sterile filter (Costar Corp, Catalog #8110). The other end of the filter attached to a 30-gauge, four inch long, hypodermic needle. The solution was dispensed through the filter and ultimately through the hypodermic

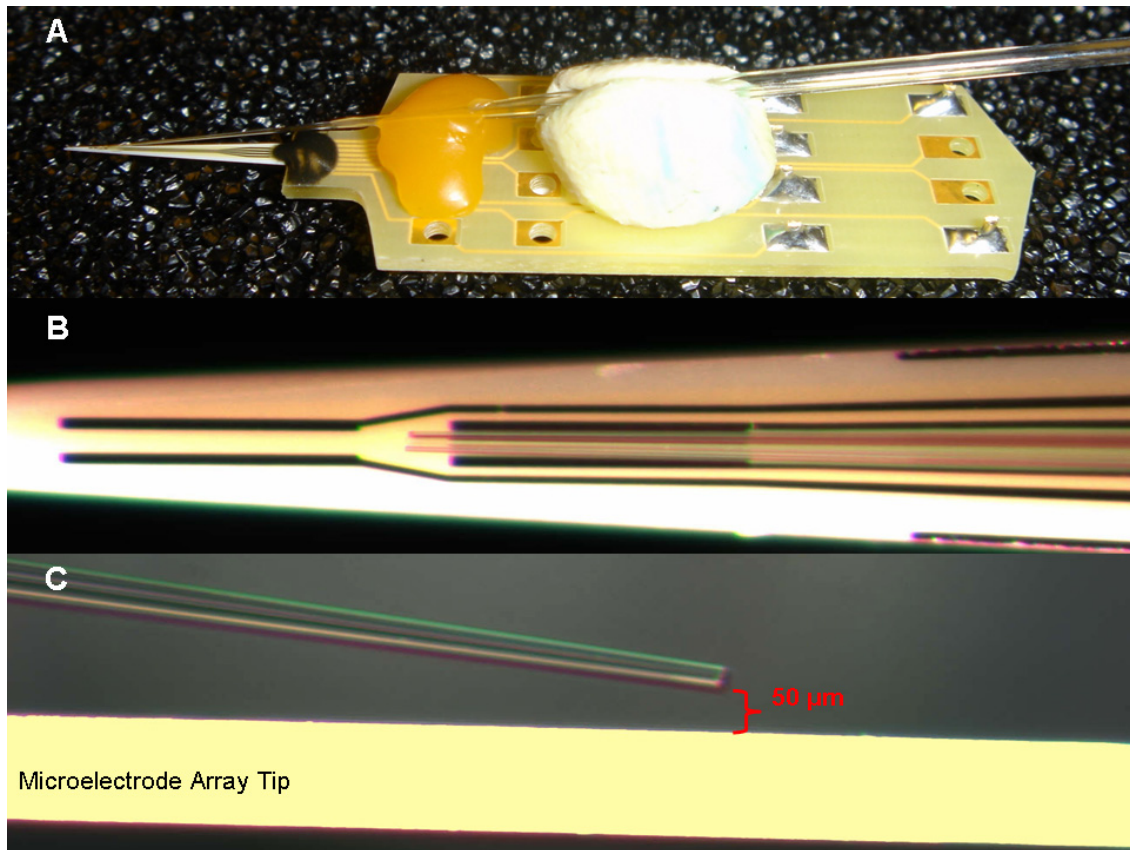


Figure 2.6: Positioning of the Glass Micropipette

Photographs of a glass micropipette attached to a multisite MEA. A.) Photograph of the glass micropipette held in place with modeling clay and Sticky Wax. B.) Photomicrograph of a glass micropipette tip positioned among the four Pt recording sites on an S2 MEA. C.) Side view photomicrograph of the glass micropipette tip held approximately 50 μm above the MEA tip.

needle. The needle was inserted into the glass micropipette and filled from the pulled tip up to the open end without creating air bubbles within the glass micropipette. Air bubbles prevented effective delivery of drugs by pressure ejection and made it difficult to determine the volume of fluid dispensed. Solutions were normally pressure ejected prior to MEA implantation into the brain to determine that there was a smooth fluid flow out of the glass micropipette. Solutions were removed from a glass micropipette by inserting the 30-gauge filling needle with an attached tuberculin syringe to draw up the solution.

Ag/AgCl Reference Electrode

While larger glass Ag/AgCl reference electrodes were suitable for mPD electropolymerization and MEA calibration, this reference electrode was too large for many biological applications. For this reason, a smaller Ag/AgCl reference electrode was made at the start of every experiment. Miniature Ag/AgCl reference electrodes were prepared by first stripping 0.25 inch of the Teflon[®] coating from each end of a silver wire (0.008 inch bare, 0.011 inch coated; A-M Systems, Inc., Catalog #786500). One of the stripped ends was soldered to a wire crimp pin (Mill-Max Mfg. Corp., Part #3603) for connection to the FAST 16 Mark II headstage. The other end was placed into a solution of 1 M HCl saturated with NaCl. A Pt wire acted as the counter electrode and was also placed into the solution. Our laboratory used a regulated power supply (Elenco Precision, Model XP-620) that outputs 9 V. However, DC adapters ranging from 1.5 V to 9 V were acceptable. The negative lead was attached to the Pt counter electrode while the positive lead was connected to the Ag wire. With both wires in solution, the applied potential attracts Cl⁻ on the wire to form AgCl thus making the Ag/AgCl reference. The plating potential was applied for approximately 10-15 minutes. When properly connected, bubbles formed around the Pt counter electrode. These miniature Ag/AgCl references were soaked in 3M NaCl prior to use *in vivo*.

MEA Preparation for Awake, Freely Moving Mice

Refer to Rutherford *et al.*, 2007 for a complete description on preparing MEAs for chronic recordings. For our awake, freely moving recordings, we used a smaller, lighter weight MEA, which is shown in figure 2.3C. Microelectrode connecting wires were prepared by first stripping both ends of 30 American Wire Gauge (AWG) varnished copper wire (RadioShack). One end of the copper connecting wire was soldered to a pin-hole on the row closest to the MEA tip. Four copper wires were soldered to the PCB, each corresponding to one of the Pt recording sites. Once all wires were soldered, the MEA tip was coated with five minute epoxy, which protected the MEA connection from potential water or other liquid damage during the remaining portion of the procedure. The MEA tip was coated with Nafion[®] (we found this exclusion layer worked longer for chronic implantations compared to mPD) and enzyme and inactive protein matrix solutions as previously described. The enzyme and inactive protein matrix solutions were allowed to cure for 48-72 hours before the MEA modifications were completed.

Once the enzyme cured, a gold-plated socket (Ginder Scientific Part #220-S02) was attached to the other end of the copper wire (figure 2.7A). Also, a miniature Ag/AgCl reference was prepared and attached to a gold socket. The gold sockets of the reference and MEA wires were inserted into a miniature, black connector (Ginder Scientific, 9-pin ABS Plug, Part #GS09PLG-220). Pliers were used to push the gold sockets into the connector so that the gold sockets were flush with the miniature, black connector. The copper wires were wrapped around the connector and the MEA tip was positioned parallel to the connector. Correct positioning of the MEA tip was essential for accurate stereotaxic placement into the brain. Five minute epoxy was used to secure the MEA and wires, making sure that all wires were covered with epoxy. The solder contacts on the gold sockets were also covered with epoxy to ensure that moisture did not penetrate the connector and disrupt the recording (figure 2.7B).

Similar to anesthetized experiments, drugs were locally applied close to the Pt recording sites for pharmacological studies in freely moving mice. Instead

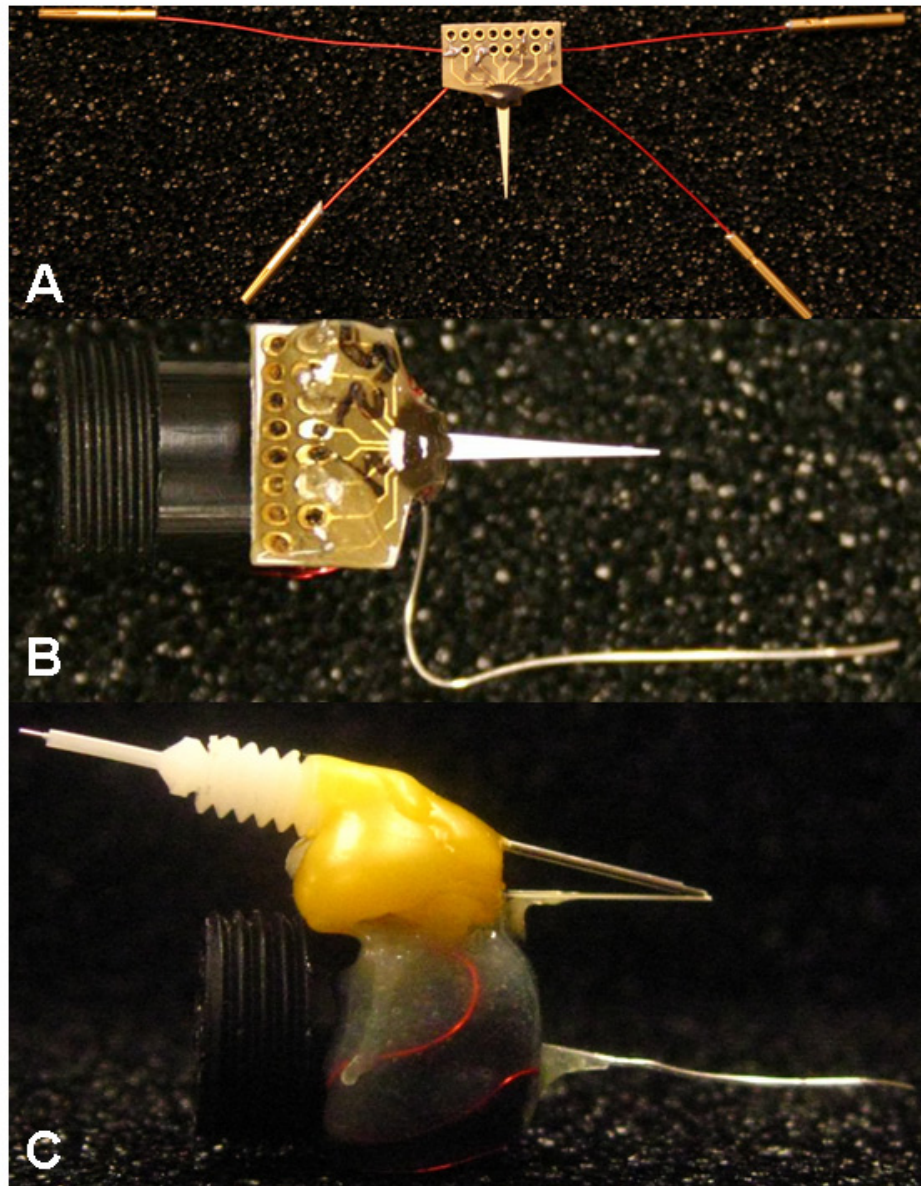


Figure 2.7: Awake, Freely Moving MEA Preparation

Photographs of the assembly process for the awake, freely moving MEAs. A.) Four copper wires were soldered to the MEA (one for each Pt recording site). Gold sockets were soldered to the other end of each copper wire. B.) The gold sockets were inserted into a black connector along with a miniature Ag/AgCl reference wire. The MEA was positioned parallel to the black connector and was held in place using five minute epoxy. C.) A fully assembled MEA with attached guide cannula was held in place with Sticky Wax. The guide cannula was held in place so an internal cannula was positioned among the four Pt recording sites.

of a glass micropipette, a 26-gauge stainless steel guide cannula (Plastics One Inc., C315G Cannula Guide 26GA 38172, PO: 052604AA, SO: 41123-1) was centered among the recording sites with sticky wax similar to the glass micropipette as previously described. A 33 gauge stainless steel internal acute cannula (Plastics One Inc., C315IA Cannula Internal Acute, PO: 121409, SO: 45203-1), slightly longer than the guide, was inserted into the guide cannula. The internal acute cannula tip was positioned among the four Pt recording sites of the MEA at a distance of approximately 70 μm above the MEA tip. To prevent clogging of the guide cannula, a stainless steel dummy cannula (Plastics One Inc., C315DC Cannula dummy, PO: 121409, SO: 45203-3) remained in the guide cannula at all times, and was only removed when solutions were locally applied through the internal acute cannula. An assembled MEA with attached guide cannula is shown in figure 2.7C.

Freely Moving Recording Apparatus

The recording headstage was slightly different from those used for *in vitro* and *in vivo* anesthetized animal recordings. This headstage screwed directly onto the mouse MEA assembly connecting the chronically implanted MEA to the FAST 16 Mark II recording system. The headstage consisted of a miniature connector with five connector pins (one connecting each of the four channels and one for the Ag/AgCl reference electrode). The connector pins led to the four channel mini-amplifier, which was positioned as close as possible to the animal in order to minimize noise artifacts. Shielded connecting wire, led to an electrical swivel (Airflyte Electronics Co., P/N 1001460-012) at the top of the recording chamber. The headstage was connected at the top center of the recording apparatus to the electrical swivel (commutator) that contained twelve electrical contacts. The commutator allowed the animal to move freely to all areas of the behavior chamber. Figure 2.8 diagrams the equipment used for freely moving recordings.

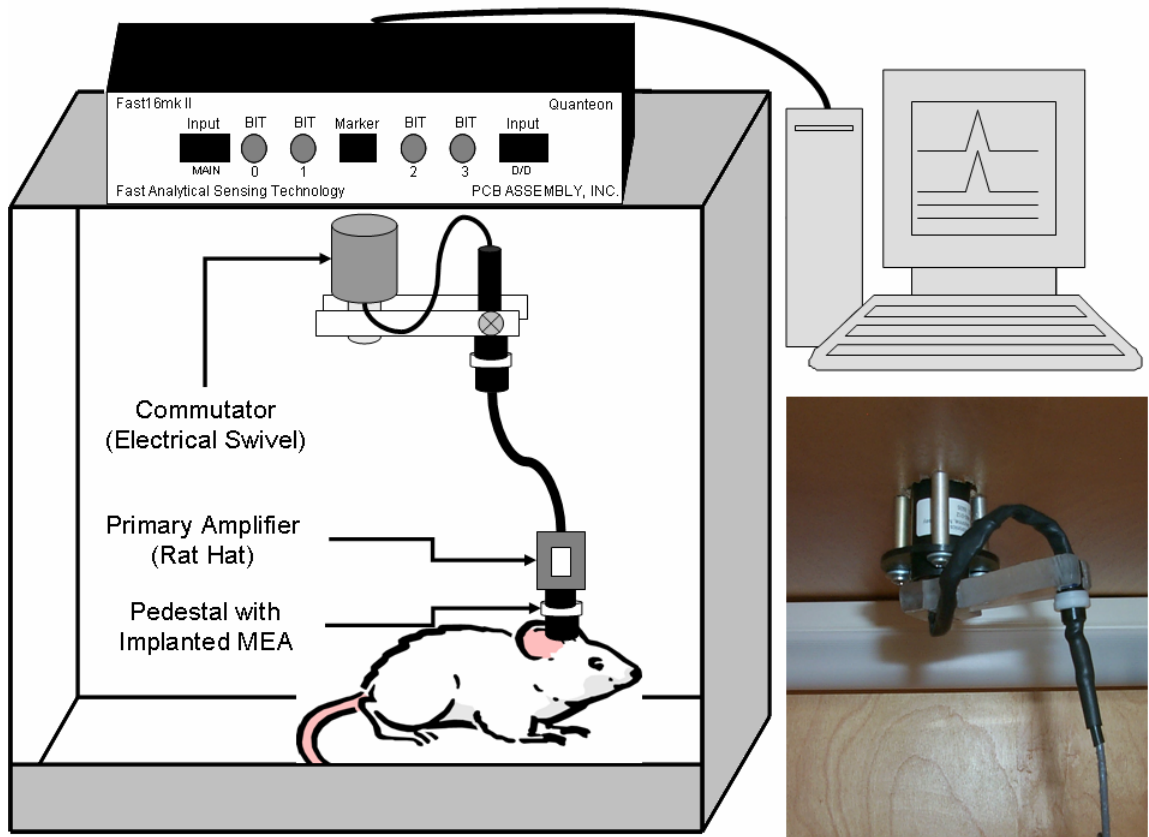


Figure 2.8: Diagram of the Freely Moving Recording Chamber

This diagram shows a mouse connected to the FAST 16 Mark II recording system for awake, freely moving recordings. Briefly, once a mouse was introduced into the recording chamber it was connected to the primary amplifier, which attached to the electrical swivel allowing the mouse to move to all areas of the recording chamber. The electrical swivel was connected to the FAST 16 Mark II recording system where the signal was amplified and digitized on a PC workstation. The bottom right inset is a photograph of the electrical swivel mounted to the top of the recording chamber.

Chronic Implantation Procedure

For chronic implantation surgeries, mice were anesthetized with isoflurane and placed in a stereotaxic apparatus fitted with a mouse adapter (David Kopf Instruments, Model 926) and mouse anesthesia mask (David Kopf Instruments, Model 907). A constant flow of isoflurane was maintained using a SurgiVet Tec 4 Vaporizer. Mouse body temperature was maintained with an isothermal heating pad at 37°C. The mouse's eyes were coated with artificial tears (www.medi-vet.com, Catalog #11970) to help maintain fluid and prevent infection. All surgeries were performed in a Vertical Laminar Flow Workstation, (Microzone Corp., VLF-2-4) with a High Efficiency Particulate Air (HEPA) filter. Prior to incision, excess fur on the head was shaved and the skin directly on top of the mouse's head (between the ears and from just behind the eyes to the neck) was wiped with a proviodine solution to keep the incision area clean and prevent infection. The skin on top of the head was reflected, making as small an incision as necessary. The mouse underwent a craniotomy to remove a 2 mm x 2 mm portion of the skull for MEA implantation. Additionally, three small holes (<0.5 mm) were drilled in the skull with a Dremel[®] engraving cutting bit (#105) for placement of the reference electrode and two stainless steel skull screws (Small Parts Inc., Part #MPX-080-02-M) that helped hold the assembly in place. Similar to the anesthetized studies, a Ag/AgCl reference electrode was implanted remotely from the recording site. For our freely moving mouse experiments, MEAs were lowered into either the right PFC (AP: +1.5, ML: 0.3; DV: -2.4 vs bregma) or right Str (AP: +0.9, ML: 1.5, DV: -3.85 vs bregma) according to the atlas of Paxinos and Franklin (2004). Figure 2.9 shows a diagram of the mouse skull with skull screws, Ag/AgCl reference wire, and MEA placement. The assembly was secured with approximately four layers of Ortho-Jet Powder (Lang Dental Manufacturing Co., Inc. REF-1330) mixed with Jet Acrylic Liquid, (Lang Dental Manufacturing Co., Inc., REF-1406), which the skull screws help anchor in place. The dental acrylic covered as much of the MEA PCB holder as possible, without adhering to the threads of the cannula or the MEA connector. The dental

Anterior

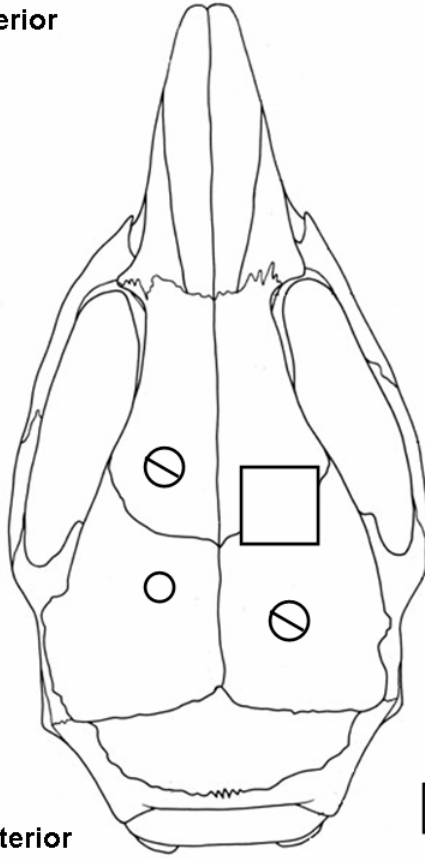


Photo Adapted from
*The Anatomy of the
Laboratory Mouse*
Margaret J. Cook

- ⊗ Skull Screw
- Ag/AgCl Reference
- MEA Implant Site

Posterior

Figure 2.9: MEA Implantation Surgery

The above figure shows an overhead view of the mouse skull and the placement of the skull screws, Ag/AgCl reference wire, and MEA implantation site.

acrylic had a smooth texture to prevent the rodent from scratching the implanted MEA. Following surgery, mice were placed on a heating pad to help maintain body temperature until they recovered from the anesthesia. Three subcutaneous injections, totaling 1 mL of Ringer's Solution, Mammal (Fisher Scientific, Catalog #S77939) were administered subcutaneously immediately following surgery. Mice were given three days to recover prior to the start of a recording session.

On experiment days, the mouse was allowed to explore the behavior chamber for 15-20 minutes before being connected to the FAST 16 Mark II recording system. Usually, the first day of recordings involved local application of an isotonic solution of 1 mM Glu (pH ~ 7.4) to determine the MEA response before behavioral or pharmacological studies were conducted. Ejected solutions were filtered and then delivered into the internal guide cannula with the aid of 28-gauge tubing (Small Parts Inc.) fitted over a 10 μ l Hamilton microsyringe. The Hamilton syringe was inserted into a repeating dispenser (Hamilton, Co; PB600-1) to provide accurate volume ejections of locally-applied chemicals. The microsyringe with repeating dispenser was placed on top of the recording chamber while the tubing was lowered through the hole drilled out for the commutator into the recording chamber. The dummy cannula was removed and the fluid cannula was inserted in its place. The animals were not restrained to insert the cannula as restraining the mouse altered behavioral studies by stressing the rodent.

Self-Referencing

An advantage of photolithographic fabrication of MEA designs was the precise control of the layout of the MEAs allowing for multiple recording sites geometrically configured in a small area. Multiple recording sites on a single MEA were used to remove chemical interferents that contributed to a portion of the analyte signal (Burmeister and Gerhardt, 2001). Our laboratory referred to this principle as 'self-referencing' and it was commonly used in our data analysis. As mentioned in the coating section, the GluOx was applied to a pair of Pt recording sites while the chemically inactive protein matrix (BSA and Glut) was

applied to the adjacent pair of recording sites referred to as 'sentinel sites'. A schematic of the coating procedure with either Nafion[®] or mPD is shown in figure 2.10.

The GluOx coated Pt recording sites detected extracellular Glu concentrations (the analyte) in addition to molecules that the inactive protein matrix coated recording sites detected (interferents). These additional molecules detected, included interferents such as AA and DOPAC as well as other neurotransmitters such as DA, NE, 5-HT. (Refer to figures 2.5A and 2.5B that show a typical Glu self-referencing calibration where the GluOx coated sites responded to Glu while the inactive protein matrix coated sites did not.)

The purpose of the inactive protein matrix on the self-referencing, or sentinel sites, was to make the response times of the sentinel sites similar to the GluOx recording sites. As mentioned earlier, protein coats altered the diffusional properties of molecules to the Pt recording surfaces. Without this inactive protein matrix layer, the sentinel sites would respond faster to interferents than the GluOx coated sites. Protein layers on both pairs of Pt recordings sites were necessary to minimize differences between the temporal recording properties of the different MEA surfaces. Ideally, the sentinel vs. analyte recording sites should be positioned side-by-side. However, our current, manual enzyme coating procedures precluded this arrangement.

Experimentally, self-referencing recordings were beneficial for providing qualitative as well as quantitative assessment of the analyte of interest. During an experiment, the FAST 16 Mark II recording software allowed the user to simultaneously view changes in Glu concentration for all four recording sites. If a peak was seen on the GluOx coated sites, but not the inactive protein matrix coated sites, this provided a good qualitative assessment that Glu was being measured. Figure 2.11 shows a screen capture of a Glu self-referencing MEA during an *in vivo* experiment.

Quantitatively, the self-referencing method was even more powerful. Since some of the response on the GluOx coated sites was attributed to

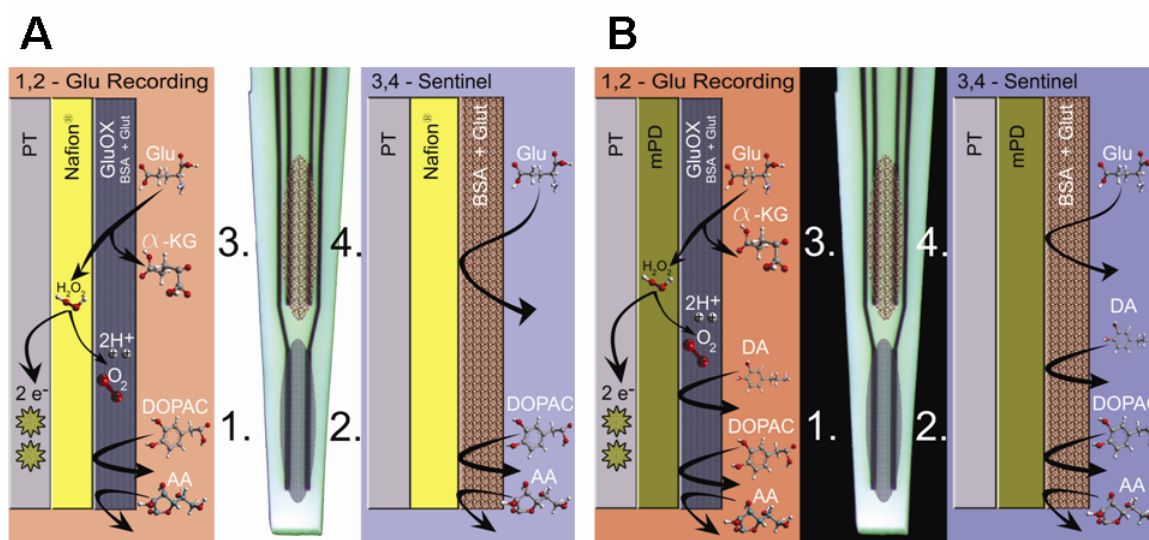


Figure 2.10: Nafion® and mPD Self-Referencing MEA Schematic

Schematics and photomicrographs of an S2, Nafion® coated (A) and mPD coated (B), self-referencing, Glu selective MEA. The left side of each schematic shows the bottom pair of Pt recording sites coated with GluOx, BSA, and Glut. The Glu that came into contact with the GluOx was converted to α -ketoglutarate and H_2O_2 . The H_2O_2 readily diffused through the Nafion® or mPD layer that blocked anionic substances such as AA and DOPAC. When the H_2O_2 came into contact with the Pt recording sites at a potential of +0.7 V versus a Ag/AgCl reference, the H_2O_2 was oxidized and the resulting two electrons were transferred to the Pt recording site and the change in current was measured by the FAST 16 Mark II system. The right side of each schematic shows the top pair of Pt recording sites coated with the inactive protein matrix of BSA and Glut, also referred to as the sentinel sites. Since no GluOx was coated onto this pair of recording sites, Glu was not converted to a reporter molecule and thus was not measured on the Pt recording sites. Once again, the Nafion® or mPD acts on these sites based on charge or size exclusion, respectively.

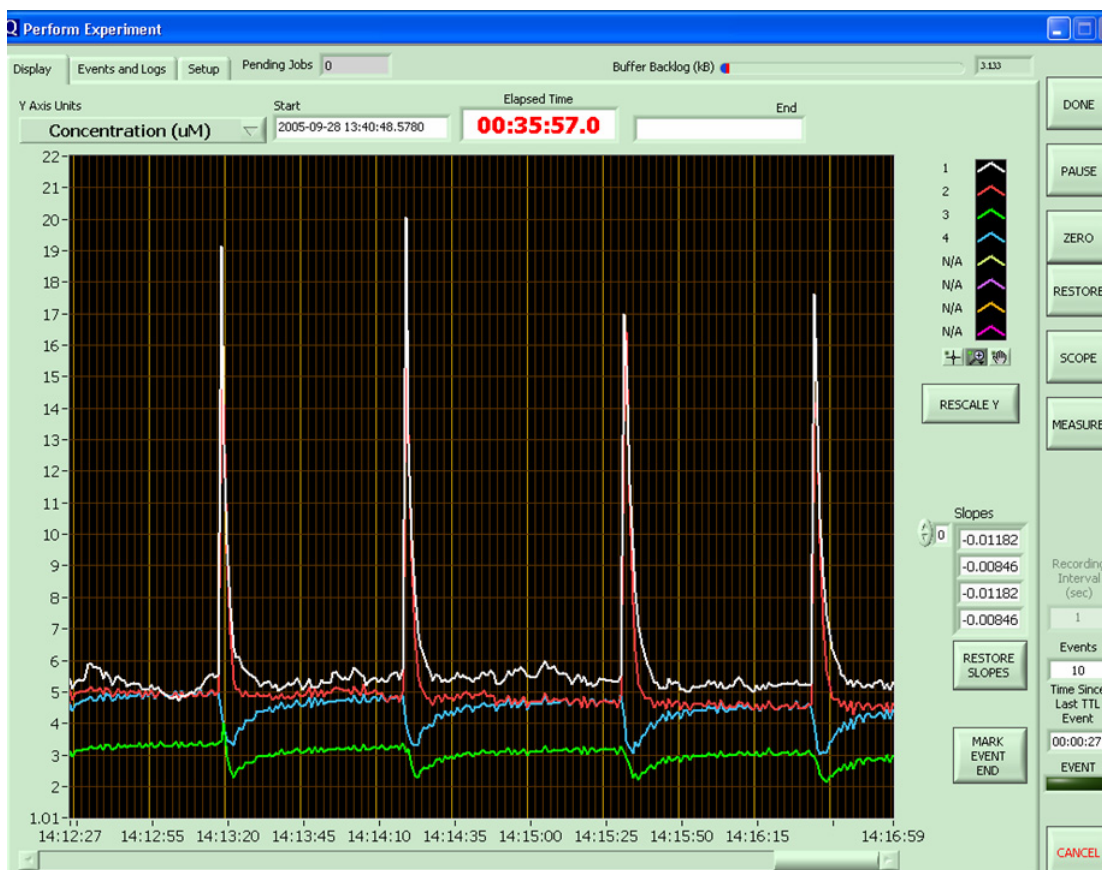


Figure 2.11: Screen Capture of an *In Vivo* Glu Response on a Self-Referencing MEA

Screen capture of the FAST-16 Mark II system with a self-referencing Glu MEA. Stimulus-evoked (70 mM KCl) Glu release was measured in the motor cortex of a rhesus monkey. Each colored line corresponds to a different Pt recording site (1=white, 2=red, 3=green, 4=blue). Sites 1 and 2 are coated with GluOx and show a rapid, robust increase in extracellular Glu compared to the two sentinel recording sites (Sites 3 and 4).

interferents, the sentinel sites were used to record the interferents contributing to the Glu response. If the recording sites' measure of Faradaic responses to DA and H₂O₂ are close (<10%) during calibration, the raw current data collected for a sentinel recording site was subtracted from the raw current obtained from the GluOx coated sites. This new raw current, once divided by the slope of the corresponding GluOx recording site, provided the adjusted concentration of Glu that was free of interferents. This unique feature of our MEAs allowed us to study resting Glu levels (Day *et al.*, 2006; Rutherford *et al.*, 2007), which is examined in more detail in chapter Five.

Besides removal of interferents that contributed to a portion of the analyte signal, self-referencing recordings removed periodic or random noise (Burmeister *et al.*, 2002). This was an obvious advantage because smaller changes in current (lower detection limits) were achieved. Figure 2.12 illustrates removal of noise using self-referencing recordings. The noisy upper trace was a response from a GluOx coated recording site, while the middle trace was the resulting sentinel site response. When the sentinel site raw current is subtracted from the GluOx raw current and divided by the slope of the GluOx coated site, the signal-to-noise ratio of the peaks was greatly improved as shown in the lower trace. This dual-channel noise subtraction approach is widely used in other methodologies such as electrophysiology and spectroscopy and is now used with the our MEAs.

Signal Analysis

A Picospritzer[®] III (Parker Hannifan, Corp, General Valve Operation) or related hardware was connected to the FAST 16 Mark II recording system, so when solutions were pressure ejected through the glass micropipette, or experimental events occurred, the software recorded these events. The FAST 16 Mark II recording system automatically saved amperometric data, time, and pressure ejection marks (external events) for all four channels for a specified time period. All calculations were performed offline using a Microsoft Office Excel[™] macro created by Jason J. Burmeister. As the FAST 16 Mark II recording

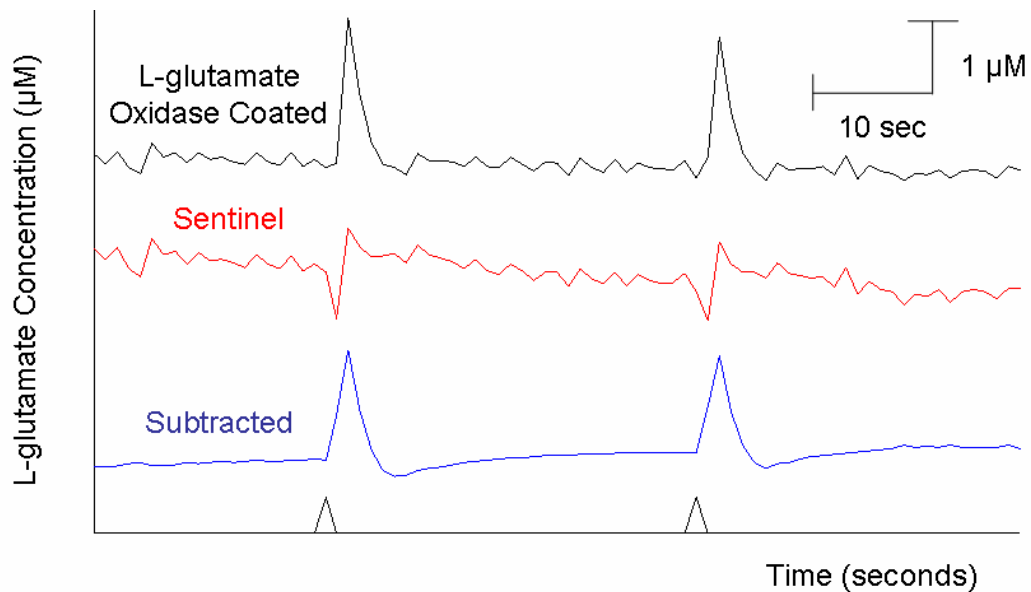


Figure 2.12: Example of Self-Referencing Subtraction

Pressure ejection of 70 mM KCl (black arrowheads) caused a release of Glu in the Str of a C57BL/6 mouse. Non-Faradaic current decreased the signal-to-noise ratio making it difficult to distinguish between current fluctuations and low Glu responses. The noise occurred on both the GluOx coated sites (top, black trace) and the sentinel recordings sites (middle, red trace). When the raw current from the sentinel recording site was subtracted from the raw current on the GluOx coated sites, the noise was removed creating a higher signal-to-noise ratio for Glu measurements (lower, blue trace).

software progressed, we analyzed individual peaks during the actual experiment. However, for the purposes of this dissertation, all data calculations were performed using the Microsoft Office Excel™ macro.

Figure 2.13A shows a typical Glu current signal (blue) and the corresponding self-referencing current (red) at 10 Hz. For Glu analysis, the absolute value of the self-referencing current was subtracted from the absolute value of the GluOx current and divided by the slope. This yielded the Glu concentration trace free of interferences as shown in figure 2.13B. A stereomicroscope mounted on a universal boom stand fitted with a reticule monitored the amount of stimulus ejected from the glass micropipette (Friedmann and Gerhardt, 1992). Pressure ejection of 70 mM KCl (70 mM KCl, 79 mM NaCl, 2.5 mM CaCl₂, pH 7.4) caused a depolarization event and released Glu into the extracellular space, causing a robust and reproducible rise in the Glu signal compared to baseline. The maximum change in concentration compared to baseline was referred to as maximum amplitude or amplitude of the Glu signal. This value was normally recorded in μM units. Next, the maximum amplitude of the signal was divided by the amount of stimulus (i.e. volume pressure ejected from the glass micropipette) necessary to elicit the Glu release. Volume displacement was calibrated according to the pipette inner diameter. (Note: the single barrel glass micropipettes had a solution volume of approximately 250 nl per mm of glass, but this varies with the inner diameter/total volume of the glass micropipette. For this reason, we suggest using the type of glass micropipettes from A-M Systems, Inc., Catalog #601500 as discussed earlier.) The volumes of stimulus ejected were recorded in nanoliters, so this calculation was referred to as amplitude per nanoliter with units $\mu\text{M}/\text{nl}$. Finally, the time period for the signal to reach the maximum amplitude from baseline was recorded (in seconds) and referred to as rise time (t_r).

Signal decay referred to the point of maximum amplitude of the signal to its return to baseline. The clearance of Glu was a result of the rapid

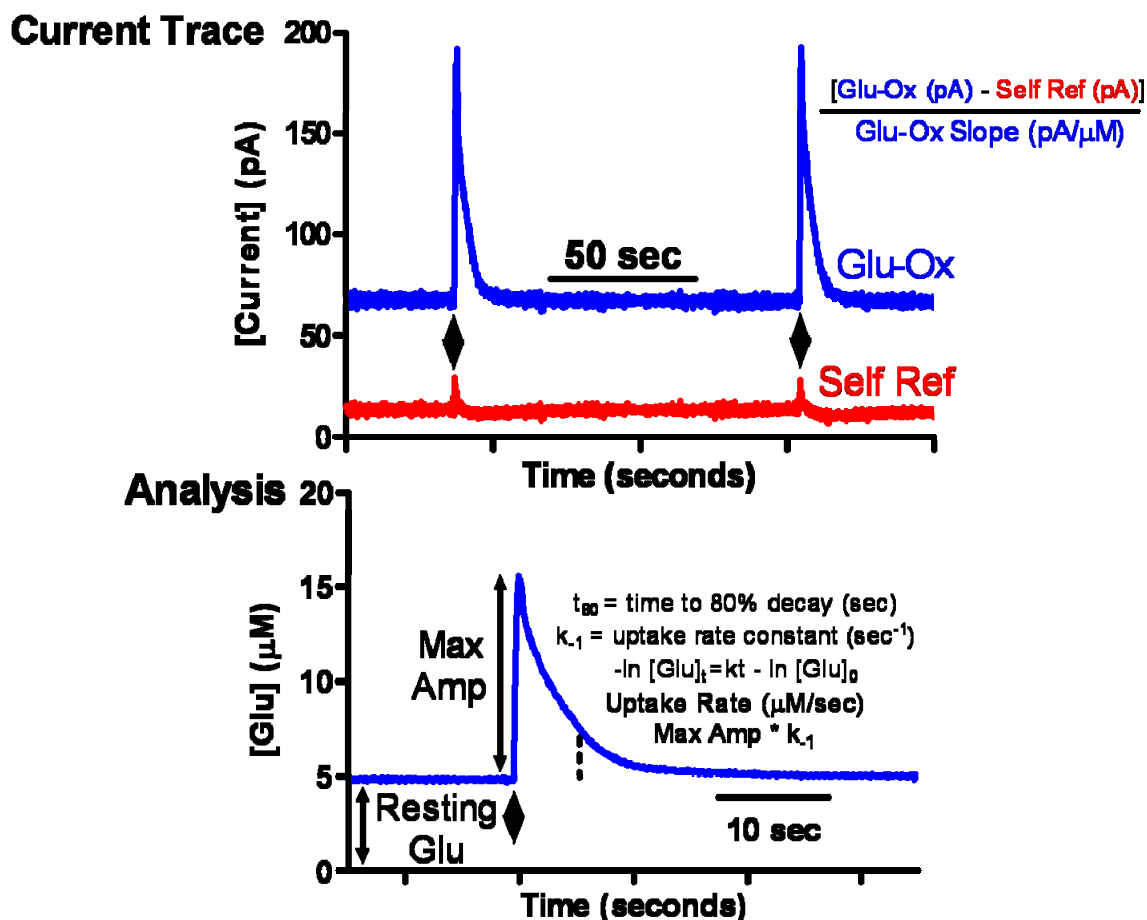


Figure 2.13: Analysis Parameters

The top graph (A) shows the absolute value of the current from a GluOx coated site (blue) and a self-referencing site (red). The bottom graph (B) is a Glu trace after the absolute value of the current from the self-referencing site was subtracted from the absolute value of the current from the GluOx coated site and divided by the slope of the GluOx coated site obtained during calibration. Additionally, this trace shows examples of resting Glu levels, maximum amplitude (Max Amp), t_{80} , and uptake rate. The diamonds on both graphs indicate local application of 0.5 μ l of 1 mM Glu.

uptake of Glu into glial and neuronal transporters (Danbolt, 2001). Glu uptake followed apparent first order decay rate. The decay of the Glu signal was fitted to the slope of the linear regression of the natural log transformation of the data over time and this was referred to as k_{-1} and had units of sec^{-1} (Parikh *et al.*, 2004). When k_{-1} was multiplied by the maximum amplitude of the signal, the uptake rate, or micromolar of Glu removed from the extracellular space per second ($\mu\text{M}/\text{sec}$), was obtained. Finally, the decay of the signal was examined at different percentages of decay. These often include t_{50} , t_{80} , and t_{100} , and follow the general format of t_D (sec), where t refers to the time from maximum amplitude for the signal to decay by D percent.

Development of Mouse Lines

All transgenic and knockout (KO) mice were developed at the University of Kansas by Dr. Elias K. Michaelis's laboratory. All transgenes were inserted into the mouse genome under the control of the Neuronal specific enolase (NSE) promoter. The NSE promoter has been shown to be expressed only in neurons of the brain and spinal cord (Choi *et al.*, 1992; Peel *et al.*, 1997). Transgenic mice were generated by injecting mouse oocytes (C57BL/6J-SJL hybrid) with vectors containing cDNA of mouse GLUD1 or rat GPT placed under the control of the NSE promoter. This promoter was excised from the pNSE-LacZ vector by first digesting the SV40 polyA tail of pNSE-LacZ vector and cloning it into pGEM-7Z. The NSE promoter was also excised and cloned into the modified pGEM-7Z. Finally, either a GLUD1 or GPT open reading frame was cloned into the pNSE-GEM-7Z to create the pNSE-GLUD1 or pNSE-GPT vector, respectively. This vector was digested, the DNA recovered, and microinjected into the nucleus of fertilized mouse oocytes to generate either the GLUD1 or GPT transgenic mice. Oocytes were transferred to surrogate C57BL/6 or BALB/C mice. Pups carrying the transgene were identified by PCR and Southern Blot Analysis.

Chapter Three: Glutamate Dynamics in Glutamate Dehydrogenase C57BL/6 and BALB/C Transgenic Mice

Introduction

Glu is the predominant excitatory neurotransmitter in the mammalian CNS with an indirect excitotoxic role implicated in several neurodegenerative disorders including PD, AD, and ALS (Doble, 1999). Evidence supports that mitochondrial damage leads to energy impairment and a decrease in intracellular ATP levels (Beal, 1992; Greene and Greenamyre, 1996; Doble, 1999). As ATP levels decrease, the Na^+/K^+ ATPase, responsible for maintaining the resting membrane potential slows down causing membrane depolarization. This can relieve the magnesium block on NMDA channels as well as open voltage-gated calcium channels. With the magnesium block removed, the NMDA receptor is more susceptible to activation by ambient or even slightly elevated levels of extracellular Glu (Beal, 1992; Greene and Greenamyre, 1996; Doble, 1999). Over prolonged periods of time (years) this process becomes similar to what is seen in acute excitotoxicity. For this reason, it has been postulated that slow, indirect excitotoxicity is partly responsible for the neuronal loss seen in several neurodegenerative disorders. Over-activation of the iGluRs are responsible for these excitotoxic effects (Gardoni and Di Luca, 2006) through the influx of calcium into the neuron (Doble, 1999). NMDA receptor antagonists have beneficial effects on experimental models of PD (Nash *et al.*, 2000; Loschmann *et al.*, 2004) as well as blocking the development of L-DOPA-induced dyskinesias (Tahar *et al.*, 2004; Wessell *et al.*, 2004). Clinical trials with memantine, an NMDA receptor antagonist, have shown functional improvement in AD patients with severe dementia (Parsons *et al.*, 1999; Winblad and Poritis, 1999; Miguel-Hidalgo *et al.*, 2002). Memantine does not accumulate in the channel during normal synaptic activity, which offers a novel approach for the treatment of AD. This drug blocks high levels of Glu at the NMDA receptor, while allowing activation by low levels of physiologically relevant neurotransmission. (Hynd *et al.*, 2004; Lipton, 2005). Finally, ALS is characterized by the selective loss of

motor neurons that leads to the muscle weakening, paralysis, and eventual respiratory failure (Williams and Windebank, 1991; Doble, 1999; Rao and Weiss, 2004). While no specific NMDA antagonist drugs have been identified for the treatment of ALS, riluzole, a drug that inhibits neuronal release of Glu, increased the lifespan of ALS patients by 3 months (McGreer and McGreer, 2005).

Few studies have examined the cause for these excessive levels of Glu in neurodegenerative disorders such as ALS, which has the largest body of evidence supporting that excitotoxicity contributes to the progression of symptoms (Doble, 1999). In ALS, several parameters involving dysfunction of glutamatergic neurotransmission have been identified including increased Glu levels in the CSF, decreased Glu uptake, and elevated amounts of Glu metabolizing enzymes (Heath and Shaw 2002). Plaitakis and Caroscio (1987) showed increased fasting plasma levels of Glu in ALS patients, and others have shown increased levels of Glu in the CSF of ALS patients (Rothstein *et al.*, 1990; Spreux-Varoquaux *et al.*, 2002). Several studies have also reported contradictory findings indicating decreases in Glu levels in various regions of post-mortem CNS tissue in ALS patients compared to controls (Perry *et al.*, 1987; Tsai *et al.*, 1990). Deficiencies in Glu transporters are also implicated for the reason behind increased Glu levels in the CNS. Rothstein and colleagues (1992) were the first to demonstrate decreased Glu transport using synaptosomes from affected brain areas of ALS patients. Furthermore, it has been shown that the EAAT2 transporter number is decreased in ALS patients compared to control (Rothstein *et al.*, 1995; Fray *et al.*, 1998; Sasaki *et al.*, 2000).

However, a study conducted by Malessa and colleagues (1991) showed alterations in Glu metabolizing enzymes in ALS patients compared to control patients. In particular, GLUD1 was upregulated in the ventral horn of the spinal cord of ALS patients compared to controls (Malessa *et al.*, 1991). This enzyme was also upregulated in the PFC of AD patients (Burbaeva *et al.*, 2005), as well as schizophrenic patients (Burbaeva, 2003, 2007). GLUD1 catalyzes a reversible reaction that favors Glu formation from ammonia and α -ketoglutarate (Yudkoff *et al.*, 1991; Kanamori and Ross, 1995; Bak *et al.*, 2006). Unfortunately,

no specific modulators for this enzyme exist, which has prevented appropriate *in vivo* study of the role this enzyme plays on glutamatergic neurotransmission. For this reason, a mouse model was created that overexpresses neuronal GLUD1 in both the C57BL/6 and BALB/C mouse strains to elucidate the role of GLUD1 on the neuronal contribution of Glu.

In the present study we examined the differences in stimulus-evoked Glu release and reuptake (using an isotonic solution of 70 mM KCl and 5 mM Glu; pH 7.4) in the Str of C57BL/6 and BALB/C GLUD1 mice compared to wildtype (WT) littermates. Stimulus-evoked Glu release provides an indication as to any differences upregulation of GLUD1 causes in the amount of Glu available for neuronal release. Examining reuptake of stimulus-evoked Glu release as well as clearance of exogenously applied Glu provided information regarding Glu transporter availability or function in the transgenic mice compared to WT controls.

Methods

All transgenic mice were developed at the University of Kansas by Dr. Elias K. Michaelis's laboratory. The GLUD1 transgene was inserted into the mouse genome under the control of the Neuronal specific enolase (NSE) promoter. The NSE promoter has been shown to be expressed only in neurons of the brain and spinal cord (Choi *et al.*, 1992; Peel *et al.*, 1997). Transgenic mice were generated by injecting mouse oocytes (C57BL/6J-SJL hybrid) with vectors containing cDNA of mouse GLUD1 placed under the control of the NSE promoter. This promoter was excised from the pNSE-LacZ vector by first digesting the SV40 polyA tail of pNSE-LacZ vector and cloning it into pGEM-7Z. The NSE promoter was also excised and cloned into the modified pGEM-7Z. Finally, a GLUD1 open reading frame was cloned into the pNSE-GEM-7Z to create the pNSE-GLUD1 vector. This vector was digested, the DNA recovered, and microinjected into the nucleus of fertilized mouse oocytes to generate the GLUD1 transgenic mice. Oocytes were transferred to surrogate C57BL/6 or BALB/C mice. Pups carrying the transgene were identified by PCR and

Southern Blot Analysis. Progeny were eventually backcrossed into both a C57BL/6 or BALB/C mouse strains. Our colleagues were interested in examining the *in vivo* effects of this enzyme in two different strains of mice, because of western blot studies that indicated exogenous expression of GLUD1 was increased in C57BL/6 mice compared to BALB/C mice (figure 3.1). Gene copy number was assayed by Southern Blot analysis and determined to be upregulated three to four-fold in the transgenic mouse strains compared to WT littermates through the first four generations of breeding.

GLUD1 transgenic and WT C57BL/6 and BALB/C mice were transported to the University of Kentucky and housed as described in Chapter Two. Male C57BL/6 and BALB/C mice between the ages of 8 and 12 months were used at the time of recordings. Mice were given 3 i.p. injections of 12.5% urethane for a total dose of 1.25 g/kg. All studies were conducted in the Str. Glu recordings were conducted using enzyme-based MEAs with a sampling rate of 1 Hz. as previously described in Chapter Two. At the time of our studies in the C57BL/6 GLUD1 transgenic mice, self-referencing techniques were not being utilized. As our MEA technology progressed, self-referencing was routinely utilized including the study with BALB/C GLUD1 transgenic mice. A craniotomy was performed over both striatal hemispheres and MEAs were positioned using the coordinates from Paxinos and Franklin (2004) (AP: +0.9 mm; ML \pm 1.5, \pm 1.7 mm; DV: -2.35, -2.85, -3.35, -3.85 mm) in order to create a depth profile of the Str in transgenic and WT mice. A glass micropipette with an internal diameter of 10-12 μ m was attached to the PCB and positioned among the 4 Pt recording sites, resting 50-100 μ m above the recording surface. Through this glass micropipette isotonic solutions of 70 mM KCl (70 mM KCl, 79 mM NaCl, 2.5 mM CaCl₂; pH 7.4) or 5 mM Glu (in 0.9% saline; pH 7.4) were locally applied to the surrounding brain tissue to study glutamatergic neurotransmission. Upon initial MEA implantation, a stable baseline recording was obtained for at least 30 minutes prior to local application of solutions. When self-referencing MEAs were used, resting Glu levels were calculated at the end of this initial baseline time period. After the initial baseline recording, solutions were locally applied at regular 30 second

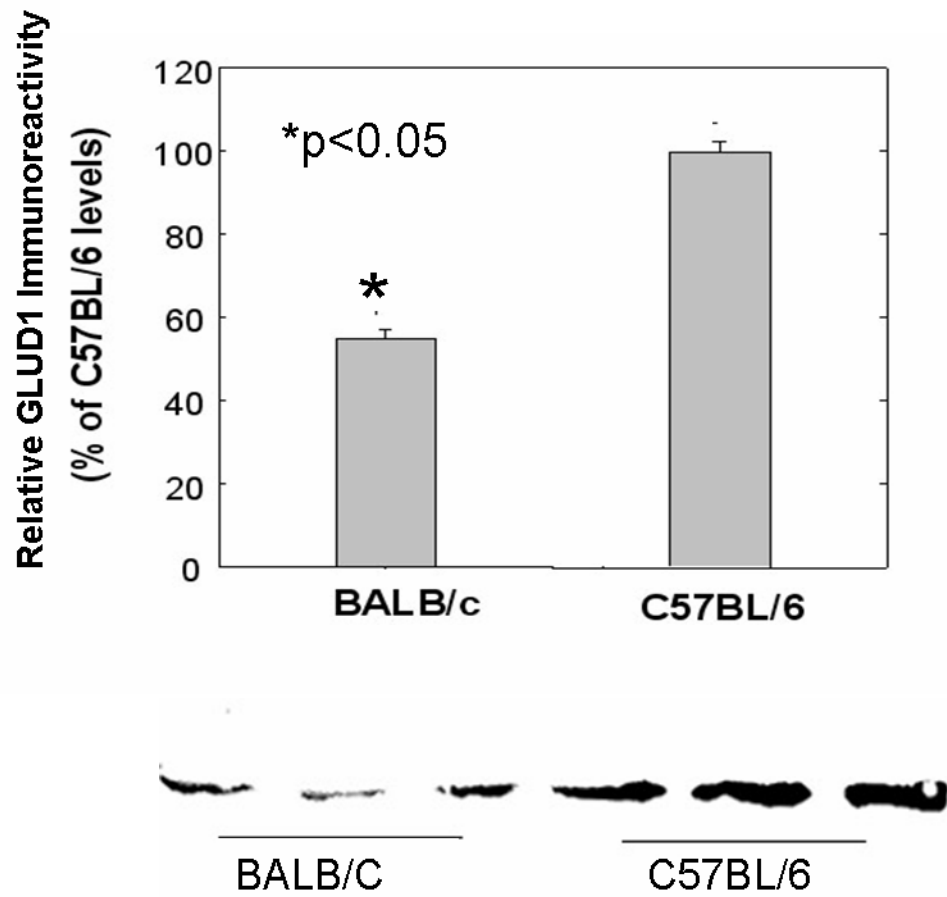


Figure 3.1: Western Blot Analysis of Exogenous GLUD1

C57BL/6 mice showed increased endogenous expression for the enzyme GLUD1 compared to BALB/C mice. BALB/C mice had approximately 55% the endogenous activity of GLUD1 compared to C57BL/6 levels. Data table and blots supplied by the University of Kansas.

intervals (for a total of 20 signals; 10 signals from each Pt recording site) to assess Glu dynamics at each dorsal ventral position. Due to the reproducibility of Glu signals *in vivo* (figure 3.2), all signals for a particular depth were averaged into a single data set for that depth. Data analysis involved a two-tailed student's t-test comparing GLUD1 transgenic to WT for each strain. All data is reported as mean \pm standard error of the mean and significance was defined as $p < 0.05$.

Results

The fact that α -ketoglutarate was a product of GluOx activity and a substrate for GLUD1, we needed to determine the concentration of α -ketoglutarate that would significantly decrease our MEA response to Glu. To do this we calibrated the same GluOx MEA in 0.05M PBS with varying concentrations of α -ketoglutarate in the buffer. We determined that approximately 5 mM α -ketoglutarate was required before a significant ($p < 0.05$) drop in MEA sensitivity to Glu was observed (figure 3.3). MEA current values after calibration in increasing buffer concentrations of α -ketoglutarate are shown in table 3.1. Dicarboxylate transporters were found on both astrocytes and neurons indicating that α -ketoglutarate existed in the same location as our recordings, the extracellular space. While no studies were found that determined the relative K_M values for these transporters with α -ketoglutarate, K_M values for similar TCA cycle substrates were found in the tens of micromolar range (Pajor, 2006). This was much less than the approximate 5 mM concentration needed to significantly reduce MEA sensitivity to Glu.

In the C57BL/6 GLUD1 transgenic and WT mice, local application of 70 mM KCl resulted in robust, reproducible Glu signals compared to baseline. We also observed that the GLUD1 transgenic mice released more Glu upon depolarization compared to WT littermates (Figure 3.4). To quantitate this finding, we volume matched the amount of stimulus locally applied to both mouse groups. Only Glu signals that were elicited by 100 to 200 nl of 70 mM KCl were used for this analysis, therefore, no significant difference in the amount of stimulus used was observed between the GLUD1 transgenic (134 ± 8 nl) and WT

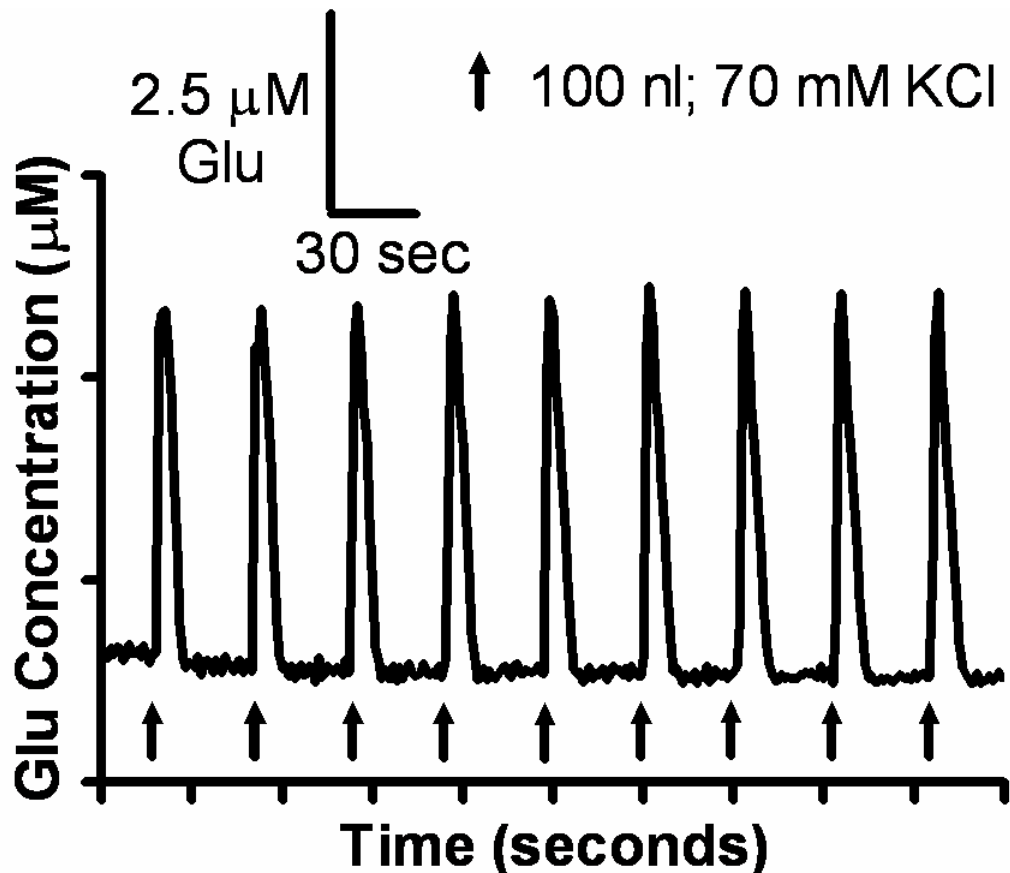


Figure 3.2: Reproducibility of Glu Signals From 70 mM KCl Depolarization

The above trace demonstrated the reproducibility of Glu signals elicited due to stimulus-evoked release by 70 mM KCl. Signals were from a GLUD1 transgenic BALB/C mouse and taken at approximately 30 second intervals. The reproducibility of the Glu signals allowed us to average the individual signals for a given depth into a single data set.

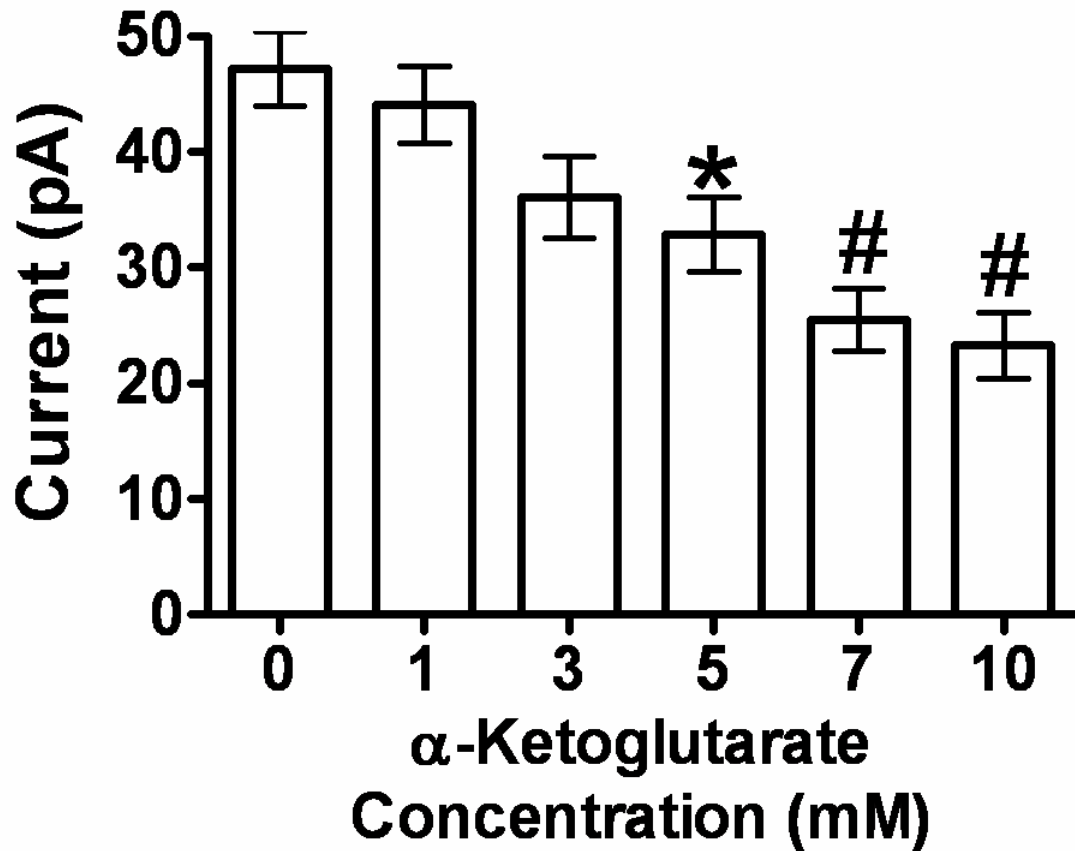


Figure 3.3: Effects of α-Ketoglutarate on MEA Sensitivity

All four sites of a Glu selective MEA were coated with GluOx and its response to Glu was determined in 0.05 M PBS with increasing concentrations of α-ketoglutarate. Concentrations of 5 mM α-ketoglutarate and higher significantly (* $p < 0.05$; # $p < 0.001$) decreased the MEA sensitivity to Glu. Data was from a single MEA over four trials. A one-way analysis of variance (ANOVA) with Tukey's post hoc was used to determine significance.

Table 3.1: Amperometric Glu Current with Increasing Buffer Concentration of α -Ketoglutarate

[α-KG] (mM)	0	1	3	5	7	10
Current (pA)	47.2 \pm 3.2	44.1 \pm 3.3	36.1 \pm 3.5	32.9 \pm 3.2	25.5 \pm 2.7	23.3 \pm 2.8

Data is averaged from a single MEA over four trials and shown as mean \pm standard error of the mean.

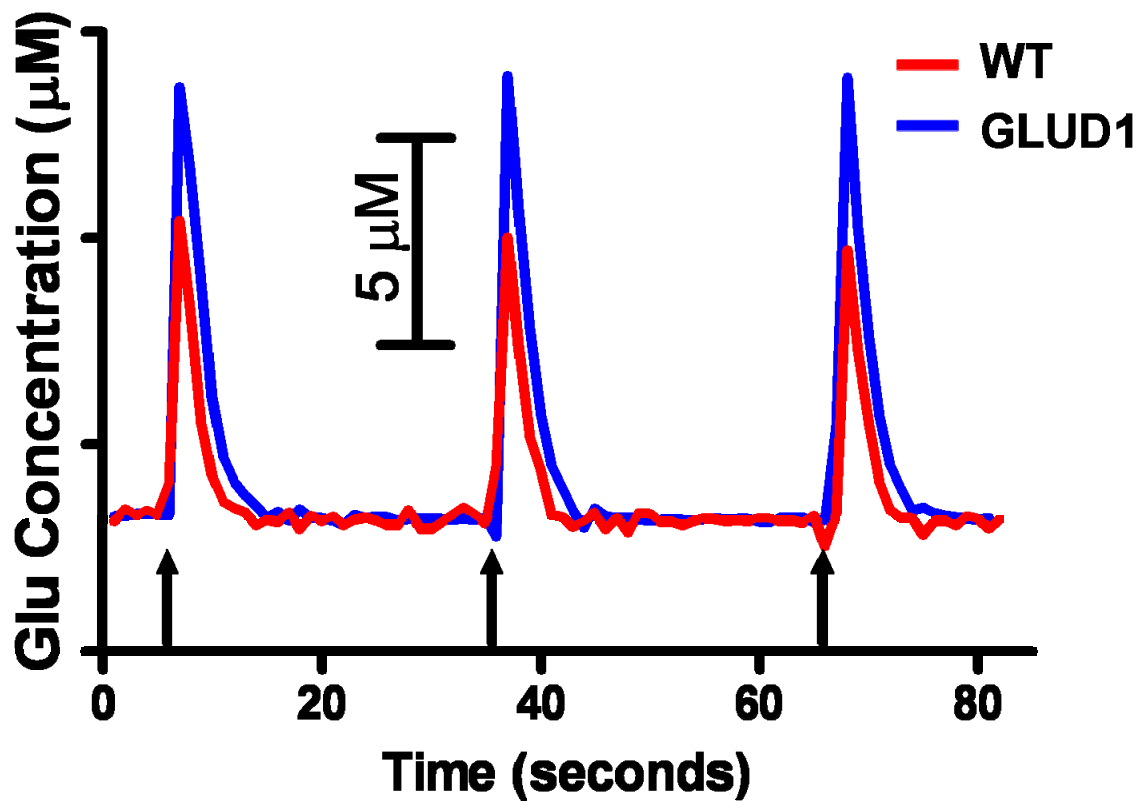


Figure 3.4: 70 mM KCl-Evoked Glu Release Traces in the C57BL/6 Mouse

Series of amperometric Glu recordings showing differences in volume matched, stimulus-evoked Glu release in WT (red) and GLUD1 (blue) transgenic C57BL/6 mice. Note the reproducibility of the signal and the significantly increased release of Glu in the GLUD1 transgenic mice compared to WT. Arrows indicate time points for local application of an isotonic solution of 70 mM KCl (pH 7.4).

(140 ± 6 nl) mice (figure 3.5A). When the average maximal amplitude of Glu release is quantitated, C57BL/6 GLUD1 transgenic mice (9.9 ± 1.4 μ M) released significantly more Glu ($p < 0.05$) compared to WT littermates (6.3 ± 0.7 μ M) (figure 3.5B). Using the same subset of signals, striatal, depth-related alterations in stimulus-evoked Glu release were also examined (figure 3.6). The average Glu release was calculated at each depth (DV -2.25 to -3.75 mm) and compared amongst C57BL/6 GLUD1 transgenic and WT mice. No significant differences were seen within groups of mice, however, a significant difference ($p < 0.05$) in Glu release was observed at depth -2.25 and -3.25 mm between GLUD1 transgenic (9.5 ± 1.4 μ M and 12.7 ± 3.0 μ M, respectively) and WT mice (5.4 ± 0.6 μ M and 5.7 ± 0.8 μ M, respectively).

Since neurotransmitter uptake follows classical Michaelis-Menten kinetics (Nicholson, 1995) and was affected by the amount of available substrate, Glu uptake was analyzed by selecting a subset of signals with maximum release values were in the range of 3-13 μ M. This range was chosen, because these peak Glu values were easily obtainable in both groups. Within this subset of signals, no significant difference in average maximum release of Glu was observed in WT (6.3 ± 0.4 μ M) and GLUD1 transgenic mice (7.8 ± 0.6 μ M), nor was a significant difference in the uptake rate of stimulus-evoked Glu release observed between WT (1.8 ± 0.2 μ M/sec) and GLUD1 transgenic mice (1.9 ± 0.3 μ M/sec) (figure 3.7).

Because Glu transporters were electrogenic (Takahashi *et al.*, 1997, Doble, 1999) and the introduction of potassium ions and subsequent membrane depolarization changed their function, we wanted to determine transporter function without membrane depolarization. To do this, we locally applied an isotonic solution of 5 mM Glu (pH 7.4) and used a subset of Glu signals that were in the same range as those used for our stimulus-evoked Glu uptake analysis, 3-13 μ M. There was no significant difference in the maximal amplitude of exogenously applied 5 mM Glu in the C57BL/6 GLUD1 transgenic (7.7 ± 0.8 μ M) and WT (9.5 ± 0.4 μ M) mice (figure 3.8A). Similar to the stimulus-evoked Glu data, there was no significant difference in the clearance rate for locally applied

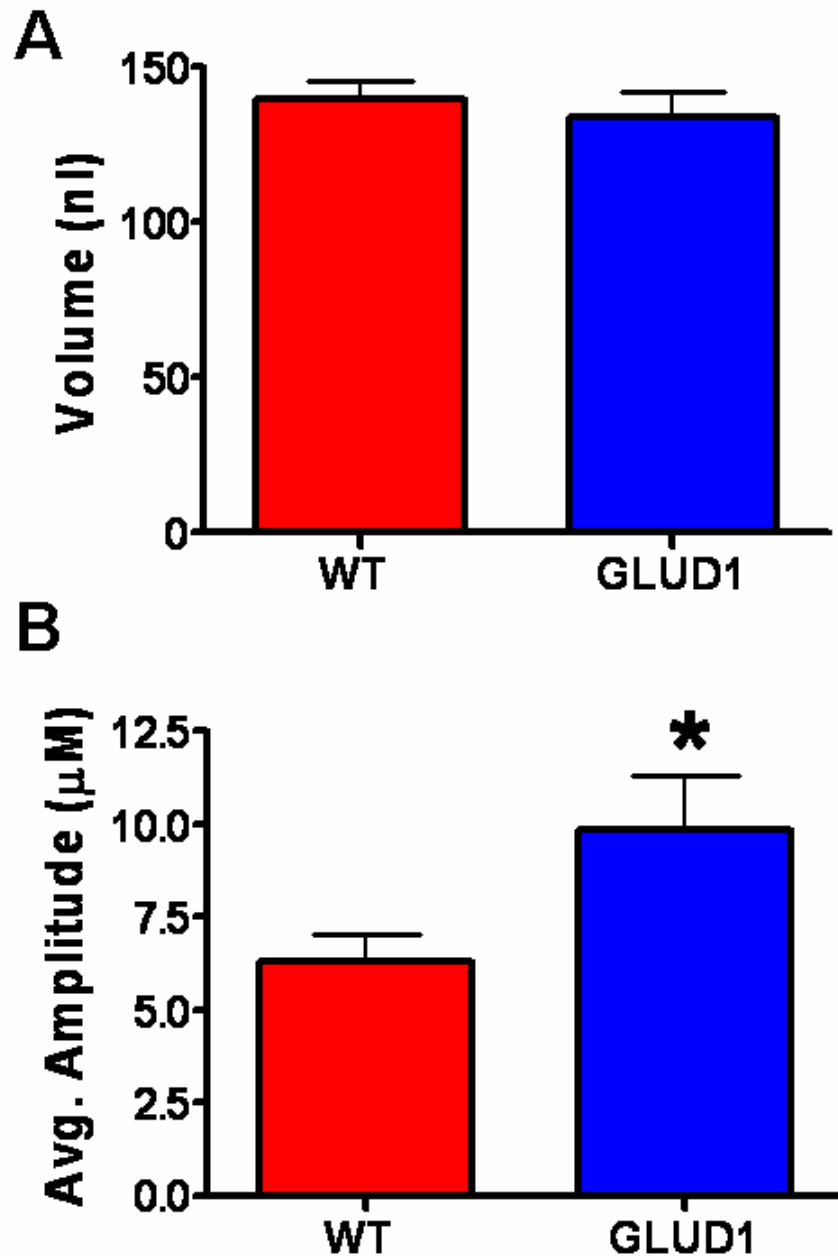


Figure 3.5: Stimulus-Evoked Glu Release in C57BL/6 GLUD1 Transgenic Mice

A) Only Glu signals that were elicited by 70 mM KCl whose volumes ranged between 100 and 200 nl were analyzed for the C57BL/6 GLUD1 transgenic (n=4) and WT (n=9) mice. Since the volumes were matched, no significant difference in the amount of stimulus locally applied was observed between WT (140 ± 6 nl) and transgenic mice (134 ± 8 nl). B) The average maximal amplitude of Glu released after local application of 70 mM KCl was significantly increased (*p < 0.05) in the GLUD1 transgenic (9.9 ± 1.4 µM) compared to WT littermates (6.3 ± 0.7 µM).

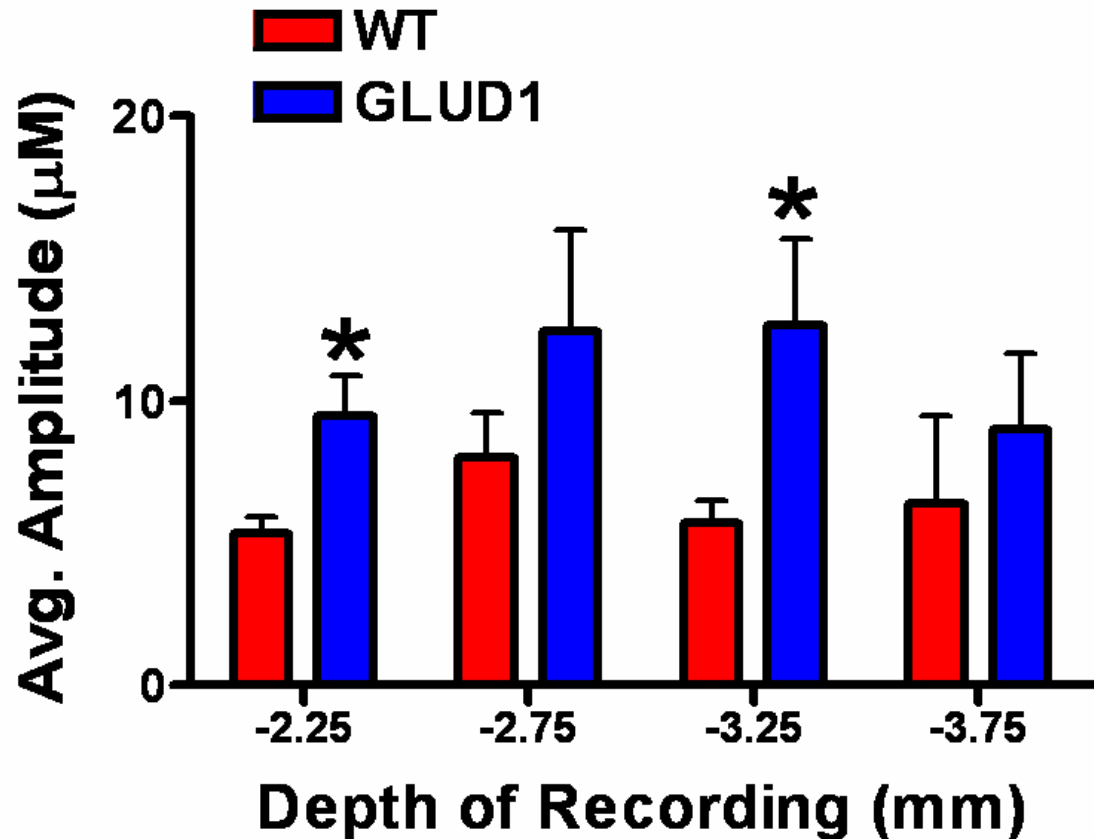


Figure 3.6: Stimulus-Evoked Glu Release Depth Profile in the C57BL/6 Mouse

Average stimulus-evoked Glu release at different recording depths within the Str of C57BL/6 GLUD1 transgenic (n=4) and WT (n=9) mice. GLUD1 transgenic mice released significantly (* $p < 0.05$) more Glu compared to WT littermates at depths -2.25 and -3.25 mm. At recording depths -2.75 and -3.75 mm there was no significant difference in the amount of Glu released between the two mouse groups. (* $p < 0.05$ based on a two-tailed t-test for comparing mouse groups at individual recording depths).

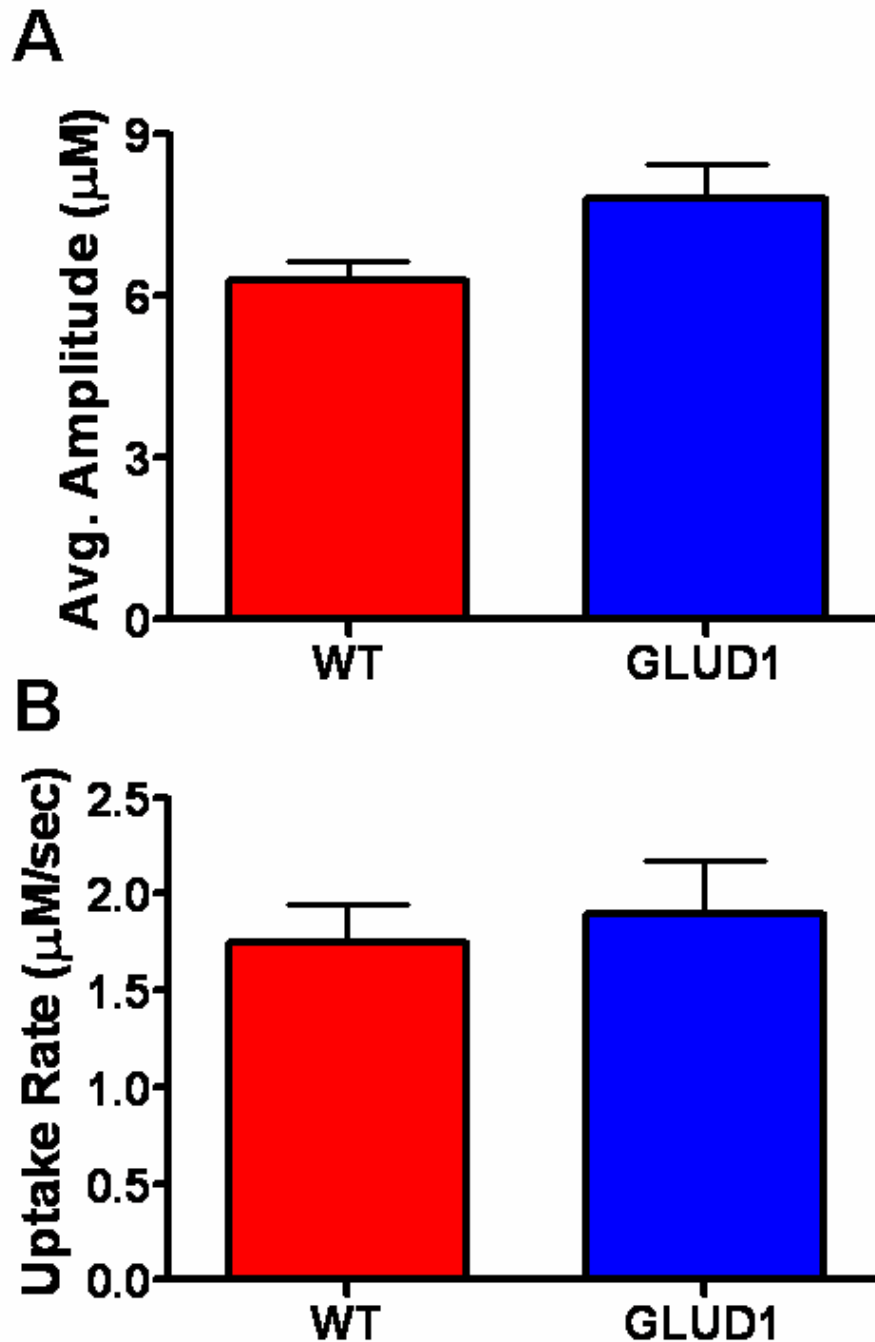


Figure 3.7: Stimulus-Evoked Glu Uptake in the C57BL/6 Mouse Groups

A) To properly study uptake kinetics, a subset of Glu signals were examined whose average maximal amplitude fell in a range of 3-13 μM for both the C57BL/6 GLUD1 transgenic (n=4) and WT (n=9) mice. No significant difference was observed between WT ($6.3 \pm 0.4 \mu\text{M}$) and GLUD1 transgenic ($7.8 \pm 0.6 \mu\text{M}$) mice. B) There was no significant difference in the uptake rate of stimulus-evoked Glu between WT ($1.8 \pm 0.2 \mu\text{M}/\text{sec}$) and GLUD1 transgenic mice ($1.9 \pm 0.3 \mu\text{M}/\text{sec}$).

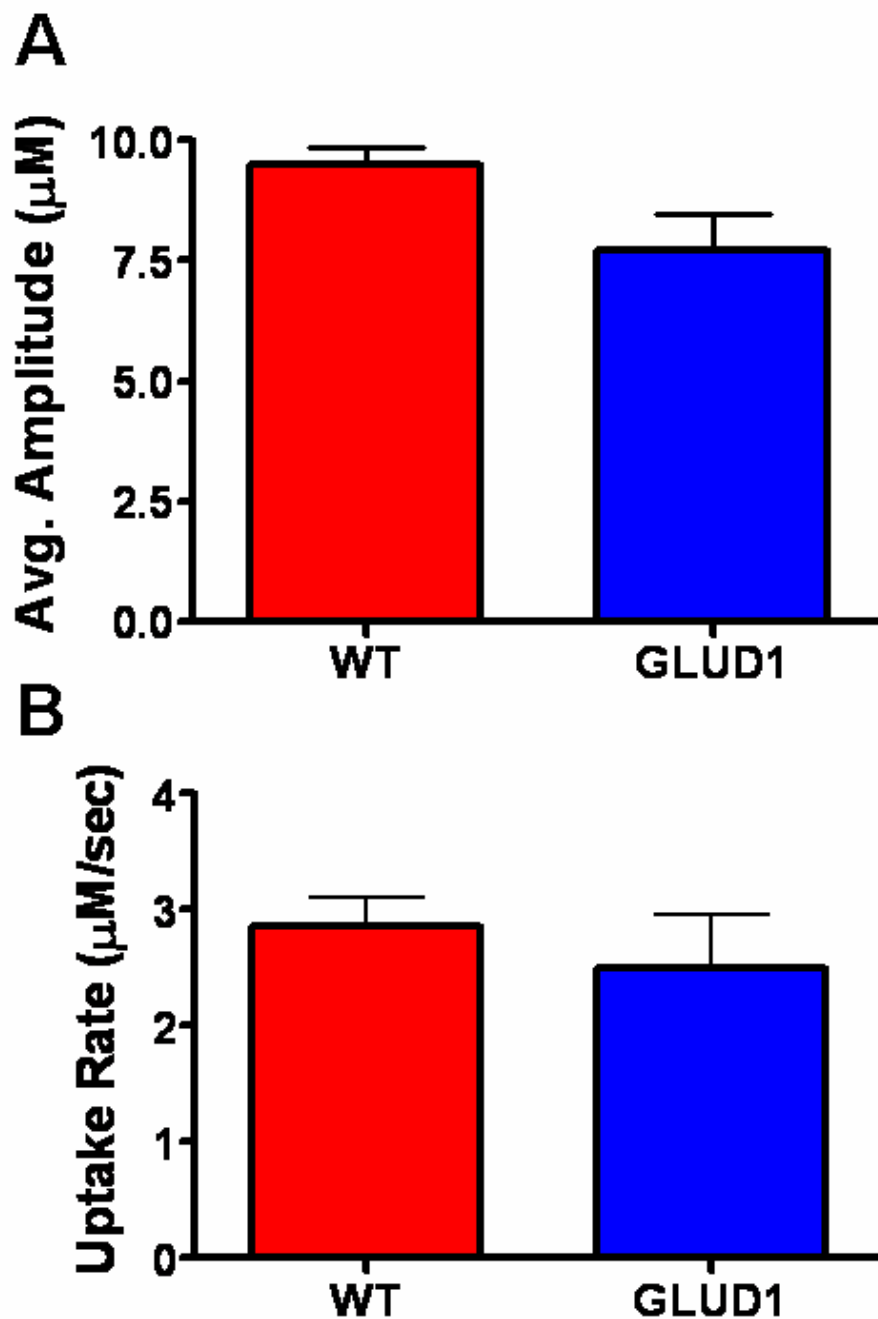


Figure 3.8: Clearance of Exogenously Applied 5 mM Glu

A) A subset of Glu signals were examined whose average maximal amplitude fell in a range of 3-13 μM for both the C57BL/6 GLUD1 transgenic (n=4) and WT (n=9) mice. No significant difference was observed between WT (9.5 \pm 0.4 μM) and GLUD1 transgenic (7.7 \pm 0.8 μM) mice.

B) There was no significant difference in the rate of Glu clearance between WT (2.9 \pm 0.2 $\mu\text{M}/\text{sec}$) and GLUD1 transgenic mice (2.5 \pm 0.5 $\mu\text{M}/\text{sec}$).

5 mM Glu in the WT ($2.9 \pm 0.2 \mu\text{M}/\text{sec}$) and GLUD1 transgenic mice ($2.5 \pm 0.5 \mu\text{M}/\text{sec}$) (figure 3.8B).

In the BALB/C GLUD1 transgenic and WT mice, local application of 70 mM KCl resulted in robust, reproducible Glu signals compared to baseline similar to what was observed in the C57BL/6 mouse groups. From these traces we noticed that the BALB/C GLUD1 transgenic mice released more Glu upon depolarization compared to WT littermates (Figure 3.9). To quantitate this finding, we volume matched the amount of stimulus locally applied to both mouse groups. Only Glu signals that were elicited by 50 to 150 nl of 70 mM KCl were used for this analysis, therefore, no significant difference in the amount of stimulus used was observed between the BALB/C GLUD1 transgenic ($106 \pm 4 \text{ nl}$) and WT ($98 \pm 5 \text{ nl}$) mice (figure 3.10A). When the average maximal amplitude of Glu release is quantitated, BALB/C GLUD1 transgenic mice ($5.2 \pm 0.4 \mu\text{M}$) released significantly more Glu ($p < 0.05$) compared to WT littermates ($3.9 \pm 0.4 \mu\text{M}$) (figure 3.10B). Using the same subset of signals, striatal, depth-related alterations in stimulus-evoked Glu release were also examined (figure 3.11). The average Glu release was calculated at each depth (DV -2.25 to -3.75 mm) and compared amongst the BALB/C mouse groups. No significant differences were seen within groups of mice, however, a significant difference ($p < 0.01$) in Glu release was observed at the ventral depth of -3.25 mm between GLUD1 transgenic ($6.1 \pm 0.7 \mu\text{M}$) and WT mice ($2.7 \pm 0.4 \mu\text{M}$).

Since neurotransmitter uptake follows classical Michaelis-Menten kinetics (Nicholson, 1995) and was affected by the amount of available substrate, Glu uptake was analyzed by selecting a subset of signals with maximum release values were in the range of 3-13 μM . This range was chosen, because these peak Glu values were easily obtainable in both groups. Within this subset of signals, no significant difference in average maximum release of Glu was observed in WT ($5.2 \pm 0.3 \mu\text{M}$) and GLUD1 transgenic mice ($5.4 \pm 0.3 \mu\text{M}$), nor was a significant difference in the uptake rate of stimulus-evoked Glu release seen between WT ($1.3 \pm 0.1 \mu\text{M}/\text{sec}$) and GLUD1 transgenic mice ($1.6 \pm 0.2 \mu\text{M}/\text{sec}$) (figure 3.12).

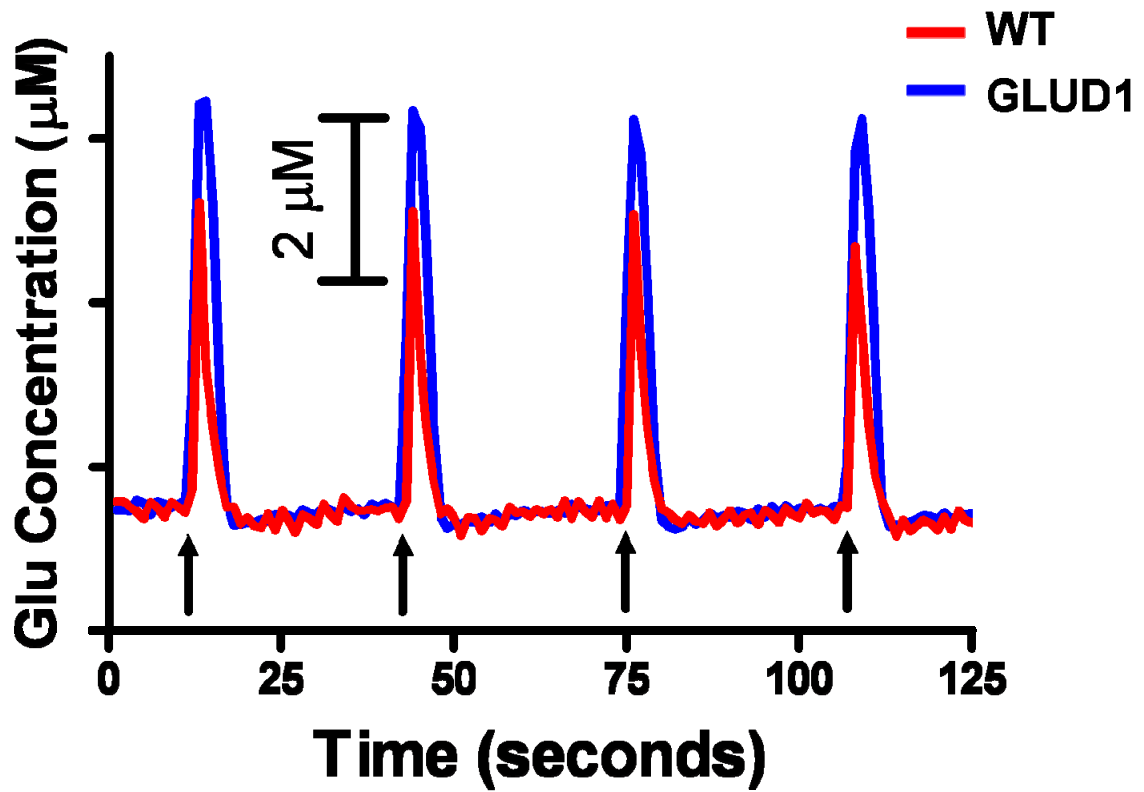


Figure 3.9: 70 mM KCl-Evoked Glu Release Traces in the BALB/C Mouse

Series of amperometric Glu recordings showed differences in volume matched stimulus-evoked Glu release in WT (red) and GLUD1 (blue) transgenic BALB/C mice. Note the reproducibility of the signal and the significantly increased release of Glu in the GLUD1 transgenic mice compared to WT. Arrows indicate time points for local application of an isotonic solution of 70 mM KCl (pH 7.4).

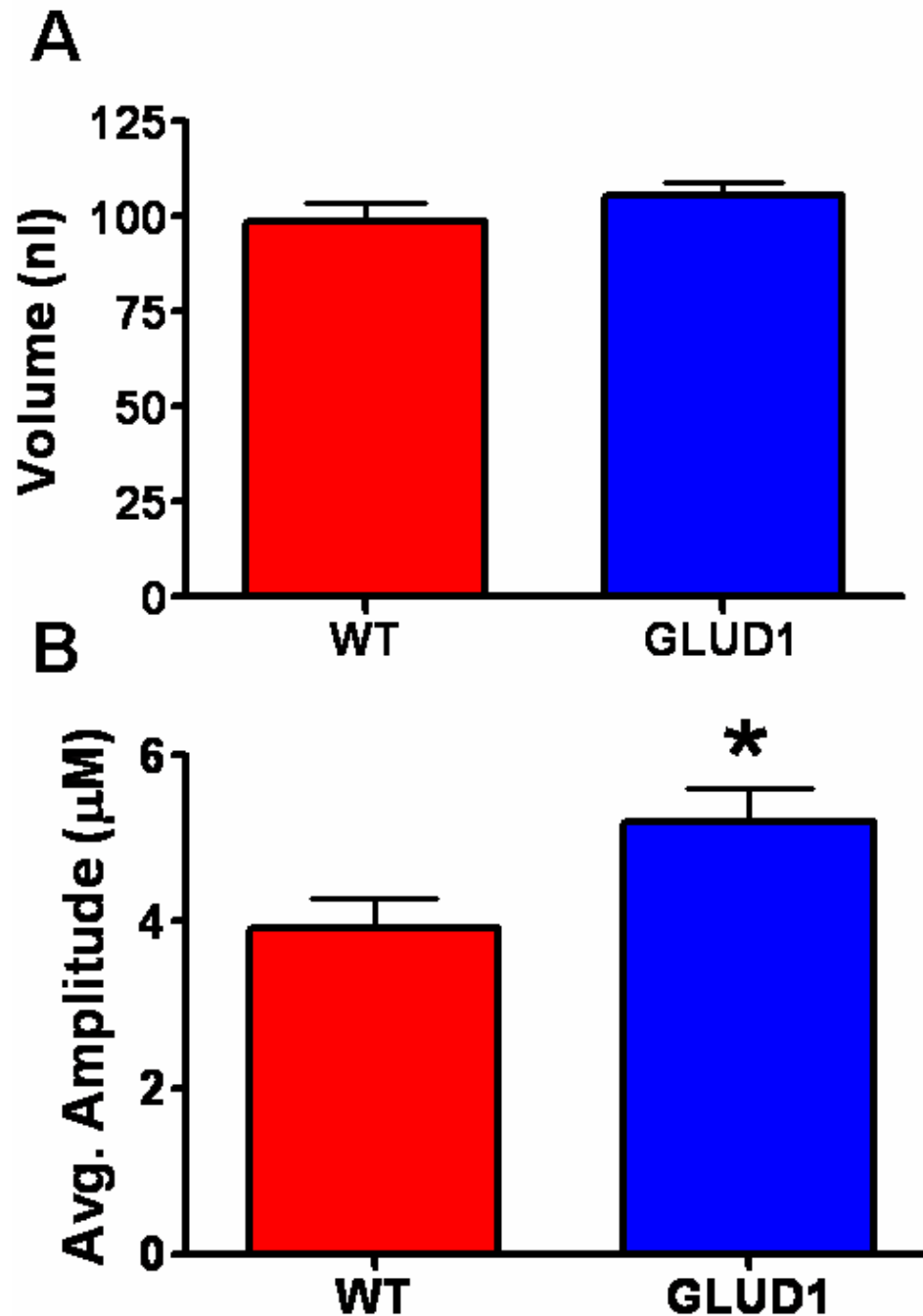


Figure 3.10: Stimulus-Evoked Glu Release in BALB/C GLUD1 Transgenic Mice

A) Only Glu signals that were elicited by 70 mM KCl whose volumes ranged between 50 and 150 nl were analyzed for the BALB/C GLUD1 transgenic (n=4) and WT (n=5) mice. Since the volumes were matched, no significant difference in the amount of stimulus locally applied was observed between WT (98 ± 5 nl) and transgenic mice (106 ± 4 nl). B) The average maximal amplitude of Glu released after local application of 70 mM KCl was significantly increased (* $p < 0.05$) in the GLUD1 transgenic (5.2 ± 0.4 µM) mice compared to WT littermates (3.9 ± 0.4 µM).

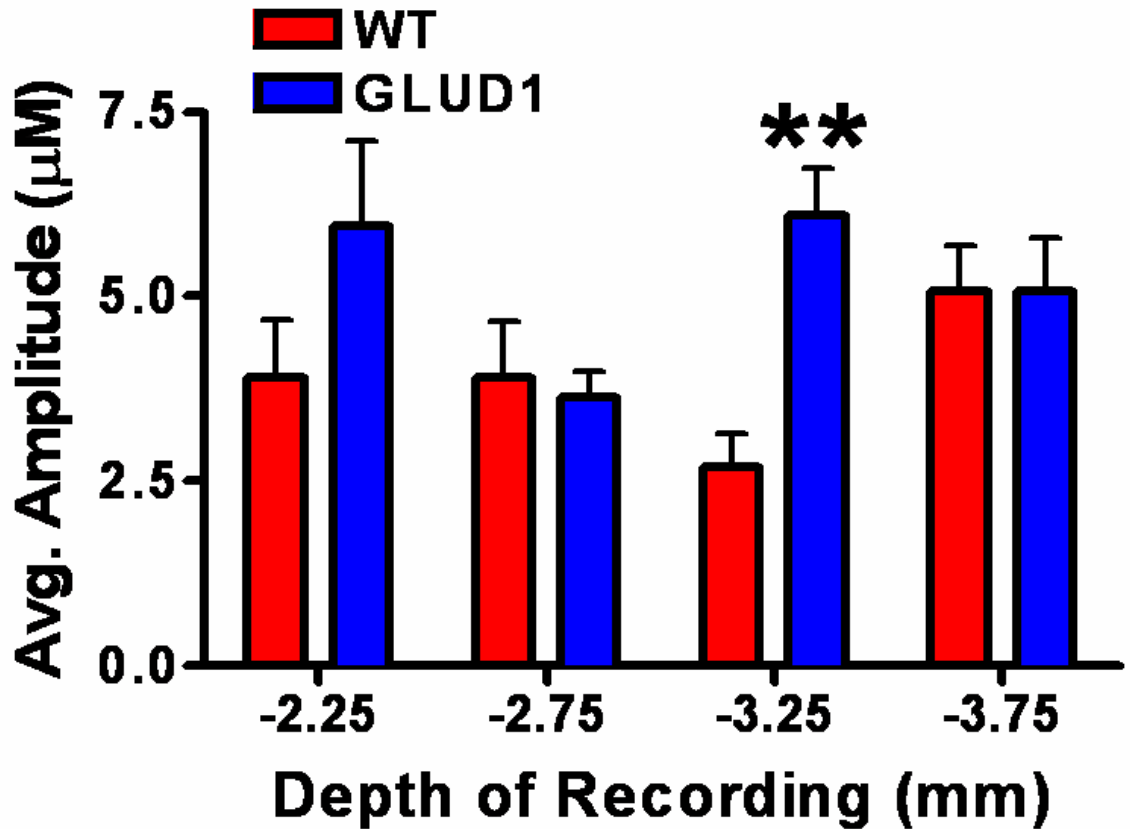


Figure 3.11: Stimulus-Evoked Glu Release Depth Profile in the BALB/C Transgenic Mice

Average stimulus-evoked Glu release at different recording depths within the Str of BALB/C GLUD1 transgenic (n=4) and WT (n=5) mice. GLUD1 transgenic mice ($6.1 \pm 0.7 \mu\text{M}$) released significantly (** $p < 0.01$) more Glu compared to WT littermates ($2.7 \pm 0.4 \mu\text{M}$) at depth -3.25 mm. At the other three recording depths, there was no significant difference in the amount of Glu released between the two mouse groups. (Significance based on a two-tailed t-test for comparing mouse groups at individual recording depths).

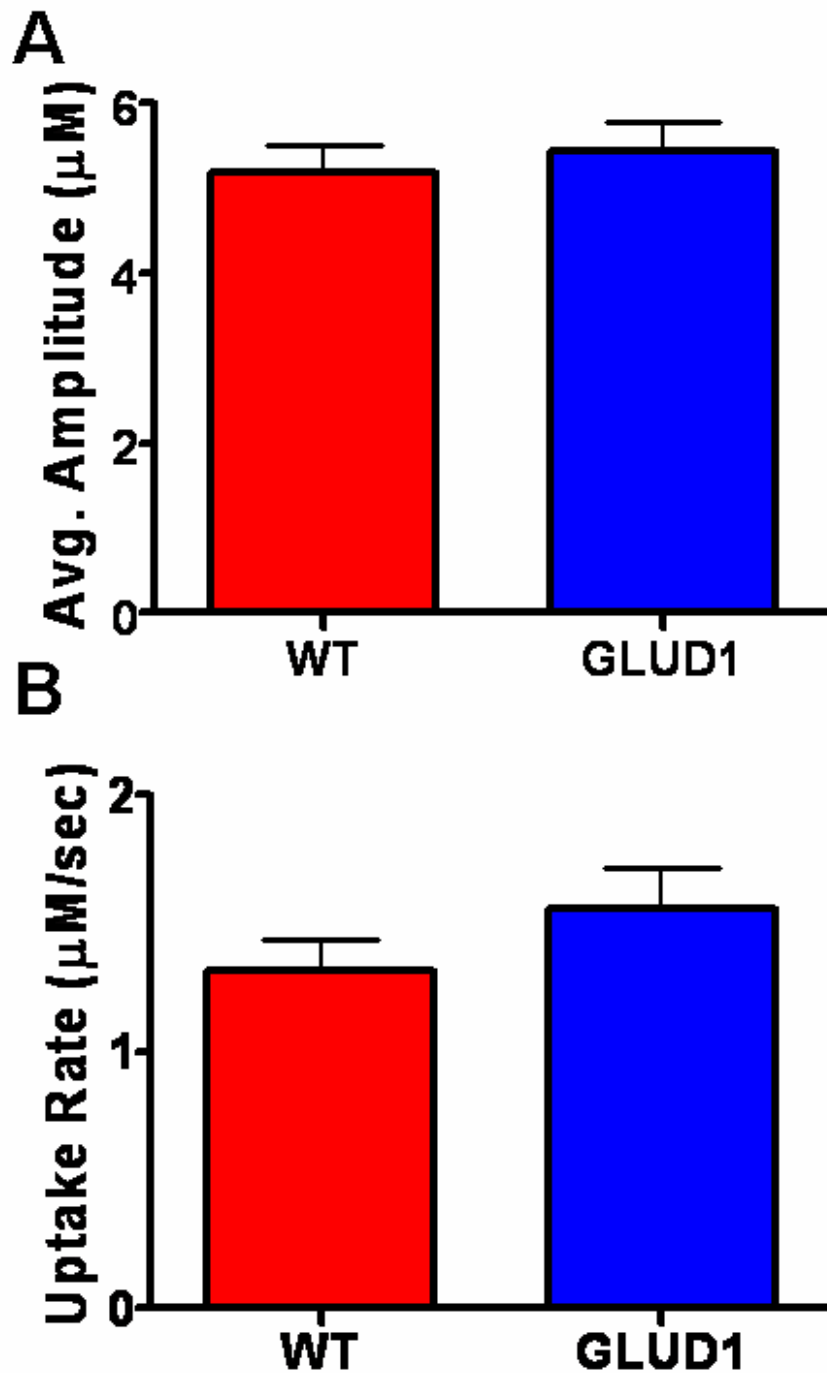


Figure 3.12: Stimulus-Evoked Glu Uptake in the BALB/C Mouse Groups

A) A subset of Glu signals were examined whose average maximal amplitude fell in a range of 3-13 μM for both the BALB/C GLUD1 transgenic (n=4) and WT (n=5) mice. No significant difference was observed between WT ($5.2 \pm 0.3 \mu\text{M}$) and GLUD1 transgenic ($5.4 \pm 0.3 \mu\text{M}$) mice. B) There was no significant difference in the rate of stimulus-evoked Glu clearance between WT ($1.3 \pm 0.1 \mu\text{M}/\text{sec}$) and GLUD1 transgenic mice ($1.6 \pm 0.2 \mu\text{M}/\text{sec}$).

Due to the electrogenic nature of Glu transporters (Takahashi *et al.*, 1997; Doble, 1999), we wanted to determine transporter function without membrane depolarization. Do to this, we locally applied an isotonic solution of 5 mM Glu (pH 7.4) and used a subset of Glu signals that were in the same range as those used for our stimulus-evoked Glu uptake analysis (3-13 μM). There was no significant difference in the maximal amplitude of exogenously applied 5 mM Glu in the BALB/C GLUD1 transgenic ($7.8 \pm 0.3 \mu\text{M}$) and WT ($8.3 \pm 0.3 \mu\text{M}$) mice (figure 3.13A). Similar to the stimulus-evoked Glu data, there was no significant difference in the clearance rate for locally applied 5 mM Glu in the WT ($2.5 \pm 0.2 \mu\text{M}/\text{sec}$) and GLUD1 transgenic mice ($2.4 \pm 0.5 \mu\text{M}/\text{sec}$) (figure 3.13B).

Since self-referencing MEAs were used to study the BALB/C GLUD1 transgenic mice, we were able to determine resting Glu levels in the Str. Thirty second baseline measures were taken prior to local application of 70 mM KCl at each recording depth. Resting Glu levels were only measured when 70 mM KCl was in the barrel of the glass micropipette. Possible diffusion of 5 mM Glu out of the barrel could cause unphysiologically elevated resting Glu levels. Using our self-referencing recording techniques, resting Glu levels were determined and found to be similar in the Str of both WT ($0.8 \pm 0.1 \mu\text{M}$) and GLUD1 transgenic mice ($0.8 \pm 0.2 \mu\text{M}$; figure 3.14A). Additionally, a depth analysis profile revealed resting Glu levels were similar at all recording depth within mouse groups and across groups of mice at individual depths (figure 3.14B).

Because the immunohistochemical data obtained from the University of Kansas revealed that endogenous expression of GLUD1 in the BALB/C mouse strain was approximately 55 percent the C57BL/6 strain (figure 3.15A), we wanted to compare maximal amplitude of stimulus-evoked Glu release in the WT and GLUD1 transgenic mouse strains. When we compared the BALB/C WT mice to the C57BL/6 WT mice we saw that the BALB/C WT mice released significantly ($p < 0.01$) less Glu upon stimulation compared to the C57BL/6 WT mice (figure 3.15B). The average maximal values in the BALB/C WT mice were approximately 62 percent of the C57BL/6 WT mice. The BALB/C GLUD1 transgenic mice released significantly ($p < 0.001$) less Glu upon stimulation

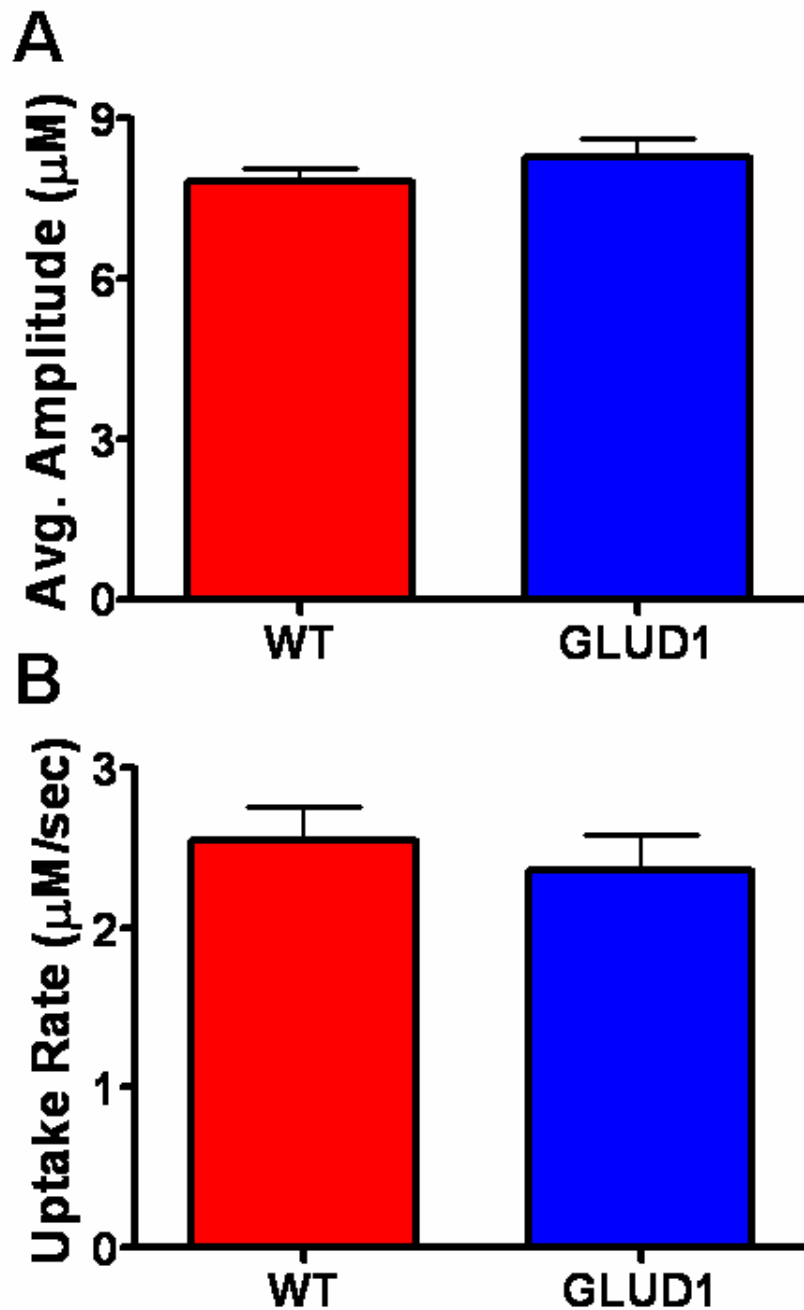


Figure 3.13: Clearance of Exogenously Applied 5 mM Glu in BALB/C Mice

A) A subset of Glu signals were examined whose average maximal amplitude fell in a range of 3-13 μM for both the BALB/C GLUD1 transgenic (n=3) and WT (n=3) mice. No significant difference was observed between WT ($7.8 \pm 0.3 \mu\text{M}$) and GLUD1 transgenic ($8.3 \pm 0.3 \mu\text{M}$) mice.

B) There was no significant difference in the rate of exogenously applied Glu clearance between WT ($2.5 \pm 0.2 \mu\text{M}/\text{sec}$) and GLUD1 transgenic mice ($2.4 \pm 0.2 \mu\text{M}/\text{sec}$).

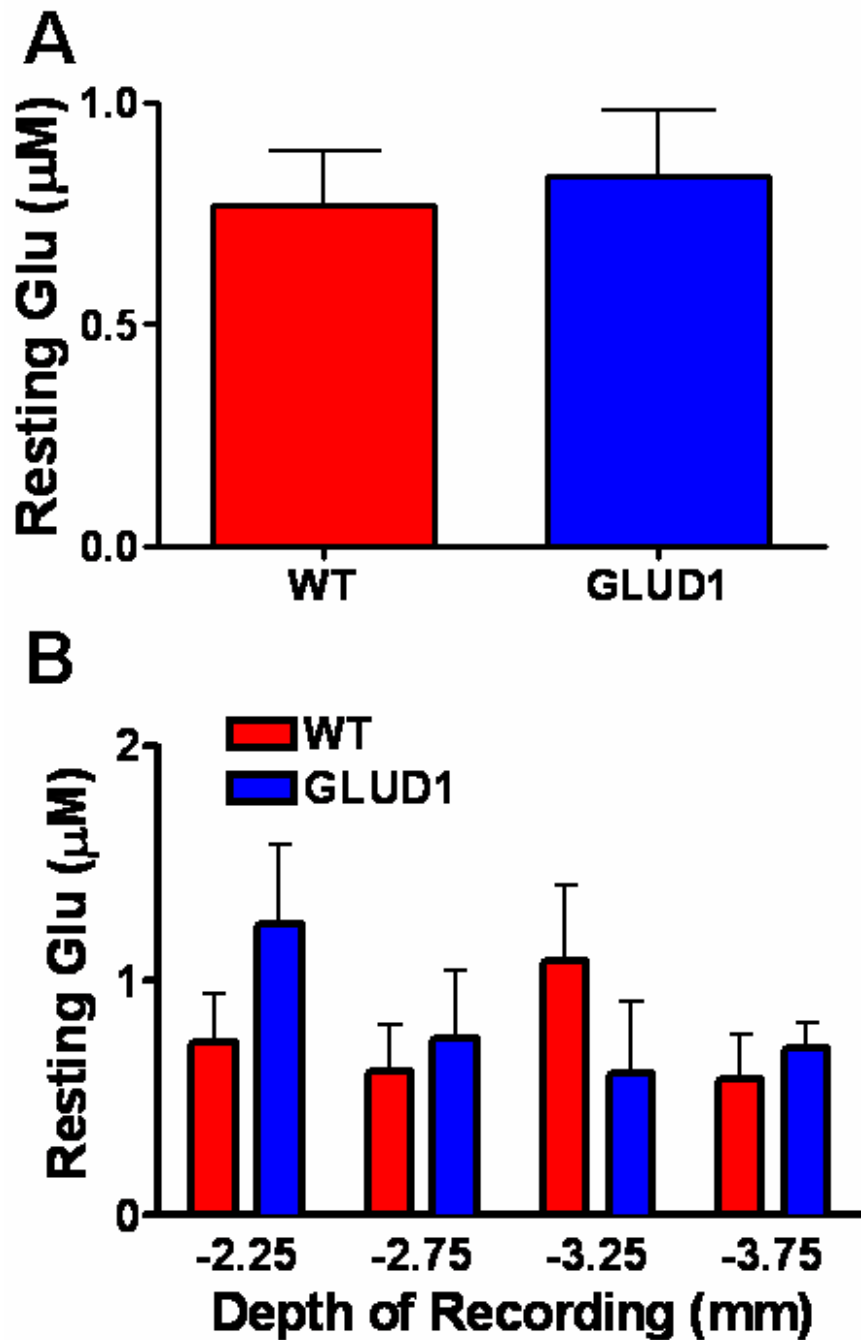


Figure 3.14: Resting Glu Levels in the BALB/C GLUD1 Transgenic Mice

A) Averaged resting Glu levels were determined for the entire Str and no significant difference was found between WT ($0.8 \pm 0.1 \mu\text{M}$) and GLUD1 transgenic mice ($0.8 \pm 0.2 \mu\text{M}$). B) Average resting Glu levels were determined for each depth within the Str. No significant difference was observed within mouse groups neither at different depths nor across mouse groups at each recording depth.

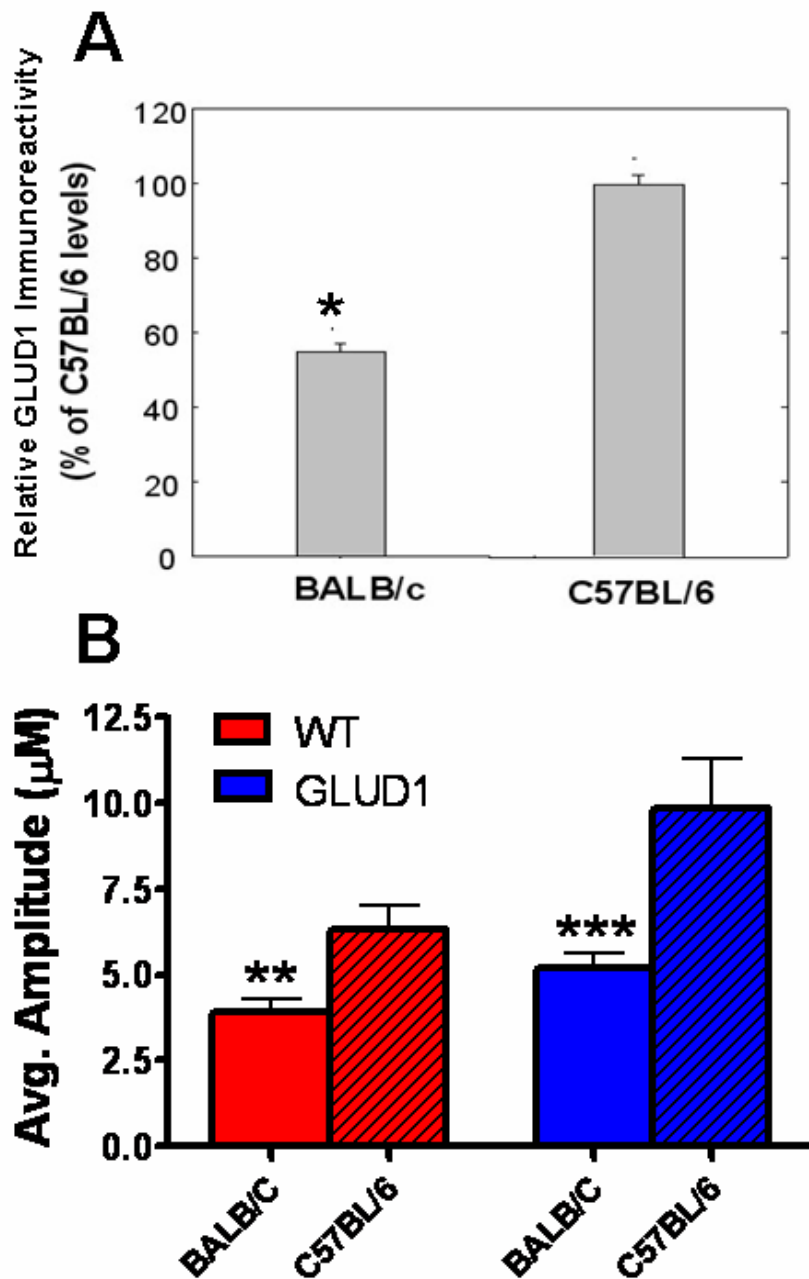


Figure 3.15: Endogenous GLUD1 Expression Correlates with Stimulus-Evoked Glu Release

A) C57BL/6 mice showed increased endogenous expression for the enzyme GLUD1 compared to BALB/C mice. BALB/C mice had approximately 55% endogenous activity of GLUD1 compared to C57BL/6 levels (* $p < 0.05$). Data table and blots supplied by the University of Kansas. B) Comparison of stimulus-evoked Glu release between WT and GLUD1 transgenic mouse groups. BALB/C WT mice released approximately 62% of the amount of Glu as compared to C57BL/6 WT mice (** $p < 0.01$) while BALB/C GLUD1 transgenic mice released approximately 53% of the amount of Glu compared to C57BL/6 GLUD1 transgenic mice (** $p < 0.001$).

compared to the C57BL/6 GLUD1 transgenic mice. The average maximal values of Glu release in the BALB/C GLUD1 transgenic mice were approximately 53 percent of the C57BL/6 GLUD1 transgenic mice. This further supports that an increase in gene copy number resulted in an increased stimulus-evoked Glu release.

A microarray study was conducted at the University of Kansas to determine any additional genes that were up or down regulated in the C57BL/6 mice due to the insertion of the pNSE-lacZ vector with the GLUD1 cDNA insert. Several genes were upregulated two fold in the C57BL/6 GLUD1 transgenic mice compared to C57BL/6 WT mice (Table 3.2). The ones related to glutamatergic neurotransmission involved a mGluR (mGluR7), two different subunits for the NMDA receptor (NMDA2A and NMDA2B), and a calcium binding protein (Calbindin-28K).

Discussion

These were the first studies demonstrated by our laboratory that our MEAs could be used to reliably study Glu in a mouse model. Local application of 70 mM KCl as well as 5 mM Glu resulted in Glu signals that were robust and reproducible in both the WT and GLUD1 transgenic mouse strains. We observed important differences between these two groups of mice that were similar across strains. First, local application of 70 mM KCl resulted in significantly ($p < 0.05$) increased release of Glu compared to WT littermates in both the BALB/C and C57BL/6 mice. When a depth profile of the Str was analyzed, there were regional differences in the amount of stimulus-evoked Glu release. Next, we determined that the rate of uptake for stimulus-evoked Glu release as well as local application of 5 mM Glu was similar in both the WT and GLUD1 transgenic mice for both mouse strains. As our MEA methodology advanced, we were able to use self-referencing techniques to determine resting Glu levels in the BALB/C mouse. There was no significant difference in resting Glu levels in the BALB/C WT and GLUD1 transgenic mice. A DNA microarray study revealed that some genes were upregulated 2 fold in the C57BL/6 GLUD1 transgenic mice compared to the WT mice.

Table 3.2: Microarray Comparison of Transgenic to WT GLUD1 C57BL/6 Mice

Gene	Protein	Transgenic/WT Gene Ratio
Grm7	mGluR7	2.092
Grin2a	NMDA2A	2.058
Grin2b	NMDA2B	2.058
Calb1	Calbindin-28K	2.056

A microarray study revealed that additional genes were upregulated two-fold in the GLUD1 transgenic C57BL/6 mouse group compared to WT littermates.

GLUD1 catalyzes a reversible reaction that favors Glu formation from ammonia and α -ketoglutarate (Yudkoff *et al.*, 1991; Kanamori and Ross, 1995; Bak *et al.*, 2006). Unfortunately, no specific modulators for this enzyme exist, which has prevented appropriate *in vivo* study of the role this enzyme plays on glutamatergic neurotransmission. For this reason, a mouse model was created that overexpresses neuronal GLUD1 in both the C57BL/6 and BALB/C mouse strains to elucidate the role of GLUD1 on the neuronal contribution of Glu. Local application of 70 mM KCl resulted in significantly increased Glu release in the GLUD1 transgenic mice compared to WT mice for both C57BL/6 and BALB/C mouse strains. In addition, when a depth profile of the Str was conducted, there were specific depths where Glu release was significantly increased in the GLUD1 transgenic mice compared to the WT mice. In the C57BL/6 GLUD1 transgenic mice, depths -2.25 and -3.25 mm showed significantly increased Glu release compared to the WT mice. Only depth -3.25 mm in the BALB/C GLUD1 transgenic mice had significantly increased stimulus-evoked Glu release compared to WT mice. Depth -2.25 mm was elevated in the BALB/C GLUD1 transgenic mice compared to WT mice, however, it was not significant. This demonstrated the advantage of our recording capability to measure discrete regions within a large brain structure. Other *in vivo* recording techniques, such as microdialysis, are too large to perform this type of analysis. Because of this advantage, we have shown that the Str is not a homogenous structure for Glu release and regional differences exist. More importantly, this was the first study that shows upregulation of a Glu metabolizing enzyme was responsible for increased neuronal release of Glu.

The uptake rate for stimulus-evoked Glu release as well as the clearance of exogenously applied Glu was determined for both mouse strains. There was no significant difference in the stimulus-evoked Glu uptake rate or clearance of exogenously applied Glu observed between GLUD1 transgenic and WT mice in both strains. However, we did observe that the uptake rate of exogenously applied Glu was increased in both strains of the GLUD1 transgenic and WT mice when compared to the uptake of stimulus-evoked Glu. Since Glu uptake was

driven by electrochemical gradients across the cell membrane to produce a negative membrane potential (Takahashi *et al.*, 1997; Doble, 1999), depolarization of glial membranes by the local application of 70 mM KCl may be responsible for the decreased stimulus-evoked Glu uptake compared to the clearance rate of exogenously applied Glu. Despite this, both chemicals showed the same trends, which indicated that Glu uptake was similar between the GLUD1 transgenic and WT mice. Even though the GLUD1 transgenic mice released significantly more Glu compared to WT mice during chemical stimulation, they removed this Glu from the extracellular space at the same rate as WT mice. This meant that extracellular concentrations of Glu in the GLUD1 transgenic mice were elevated for longer periods of time upon stimulation compared to WT mice. Over a prolonged period of time, these elevated levels may lead to slow-indirect excitotoxicity.

Using our self-referencing recording techniques, we were able to record resting Glu levels in the Str of BALB/C WT and GLUD1 transgenic mice. Resting Glu levels were similar in the WT and GLUD1 transgenic BALB/C mice. This indicated that ambient levels of Glu were not elevated in the GLUD1 transgenic mice despite the fact that more Glu was released upon stimulation. One possible explanation for this finding was that resting Glu levels were analyzed in anesthetized mice. Anesthetics such as urethane, which was used in these experiments, exert their effects by enhancing inhibitory synaptic neurotransmission as well as inhibiting excitatory neurotransmission (Hara and Harris, 2002). Our lab has also demonstrated that urethane significantly decreased resting Glu levels by 58 percent (Rutherford *et al.*, 2007). Because of these two factors, anesthetized animal models may not provide accurate measures of resting Glu and future experiments in awake, freely moving GLUD1 transgenic mice are needed to better determine unstimulated levels of Glu.

To determine additional genes that may have been up or down regulated due to the introduction of the GLUD1 vector, a DNA microarray study was conducted on the C57BL/6 mouse strain at the University of Kansas. This study revealed that gene expression encoding several receptors for Glu signaling were

increased two fold (table 3.2). The mGluR7 gene was increased. This is a G-protein coupled inhibitory autoreceptor found on both pre- and post-synaptic neurons. In addition, two subunits of the NMDA receptor, the NMDA2A and NMDA2B were increased. The NMDA2A receptor is the subunit for which Glu binds to open the calcium pore (Furukawa *et al.*, 2005). Finally, the gene for an intracellular calcium binding protein, Calbindin-28K, was also upregulated. Calbindin-28K buffers high levels of intracellular calcium, but Calbindin-28K is found in low levels in motor neurons and is non-existent in spinal motor neurons (Van Den Bosch *et al.*, 2006). While the microarray study did not correlate gene copy number to actual protein levels, it seemed evident that the GLUD1 transgenic mice were attempting to compensate for the increased amount of stimulus-evoked Glu release and the possibility of slow, indirect excitotoxicity.

Upon completion of the study with the GLUD1 transgenic C57BL/6 mouse, it was decided to let a small group of the transgenic mice age to determine if any phenotypic traits developed. At 16 months of age, we noticed that the mice developed lower limb abnormalities that affected their movement, gait, and righting behavior. As of yet, BALB/C mice have not displayed such characteristics. Upon further histological examination conducted at the University of Kansas, it was determined that the GLUD1 transgenic mice had severe atrophy of Betz cells in layer IV of the motor cortex (figure 3.16) as well as atrophy of the lower motor neuron in the ventral horn of the spinal cord (figure 3.17). These two areas were associated with motoric movement and helped to explain the motor deficits seen in the GLUD1 transgenic mice at 16 months of age.

The histology from the University of Kansas was not easily explained by itself, however, taken as a whole with our *in vivo* amperometric data we have proposed a working hypothesis as outlined in figure 3.18. Upregulation of GLUD1 genes leads to production of more GLUD1 protein. This in turn lead to the synthesis of Glu from α -ketoglutarate and subsequent increased vesicle packaging of Glu in glutamatergic neurons. With increased amounts of Glu in

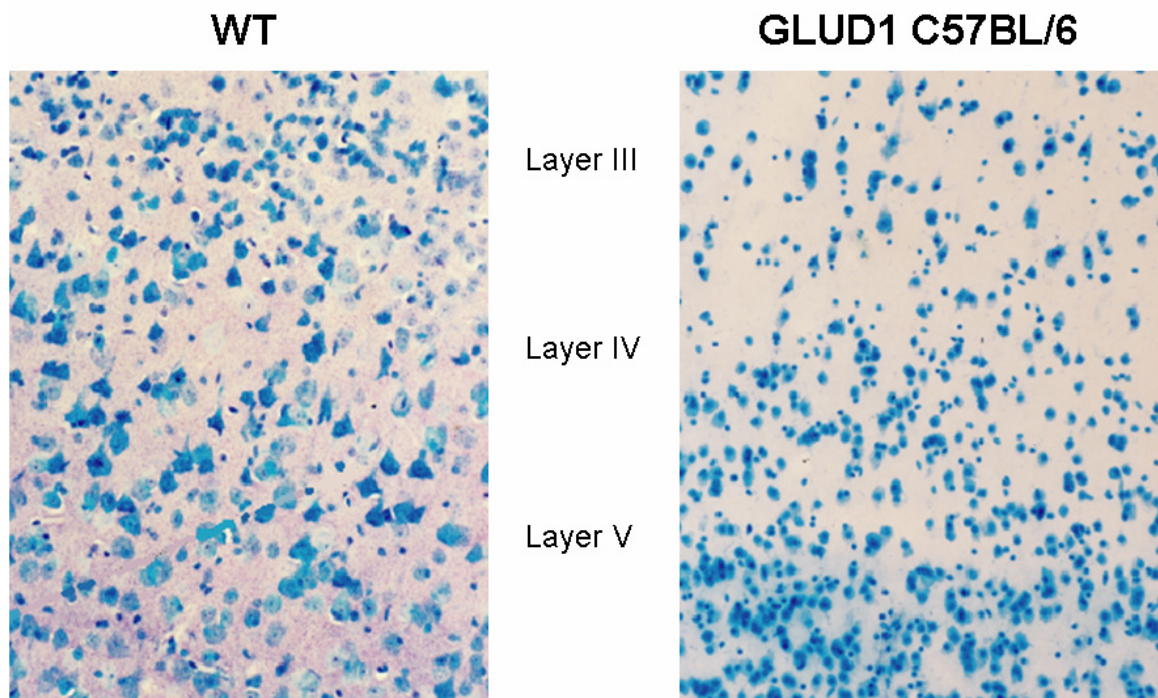


Figure 3.16: C57BL/6 GLUD1 Transgenic Mouse Motor Cortex Histology

The motor cortex of WT (left) and GLUD1 transgenic (right) C57BL/6 mice were stained for neurons. GLUD1 transgenic mice showed severe atrophy of the large pyramidal neurons in Layer IV of the motor cortex associated with motor movement. Staining and figures courtesy of the University of Kansas, Dr. Elias K. Michaelis' laboratory.

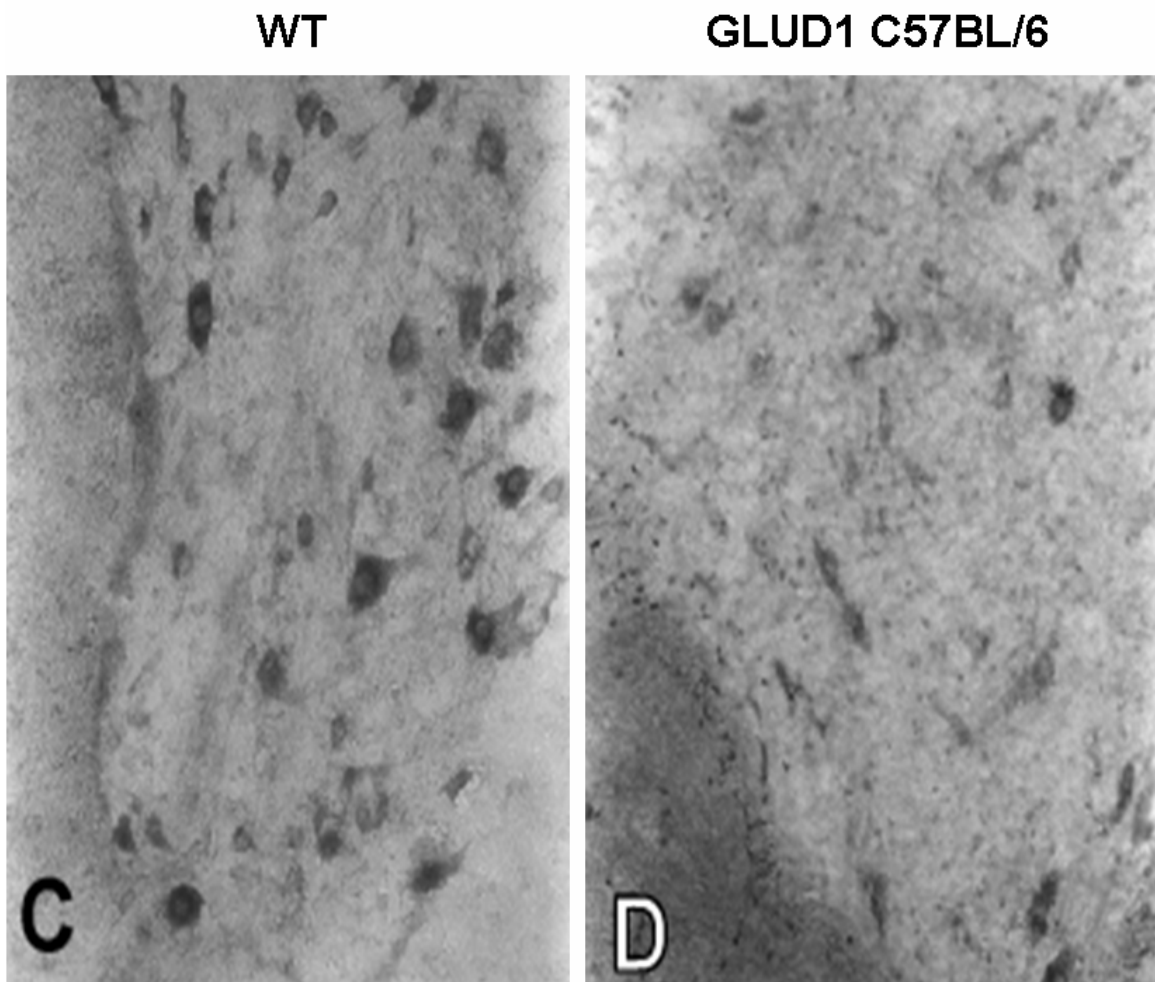


Figure 3.17: C57BL/6 GLUD1 Transgenic Mouse Spinal Cord Histopathology

The ventral horn of the spinal cord in WT (left) and GLUD1 transgenic (right) C57BL/6 mice were stained for neurons. GLUD1 transgenic mice showed severe atrophy of the large lower motor neurons in the ventral horn of the spinal cord associated with motor movement. Staining and figures courtesy of the University of Kansas, Dr. Elias K. Michaelis' laboratory.

vesicles, the GLUD1 transgenic mice release more Glu into the extracellular space upon stimulus-evoked Glu release as compared to WT mice as shown with our amperometry data. Recent data have shown that pre-synaptic cytoplasmic Glu availability affects the mean quantal amplitude, which implies increased vesicular filling of Glu and more Glu released upon depolarization. (Ishikawa *et al.*, 2002; Wilson *et al.*, 2005; Wu *et al.*, 2007). Our amperometry data also showed that Glu uptake was the same rate in the GLUD1 transgenic mice compared to WT mice. This means that more Glu is available in the synaptic cleft to activate iGluRs and mGluRs; in particular the NMDA receptor, whose Glu binding domain has been shown by DNA microarray data to be upregulated in GLUD1 transgenic mice. Since motor neurons have little to no calcium sequestering proteins (Van Den Bosch *et al.*, 2005) mitochondria are forced to buffer the intracellular calcium. Over time, if the mitochondria become damaged by excessive intracellular calcium, proteases, oxygenases, and reactive oxygen species (ROS) form, which are key mediators of excitotoxic cell death (Nicholls and Budd, 2001). This may explain the severe motor impairments and histological motor neuron atrophy staining seen in GLUD1 transgenic mice at 16 months of age.

Using *in vivo* amperometry with our Glu selective MEAs, we demonstrated that upregulation of GLUD1 led to a significant increase in stimulus-evoked Glu release in both the C57BL/6 and BALB/C mouse strains. Stimulus-evoked Glu release was also significantly higher in the C57BL/6 mouse strain compared to the BALB/C strain possibly due to the higher endogenous activity of GLUD1 in C57BL/6 mice. We hypothesize that this increased stimulus-evoked Glu release caused excitotoxicity over time (16 months) that selectively damaged motor neurons in both the motor cortex and spinal cord leading to severe motoric deficits in the GLUD1 transgenic mice. Despite the fact that stimulus-evoked Glu release was elevated in the BALB/C mice, it was not sufficient to cause excitotoxicity since the same phenotypic traits were not observed in this strain of mouse. To our knowledge, the GLUD1 transgenic C57BL/6 mouse model was the first animal model that showed spontaneous motor neurodegeneration.

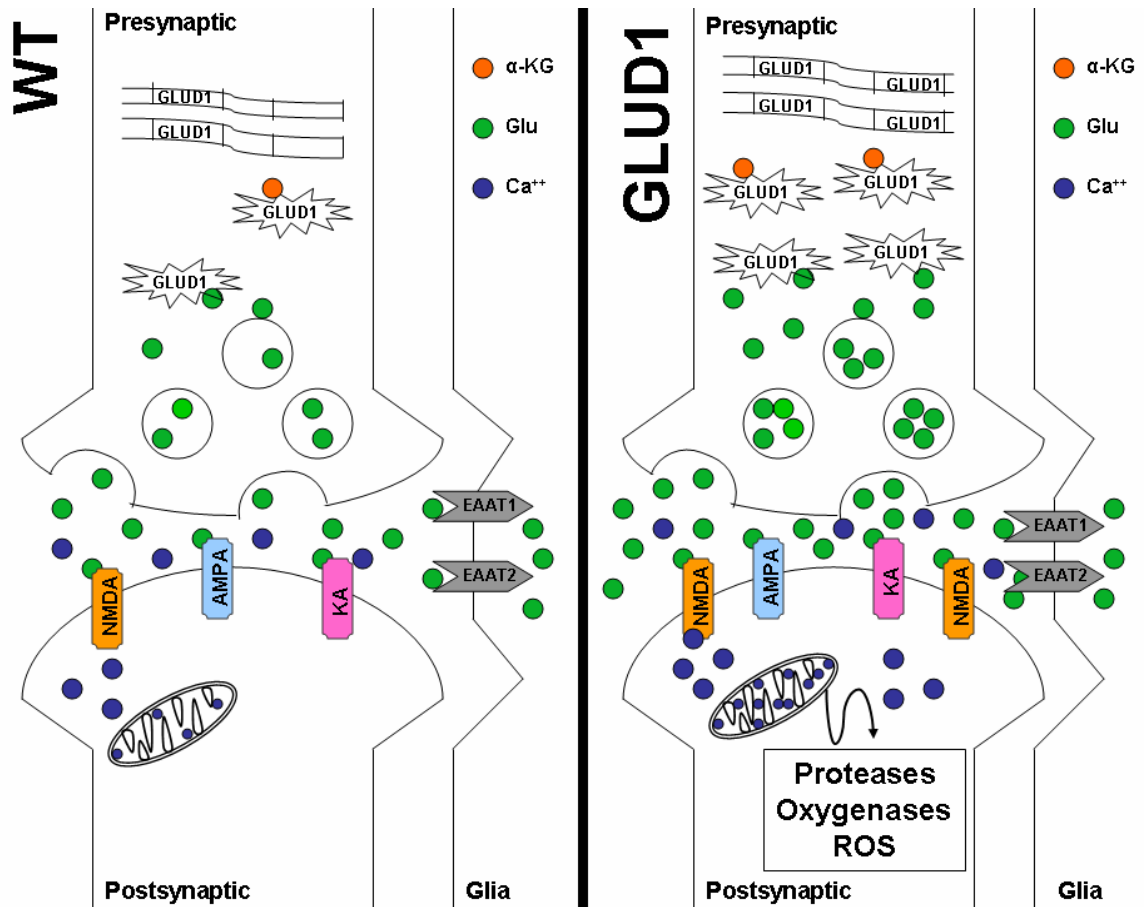


Figure 3.18: Proposed Excitotoxic Mechanism for GLUD1 C57BL/6 Mice

Our proposed hypothesis of the excitotoxic mechanism underlying the motor deficits seen in GLUD1 C57BL/6 transgenic mice. The above figure depicted two synapses, one from a healthy, WT mouse (left) and the other synapse from GLUD1 transgenic C57BL/6 mice (right). Upregulation of GLUD1 genes led to production of more GLUD1 protein. This in turn led to the synthesis of Glu from α -ketoglutarate and subsequent increased vesicle packaging of Glu in glutamatergic neurons. With increased amounts of Glu in vesicles, the GLUD1 transgenic mice released more Glu into the extracellular space after stimulus compared to WT. Glu uptake was similar between GLUD1 transgenic mice and WT mice. More Glu was available in the synaptic cleft of GLUD1 transgenic mice to activate iGluRs and mGluRs; in particular the NMDA receptor, whose gene for the Glu binding domain was upregulated in GLUD1 transgenic mice. Since motor neurons had little to no calcium sequestering proteins, mitochondria were forced to buffer the intracellular calcium. Over time, if the mitochondria became damaged by excessive intracellular calcium, proteases, oxygenases, and reactive oxygen species (ROS) formed, which were key mediators of excitotoxic cell death.

Copyright © Kevin Nicholas Hascup

Chapter Four: Glutamate Dynamics in Glutamate Pyruvate Transaminase Transgenic and Knockout C57BL/6 Mice

Introduction

The glutamate-glutamine cycle is a well understood mechanism that is essential for glutamatergic neurotransmission. Upon depolarization and vesicular release of Glu, the neurotransmitter is taken up into astrocytes by high affinity transporters (Danbolt, 2001). Once in the astrocytes, Glu is degraded into glutamine by glutamine synthetase that is localized only in astrocytes. Glutamine is not neurotoxic and therefore it can be safely transported out of the astrocytes through System N located on astroglial cells. In the extracellular space, glutamine is transported into neurons through System A (Bak *et al.*, 2006). When returned to the neuron, glutamine is converted back into Glu by PAG, which is located on the inner mitochondrial membrane (Kvamme *et al.*, 2000). This Glu formed is returned to the cytosol and subsequently packaged into vesicles for future neurotransmitter signaling.

Since neurons are incapable of net synthesis of Glu from glucose (Waagepetersen *et al.*, 2005), the Glutamate-glutamine cycle was previously thought to provide neurons with all the Glu necessary for neurotransmitter signaling. Because of this theory, the glutamate-glutamine cycle was originally thought to operate in a stoichiometric one-to-one ratio. For every Glu released, one glutamine was transported into neurons to replenish the neurotransmitter pool of Glu. However, recent evidence suggests this theory is simplistic (Broman *et al.*, 2000; Fonnum, 1993; Peng *et al.*, 1993; Danbolt, 2001; Waagepetersen *et al.*, 2000; Hertz, 2004; Waagepetersen *et al.*, 2005) due to recent ¹³C NMR data that suggests one-third of the Glu in the Glutamate-glutamine cycle is newly synthesized from glucose (Gruetter *et al.*, 2001; Hertz, 2004). This indicates that other enzymes must be responsible for synthesis and degradation of Glu for the neurotransmitter pool. Glu is closely related metabolically to the TCA cycle (Hertz, 2004; Waagepetersen *et al.*, 2005). For example, when Glu is transported into astrocytes, it can be metabolized into glutamine by glutamine

synthetase or transaminated into α -ketoglutarate. Alpha-ketoglutarate can then enter the TCA cycle where it eventually metabolizes into malate, which decarboxylates into pyruvate and reduces to lactate. Lactate can be transported out of astrocytes and into neurons by monocarboxylate transporters (Gladden, 2004). Once in the neurons, lactate can oxidize to pyruvate and either re-enter the TCA cycle or transaminates back into Glu for neurotransmitter packaging and signaling (Refer to figure 1.2). This example demonstrates one of the many possible fates of Glu and is used to show the complicated competition for Glu between cellular energy demands and neurotransmitter signaling. Furthermore, Hassel and Bråthe (2000) demonstrate that it is possible to obtain Glu formation independent of glutamine. This implies that enzymes other than PAG and glutamine synthetase are responsible for *de novo* synthesis or degradation of Glu. Two such Glu metabolizing enzymes found in neurons are GPT and GLUD1. Chapter Three highlighted the effects of upregulation of GLUD1 on increasing Glu for neurotransmitter release. We wanted to characterize how upregulation or knockout of the GPT gene affects the neurotransmitter pool of Glu in the mouse Str.

GPT exists as a dimer with a molecular mass of approximately 100 kDa in most species (Saier and Jenkins, 1967). The enzyme catalyzes a reversible transaminase reaction using pyruvate as a co-substrate to form alanine and α -ketoglutarate (Figure 1.3A). Biochemical studies show GPT activity in both the cytosol and mitochondria of astrocytes and neurons (Balazs and Haslam, 1965; Erecińska *et al.*, 1994), but the greatest activity is found in astrocytes of the cerebral cortex (Westergaard *et al.*, 1993). It is debated throughout the literature whether GPT favors Glu degradation (Saier Jr. and Jenkins, 1967; Ruščák *et al.*, 1982; Erecińska *et al.*, 1994) or synthesis (Peng *et al.*, 1991, 1993; Schousboe *et al.*, 2003). This process most likely depends on the amount of substrates/products available. However, Matthews and colleagues (2000, 2003) demonstrated that GPT is an active Glu degrading enzyme that acts as an effective neuroprotectant in cell culture models of exogenous and endogenous Glu excitotoxicity. Unfortunately, GPT does not exist in the extracellular space

and, due to its large size, is unable to cross the blood-brain barrier. This makes it an unsuitable candidate for excitotoxicity therapeutics; nevertheless these studies demonstrate the propensity for GPT to metabolize Glu.

Due to the broad spectrum of transaminase molecules found in the brain, there are no specific modulators for this enzyme. To determine the role GPT plays on the neurotransmitter pool of Glu, two different mouse models were created. The first model has upregulated activity of GPT, while the second model has removed this gene altogether. In the present study we examined the differences in stimulus-evoked Glu release and reuptake (using an isotonic solution of 70 mM KCl and 5 mM Glu; pH 7.4) in the Str of GPT transgenic as well as knockout (KO) C57BL/6 mice. Stimulus-evoked Glu release provides an indication as to any differences upregulation or KO of GPT causes in the amount of Glu available for neuronal release. Examining reuptake of stimulus-evoked Glu release and clearance of exogenously applied Glu provides information regarding Glu transporter availability or function in the transgenic and KO mice compared to WT controls.

Methods

All transgenic mice were developed at the University of Kansas by Dr. Elias K. Michaelis's laboratory. A rat GPT transgene was inserted into the mouse genome under the control of the Neuronal specific enolase (NSE) promoter. The NSE promoter has been shown to be expressed only in neurons of the brain and spinal cord (Choi *et al.*, 1992; Peel *et al.*, 1997). Transgenic mice were generated by injecting mouse oocytes (C57BL/6J-SJL hybrid) with vectors containing cDNA of rat GPT placed under the control of the NSE promoter. This promoter was excised from the pNSE-LacZ vector by first digesting the SV40 polyA tail of pNSE-LacZ vector and cloning it into pGEM-7Z. The NSE promoter was also excised and cloned into the modified pGEM-7Z. Finally, a GPT open reading frame was cloned into the pNSE-GEM-7Z to create the pNSE-GPT vector for the GPT transgenic mice. To create the GPT KO line, a nonfunctional rat GPT open reading frame was cloned into the pNSE-GEM-7Z vector. The vector was digested, the DNA recovered, and microinjected into the

nucleus of fertilized mouse oocytes to generate either the GPT transgenic or KO mice. Oocytes were transferred to surrogate C57BL/6 mice. Pups carrying the transgene were identified by PCR and Southern Blot Analysis. Progeny were eventually backcrossed into a C57BL/6 mouse strain. Gene copy number was assayed by Southern Blot analysis and determined to be upregulated three to four-fold in the transgenic mouse strains compared to WT littermates through the first four generations of breeding.

GPT transgenic and KO C57BL/6 mice were transported to the University of Kentucky and housed as described in Chapter Two. For the GPT C57BL/6 mice, males between the ages of 8 and 12 months were used at the time of recordings. For the GPT KO study, both male and female mice were studied. Only the results from the female analysis were included in this chapter. Breeding prevented sufficient numbers of male homozygous mice for complete analysis. All data regarding male GPT KO mice are found in Appendix A. Mice were given 3 i.p. injections of 12.5% urethane for a total dose of 1.25 g/kg. All studies were conducted in the Str. Glu recordings were conducted using enzyme-based MEAs with a sampling rate of 1 Hz as previously described in Chapter Two. At the time of our studies in the C57BL/6 GPT transgenic mice, self-referencing techniques were not utilized. As our MEA technology progressed, self-referencing was routinely utilized including the study with GPT KO mice. A craniotomy was performed over both striatal hemispheres and MEAs were stereotaxically placed using the coordinates from Paxinos and Franklin (2004) (AP: +0.9 mm; ML \pm 1.5, \pm 1.7 mm; DV: -2.25, -2.75, -3.25, -3.75 mm vs bregma) in order to create a depth profile of the Str. A glass micropipette with an internal diameter of 10-12 μ m was attached to the PCB and positioned among the four Pt recording sites, resting 50-100 μ m above the recording surface. Through this glass micropipette isotonic solutions of 70 mM KCl (70 mM KCl, 79 mM NaCl, 2.5 mM CaCl₂; pH 7.4) and 5 mM Glu (in 0.9% saline; pH 7.4) were locally applied to the surrounding brain tissue to study glutamatergic neurotransmission. Upon initial MEA placement, a stable baseline recording was obtained for at least 30 minutes prior to local application of solutions. When self-referencing MEAs were

used, resting Glu levels were calculated during this initial baseline time period. After the initial baseline recording, solutions were locally applied at regular 30 second intervals (for a total of 20 signals; 10 signals from each Pt recording site) to assess Glu dynamics at each dorsal ventral position. Due to the reproducibility of Glu signals *in vivo* (figure 4.1), all signals for a particular depth were averaged into a single data set for that depth. Data analysis involved a two-tailed student's t-test comparing GPT transgenic to WT mice. An ANOVA with a Tukey's post hoc test was used to analyze the GPT KO data to compare heterozygous and homozygous to control. All data was reported as mean \pm standard error of the mean and significance was defined as $p < 0.05$.

Results

In the C57BL/6 GPT transgenic and WT mice, local application of 70 mM KCl resulted in robust, reproducible Glu signals compared to baseline (figure 4.2). We did not observe any significant difference in the amount of Glu released between transgenic and WT mice. To quantitate this finding, we volume matched the amount of stimulus locally applied to both mouse groups. Only Glu signals that were elicited by 100 to 200 nl of 70 mM KCl were used for this analysis, therefore, no significant difference in the amount of stimulus applied was observed between the GPT transgenic (131 ± 7 nl) and WT (140 ± 6 nl) mice (figure 4.3A). When the average maximal amplitude of Glu release was quantitated, there was no significant difference in the amount of Glu released between WT (6.3 ± 0.7 μ M) and GPT transgenic (6.1 ± 0.9 μ M) mice (figure 4.3B). Using the same subset of signals, any striatal, depth-related alterations in stimulus-evoked Glu release were also examined (figure 4.4). The average Glu release was calculated at each depth (DV -2.25 to -3.75 mm) and compared amongst groups. No significant differences were seen within groups of mice across the different depths. On average, GPT transgenic mice released slightly more Glu compared to WT mice at depth -2.25, 3.25, and 3.75 mm; however, it was not a significant difference.

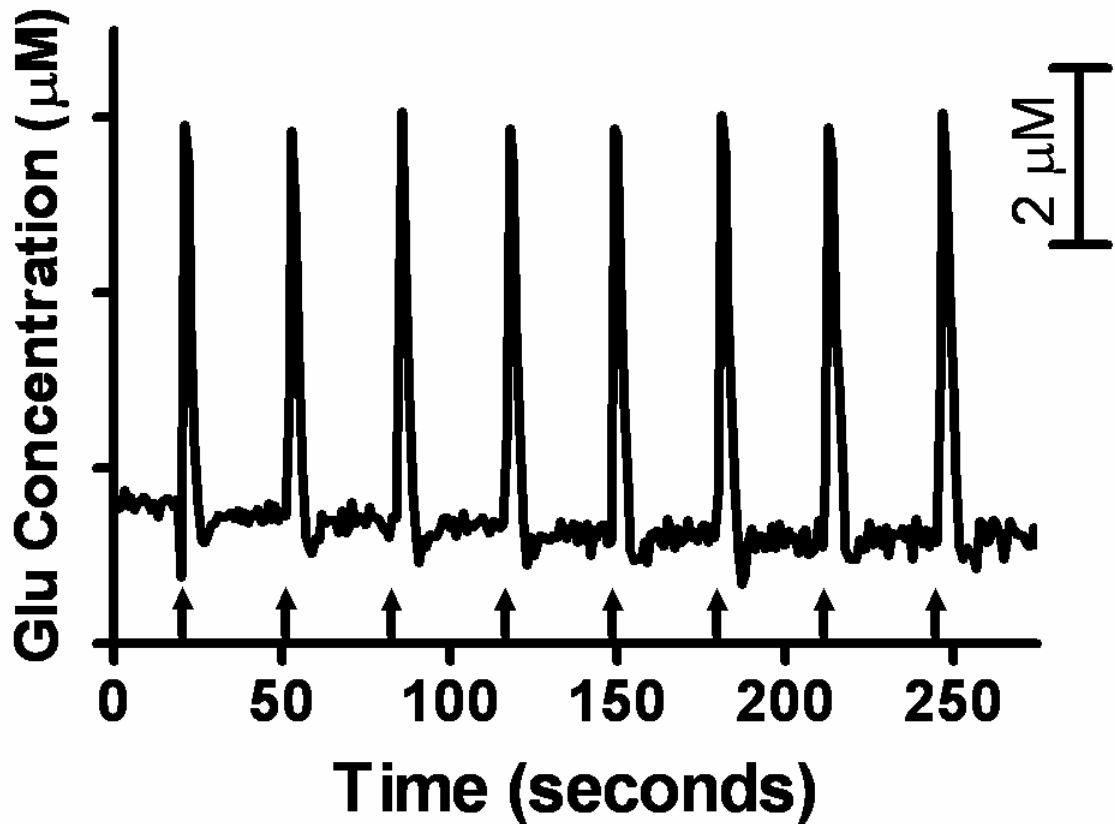


Figure 4.1: Reproducibility of Glu Signals from 70 mM KCl Depolarization

The above trace demonstrated the reproducibility of Glu signals elicited due to stimulus-evoked release by 70 mM KCl. Signals were from a GPT KO homozygous C57BL/6 mouse and taken at approximately 30 second intervals. The reproducibility of the Glu signals allowed us to average the individual signals for a given depth into a single data set. Arrows indicated time point of local application of an isotonic solution of 70 mM KCl.

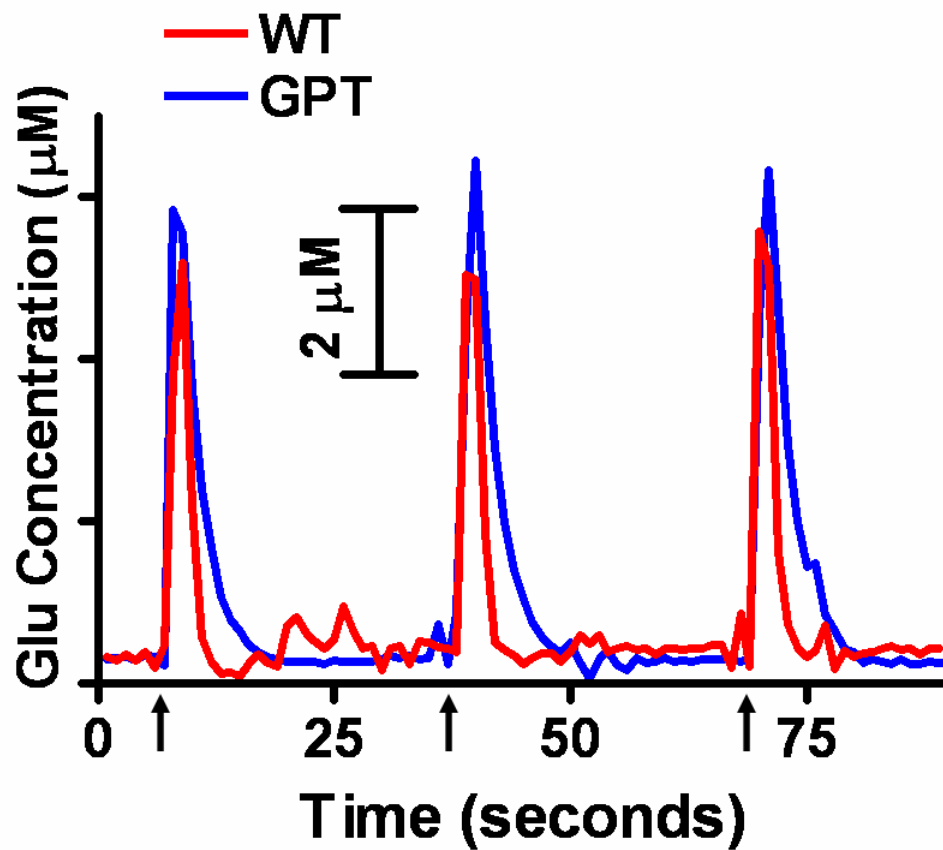


Figure 4.2: 70 mM KCl-Evoked Glu Release Traces in the GPT Transgenic Mice

Series of amperometric Glu recordings showing differences in volume matched stimulus-evoked Glu release in WT (red) and GPT (blue) transgenic mice. Note the reproducibility of the signal in both WT and GPT transgenic mice. Arrows indicate time points for local application of an isotonic solution of 70 mM KCl (pH 7.4).

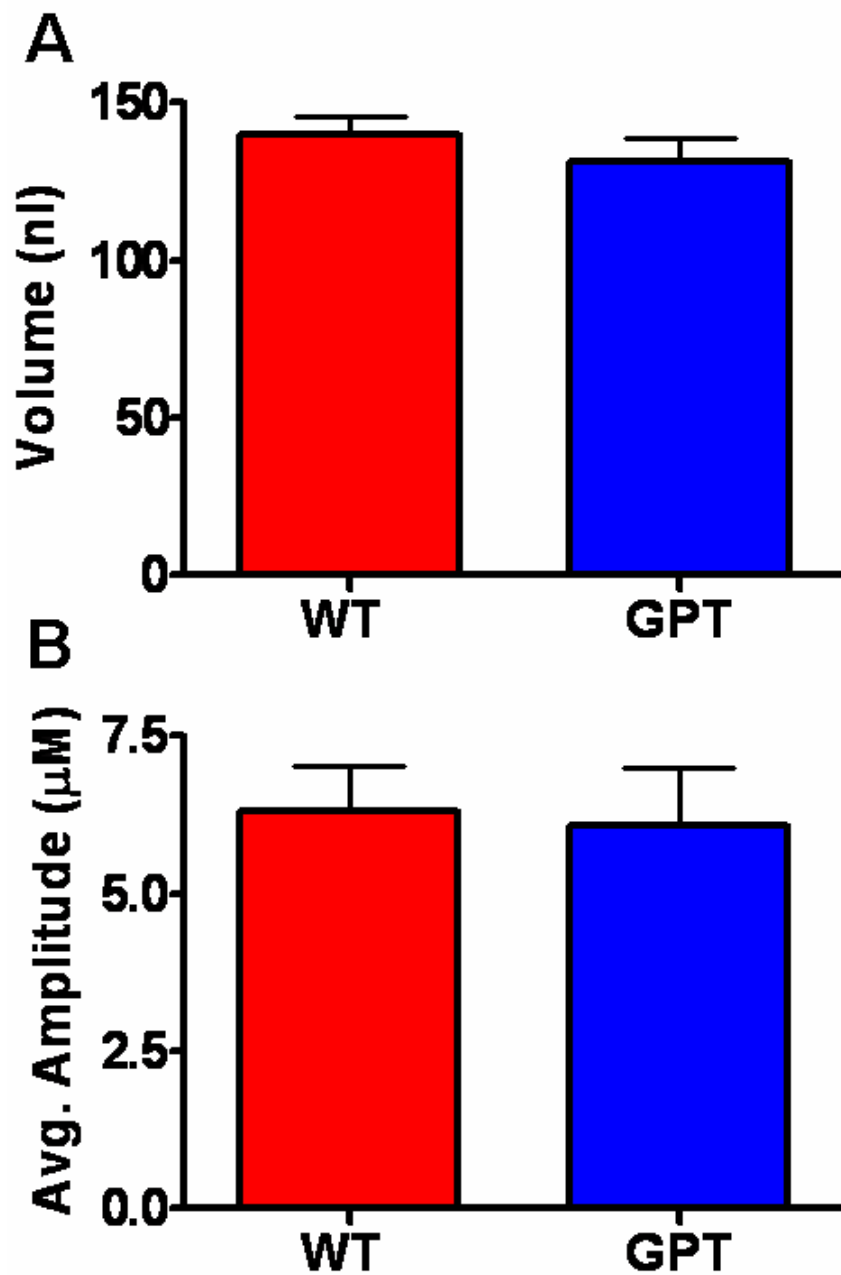


Figure 4.3: Stimulus-Evoked Glu Release in GPT Transgenic Mice

A) Only Glu signals that were elicited by 70 mM KCl whose volumes ranged between 100 and 200 nl were analyzed for the GPT transgenic (n=4) and WT (n=9) mice. Since the volumes were matched, no significant difference in the amount of stimulus locally applied was observed between WT (140 ± 6 nl) and transgenic mice (131 ± 7 nl). B) The average maximal amplitude of Glu released upon local application of 70 mM KCl was not significantly different in the GPT transgenic (6.1 ± 0.9 µM) compared to WT littermates (6.3 ± 0.7 µM).

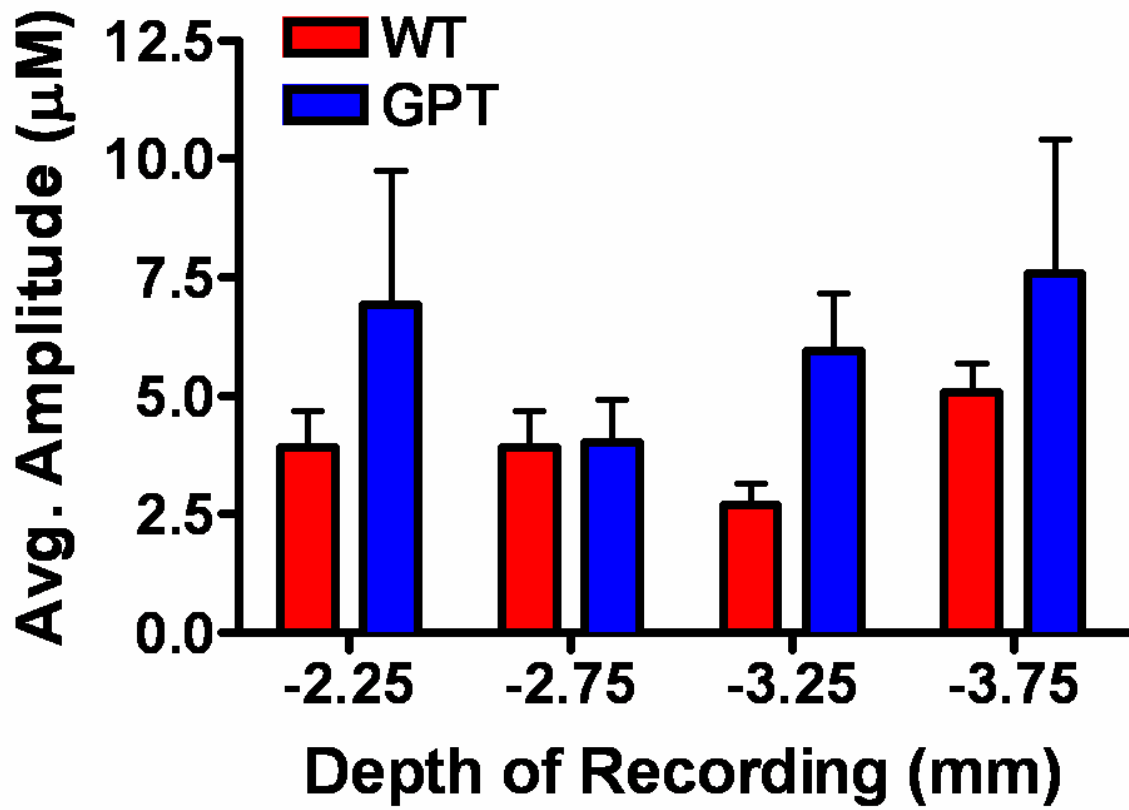


Figure 4.4: Stimulus-Evoked Glu Release Depth Profile in the GPT Transgenic Mouse

Average stimulus-evoked Glu release at different recording depths within the Str of GPT transgenic (n=4) and WT (n=9) mice. No significant differences were observed within groups of mice across the different depths. On average, GPT transgenic mice released slightly more Glu compared to WT mice at depths -2.25, 3.25, and 3.75 mm; however, it was not a significant difference. A two-tailed t-test was conducted at each depth for statistical analysis.

Since neurotransmitter uptake follows classical Michaelis-Menten kinetics (Nicholson, 1995) and was affected by the amount of available substrate, Glu uptake was analyzed by selecting a subset of signals with maximum release values were in the range of 3-13 μM . This range was chosen, because these peak Glu values were easily obtainable in both groups. Within this subset of signals, no significant difference in average maximum release of Glu was observed in WT ($6.3 \pm 0.4 \mu\text{M}$) and GPT transgenic ($6.3 \pm 0.6 \mu\text{M}$) mice (figure 4.5A). We did observe a significant decrease in the uptake rate of stimulus-evoked Glu seen between WT ($1.8 \pm 0.2 \mu\text{M}/\text{sec}$) and GPT transgenic ($0.7 \pm 0.1 \mu\text{M}/\text{sec}$) mice (figure 4.5B). Using the same subset of signals, we wanted to examine if there was any depth related alterations in the uptake rate of stimulus-evoked Glu release (figure 4.6). No significant differences were seen within groups of mice across the different depths. On average, GPT transgenic mice had slower uptake of Glu compared to WT mice over all depths. This decrease was only significant (** $p < 0.01$) at DV -3.25 mm between WT ($2.0 \pm 0.3 \mu\text{M}/\text{sec}$) and GPT transgenic ($0.6 \pm 0.2 \mu\text{M}/\text{sec}$) mice.

Because Glu transporters are electrogenic (Takahashi *et al.*, 1997; Doble, 1997) and the introduction of potassium ions and subsequent membrane depolarization changed their function, we wanted to determine transporter function without membrane depolarization. To do this, we locally applied an isotonic solution of 5 mM Glu (pH 7.4) and used a subset of Glu signals that were in the range of 3-13 μM , which was the same range used to analyze the uptake of stimulus-evoked Glu. Since we amplitude matched, there was no significant difference in the maximal amplitude of exogenously applied 5 mM Glu in the GPT transgenic ($8.3 \pm 0.6 \mu\text{M}$) and WT ($9.5 \pm 0.4 \mu\text{M}$) mice (figure 4.7A). Similar to the stimulus-evoked Glu uptake data, there was a significant decrease (** $p < 0.01$) in the clearance rate for locally applied 5 mM Glu for the GPT transgenic ($1.7 \pm 0.2 \mu\text{M}/\text{sec}$) mice compared to WT ($2.9 \pm 0.2 \mu\text{M}/\text{sec}$) mice (figure 4.7B). Using the same subset of signals, we wanted to examine if there was any depth related alterations in the clearance of exogenously applied Glu (figure 4.8). No significant differences were seen within groups of mice across the different

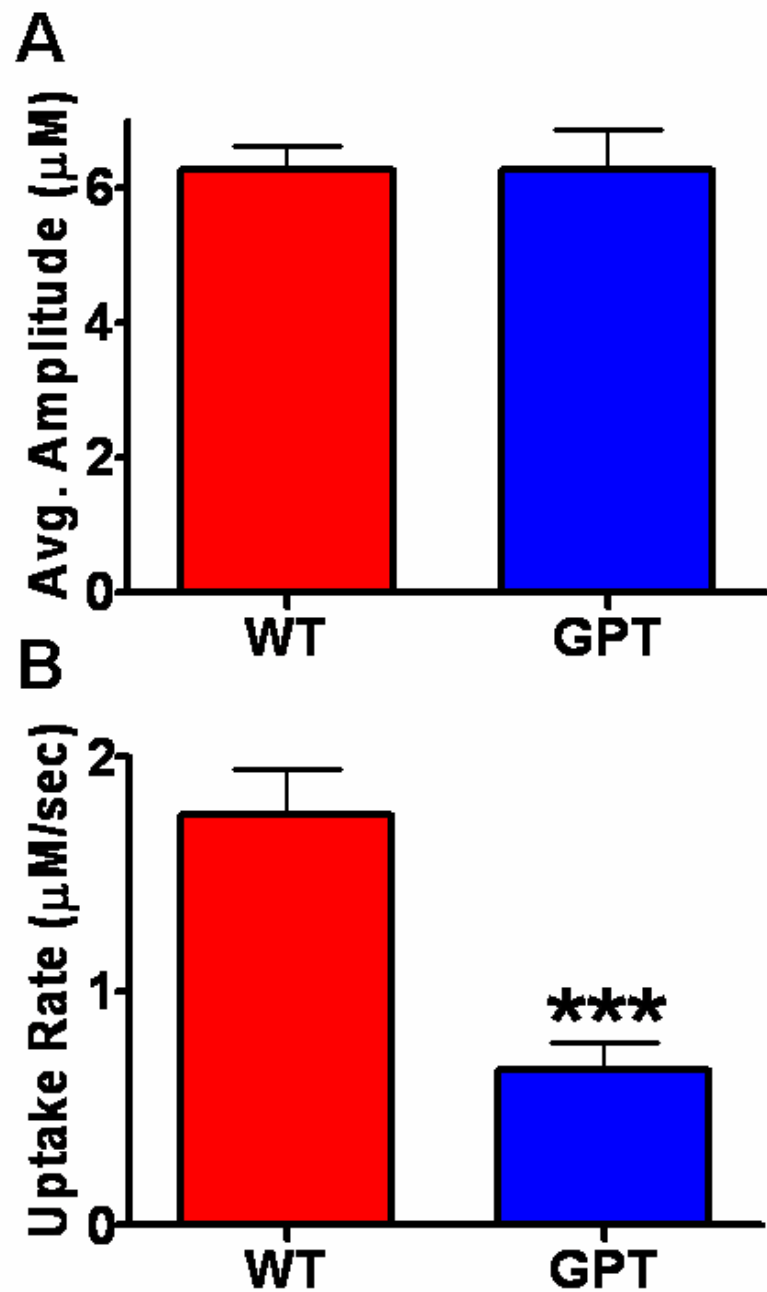


Figure 4.5: Stimulus-Evoked Glu Uptake in the GPT Transgenic Mouse Groups

A) A subset of Glu signals were examined whose average maximal amplitude fell in a range of 3-13 μM for both the GPT transgenic (n=4) and WT (n=9) mice. No significant difference was observed between WT ($6.3 \pm 0.4 \mu\text{M}$) and GPT transgenic ($6.3 \pm 0.6 \mu\text{M}$) mice. B) When the uptake rate of stimulus-evoked Glu was examined, GPT transgenic ($0.7 \pm 0.2 \mu\text{M}/\text{sec}$) mice cleared Glu significantly (***) slower compared to WT ($1.8 \pm 0.2 \mu\text{M}/\text{sec}$) mice.

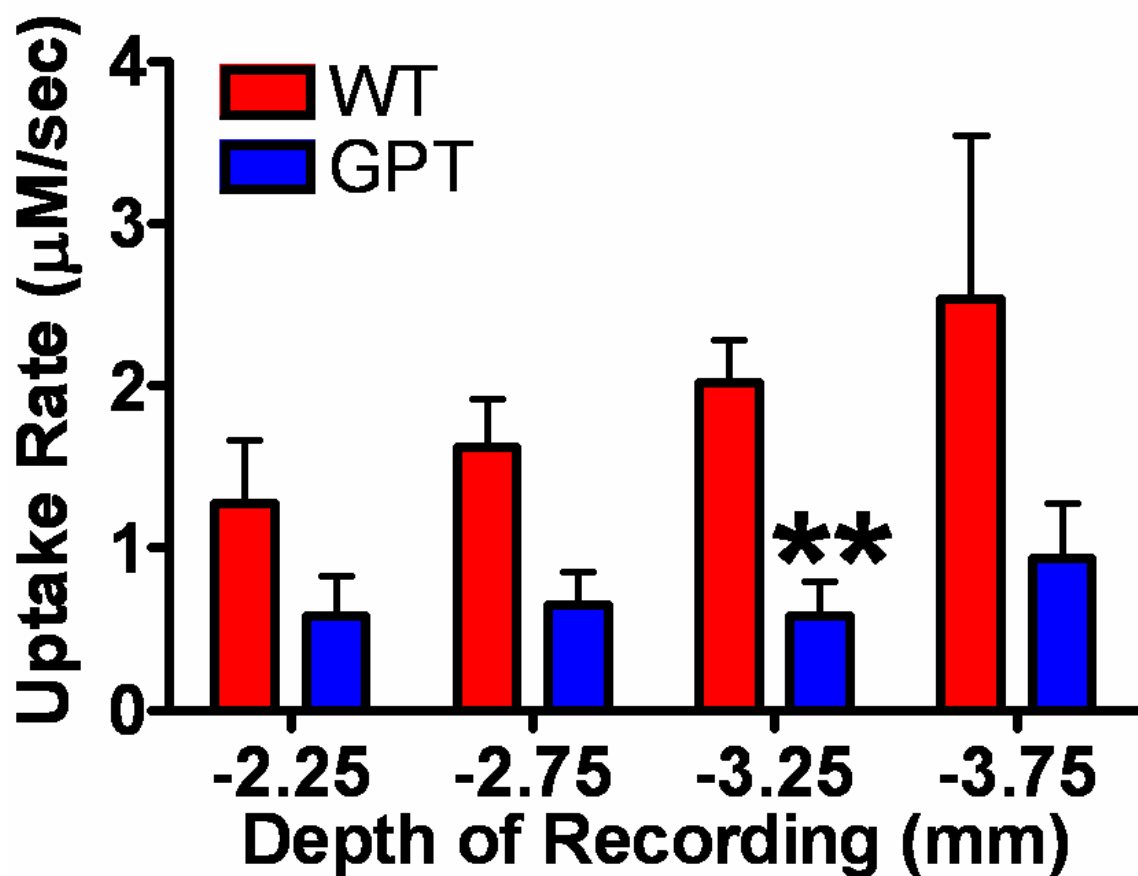


Figure 4.6: Stimulus-Evoked Glu Uptake Depth Profile in the GPT Transgenic Mouse

Average stimulus-evoked Glu release at different recording depths within the Str of GPT transgenic (n=4) and WT (n=9) mice. No significant differences were observed within groups of mice across the different depths. On average, GPT transgenic mice had slower uptake of Glu compared to WT mice across all depths. This decrease was only significant (**p<0.01) at DV -3.25 mm between WT (2.0 ± 0.3 µM/sec) and GPT transgenic (0.6 ± 0.2 µM/sec) mice. A two-tailed t-test was conducted at each depth for statistical analysis.

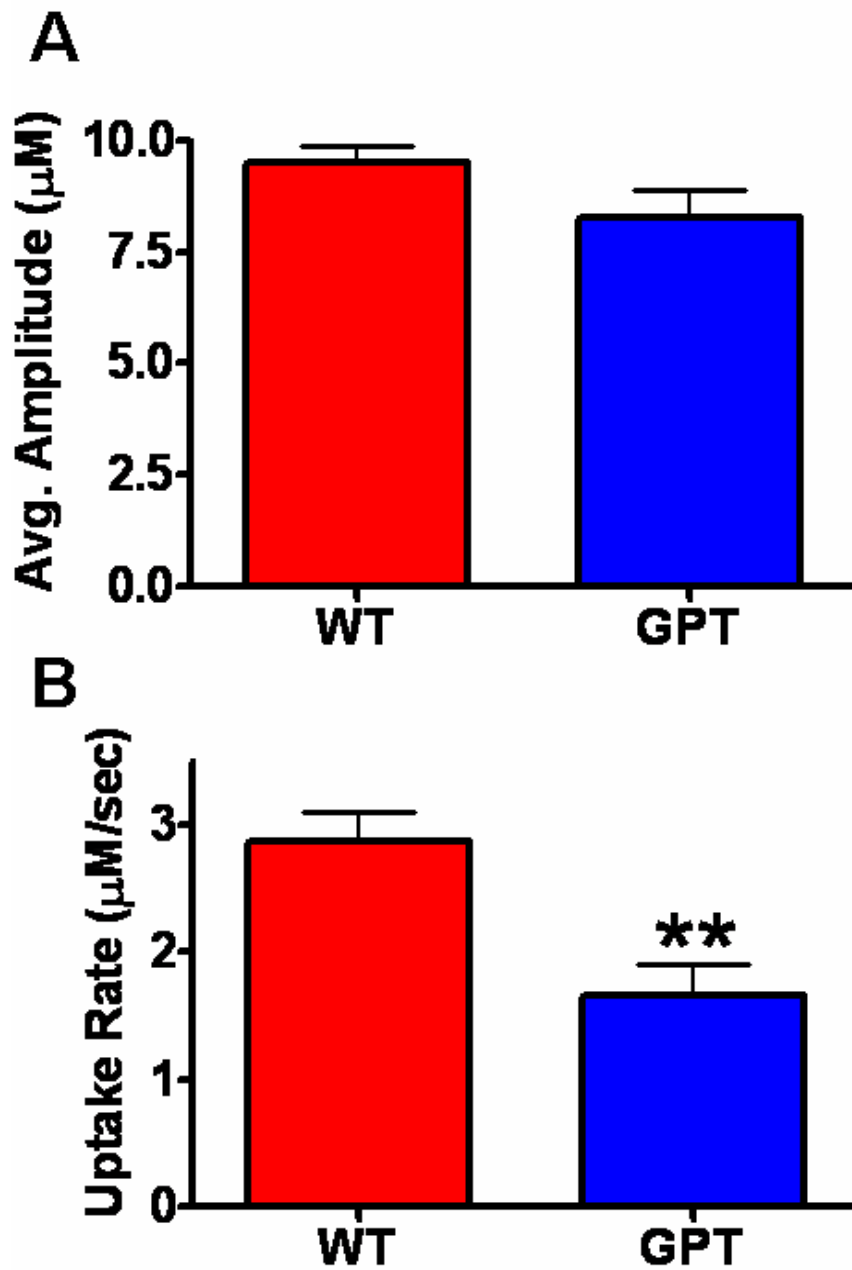


Figure 4.7: 5 mM Glu Clearance in the GPT Transgenic Mouse Groups

A) A subset of Glu signals were examined whose average maximal amplitude fell in a range of 3-13 μM for both the GPT transgenic (n=4) and WT (n=9) mice. No significant difference was observed between WT ($9.5 \pm 0.4 \mu\text{M}$) and GPT transgenic ($8.3 \pm 0.6 \mu\text{M}$) mice. B) When the clearance of exogenously applied Glu was examined, GPT transgenic ($1.7 \pm 0.2 \mu\text{M}/\text{sec}$) mice cleared Glu significantly (**p < 0.01) slower than WT ($2.9 \pm 0.2 \mu\text{M}/\text{sec}$) mice.

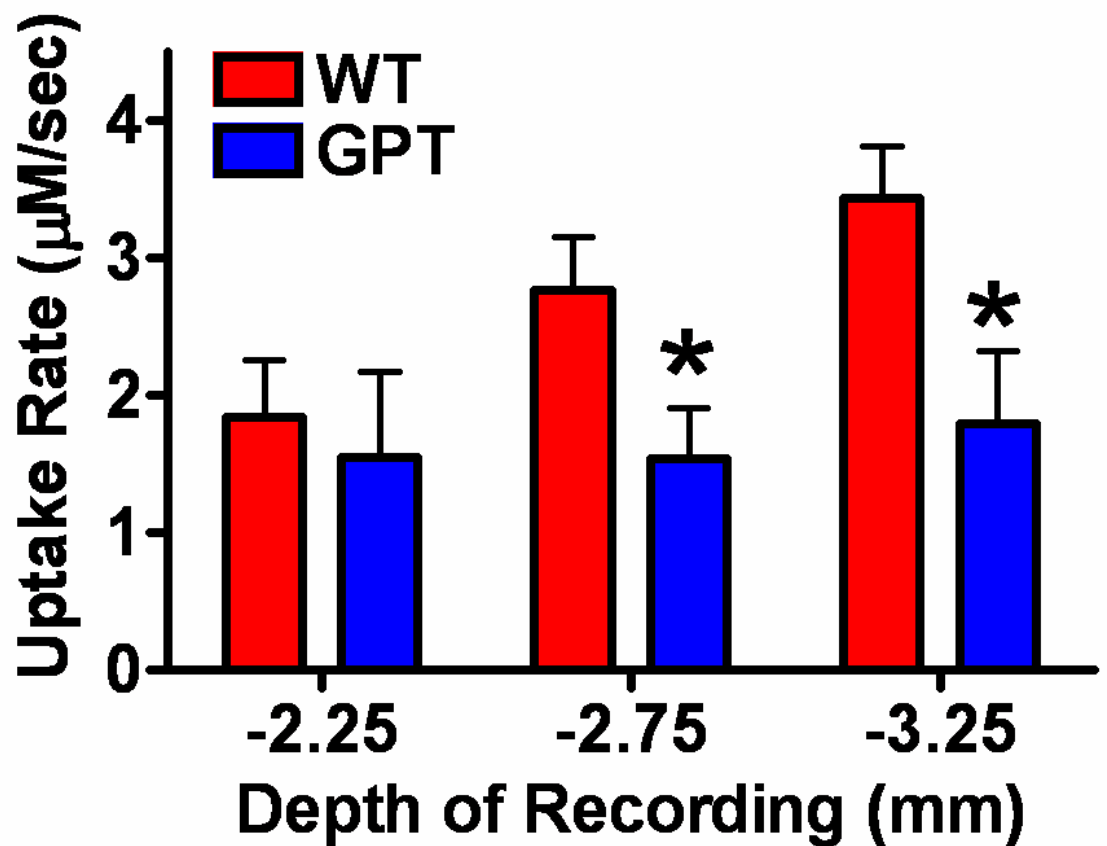


Figure 4.8: Exogenously Applied 5 mM Glu Clearance Depth Analysis

Average uptake rate of exogenously applied 5 mM Glu at different recording depths within the Str of GPT transgenic (n=4) and WT (n=9) mice. No significant differences were observed within groups of mice across the different depths. GPT transgenic mice had significantly (*p<0.05) slower uptake than WT mice at depths -2.75 mm (1.5 ± 0.4 µM/sec and 2.8 ± 0.4 µM/sec, respectively) and -3.25 mm (1.8 ± 0.5 µM/sec and 3.4 ± 0.4 µM/sec, respectively). A two-tailed t-test was conducted at each depth for statistical analysis.

depths. We observed that GPT transgenic mice had a significantly ($p < 0.05$) slower uptake rate of exogenously applied 5mM Glu compared to WT mice at depths -2.75 mm ($1.5 \pm 0.4 \mu\text{M}/\text{sec}$ and $2.8 \pm 0.4 \mu\text{M}/\text{sec}$, respectively) and -3.25 mm ($1.8 \pm 0.5 \mu\text{M}/\text{sec}$ and $3.4 \pm 0.4 \mu\text{M}/\text{sec}$, respectively).

Next, we wanted to perform the same series of recordings in the GPT KO mouse groups. Local application of 70 mM KCl resulted in robust, reproducible Glu signals compared to baseline similar to what was observed in the GPT transgenic mouse groups. From these traces we noticed that the GPT heterozygous and WT mice released similar amounts of Glu upon depolarization, however, the homozygous mice released significantly more Glu than either group (figure 4.9). To quantitate this finding, we volume matched the amount of stimulus locally applied to both mouse groups. Only Glu signals that were elicited by 50 to 150 nl of 70 mM KCl were used for this analysis, therefore, no significant difference in the amount of stimulus used was observed between the GPT WT ($101 \pm 4 \text{ nl}$), heterozygous ($93 \pm 8 \text{ nl}$) and homozygous ($107 \pm 5 \text{ nl}$) mice (figure 4.10A). When the average maximal amplitude of Glu release was quantitated, GPT homozygous mice ($5.9 \pm 0.8 \mu\text{M}$) released significantly more Glu ($p < 0.05$) compared to WT ($4.1 \pm 0.3 \mu\text{M}$) and heterozygous ($4.0 \pm 0.7 \mu\text{M}$) littermates (figure 4.10B). Using the same subset of signals, striatal, depth-related alterations in stimulus-evoked Glu release were also examined (figure 4.11). The average Glu release was calculated at each depth (DV -2.25 to -3.75 mm) and compared amongst the GPT KO mouse groups. No significant differences were seen within groups of mice across all depths. On average, the GPT homozygous mice released more Glu compared to WT and heterozygous mice at each recording depth, however, it was not a significant difference at any recording depth.

Since neurotransmitter uptake follows classical Michaelis-Menten kinetics (Nicholson, 1995) and was affected by the amount of available substrate, Glu uptake was analyzed by selecting a subset of signals with maximum release values were in the range of 3-13 μM . This range was chosen, because these peak Glu values were easily obtainable in both groups. Within this subset of

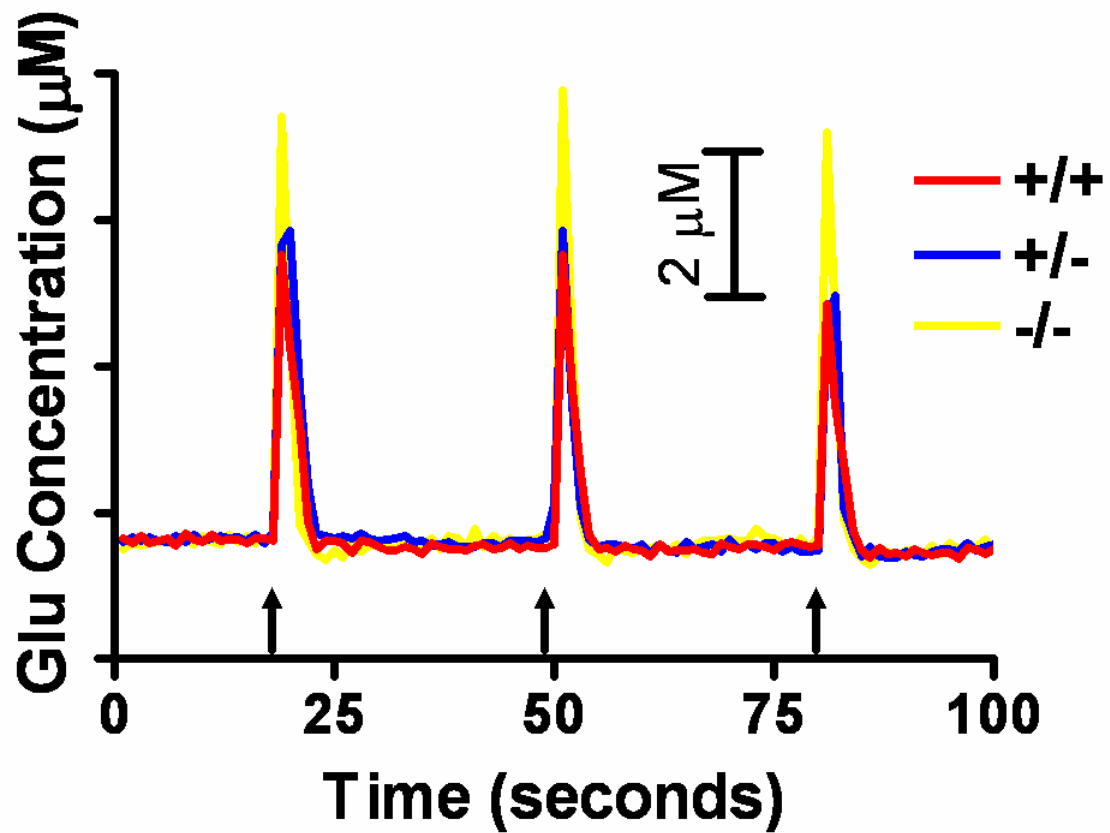


Figure 4.9: 70 mM KCl-Evoked Glu Release Traces in the Female GPT KO Mice

Series of amperometric Glu recordings showed differences in volume matched stimulus-evoked Glu release in WT (+/+; red), heterozygous (+/-; blue) and homozygous (-/-; yellow) mice. Note the reproducibility of the signal in all three groups. The heterozygous mice had similar amounts of stimulus-evoked Glu release compared to WT mice, while the homozygous mice had increased release compared to either group. Arrows indicated time points for local application of an isotonic solution of 70 mM KCl (pH 7.4).

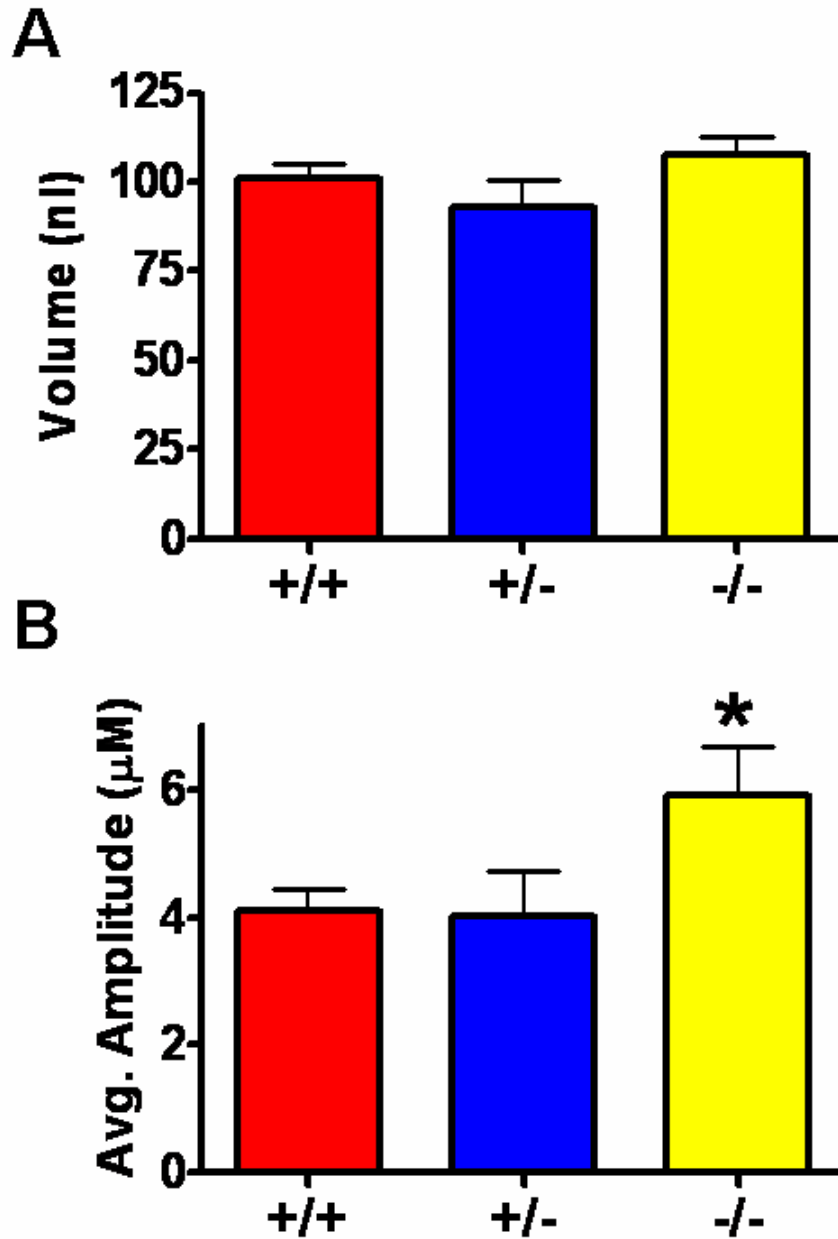


Figure 4.10: Stimulus-Evoked Glu Release in the Female GPT KO Mice

A) Only Glu signals that were elicited by 70 mM KCl whose volumes ranged between 50 and 150 nl were analyzed for the GPT WT (n=5; +/+; red), heterozygous (n=4; +/-; blue) and homozygous (n=4; -/-; yellow) mice. Since the volumes were matched, no significant difference in the amount of stimulus locally applied was observed between WT (101 ± 4 nl), heterozygous (93 ± 8 nl), homozygous (107 ± 5 nl) mice. B) The average maximal amplitude of Glu released upon local application of 70 mM KCl was significantly increased (*p < 0.05) in the GPT homozygous mice (5.9 ± 0.8 µM) compared to WT (4.1 ± 0.3 µM) and heterozygous (4.0 ± 0.7 µM) littermates.

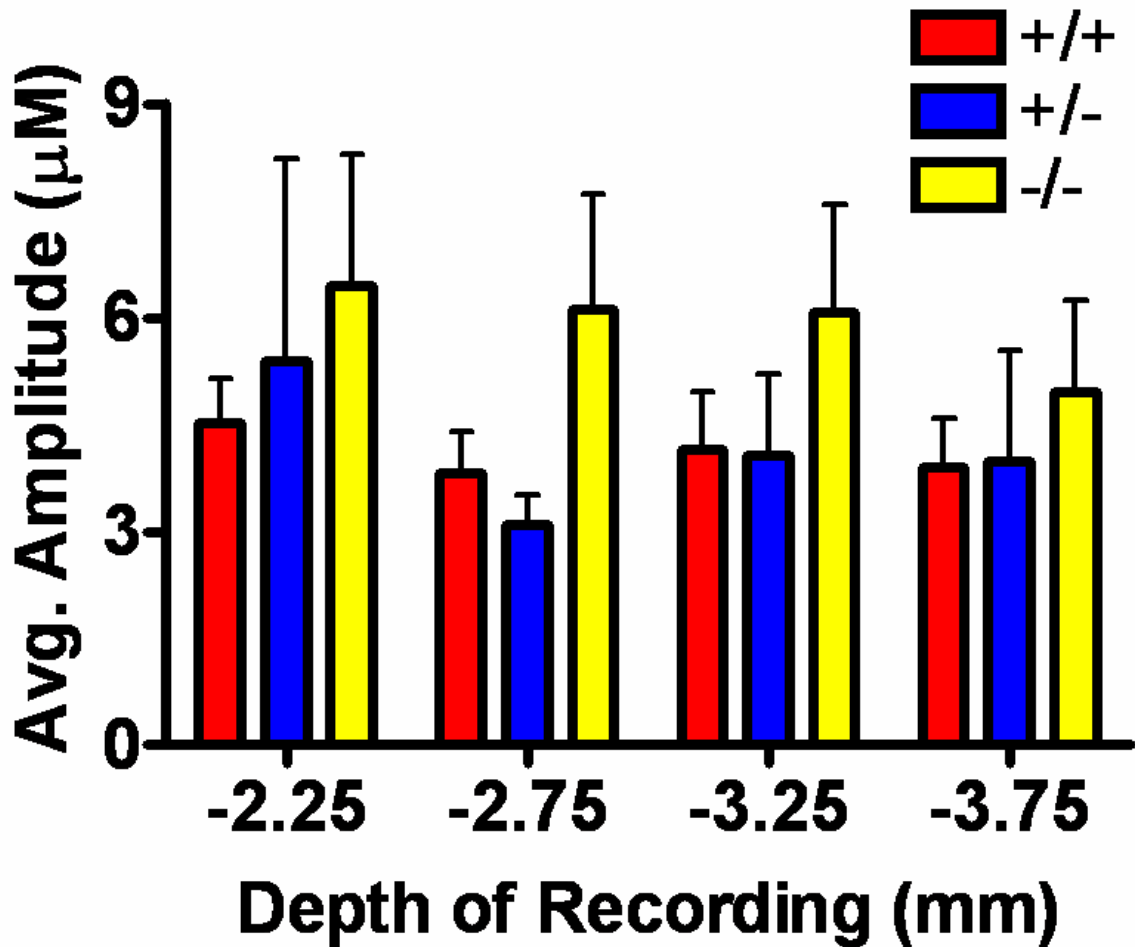


Figure 4.11: Stimulus-Evoked Glu Release Depth Profile in the Female GPT KO Mice

Average stimulus-evoked Glu release at different recording depths within the Str of GPT WT (n=5; +/+; red), heterozygous (n=4; +/-; blue), and homozygous (n=4; -/-; yellow) mice. No significant differences were observed within groups of mice across the different depths. On average, GPT homozygous mice released slightly more Glu compared to WT and heterozygous mice at all recording depths; however, it was not a significant difference. A one-way ANOVA with Tukey's post hoc was conducted at each depth for statistical analysis.

signals, no significant difference in average maximum release of Glu was observed in WT ($4.8 \pm 0.3 \mu\text{M}$), heterozygous ($6.0 \pm 0.5 \mu\text{M}$) and homozygous ($6.1 \pm 0.4 \mu\text{M}$) mice, nor was a significant difference in the uptake rate of stimulus-evoked Glu release observed between WT ($1.5 \pm 0.1 \mu\text{M}/\text{sec}$), heterozygous ($1.8 \pm 0.2 \mu\text{M}/\text{sec}$), and homozygous ($1.6 \pm 0.2 \mu\text{M}/\text{sec}$) mice (figure 4.12).

Due to the electrogenic nature of Glu transporters (Takahashi *et al.*, 1997; Doble, 1997), we wanted to determine transporter function without membrane depolarization. To do this, we locally applied an isotonic solution of 5 mM Glu (pH 7.4) and examined a subset of Glu signals that were in the range of 3-13 μM , which was the same range as those used for our stimulus-evoked Glu uptake analysis. There was no significant difference in the maximal amplitude of exogenously applied 5 mM Glu in the GPT WT ($8.6 \pm 0.3 \mu\text{M}$), heterozygous ($8.4 \pm 0.4 \mu\text{M}$), and homozygous ($7.8 \pm 0.3 \mu\text{M}$) mice (figure 4.13A). Unlike the stimulus-evoked Glu uptake, we observed slower clearance in the heterozygous ($2.5 \pm 0.3 \mu\text{M}/\text{sec}$) mice compared to the WT ($3.1 \pm 0.2 \mu\text{M}/\text{sec}$) mice. The homozygous mice ($2.3 \pm 0.2 \mu\text{M}/\text{sec}$) had a significantly ($p < 0.05$) slower clearance of exogenously applied Glu compared to WT mice (figure 4.13B). Using the same subset of signals, striatal depth-related alterations in exogenously applied 5 mM Glu clearance was examined (figure 4.14). The average clearance rate was calculated at each recording depth (DV -2.25 to -3.75 mm) and compared amongst the GPT KO mouse groups. No significant differences were seen within groups of mice across all depths. On average, the GPT homozygous mice had slower clearance of exogenously applied 5 mM Glu compared to WT mice at each recording depth, however, it was not a significant difference at any recording depth.

Since self-referencing MEAs were used to study the GPT KO mice, we were able to determine resting Glu levels in the Str. Thirty second baseline measures were taken prior to local application of 70 mM KCl. Resting Glu levels were only measured when 70 mM KCl was in the barrel of the glass micropipette. Possible diffusion of 5 mM Glu out of the barrel caused unphysiologically

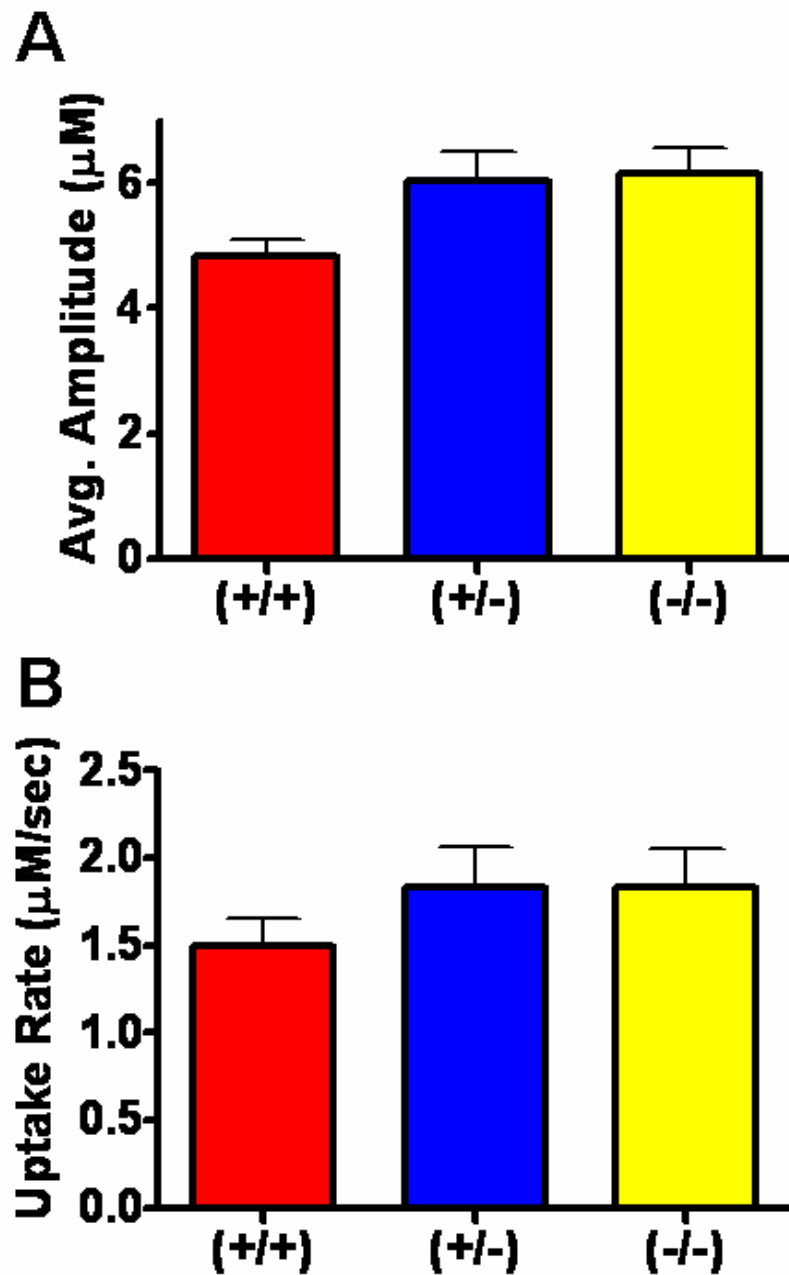


Figure 4.12: Stimulus-Evoked Glu Uptake in the Female GPT KO Mice

A) Subset of Glu signals were examined whose average maximal amplitude fell in a range of 3-13 μM for both the GPT WT (n=5; +/+; red), heterozygous (n=4; +/-; blue), and homozygous (n=4; -/-; yellow) mice. No significant difference was observed between WT ($4.8 \pm 0.3 \mu\text{M}$), heterozygous ($6.0 \pm 0.5 \mu\text{M}$) and homozygous ($6.1 \pm 0.4 \mu\text{M}$) mice. B) When the uptake rate of stimulus-evoked Glu was examined, no significant differences were seen between WT ($1.5 \pm 0.1 \mu\text{M/sec}$), heterozygous ($1.8 \pm 0.2 \mu\text{M/sec}$), and homozygous ($1.6 \pm 0.2 \mu\text{M/sec}$) mice.

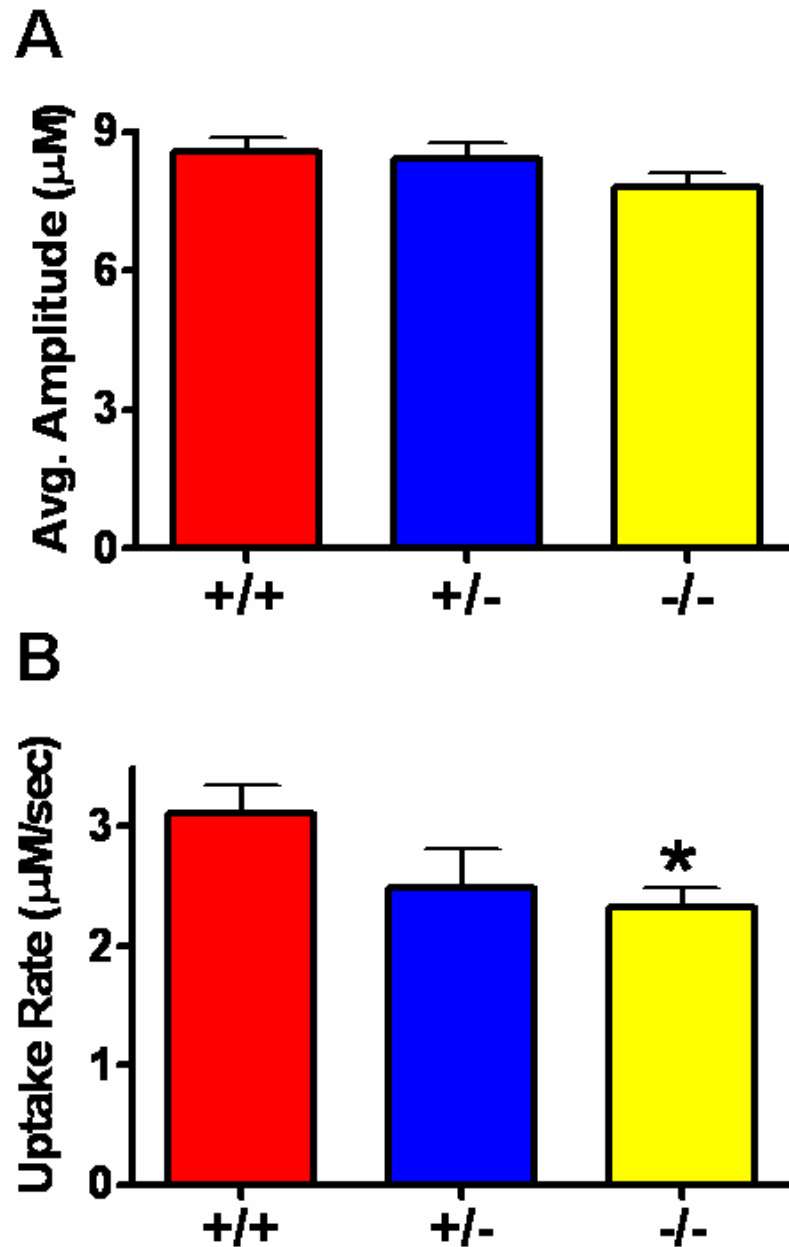


Figure 4.13: 5 mM Glu Clearance in the Female GPT KO Mice

A) A subset of Glu signals were examined whose average maximal amplitude fell in a range of 3-13 μM for the GPT WT (n=5; +/+; red), heterozygous (n=4; +/-; blue), and homozygous (n=4; -/-; yellow) mice. There was no significant difference in the maximal amplitude of exogenously applied 5 mM Glu in the GPT WT ($8.6 \pm 0.3 \mu\text{M}$), heterozygous ($8.4 \pm 0.4 \mu\text{M}$), homozygous ($7.8 \pm 0.3 \mu\text{M}$) mice. B) We observed slower clearance in the heterozygous ($2.5 \pm 0.3 \mu\text{M}/\text{sec}$) mice compared to the WT ($3.1 \pm 0.2 \mu\text{M}/\text{sec}$) mice. The homozygous mice ($2.3 \pm 0.2 \mu\text{M}/\text{sec}$) had a significantly ($*p < 0.05$) slower clearance rate of exogenously applied Glu compared to WT mice.

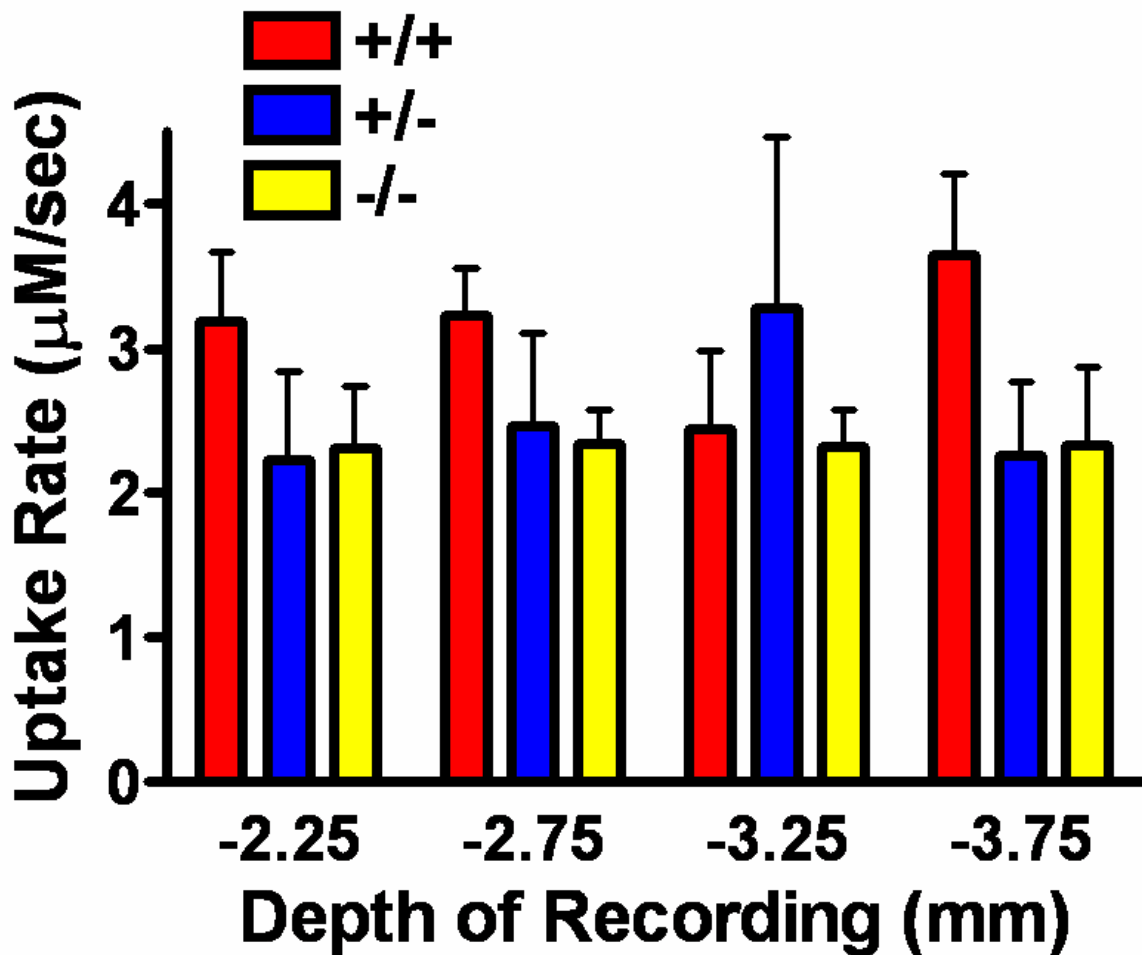


Figure 4.14: 5 mM Glu Clearance Depth Profile in the Female GPT KO Mice

Average stimulus-evoked Glu release at different recording depths within the Str of GPT WT (n=5; +/+; red), heterozygous (n=4; +/-; blue), and homozygous (n=4; -/-; yellow) mice. No significant differences were observed within groups of mice across the different depths. On average, GPT homozygous mice had slower clearance of exogenously applied 5 mM Glu compared to WT mice at all recording depths; however, it was not a significant difference. A one-way ANOVA with a Tukey's post hoc was conducted at each depth for statistical analysis.

elevated levels of resting Glu. Using our self-referencing recording techniques, resting Glu levels were similar in the Str of WT ($0.9 \pm 0.1 \mu\text{M}$), heterozygous ($1.4 \pm 0.4 \mu\text{M}$) and homozygous ($1.0 \pm 0.1 \mu\text{M}$) mice (figure 4.15A). Additionally, a depth analysis profile revealed resting Glu levels were similar at all recording depth within mouse groups. On average, GPT heterozygous mice had elevated resting Glu levels at all recording depths, but this was not significant (figure 4.15B).

Discussion

GPT catalyzes a reversible transaminase reaction using pyruvate as a co-substrate to form alanine and α -ketoglutarate. It is debated throughout the literature whether GPT favors Glu degradation (Saier Jr. and Jenkins, 1967; Ruščák *et al.*, 1982; Erecińska *et al.*, 1994) or synthesis (Peng *et al.*, 1991, 1993; Schousboe *et al.*, 2003). This process most likely depends on the amount of substrates/products available. Matthews and colleagues (2000, 2003) demonstrated that GPT was an active Glu degrading enzyme that acted as an effective neuroprotectant in cell culture models of exogenous and endogenous Glu excitotoxicity. The broad spectrum of transaminase molecules in the brain made it difficult to develop specific modulators for this enzyme. To determine the role GPT played in glutamatergic neurotransmission, two different mouse models were created. The first model had upregulated activity of GPT while the second model had removed this gene altogether.

Local application of 70 mM KCl resulted in robust, reproducible Glu signals in both the GPT transgenic and GPT KO mouse groups. When the average maximal amplitude of Glu release was quantitated we saw no significant differences between the GPT transgenic and WT littermates nor any significant depth related differences in stimulus-evoked Glu release between the two groups. We observed that the GPT transgenic mice had significantly slower uptake rates of stimulus-evoked Glu as well as clearance of exogenously applied 5 mM Glu. A depth profile revealed GPT transgenic mice, on average, had a slower rate of Glu uptake compared to WT mice, which became significant at

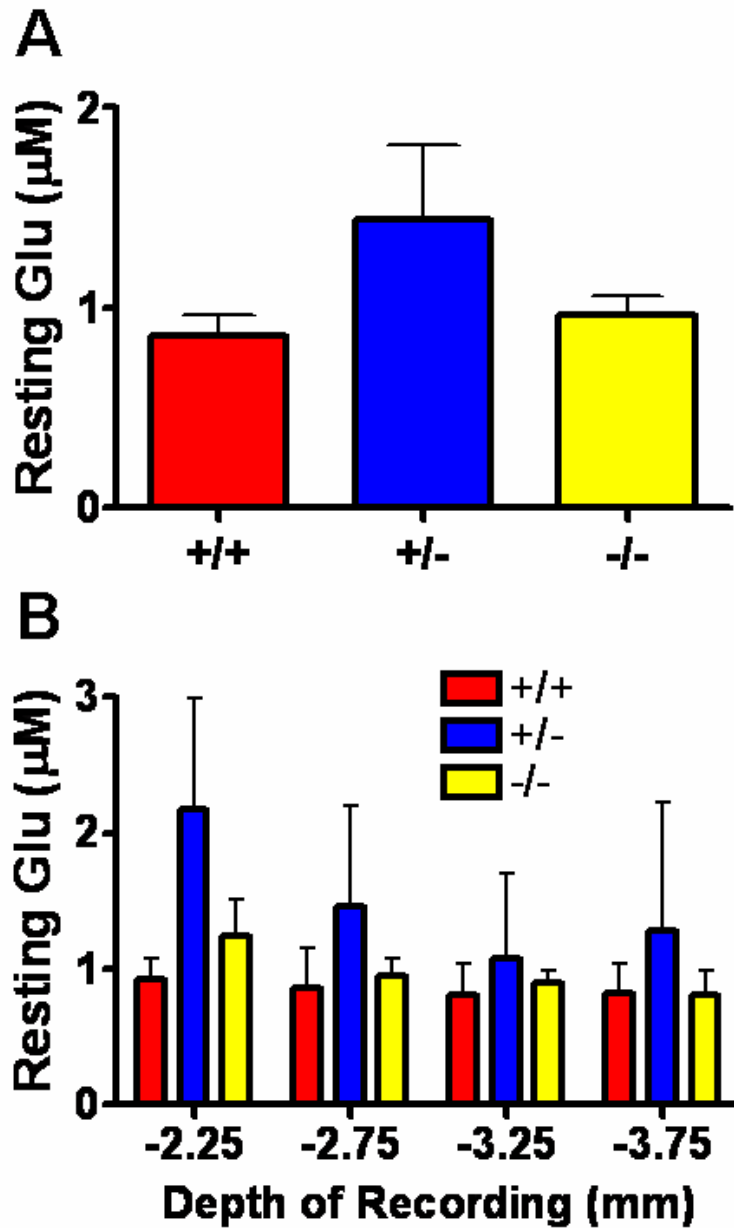


Figure 4.15: Resting Glu Levels in the Female GPT KO Mice

A) Resting Glu levels were averaged through the entire Str and no significant ($p=0.16$) differences were found between WT ($0.9 \pm 0.1 \mu\text{M}$), heterozygous ($1.4 \pm 0.4 \mu\text{M}$) and homozygous ($1.0 \pm 0.1 \mu\text{M}$) mice. B) Average resting Glu levels were determined for each depth within the Str of WT (+/+; red), heterozygous (+/-; blue), and homozygous (-/-; yellow). No significant difference was observed within mouse groups over the different recording depths. On average, GPT heterozygous mice had elevated resting Glu levels at all recording depths, but this was not significant. A one-way ANOVA with a Tukey's post hoc was conducted at each depth for statistical analysis.

recording depths -2.75 mm and -3.25 mm. In the GPT KO, homozygous mice had a significantly increased release of Glu compared to WT after local application of 70 mM KCl. A depth profile revealed that GPT homozygous KO mice, on average, released more Glu at all recording depths compared to WT mice. These values were not significant at any recording depth. We observed no significant difference in the uptake rate of stimulus-evoked Glu release, but found that the clearance rate after local application of 5 mM Glu in the homozygous mice was significantly slower compared to WT. A depth profile showed no significant difference at any of the recording depths. Since self-referencing MEAs were used for the GPT KO study, we were able to record resting Glu levels in these mice. We saw no significant difference in Glu resting levels among the mouse groups, but GPT heterozygous mice, on average, had nonsignificantly ($p=0.16$) higher Glu resting levels compared to WT and homozygous mice. This was also observed at all recording depths.

We observed no significant difference in stimulus-evoked Glu release in the GPT transgenic mouse groups. The same experiment in the GPT KO mice revealed that homozygous mice released significantly more Glu compared to WT littermates. Depth profiles of the Str showed no significant differences among the GPT transgenic as well as the GPT KO mice. The GPT homozygous mice showed a trend of higher stimulus-evoked Glu release. Our depth profile analysis demonstrated the advantage of our recording capability to measure discrete regions within a large brain structure. Other *in vivo* recording techniques, such as microdialysis, were too large to perform this type of analysis. Because of this advantage we showed that the Str was not a homogenous structure for Glu release and regional differences exist. More importantly, we demonstrated that knockout of a Glu metabolizing enzyme is responsible for increased neuronal release of Glu. Since cell culture studies have demonstrated the propensity for GPT to metabolize Glu (Matthews *et al.*, 2000, 2003) it was reasonable to hypothesize that dysfunction of this gene led to an increase in Glu availability for vesicular release from neurons. What was more difficult to explain was the fact that upregulation of the same gene showed no decrease in stimulus-

evoked Glu release. Increasing the gene copy number did not necessarily correlate to an increase in enzyme production. Also, since Glu is the predominant excitatory pathway throughout the mammalian CNS, a minimum amount of Glu must be made available for neurotransmission to maintain normal brain function (Wojcik *et al.*, 2004; Takamori, 2006). Other Glu metabolizing enzymes (such as GLUD1, PAG and/or aspartate aminotransferase) may compensate for the increased activity of GPT and return Glu to those levels seen for normal neurotransmission as in WT mice. A quantitative western blot analysis of Glu metabolizing enzymes must be run to test this hypothesis.

The uptake rate for stimulus-evoked Glu release as well as clearance of exogenously applied Glu was determined for both GPT transgenic and KO groups. We determined that Glu uptake of stimulus-evoked Glu as well as clearance of exogenously applied Glu was significantly decreased in the GPT transgenic mice. In the GPT KO mice we saw no significant change in uptake of stimulus-evoked Glu, but did see a significant decrease in the clearance rate of exogenously applied 5 mM in the homozygous mouse group. Since Glu uptake was driven by electrochemical gradients across the cell membrane to produce a negative membrane potential (Takahashi *et al.*, 1997; Doble, 1999), depolarization of glial membranes by the local application of 70 mM KCl may be responsible for the differences in the uptake rates when compared to clearance rates of exogenously applied 5 mM Glu in the GPT KO mice. This may also explain why the uptake rate in both the GPT transgenic and GPT KO was faster for exogenously applied 5 mM Glu compared to stimulus-evoked Glu uptake. What was more difficult to explain was how a Glu metabolizing enzyme affected Glu transporter function. Investigation of the mouse genome revealed that the mouse GPT and EAAT1 gene are both located on chromosome 15. We hypothesize that insertion or disruption of the GPT gene had downstream effects on the EAAT1 gene. If production of the EAAT1 protein was compromised, this may explain the significantly decreased uptake rate compared to WT littermates. Further studies on transporter number or function need to be completed to address these issues.

Using our self-referencing recording techniques, we were able to record resting Glu levels in the Str of GPT KO mice. Resting Glu levels were similar in the WT, heterozygous, and homozygous mouse groups, despite the differences seen in stimulus-evoked Glu release as well as decreases in the clearance rate of exogenously applied Glu in the homozygous mice. These two factors led one to hypothesize that resting Glu levels were elevated in the homozygous mice compared to WT littermates. One possible explanation for this finding was that resting Glu levels were analyzed in anesthetized mice. Anesthetics such as urethane exert their effects by enhancing inhibitory synaptic neurotransmission as well as inhibiting excitatory neurotransmission (Hara and Harris, 2002). Our laboratory has also demonstrated that urethane significantly decreased resting Glu levels by 58 percent (Rutherford *et al.*, 2007). Because of these two factors, anesthetized mouse models may not provide accurate measures of resting Glu.

Using *in vivo* amperometry with our Glu selective MEAs, we demonstrated that upregulation of GPT did not change stimulus-evoked Glu release, but significantly decreased the rate at which Glu was cleared from the extracellular space. Stimulus-evoked Glu release was significantly higher in the homozygous GPT KO mice. The GPT homozygous mice also showed a significantly slower ability to clear exogenously applied 5 mM Glu from the extracellular space. Despite these alterations on glutamatergic neurotransmission, we have not observed any phenotypic changes in either the GPT transgenic or the GPT KO mice. The significantly decreased uptake rate seen in GPT transgenic as well as the GPT homozygous mice was an interesting finding. Studies have found that EAAT expression or uptake of Glu was decreased in several neurological disorders including ALS, Huntington's disease (HD), and AD (Beart and O'Shea 2007). One would hypothesize to observe similar characteristics as the aforementioned neurological disorders in these transgenic and KO mice due to decreased Glu uptake.

Chapter Five: Understanding L-Glutamate Dynamics in the Awake, Freely Moving C57BL/6 Mouse

Introduction

Previous sections have focused on Glu neurotransmission in ethyl carbamate (urethane) anesthetized transgenic mouse models. Urethane is an injectible anesthetic widely used in animal research (Hara and Harris, 2002; Sabeti *et al.*, 2003) that modulates ligand-gated ion channels to mediate anesthesia-induced CNS depression (Yamakura *et al.*, 2001). It has already been shown that urethane has minimal effects on dopamine clearance (Sabeti *et al.*, 2003), which is the reasoning for using this anesthetic by our laboratory for non-survival surgeries. However, data indicates that urethane inhibits responses of NMDA and AMPA receptors (Hara and Harris, 2002). Rutherford and colleagues (2007) have also demonstrated that urethane can lower resting Glu levels by 58 percent. In addition, general anesthetics such as isoflurane, can inhibit NMDA and AMPA receptors (Yamakura *et al.*, 2001; Mellon *et al.*, 2007) as well as inhibiting potassium-evoked release (Larsen and Langmoen, 1998; Liachenko *et al.*, 1999) and re-uptake (Liachenko *et al.*, 1999) of Glu. These are just two examples of commonly used anesthetics in animal laboratories. Many other general anesthetics affect iGluRs (Perouansky *et al.*, 1998; Yamakura *et al.*, 2001; Mellon *et al.*, 2007). These studies indicate that most anesthetics exert some action or affect on the glutamatergic system. In an attempt to better understand Glu neurotransmission without the effects of anesthesia, our laboratory has begun to use the MEA technology in awake, freely moving animals.

Currently, *in vivo* microdialysis is the most commonly used technique to study extracellular Glu in freely moving mice (Olive *et al.*, 2000; Uezono *et al.*, 2001; Wang *et al.*, 2005; Holmer *et al.*, 2005; Zuo *et al.*, 2006; Hao *et al.*, 2007; Win-Shwe *et al.*, 2007). Microdialysis utilizes semipermeable membranes to restrict the diffusion of extracellular molecules or neurotransmitters along their concentration gradients (Ungerstedt, 1984; Di Chiara *et al.*, 1996). With

microdialysis, several analytes can be measured simultaneously allowing for studies of multiple neurotransmitter systems. However, the temporal and spatial resolution of this technique may be inadequate to properly measure the fast dynamics of Glu neurotransmission. Strides are being made to increase the temporal resolution into several second intervals by coupling microdialysis with capillary electrophoresis (Tucci *et al.*, 1997; Kennedy *et al.*, 2002; Rossell *et al.*, 2003). Even with these recent improvements, it is unlikely that microdialysis can achieve the sub-second response time necessary for studying *in vivo* Glu dynamics due to diffusion processes required for molecules to cross the dialysis membrane. While collection and analyzing of microdialysis samples corresponding to one second intervals is possible (Rossell *et al.*, 2003), work by Kennedy's group shows that band broadening of the sample within the tubing prevents this technique from achieving response times faster than ten seconds (Lada *et al.*, 1997). Since Glu neurotransmission occurs on a sub-second to second time scale (Kinney *et al.*, 1997), faster recording techniques are necessary to understand its release and uptake dynamics. Furthermore, several microdialysis studies report that the Glu overflow measured with microdialysis is not TTX – dependent (Timmerman and Westerink, 1997; Baker *et al.*, 2002; Melendez *et al.*, 2005). This suggests that Glu signals measured from microdialysis are not neuronally derived, which does not fulfill the classical criteria for exocytotic release and questions the source of resting Glu levels

To make matters worse, the large size of the microdialysis probe causes substantial short- and long-term trauma, which is evidenced by histological, physiological, and biochemical changes in nearby CNS tissue (Bungay *et al.*, 2003). During the first hours after implantation the blood-brain barrier is disrupted, blood flow to the tissue surrounding the probe is decreased and release of neurotransmitters is altered (Westerink, 1995). Positron emission tomography (PET) imaging has revealed that glucose metabolism is drastically and irreversibly altered by chronic implantation of a microdialysis cannula/probe (Schiffer *et al.*, 2006). Three days after implantation a glial barrier is observed and may account for probe blockage (Benveniste and Diemer, 1987). This glial

barrier is markedly increased if nonfunctional microdialysis probes are removed and functional probes are reinserted in an attempt to continue freely moving studies within the same animal (Georgieva *et al.*, 1992). Clapp-Lilly and colleagues (1999) demonstrate that ultrastructural damage occurs up to 1.4 mm away from a microdialysis probe implant site. In addition, normal dialysate perfusion and removal of material by the probe may produce concentration gradients that damage tissue up to several millimeters away from the implant site (Bungay *et al.*, 1990). The implantation damage caused by microdialysis probes has drastic effects on local neurotransmitter dynamics. Carbon fiber microelectrodes coupled with voltammetric techniques were used to show that stimulus-evoked dopamine release is attenuated up to 220-250 μm from the probe implant site (Yang *et al.*, 1998; Borland *et al.*, 2005). If this probe-induced trauma along with glial barrier formation is not taken into account for microdialysis analysis, the estimation of extracellular concentrations and clearance of neurotransmitters such as DA and Glu can be underestimated (Lu *et al.*, 1998; Yang *et al.*, 1998; Bungay *et al.*, 2003). Furthermore, Frumberg and colleagues (2007) demonstrated that rats implanted with microdialysis probes in the right Str performed significantly worse in object recognition tasks despite no change in locomotor activity. These studies demonstrate the excessive damage caused by a dialysis probe as well as question the physiological validity of dialysis samples.

Within the past decade, several groups have developed Glu selective microelectrodes to address the above inconsistencies with microdialysis studies on glutamatergic physiology (Hu *et al.*, 1994; Rahman *et al.*, 2005) and some studies utilizing these microelectrodes show that Glu is TTX-dependent (Kulagina *et al.*, 1999; Day *et al.*, 2006; Oldenziel *et al.*, 2006). Our laboratory has developed an enzyme-based MEA that is capable of detecting low levels of Glu on a sub-second time scale (500-800 msec) that is free from CNS interferents such as DOPAC and AA (Burmeister and Gerhardt, 2001; Burmeister *et al.*, 2002). These MEAs have been successfully used by our laboratory to measure Glu dynamics in aged Fischer 344 rats (Nickell *et al.*, 2004; Nickell *et al.*, 2007)

as well as resting Glu levels in Fischer 344 rats (Day *et al.*, 2006). Even more recently, our laboratory has successfully modified these MEAs for chronic recordings in awake, freely moving rats (Rutherford *et al.*, 2007). The present study concerns the adaptation and validation of these MEAs for selective Glu recordings in the awake, freely moving mouse model. First, we have adapted our methodology for chronic recordings of resting and phasic (rapid) changes in Glu in awake mice. Next, we investigated the reproducibility of such methods for measures in the C57BL/6 PFC and Str. Finally, we studied the pharmacological effects TTX and THA have on resting Glu levels in the mouse Str.

Methods

All materials and methods for freely moving recording were thoroughly outlined in Chapter Two. Male C57BL/6 between the ages of 5 and 6 months were used at the time of recordings. Glu recordings were conducted using self-referencing, enzyme-based MEAs with a sampling rate of 1 Hz. A craniotomy was performed over the Str (AP: +0.9 mm; ML: -1.5 mm; DV: -3.85 mm vs. bregma) or PFC (AP: +1.54 mm, ML: 0.3 mm, DV: -2.45 mm vs. bregma) and MEAs were implanted using the coordinates from Paxinos and Franklin (2004). A stainless steel guide cannula was attached to the PCB and positioned so an internal, acute stainless steel cannula was positioned among the 4 Pt recording sites, resting 50-100 μ m above the recording surface. Through this internal cannula isotonic solutions of 1 mM Glu (in 0.9% saline; pH 7.4); 0.9% physiological saline, citrate, 100 μ M THA, and 1 μ M TTX (all pH 7.4) were locally applied to the surrounding brain tissue to study glutamatergic neurotransmission. Prior to connecting the mouse pedestal with the FAST 16 Mark II recording system, mice were allowed to freely roam around the recording chamber for at least 30 minutes to acclimate to their environment. Once connected to the FAST 16 Mark II recording system, the mice underwent a minimum 60 minute acclimation period to establish a stable baseline recording. Following this acclimation period, the dummy cannula was removed and the internal, acute cannula (connected to a 10 μ l Hamilton Syringe) was inserted into the guide

cannula on recording sessions when chemicals were locally applied. After the internal cannula was inserted, another acclimation period of 30 minutes was allowed to reestablish baseline. Following this period, resting Glu, the effects of locally applied Glu, TTX or THA were studied for up to three additional hours. The volumes of locally applied Glu were kept constant at 0.5 μ l while the volumes for locally applied TTX, THA, and appropriate controls, saline (THA) and citrate (TTX), were kept at 1.0 μ l.

Following completion of all recording sessions (after multiple days of recording), mice were anesthetized with isoflurane and transcardially perfused with 0.9% saline followed by 4% paraformaldehyde. The brain was removed and stored in 4% paraformaldehyde for three days followed by storage in 0.1 M phosphate buffer (10% sucrose) for sectioning and staining to confirm MEA placement.

Data analysis involved a one-way ANOVA with Tukey's post hoc to examine any differences in resting Glu levels, maximal amplitude, t_{80} and uptake rate of Glu over multiple days post-implantation. A two-tailed student's t-test was used to compare different brain regions on similar days as well as differences in resting Glu after local application of THA or TTX compared to appropriate controls (0.9% saline and citrate, respectively). All data were reported as mean \pm standard error of the mean and significance was defined as $p < 0.05$.

Results

The FAST 16 Mark II recording system along with our modified MEA allowed for reliable second-by-second recordings of Glu in the Str and PFC of awake, freely moving mice. We consistently implanted the pedestal assemblies and recorded Glu for as long as 2 weeks in awake mice. Local application of an isotonic solution of Glu (1 mM; 0.5 μ l; pH 7.4) through the internal cannula was used to verify Glu recordings *in vivo*. Figure 5.1 shows representative Glu signals in the Str (A) and PFC (B) of awake, freely moving mice. Glu measures were robust and reproducible within brain regions, and over multiple days (figure 5.2).

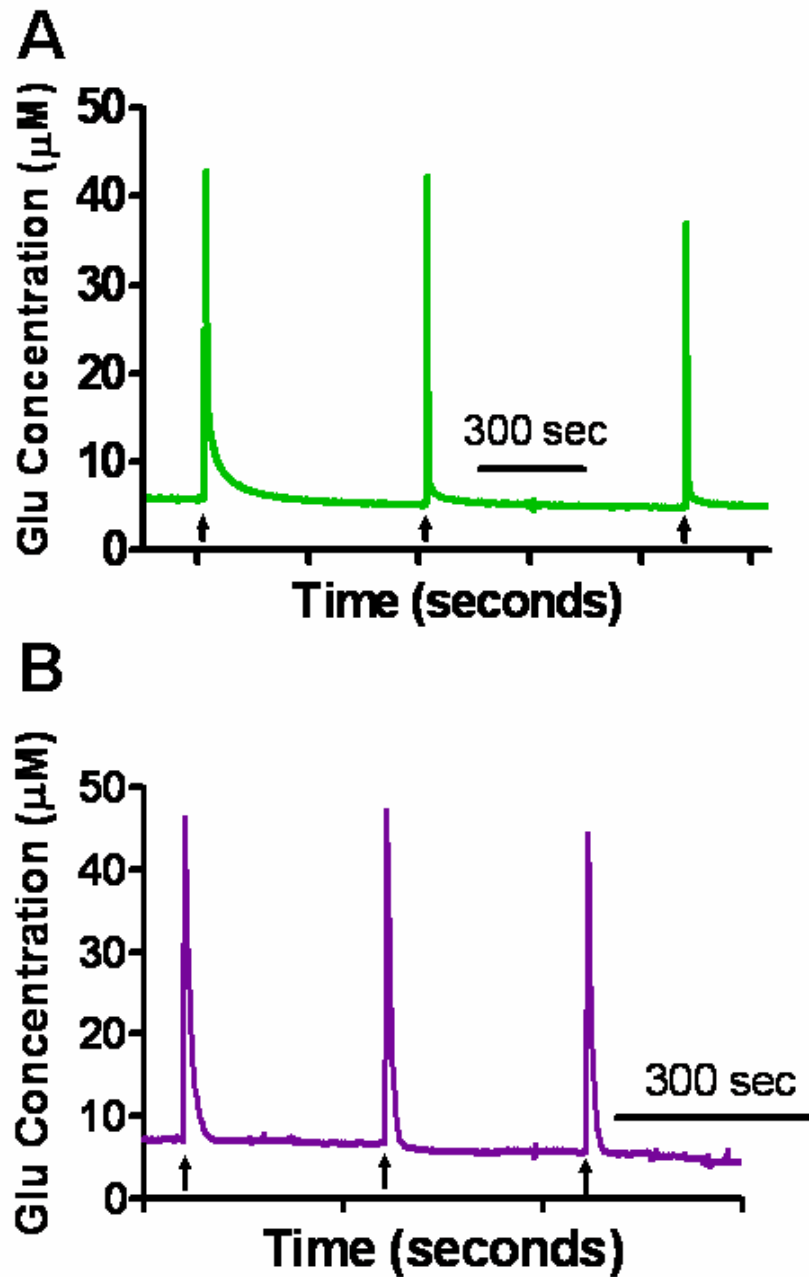


Figure 5.1: Representative Glu Traces After Local Application of 1 mM Glu

Representative traces of locally applied Glu (1 mM; 0.5 μ l) in the Str (A) and PFC (B) of male C57BL/6 mice. Glu was locally applied at the time points indicated by the arrows. A rapid, reproducible spike was recorded in both brain regions using self-referencing MEAs. Maximal peak height suggests *in vivo* Glu signal from local application of Glu (arrows), while baseline measures suggest resting Glu levels.

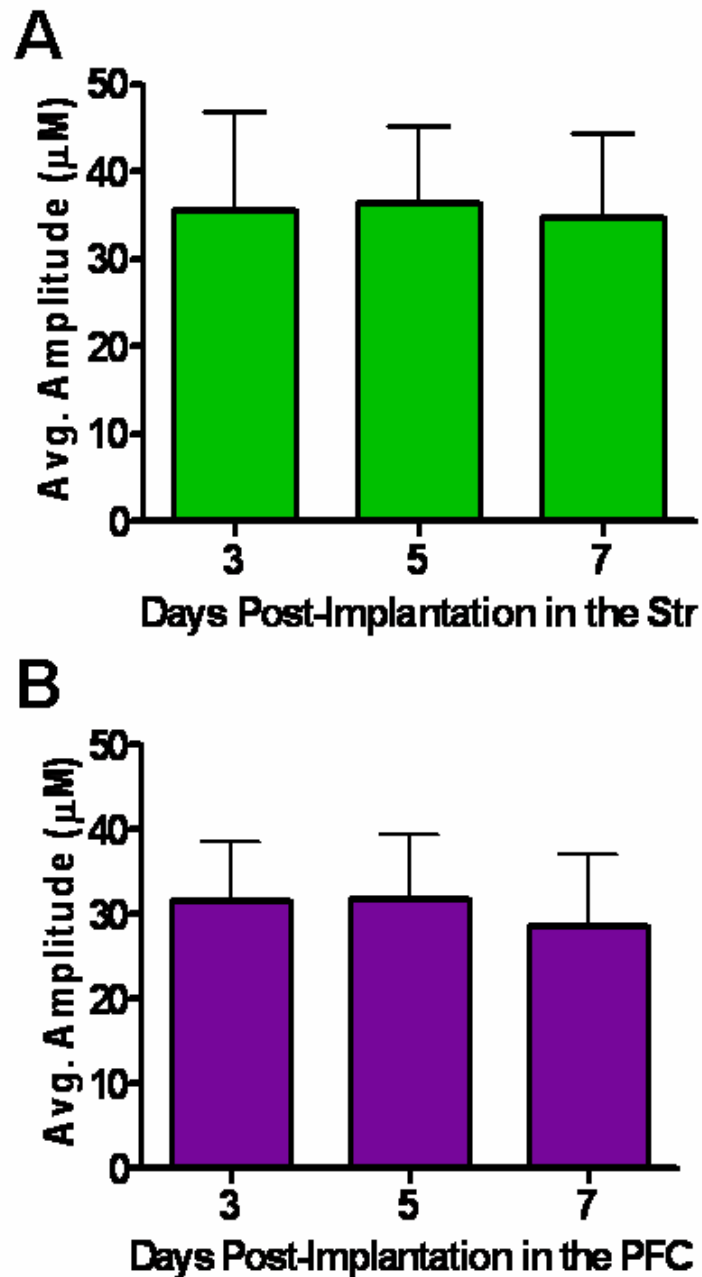


Figure 5.2: Local Application of Glu in the PFC and Str

Locally applied Glu data for days 3, 5, and 7 post-implantation in the Str (A, n=8) and PFC (B, n=6) of C57BL/6 mice. Glu (0.5 µl, 1 mM) was locally applied in both brain regions over multiple days and recorded using a self-referencing MEA. Substantial and stable Glu recordings were observed over all days measured indicating reliable, *in vivo* Glu measurements for at least 7 days post-implantation. Average maximum amplitude over days within brain regions as well as between the PFC (30.5 ± 7.8) and the Str (35.6 ± 9.9) was not significantly different.

An isotonic solution of Glu (1 mM; 0.5 μ l; pH 7.4) was locally applied in the PFC and Str of male, C57BL/6 mice on days 3, 5, and 7 post-implantation. As shown in figure 5.2, Glu signals were reproducible over multiple days within the Str (figure 5.2A) and PFC (figure 5.2B) as well as similar between the two brain regions. Table 5.1 provides a list of the average maximum amplitude values on days 3, 5 and 7 post-implantation for both brain regions.

No significant difference in maximal Glu response was observed between brain regions after local application of 1 mM Glu. We observed differences in the clearance of locally applied Glu as shown by the traces in figure 5.3. When we examined the uptake rate of locally applied 1 mM Glu (figure 5.4) we found that both the Str (figure 5.4A) and PFC (figure 5.4B) cleared exogenously applied Glu slower over days, however, this was not significant. We also observed that the Str (13.4 ± 4.2 μ M/sec), on average, had a faster clearance of Glu compared to the PFC (5.8 ± 1.9 μ M/sec), but this was not significant ($p=0.17$) between brain regions on either day 3, 5, or 7 post implantation (figure 5.4C). Table 5.2 provides a list of the average uptake rate values on days 3, 5 and 7 post-implantation. Due to the long duration of decay signals coupled with the fact that our uptake rate analysis only factors the first 5 seconds of signal decay, we wanted to examine the time period it takes to clear 80% of the Glu signal (t_{80}) (figure 5.5). We did not observe any significant difference in the t_{80} of locally applied Glu over days in the Str (figure 5.5A) and PFC (figure 5.5B) of C57BL/6 mice. We noticed a nonsignificant increase in t_{80} over days in both brain regions. Also, the average t_{80} was increased in the PFC compared to the Str, which became significant ($p<0.05$) on day 7 post-implantation (17.2 ± 2.9 sec and 10.0 ± 1.6 sec, respectively). Table 5.2 provides a list of the average t_{80} values for days 3, 5 and 7 post-implantation for both brain regions.

Resting Glu measures in the awake mice were measured in the PFC and Str of male, C57BL/6 mice on days 3 through 7 post-implantation using the self-referencing technique described in Chapter Two. Briefly, the self-referencing site current was subtracted from the Glu recording site current, and divided by the Glu recording site slope obtained from *in vitro* calibration. We observed no

Table 5.1: Local Application and Resting Glu Measures on Days 3 through 7 Post-Implantation

		Days Post-Implantation					
	Brain Region	3	4	5	6	7	Average
Locally Applied Glu (μM)	PFC (n=6)	31.4 \pm 7.2	n/a	31.7 \pm 7.7	n/a	28.4 \pm 8.6	30.5 \pm 7.8
	Str (n=8)	35.6 \pm 11.3	n/a	36.4 \pm 8.7	n/a	34.7 \pm 9.7	35.6 \pm 9.9
Resting Glu (μM)	PFC (n=8)	3.3 \pm 1.3	3.2 \pm 1.1	4.0 \pm 0.9	3.0 \pm 0.9	3.0 \pm 1.0	3.3 \pm 1.0
	Str (n=10)	5.5 \pm 1.3	5.0 \pm 1.0	5.1 \pm 1.1	4.4 \pm 1.1	4.9 \pm 1.2	5.0 \pm 1.2

The extracellular Glu concentrations in the PFC and Str from local application of 1 mM Glu (0.5 μl) and resting Glu levels on days 3 through 7 post-implantation.

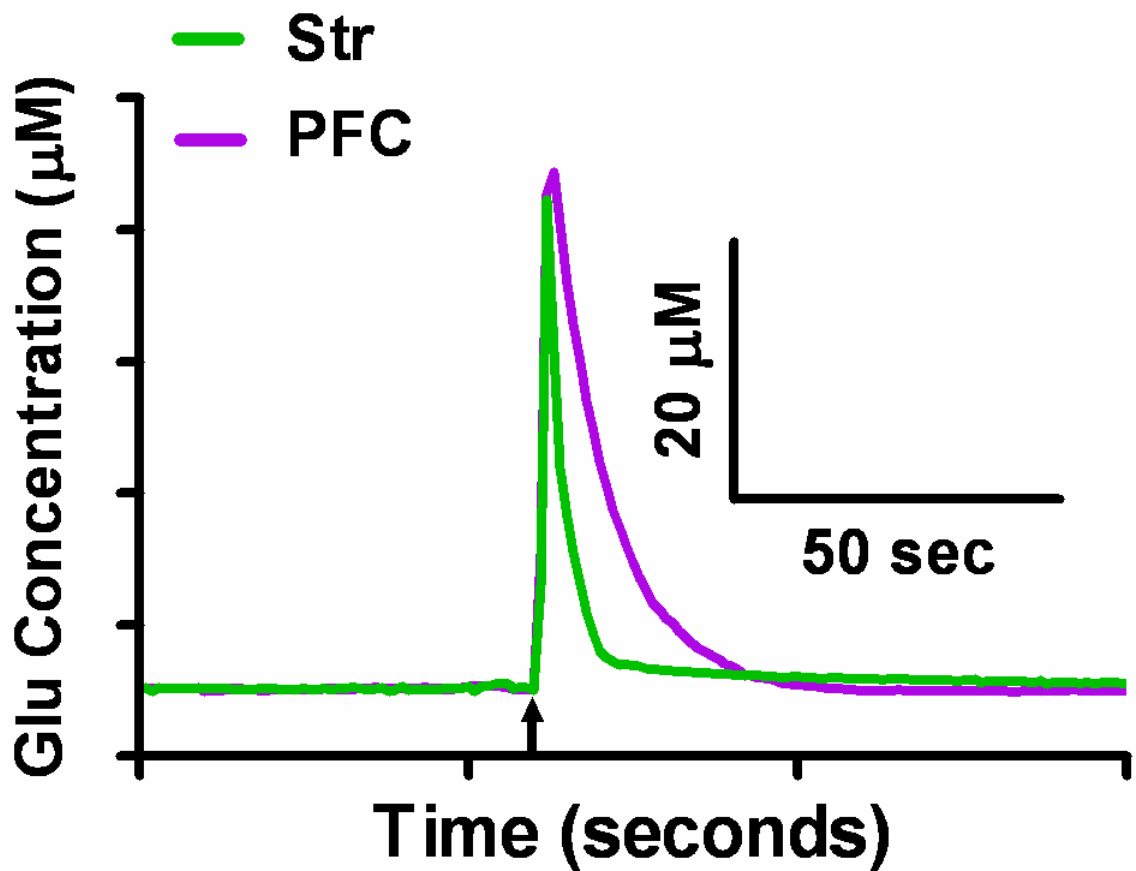


Figure 5.3: Representative Traces of Glu Clearance in the Str and PFC

Local application of 1 mM Glu (0.5 µl; pH 7.4) resulted in similar maximal amplitude between MEAs implanted in the Str and PFC of C57BL/6 mice. We observed that clearance kinetics were different between the two brain regions. Traces were from day 3 post-implantation for both brain regions.

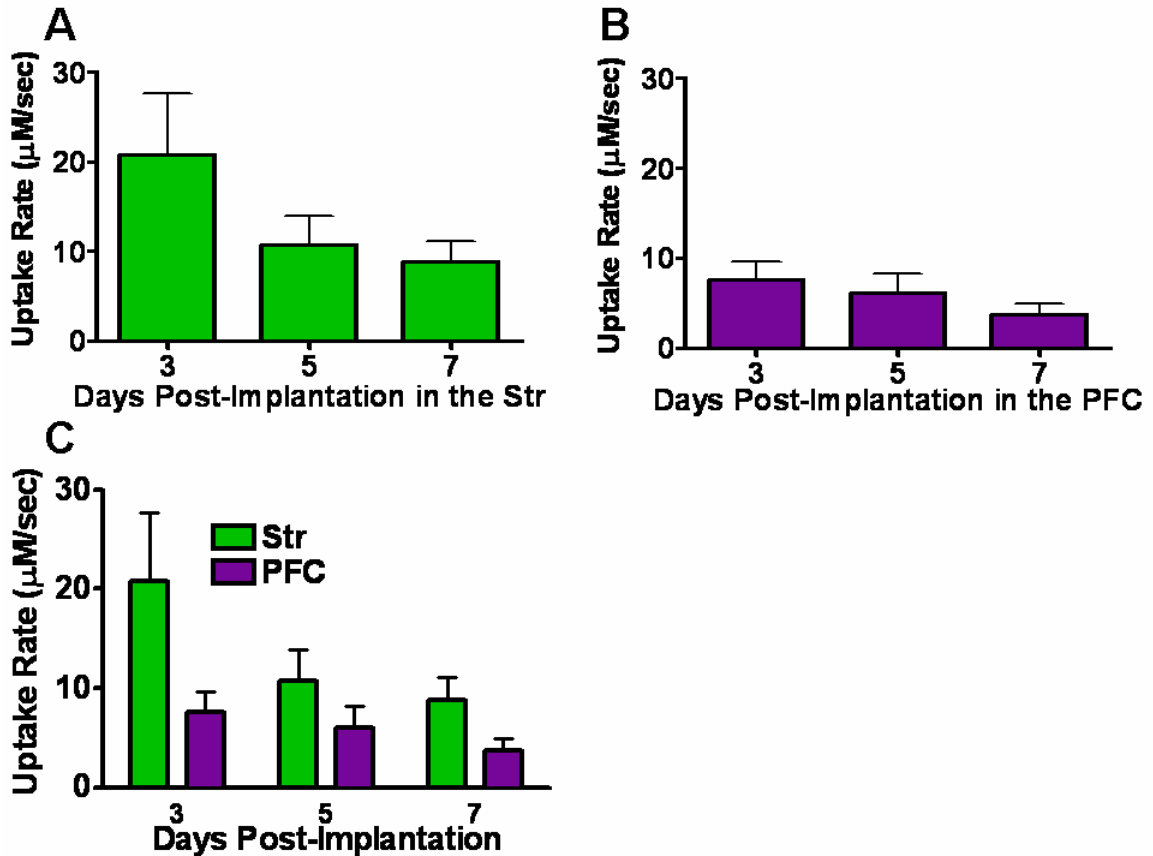


Figure 5.4: Clearance Rate of Locally Applied 1 mM Glu

Clearance rate of locally applied 1 mM Glu in the Str (A, n=8) and PFC (B, n=6) of C57BL/6 mice on days 3, 5, and 7 post-implantation. There was non significant decrease in the clearance of Glu over days within a brain region ($p=0.17$, Str; $p=0.37$, PFC). C) Comparison of clearance rate between brain regions over days. When a two-tailed t-test was used to compare brain regions over days there was no significant difference in the clearance of exogenously applied 1 mM Glu on either day 3 ($p=0.16$), 5 ($p=0.28$), or 7 ($p=0.12$).

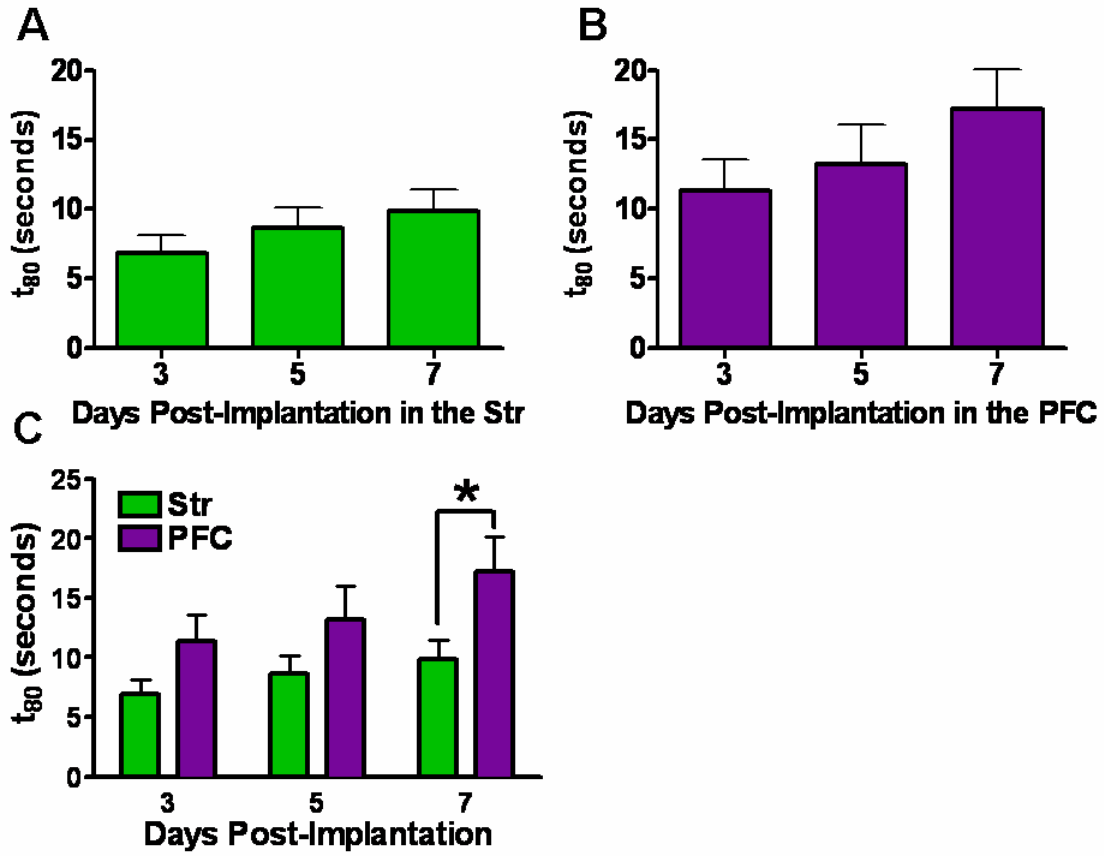


Figure 5.5: t_{80} of Locally Applied 1 mM Glu

The time period for 80 percent of the Glu signal to decay (t_{80}) in the Str (A, $n=8$) and PFC (B, $n=6$) of C57BL/6 mice. There was a nonsignificant trend towards increasing t_{80} over increasing days post-implantation ($p=0.35$, Str; $p=0.32$, PFC). The PFC of C57BL/6 mice cleared exogenously applied 1 mM Glu slower compared to the Str of C57BL/6 mice, which was significant ($*p<0.05$) on day 7 post-implantation, but not on days 3 ($p=0.08$) or 5 ($p=0.22$) post implantation (two-tailed t-test between Str and PFC on day 7 post-implantation).

Table 5.2: Clearance Kinetics of Exogenously Applied 1 mM Glu

	Brain Region	Days Post-Implantation			Average
		3	5	7	
Uptake Rate ($\mu\text{M}/\text{sec}$)	PFC (n=6)	7.5 ± 2.1	6.1 ± 2.2	3.7 ± 1.3	5.8 ± 1.9
	Str (n=8)	20.7 ± 7.0	10.7 ± 3.2	8.8 ± 2.3	13.4 ± 4.2
t_{80} (sec)	PFC (n=6)	7.5 ± 2.1	13.2 ± 2.8	17.2 ± 2.9	12.6 ± 2.6
	Str (n=8)	6.9 ± 1.3	8.7 ± 1.5	10.0 ± 1.6	8.5 ± 1.5

The clearance of extracellular Glu concentrations after local application of 1 mM Glu (0.5 μl) in the PFC and Str on days 3 through 7 post-implantation.

significant difference in resting Glu over days in the Str (figure 5.6A) and the PFC (figure 5.6B). However, the average resting Glu levels were decreased in the PFC compared to the Str although not significantly ($p=0.31$). Table 5.1 provides a list of the average resting Glu levels for days 3 through 7 post-implantation for both brain regions.

We wanted to determine how blocking the high-affinity transporters located on glial cells (Danbolt, 2001) affected resting Glu levels in the Str. To test this we locally applied 100 μM of THA, a transportable, competitive inhibitor for all excitatory amino acid transporters (EAAT) (Anderson *et al.*, 2001; Chatton *et al.*, 2001; Gaillet *et al.*, 2001), in the Str of C57BL/6 mice. Figure 5.7A shows Glu tracings after local application of 100 μM THA (1.0 μl) in 0.9% saline (pH 7.4) and 0.9% saline control (1.0 μl , pH 7.4). Local application of 100 μM THA in saline caused a significant increase ($p < 0.05$) in resting Glu levels ($2.9 \pm 1.2 \mu\text{M}$; $n=7$) compared to saline control ($0.3 \pm 0.1 \mu\text{M}$; $n=7$) (figure 5.7B). This was approximately a 60% increase in resting Glu levels in the Str when compared to our study in table 5.1.

We further investigated the source of resting Glu by determining the extent of exocytotic release from neurons. To test this, we locally applied TTX, a sodium channel blocker that prevented depolarization and subsequently terminated the action potential-dependent vesicular release of Glu. Local application of 1 μM TTX (1.0 μl , pH 7.4), in an isotonic solution of citrate, in the Str of C57BL/6 mice caused a significant decrease ($*p < 0.05$) in resting Glu levels ($-1.0 \pm 0.2 \mu\text{M}$; $n=6$) compared to an isotonic solution of citrate control (1.0 μl , pH 7.4) ($-0.3 \pm 0.1 \mu\text{M}$; $n=6$) (figure 5.8). This was approximately a 20% decrease in resting Glu in the Str when compared to our study in table 5.1.

Finally, we wanted to study the affects of a stressor on resting Glu levels. To do this, we applied fox urine on a cotton ball and introduced it into the recording chamber for 5 minutes. The Glu trace in figure 5.9 shows that the fox urine stressor caused a robust increase ($\sim 7 \mu\text{M}$) in Glu levels in the Str of C57BL/6 mice throughout the duration of the stressor (black line). Glu levels returned to baseline approximately 15 minutes after the stressor was removed.

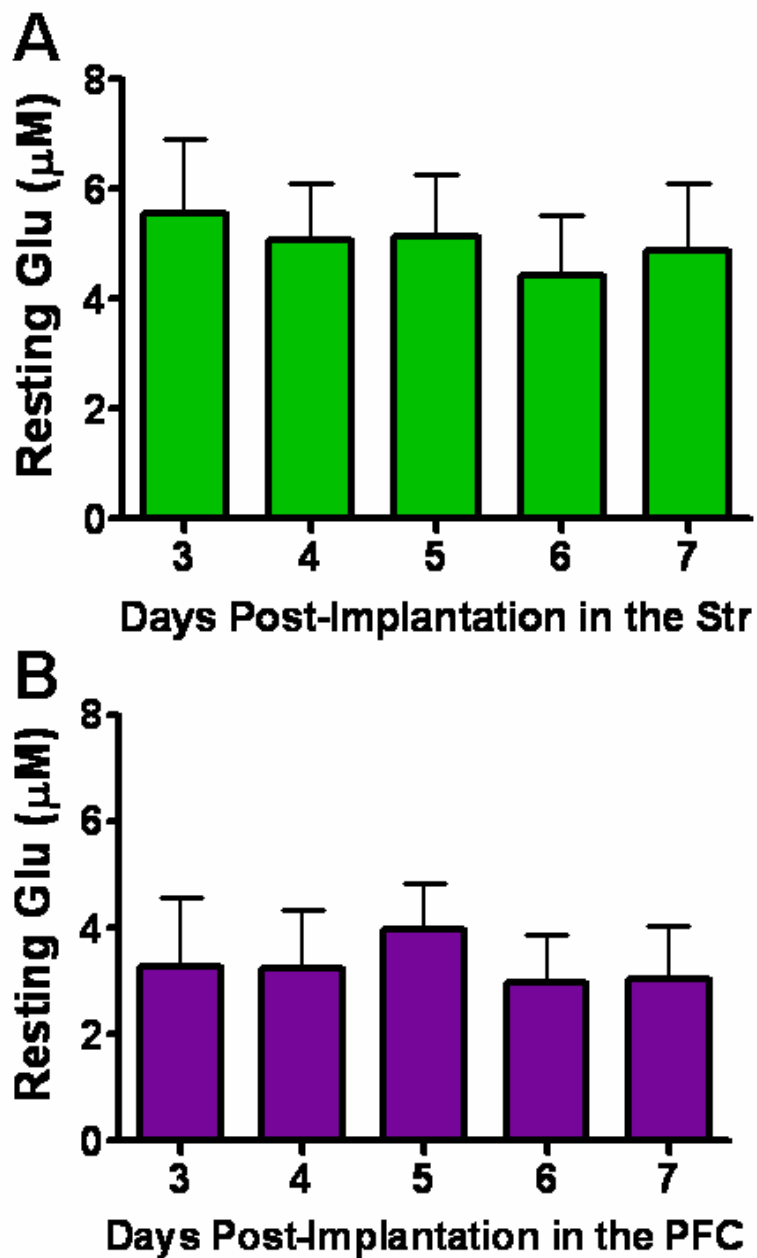


Figure 5.6: Resting Glu Levels in the Str and PFC

Resting Glu levels were assessed on days 3 through 7 post-implantation in the Str (A, n=10) and PFC (B, n=8) of C57BL/6 mice. Self-referencing MEAs were used to determine resting Glu levels. The self-referencing site current was subtracted from the GluOx coated site current, and divided by the GluOx slope, to yield resting Glu levels. Average resting Glu over days between the PFC (3.3 ± 1.0) and the Str (5.0 ± 1.2) of male C57BL/6 mice was not significantly ($p=0.31$) different.

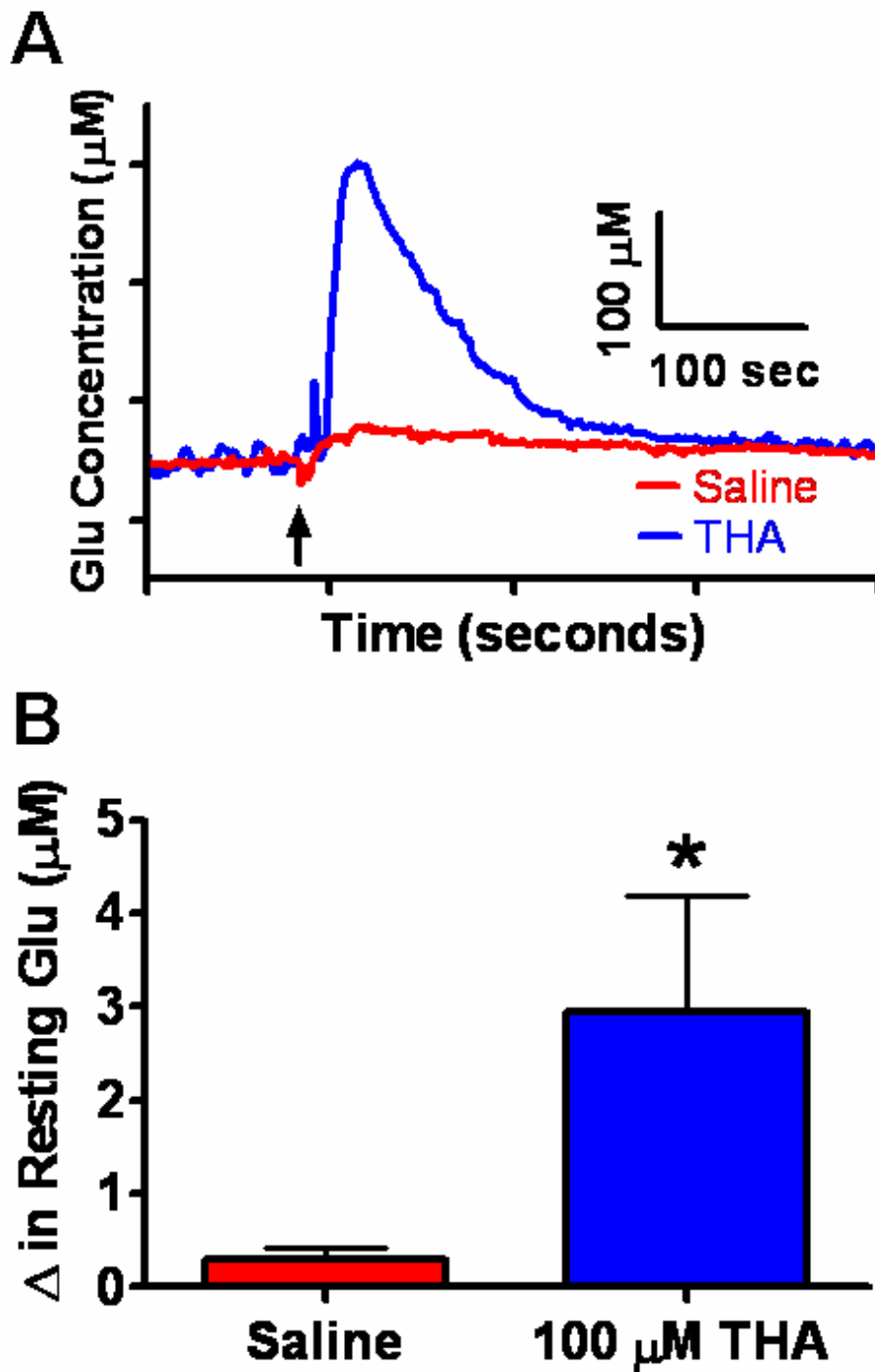


Figure 5.7: Local Application of 100 μM THA

Effects of local application of THA. A) Representative tracings of local application of THA (1.0 μl ; 100 μM) and 0.9% saline control (1.0 μl) in the Str of C57BL/6 mice. Local application of THA resulted in a robust, sustained increase in extracellular Glu compared to saline control. B) Change in resting Glu levels were significantly increased with local application of THA (2.9 \pm 1.2 μM ; n=7) compared to saline control (0.3 \pm 0.1 μM ; n=7) (*p < 0.05).

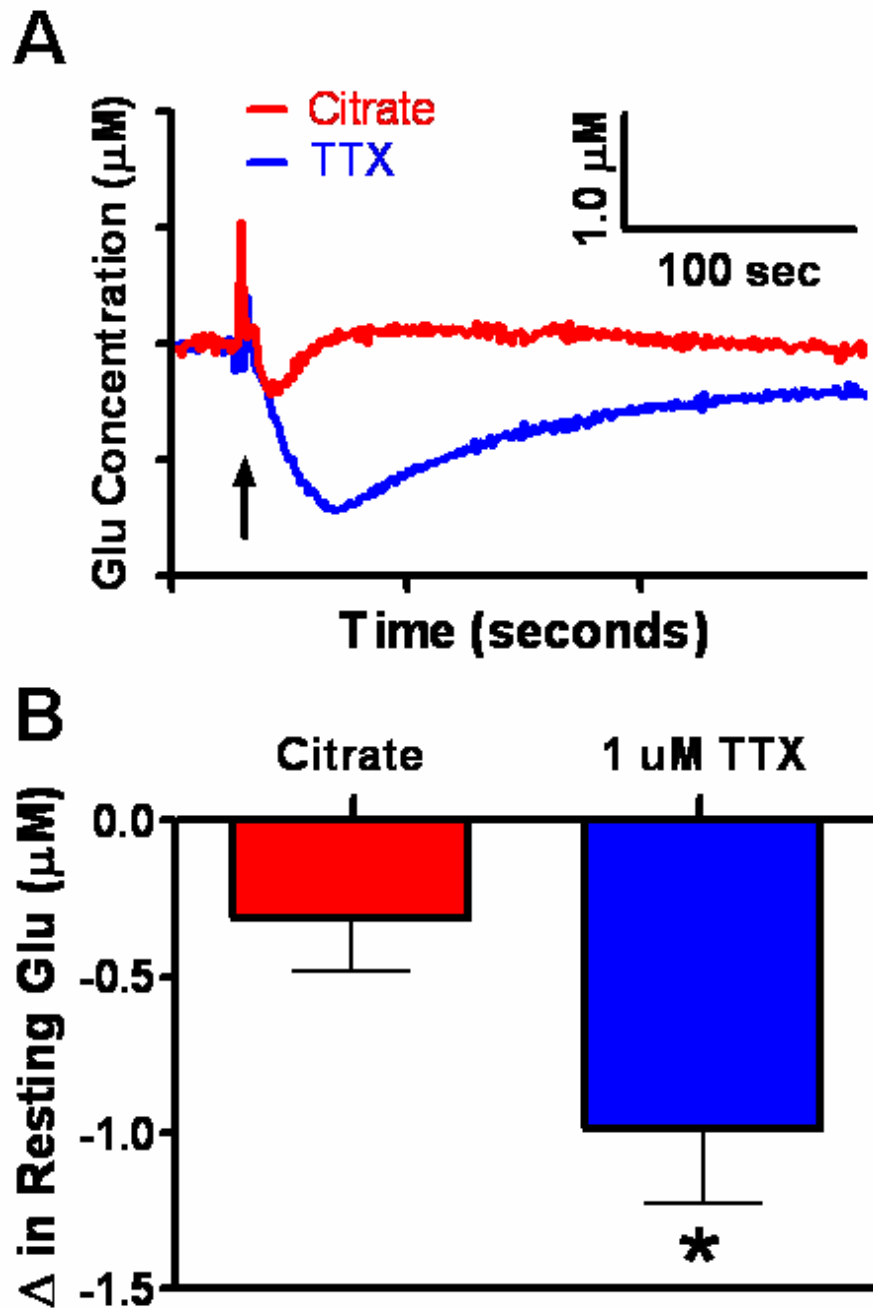


Figure 5.8: Local Application of 1 μM TTX

Effects of local application of TTX. A) Representative tracings of local application of TTX (1.0 μl ; 1 μM) and citrate control (1.0 μl) in the Str of C57BL/6 mice. Local application of TTX resulted in a robust, sustained decrease in extracellular Glu compared to citrate control. B) Change in resting Glu levels were significantly decreased with local application of TTX ($-1.0 \pm 0.2 \mu\text{M}$; $n=6$) compared to citrate control ($-0.3 \pm 0.1 \mu\text{M}$; $n=6$) ($*p < 0.05$).

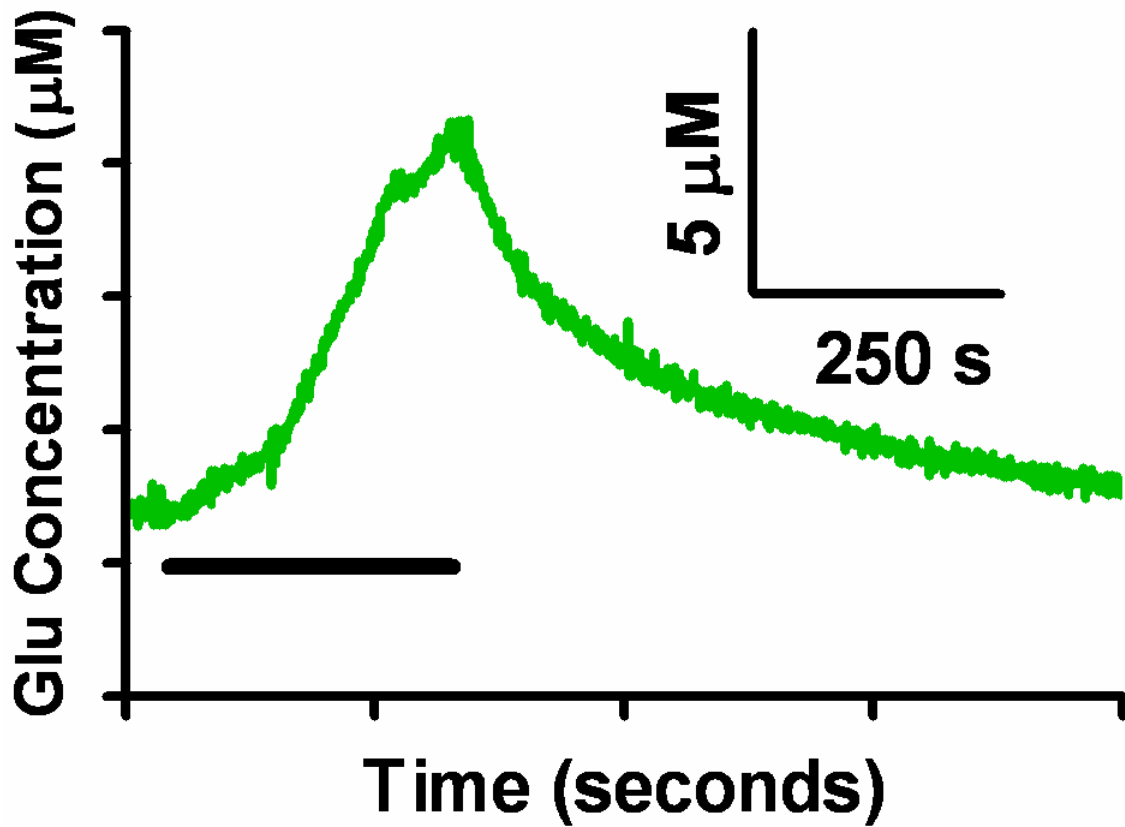


Figure 5.9: Fox Urine Affects Resting Glu Levels

A fox urine soaked cotton ball was introduced into the recording chamber for 5 minutes (black line). During this time period Glu levels rose to approximately 7 µM above baseline until the fox urine soaked cotton ball was removed. Glu levels returned to baseline approximately 15 minutes after removal of the cotton ball.

Discussion

The objective of this study was to adapt our current method for enzyme-based second-by-second Glu detection used in anesthetized animals or isolated preparations, to a system that can be used in awake, freely moving mice over multiple days. The small size and lightweight design of the pedestal allowed for chronic recordings with limited effects on the mouse's behavior and ability to perform everyday activities. We also wanted to develop a technology that was able to record second-by-second measures of Glu over multiple days, unlike microdialysis studies in freely moving mice, or other animals, that are normally performed in a single day over minute time scales (Olive *et al.*, 2000; Uezono *et al.*, 2001; Wang *et al.*, 2005; Holmer *et al.*, 2005 a,b; Zuo *et al.*, 2006; Hao *et al.*, 2007; Win-Shwe *et al.*, 2007). Similar to the work conducted by Rutherford and colleagues (2007) this study demonstrated the ability of our enzyme-based MEAs to reliably measure Glu for at least 7 days post-implantation. In addition, the small size of the ceramic tip of our MEA produced less damage than a chronically implanted microdialysis probe (Clapp-Lilly *et al.*, 1999; Borland *et al.*, 2005; Rutherford *et al.*, 2007), which allowed us to sample physiologically relevant Glu (Drew *et al.*, 2004). The small size of our MEAs, in conjunction with our self-referencing capability (Burmeister and Gerhardt, 2001), allowed us to measure resting levels of Glu and determine that a portion was TTX-dependent and not from reversal of the high-affinity transporters for Glu as demonstrated using THA to block the EAATs.

When using *in vivo* amperometry, the ability to selectively identify the molecule of interest was questioned; however, our laboratory overcame these issues. First, the enzyme-based MEAs differentially recorded a specific molecule, in this case Glu, due to the high selectivity of GluOx for its substrate (Glu) (Kusakabe *et al.*, 1983). Varying the applied potential to the Pt recording surface is another way we identify the molecule of interest. The reporter molecule, H₂O₂ that was produced from the metabolism of Glu by GluOx was predominantly oxidizable at +0.7 V vs. a Ag/AgCl reference electrode. When the applied potential is dropped to +0.2 V vs. a Ag/AgCl reference electrode, much of

the H₂O₂ was no longer oxidized at the Pt recording surface resulting in a decrease in signal (Day *et al.*, 2006; Rutherford *et al.*, 2007). Finally, the ability to perform self-referencing and subtract off interferents from the Glu signal enhanced the selectivity of our MEA. Since the sentinel sites were not coated with GluOx, they did not respond to changes in extracellular concentrations of Glu, thereby allowing us to qualitatively visualize responses that were solely from a Glu source. Furthermore, the offline subtraction method allowed us to remove any possible interferents or noise artifacts that quantitatively added to the extracellular Glu concentration. Self-referencing methods were employed throughout this study to ensure that resting and peak responses (maximum amplitude) were due primarily to changes in extracellular Glu levels.

We locally applied an isotonic solution of Glu (0.5 μ l, 1mM) in the PFC and Str of the C57BL/6 mouse on days 3, 5 and 7 post-implantation to determine the longevity of the enzyme-based MEA *in vivo*. We saw no significant change in MEA sensitivity for Glu in either brain region on days 3 - 7 post-implantation. Both brain regions had similar responses to local application (0.5 μ l) of 1 mM Glu with the Str ($35.6 \pm 9.9 \mu$ M) having slightly higher responses ($p=0.71$), on average, compared to the PFC ($30.5 \pm 7.8 \mu$ M) as shown in table 5.1. Rutherford and colleagues (2007) observed similar *in vivo* MEA longevity to Glu in the PFC and Str of Fischer 344 and Long Evans rat strains. Since there was no decline in MEA response for Glu we concluded that the enzyme activity of GluOx, when adhered to our Pt recordings sites of our MEA, was viable for at least 7 days *in vivo*. This had important implications as we progress this technology to study behavior related changes in extracellular Glu over days in the awake, freely moving mouse.

To better understand the clearance of exogenously applied 1 mM Glu we examined the uptake rate and time for 80% decay (t_{80}) of the Glu signals on days 3, 5 and 7 post-implantation. We found that in both the PFC and Str there was a nonsignificant decrease in uptake rate over days. We also noticed that the average Glu uptake rate in the Str ($13.4 \pm 4.2 \mu$ M/sec) was increased compared to the PFC ($5.8 \pm 1.9 \mu$ M/sec), but not significantly ($p=0.17$). Due to the long

duration of Glu uptake after local application of 1 mM Glu in the freely moving mice we also decided to look at the time period for 80 percent of the signal to decay (t_{80}). Both the Str ($p=0.35$) and PFC ($p=0.32$) had a nonsignificant increase in t_{80} over days, which was to be expected since the uptake rate decreased over days. On average, the PFC (12.6 ± 2.6 sec) had a longer t_{80} compared to the Str (8.5 ± 1.5 sec), which was significant ($p<0.05$) on day 7 post-implantation. Since we saw a slower uptake rate in the PFC compared to the Str, it was expected that the duration of clearance was longer in the PFC. These differences indicate several possibilities. Clearance differences between brain regions could indicate that there was a variation in Glu transporter number between the two brain regions, with the Str having a higher density of transporters resulting in faster clearance. Addressing changes in Glu clearance over days within a brain region was more difficult to explain. Differences in cellular density and number of synapses between brain regions (and even within the neocortex) could affect diffusion of neurotransmitters as well as transporter numbers (DeFelipe *et al.*, 2002). We know that our MEAs caused only limited damage to the surrounding brain tissue (Rutherford, *et al.*, 2007); however, we were uncertain on the extent of damage caused by the guide cannula; especially, when factoring in removal/insertion of the dummy and internal cannula over multiple days. If we were damaging the surrounding glia, it would go to reason there would be less transporters available thus slowing Glu uptake over days in both brain regions (Yi and Hazell, 2006; Beschorner *et al.*, 2007). We were also unsure of what local application of 1 mM Glu does to the surrounding CNS tissue. This could induce transporter trafficking to and from the plasma membrane thus affecting clearance kinetics over days (Fournier, *et al.*, 2004).

Our MEA self-referencing recording techniques were also used to effectively and reliably measure resting Glu levels (Day *et al.*, 2006; Rutherford *et al.*, 2007). As shown in table 5.1 our data indicated that there was no significant ($p=0.31$) change in resting Glu levels over days within the PFC and the Str nor averaged across brain regions (3.3 ± 1.0 μ M; 5.0 ± 1.2 μ M, respectively). The limited number of publications using microdialysis in freely moving C57BL/6 mice

to study resting Glu levels made it difficult to compare the techniques. We were unaware of any studies using microdialysis in the PFC of freely moving C57BL/6 mice, but Meshul's group had three separate studies with probe placement in the Str (Holmer *et al.*, 2005 a,b; Shakil *et al.*, 2005). In table 5.3, our resting Glu values utilizing our enzyme-based MEA technology coupled with *in vivo* amperometry in the Str of freely moving C57BL/6 mice were higher (at least double in two studies) compared to what Meshul's group observed using microdialysis. These discrepancies may be explained by the difference in sampling time and method as well as the origin of the Glu pool being sampled. The small size of our MEA tips caused less damage compared to a microdialysis probe (Clapp-Lilly *et al.*, 1999; Peters *et al.*, 2004; Borland *et al.*, 2005; Rutherford *et al.*, 2007) which helped to improve the spatial resolution of the sampling method (Drew *et al.*, 2004). Furthermore, our considerably faster sampling rate allowed us to measure Glu closer to the synapse and subsequently the neuronal pool of Glu (Drew *et al.*, 2004).

Our laboratory was also interested in determining how resting Glu levels in the Str were affected by blocking all EAATs using the transportable competitive inhibitor, THA (Figure 7). Local application of an isotonic solution of 100 μ M THA (1.0 μ l, pH 7.4) caused a significant ($p < 0.05$) increase ($2.9 \pm 1.2 \mu$ M) in resting Glu levels when compared to 0.9% saline control ($0.3 \pm 0.1 \mu$ M). This was an approximate 60% increase in resting Glu levels in the Str when compared to averaged resting Glu Str values from table 5.1. Furthermore, local application of THA resulted in sustained Glu elevation when compared to our data from local application of exogenous Glu. This was expected since resting Glu was now competing for uptake with THA whereas exogenously applied Glu induced an immediate effect without competition for uptake present. When blocking the high affinity transporters, resting Glu levels were from diffusion from the synapse and essentially neuronal sources. Unfortunately, heteroexchange of Glu from astrocytes cannot be ruled out with transportable inhibitors, however, even non-transportable inhibitors such as D,L-*threo*- β -benzyloxyaspartate (TBOA) were

Table 5.3: Comparison of Resting Glu Levels in the Str of C57BL/6 Mice

Author	Technique	Sampling Interval	Location	Resting Glu (μM)
Hascup, K.N. <i>et al.</i>	amperometry	1 sec	Striatum	5.0 ± 1.2
Holmer, H.K. <i>et al.</i>	microdialysis	15 min	Striatum	3.5 ± 0.1 to 4.2 ± 0.1
Holmer, H.K. <i>et al.</i>	microdialysis	15 min	Striatum	~ 2.75
Shakil, S.S. <i>et al.</i>	microdialysis	15 min	Striatum	1.2 ± 0.1 to 1.8 ± 0.1

Resting Glu levels in the Str of C57BL/6 mice when measured using MEAs compared to studies using microdialysis probes.

shown to induce heteroexchange at similar concentrations (Anderson *et al.*, 2001).

To determine the neuronal contribution to resting Glu levels in the Str, the sodium channel blocker, TTX, was locally applied adjacent to the MEA. Local application of an isotonic solution of 1 μM TTX (1.0 μl ; pH 7.4) ($-1.0 \pm 0.2 \mu\text{M}$) caused a significant decrease ($p < 0.05$) in resting Glu levels compared to citrate control (1.0 μl ; pH 7.4) ($-0.3 \pm 0.1 \mu\text{M}$). This was an approximate 20% decrease in resting Glu levels in the Str when compared to averaged resting Glu levels from table 5.1. This observation was in contrast with several microdialysis studies examining TTX-dependency in rats (Timmerman and Westerink, 1997) and further supported findings conducted by our laboratory in rats (Day *et al.*, 2006) and others using microelectrodes (Kulagina *et al.*, 1999; Oldenziel *et al.*, 2006). Unlike other TTX studies using Glu selective microelectrodes in anesthetized rats, our freely moving mouse studies did not completely attenuate resting Glu levels for two possible reasons. First, our laboratory demonstrated that the use of anesthetic significantly decreased resting Glu levels (Rutherford, *et al.*, 2007) in rats. Anesthetics such as chloral hydrate and urethane exert their effects by enhancing inhibitory synaptic neurotransmission as well as inhibiting excitatory neurotransmission (Hara and Harris, 2002); possibly making the glutamatergic system more susceptible to blockade of sodium channels by TTX. Second, our concentration of TTX (1 μM) used was 100 fold lower compared to those used in the anesthetized rat studies (Kulagina *et al.*, 1999; Day *et al.*, 2006; Oldenziel *et al.*, 2006). It should be noted that TTX concentrations of 5 μM and higher were locally applied and resulted in severe lower limb paralysis forcing us to immediately euthanize these mice according to our approved protocols.

Finally, we wanted to study the effects of a stressor on resting Glu levels. To do this, we applied fox urine on a cotton ball and introduced it into the recording chamber for 5 minutes, which resulted in a $\sim 7 \mu\text{M}$ increase in Glu levels. Glu levels rose throughout the 5 minute stressor and took approximately 15 minutes to return to baseline after removal. Since this was an odor stressor, it

took time for the smell to diffuse out of the recording chamber once the cotton ball was removed, which may explain the prolonged time period for levels to return to baseline. This experiment demonstrated our ability to record changes in Glu due to behaviorally related stimuli.

In summary, the present studies using MEAs configured for second-by-second Glu measurements were viable for at least 7 days post-implantation in the awake, freely moving mouse. This increased recording time span has helped us to better understand resting Glu levels. We observed a nonsignificant difference in resting Glu levels between the PFC and Str of awake C57BL/6 mice. We also observed that local application of pharmacological agents such THA and TTX altered resting Glu levels. We saw a significant increase in resting Glu levels with the addition of THA and a significant decrease in resting Glu levels with the addition of TTX, which indicated that resting Glu levels were neuronally derived. These findings provided evidence that the high spatial and low temporal resolution provided by our MEA technology was necessary to better understand resting Glu levels. Furthermore the ability to monitor Glu without anesthesia allowed us to study Glu dynamics for at least 7 days post-implantation. When we couple this finding with our changes in Glu from a stressor such as fox urine we can design behavioral paradigms to better understand physiological release and uptake of Glu.

Copyright © Kevin Nicholas Hascup

Chapter Six: Conclusion

Introduction

The most important findings from our GLUD1 transgenic mouse studies is their increased stimulus-evoked Glu release as well as their spontaneous motor neuron degeneration. It is well known that excessive Glu release and activation of post-synaptic receptors can kill neurons (Olney, 1978). This has undoubtedly led us to the model excitotoxicity proposed in Chapter III. Upregulation of GLUD1 gene leads to production of more GLUD1 protein. This in turn leads to the synthesis of Glu from α -ketoglutarate and subsequent increased vesicle packaging of Glu in glutamatergic neurons. With increased amounts of Glu in vesicles, the GLUD1 transgenic mice released more Glu into the extracellular space after stimulus compared to WT. Since there is not a compensatory increase in Glu uptake in the GLUD1 transgenic mice, more Glu is available in the synaptic cleft of GLUD1 transgenic mice to activate iGluRs and mGluRs. In particular the NMDA receptor, whose gene for the Glu binding domain was upregulated in GLUD1 transgenic mice. Since motor neurons have little to no calcium sequestering proteins (Van Den Bosch *et al.*, 2005), mitochondria are forced to buffer the intracellular calcium. Over time, if the mitochondria become damaged by excessive intracellular calcium, proteases, oxygenases, and reactive oxygen species (ROS) form, which are key mediators of excitotoxic cell death. Despite this model, it doesn't explain what neurological disease state these mice most closely represent. Unfortunately, there is not a simple relationship between high extracellular levels of glutamate and neuronal death (Obrenovitch and Urenjak, 1997), which makes narrowing this transgenic mouse down to a specific disease state a daunting task.

Alzheimer's Disease

AD is a chronic degenerative neurological disorder characterized by progressive loss of memory and cognition (Katzman and Saitoh, 1991). Pathologically, AD is characterized by three major hallmarks: senile plaques

consisting of amyloid β -peptide ($A\beta$), neurofibrillary tangles consisting of hyperphosphorylated tau protein, and loss of synapses (Katzman and Saitoh, 1991). Since Glu is involved in cognition, it goes to reason that this neurotransmitter plays a key role in the progression of AD. Recent studies suggest that glutamate-induced NMDA receptor activation stimulates amyloid precursor protein to produce $A\beta$ (Gordon-Krajcer *et al.*, 2002). Burbaeva and colleagues (2005) determined that GLUD1 was increased in brain tissue homogenate from the prefrontal cortex (PFC) of Alzheimer's disease (AD) patients compared to control patients. This group concludes that alterations in Glu metabolizing enzymes may be responsible for changes in the extracellular concentration of Glu. If an increase in GLUD1 is causing an increase in extracellular concentrations of Glu, this may lead to over stimulation of NMDA receptors and excess $A\beta$ production with consequent oxidative stress-induced neuroexcitotoxicity. Studies have also shown that the EAAT2 activity is significantly reduced in the brains of AD patients (Masliah, *et al.*, 1996). Other studies have found a correlation between loss of glutamine synthetase and cognitive and functional status of AD patients (Antuono *et al.*, 2001). Inhibition of Glu transport, coupled with decreased activity of glutamine synthetase or increased activity of GLUD1, may lead to increased extracellular levels of Glu. These increased levels of extracellular Glu can cause excessive stimulation of NMDA receptors and excitotoxic processes involving excess intraneuronal Calcium accumulation and eventual neuronal death.

The information provided above presents some potential similarities between the GLUD1 transgenic mice as a model of AD. Our studies have not directly examined the GLUD1 transgenic mouse brains for formation of senile plaques or tauopathies. Staining at the University of Kansas has shown ubiquitinated protein aggregates in the hippocampus of 16-20 month old GLUD1 mice. These results suggested the appearance of aggresome-like structures in vulnerable neurons of GLUD1 transgenic mice, indicating neuronal stress. AD patients show that CA1 neurons are selectively damaged at an early stage of the disease and the same neurons show accumulations of ubiquitinated-proteins.

We cannot make definitive conclusions regarding the levels of EAAT2 transporters in the GLUD1 transgenic mice because the appropriate experiments to examine this have not been conducted. However, no difference in Glu uptake was observed with our MEA studies. In addition, no studies were conducted to determine activity of glutamine synthetase. The oxidative stress due to A β may explain EAAT2 and glutamine synthetase dysfunction, but this has not been elucidated in the GLUD1 motor deficient mice. The biggest drawback to elucidating this mouse as a model of AD is the fact that the mice show no cognitive impairment in behavioral memory studies, a hallmark of AD in humans. More studies are needed to examine these factors to provide additional information to better characterize these mice as a model of AD.

Amyotrophic Lateral Sclerosis

ALS is a chronic progressive disorder characterized by the selective degeneration of motor neurons in the cerebral cortex, brainstem, and spinal cord (Danbolt, 2001). Symptoms normally are muscular weakness and atrophy which leads to extensive paralysis and death due to respiratory failure generally within 2-5 years from diagnosis (McGeer and McGeer, 2005). There is a growing body of evidence implicating excitotoxicity as a contributing factor to motor neuron injury either as a primary or secondary mechanisms (Heath and Shaw, 2002). A study conducted by Malessa and colleagues (1991) have shown that GLUD1 is upregulated in the ventral horn of the spinal cord of ALS patients. It is well documented that Glu levels are increased in the CSF of ALS patients (Rothstein *et al.*, 1990; Doble, 1999; Heath and Shaw, 2002; Spreux-Varoquaux *et al.*, 2002). Since the GLUD1 reaction favors Glu formation, this finding by Malessa and colleagues, suggests a causative relation for the increased levels of Glu. These CSF Glu levels may be high enough to cause excitotoxicity and damage motor neurons—a hallmark of ALS. Other studies have shown that EAAT2 levels are lower resulting in reduced uptake of extracellular Glu (Rothstein *et al.*, 1992). Currently, it is not clear if the reduced EAAT2 expression is the primary event leading to motor neuron death and ALS or if the reduced expression is secondary

to the neuron loss; however, available data suggests it to be the later (Danbolt, 2001).

The information presented above provides a strong case for categorizing the GLUD1 transgenic mice as a model of ALS. We know from our electrochemical studies that increased gene copy number leads to an increase of stimulus-evoked Glu release. At 16 months of age, these mice have obvious movement and righting impairments. Histological data provided by the University of Kansas clearly show upper and lower motor neuron atrophy and necrosis in the GLUD1 transgenic mice. The only piece of evidence not supporting a model of ALS is a decrease in the EAAT2 levels. We cannot make definitive conclusions regarding the levels of EAAT2 transporters in the GLUD1 transgenic mice because the appropriate experiments to examine this have not been conducted. However, no difference in Glu uptake was observed with our MEA studies. If transporter levels are decreased as a secondary mechanism, it might go to reason that we should not have seen differences in Glu clearance since all our electrochemical studies were conducted in GLUD1 mice that were 8-12 months of age. Similar studies in the 16 month motor deficient GLUD1 transgenic mice might help elucidate this question as well as provide us with more information to better characterize these mice as a model of ALS.

Epilepsy

Epilepsy is a chronic neurological disorder characterized by recurring seizures. As the principal excitatory neurotransmitter, Glu inevitably plays a role in the initiation and spreading of seizure activity (Danbolt, 2001). Studies have shown that Glu levels are elevated in patients with various epilepsies and it has been shown that Glu is elevated patients just prior to the onset of seizures (Danbolt, 2001). It is not known if defective uptake plays a role in epilepsy in humans, but reduced expression of transporters has been shown to cause or be associated with seizures in animal models (Danbolt, 2001). For example, mice lacking EAAT2 develop spontaneous seizures.

The motor deficient GLUD1 mice would not be categorized well as a model of epilepsy. Despite the fact that force plate actometer studies conducted at the University of Kansas have noted seizure like activity during behavioral studies in some of the GLUD1 motor deficient mice. However, this does not explain the motor deficits observed in these mice. Also, we cannot make definitive conclusions regarding the levels of EAAT2 transporters in the GLUD1 transgenic mice because the appropriate experiments to examine this have not been conducted. However, no difference in Glu uptake was observed with our MEA studies. Based on these findings the GLUD1 motor deficient mice are not a good model of epilepsy.

Huntington's Disease

Huntington's disease (HD) is a neurodegenerative disorder characterized by adult onset with choreic movements combined with mental impairments. The gene responsible for HD is localised on chromosome 4 that encodes the protein huntingtin. The disease is caused by the presence of strings of CAG repeats in the DNA that introduce polyglutamine sequences into the protein that endows the protein with neurotoxic properties (Doble, 1999). Initial observations showed that the NMDA agonist, quinolinic acid, reproduce the lesions seen in HD. Additional studies suggest that selective neurodegeneration can be produced by energy impairment, which sensitizes striatal neurons to the excitotoxic effects of Glu, which is a classic case of slow excitotoxicity.

The motor deficient GLUD1 mice would not be categorized well as a potential model of HD. The main similarities are centered on the movement disorders. Histological studies show that the large upper and lower motor neurons are deteriorating in the GLUD1 mice. This is unlike HD where the larger neurons are spared and the medium sized neurons atrophy. Also, there is no indication that the huntingtin protein is altered in these mice, but a direct examination of this protein in the GLUD1 mice is needed before anything definitive can be claimed. But based on these early observations, the GLUD1 motor deficient mice is not a good model of HD.

Parkinsons Disease

PD is a progressive degenerative neurological disorder pathologically characterized by motor symptoms that include rigidity, hypokinesia and tremor, which is a result of massive and selective loss of dopaminergic neurons in the nigrostriatal pathway (Doble, 1999). This causes imbalance in the motor circuits in the basal ganglia, which leads to a net increase in inhibitory output from the basal ganglia to the thalamus (Doble, 1999). This results in profound modifications of glutamatergic firing throughout the basal ganglia. Some experimental evidence suggests that neurodegeneration of dopaminergic neurons in substantia nigra involves a toxic action exerted by Glu on the NMDA receptor.

The motor deficient GLUD1 mice would not be categorized well as a potential model of HD. The main similarities are centered around the movement disorders. The main difference is the fact that there appears to be no loss of dopaminergic neurons in the GLUD1 motor deficient mice. Preliminary studies conducted in Dr. Don Gash's laboratory showed no loss of dopaminergic neurons as well as tyrosine hydroxylase staining for catecholamines. Since loss of dopaminergic neurons is a hallmark sign of PD in humans, based on these preliminary studies, it would be impossible to use the GLUD1 motor deficient mice as a model of PD.

Final Notes

Based on the data presented for the predominant neurological disorders described in this chapter, the most likely candidate that the GLUD1 motor deficient mice would model is ALS. The GLUD1 mice show spontaneous motoneuron degeneration around 16 months of age, which is slightly past the half-way time point of a mouse's lifespan. This is similar age of onset for people who develop ALS. The histopathology is similar between ALS and the GLUD1 mice. In both, the spontaneous degeneration is limited to the large upper and lower pyramidal neurons. More studies are needed to provide a stronger case.

For example, we have not studied the role of Calcium ions, which is speculated to lead to formation of reactive oxygen species, which is implicated in models of excitotoxicity. A long term goal of this project is to provide evidence that shows the increased levels stimulus-evoked Glu release due to upregulation of the GLUD1 gene leads to overstimulation of the NMDA receptor and subsequent Calcium influx and eventual reactive oxygen species formation leading to motor neuron degeneration. But these early studies indicate something not normally studied when it comes to neurological disorders. Dysregulation of Glu metabolizing enzymes may be the initial event that leads to a cascade of problems that overtime causes the severe memory or motor impairments. More studies throughout the scientific community need to be conducted in animal models of neurological diseases to address this issue.

Copyright © Kevin Nicholas Hascup

Appendix A: L-Glutamate Dynamics in Male Glutamate Pyruvate Transaminase Knock Out Mice

Introduction

The development of the GPT KO mouse line was one of several transgenic mouse lines bred in Dr. Elias Michaelis's research laboratory at the University of Kansas. Unfortunately, their laboratory was not equipped or funded to maintain a large breeding colony for each transgenic model being studied. For this reason, litters were kept small, which forced our early studies to examine both male and female GPT KO mice. Our preliminary studies indicated several gender differences in Glu regulation when examining this first set of GPT KO mice. This was expected since the limited data examining hormonal regulation on Glu neurotransmission indicates that female hormones act as antagonists on iGluRs (Bergeron *et al.*, 1996). Because of its antagonistic effects on iGluRs, progesterone has been shown to be a successful post-injury treatment for stroke and traumatic brain injury in both males and females (Stein, 2001). In addition, recent work suggests that the estrogen receptor alpha (ER α) is found at extranuclear sites on neurons where they directly modulate excitation or inhibition (Stein, 2001 and Toran-Allerand, 1996). Since females, not males maintain circulating blood plasma levels of progesterone and occasionally estrogen, we hypothesized that male and female GPT KO mice would differ in Glu neurotransmission.

These differences we observed in our preliminary studies warranted further examination with a larger number of animals for both male and female GPT KO mice. However, due to the age range used in these studies, the small litters, and the fact that the University of Kansas was performing behavioral and histological studies on these mice, few male GPT homozygous mice were available for study. This made it difficult to statistically compare the male and female GPT KO groups. All data regarding the male GPT KO mice are given below and general comparisons between genders are discussed.

Methods

All transgenic mice were developed at the University of Kansas by Dr. Elias K. Michaelis's laboratory. A nonfunctional rat GPT transgene was inserted into the mouse genome under the control of the Neuronal specific enolase (NSE) promoter. The NSE promoter has been shown to be expressed only in neurons of the brain and spinal cord (Choi *et al.*, 1992; Peel *et al.*, 1997). Transgenic mice were generated by injecting mouse oocytes (C57BL/6J-SJL hybrid) with vectors containing cDNA of nonfunctional rat GPT placed under the control of the NSE promoter. This promoter was excised from the pNSE-LacZ vector by first digesting the SV40 polyA tail of pNSE-LacZ vector and cloning it into pGEM-7Z. The NSE promoter was also excised and cloned into the modified pGEM-7Z. Finally, a nonfunctional GPT open reading frame was cloned into the pNSE-GEM-7Z to create the pNSE-GPT vector for the GPT transgenic mice. The vector was digested, the DNA recovered, and microinjected into the nucleus of fertilized mouse oocytes to generate the GPT KO mice. Oocytes were transferred to surrogate C57BL/6 mice. Pups carrying the transgene were identified by PCR and Southern Blot Analysis. Progeny were eventually backcrossed into a C57BL/6 mouse strain.

GPT KO C57BL/6 mice were transported to the University of Kentucky and housed as described in Chapter Two. For the GPT KO study, both male and female mice were studied. Only the results from the male analysis are included in this Appendix; the female analysis is found in Chapter Four. Breeding limited sufficient numbers of male homozygous mice (n=2) for complete analysis and comparison between genders

Mice were given 3 i.p. injections of 12.5% urethane for a total dose of 1.25 g/kg. All studies were conducted in the Str. Glu recordings were conducted using enzyme-based MEAs with a sampling rate of 1 Hz as previously described in Chapter Two. A craniotomy was performed over both striatal hemispheres and MEAs were stereotaxically placed using the coordinates from Paxinos and Franklin (2004) (AP: +0.9 mm; ML: \pm 1.5, \pm 1.7 mm; DV: -2.25, -2.75, -3.25, -3.75

mm vs bregma) in order to create a depth profile of the Str in transgenic and WT mice. A glass micropipette with an internal diameter of 10-12 μm was attached to the PCB and positioned among the four Pt recording sites, resting 50-100 μm above the recording surface. Through this glass micropipette isotonic solutions of 70 mM KCl (70 mM KCl, 79 mM NaCl, 2.5 mM CaCl_2 ; pH 7.4) and 5 mM Glu (in 0.9% saline; pH 7.4) were locally applied to the surrounding brain tissue to study glutamatergic neurotransmission. Upon initial MEA placement, a stable baseline recording was obtained for at least 30 minutes prior to local application of solutions. Since self-referencing MEAs were used, resting Glu levels were calculated during this initial baseline time period. After the initial baseline recording, solutions were locally applied at regular 30 second intervals (for a total of 20 signals; 10 signals from each Pt recording site) to assess Glu dynamics at each recording depth. Due to the reproducibility of Glu signals *in vivo*, all signals for a particular depth were averaged into a single data set for that depth. Data analysis involved an ANOVA with a Tukey's post hoc test to compare GPT KO groups. All data was reported as mean \pm standard error of the mean and significance was defined as $p < 0.05$.

Results

Local application of 70 mM KCl resulted in robust, reproducible Glu signals compared to baseline. To quantitate the amount of Glu released, we volume matched the amount of stimulus locally applied to all three mouse groups. Only Glu signals that were elicited by 50 to 150 nl of 70 mM KCl were used for this analysis, therefore, no significant difference in the amount of stimulus used was observed between the GPT WT (107 ± 4 nl), heterozygous (97 ± 4 nl) and homozygous (109 ± 9 nl) mice (figure A.1A). When the average maximal amplitude of Glu release was quantitated, GPT heterozygous mice (10.9 ± 1.3 μM) released significantly more Glu ($p < 0.001$) compared to WT (2.9 ± 0.5 μM) and ($p < 0.05$) homozygous (3.9 ± 1.2 μM) littermates (figure A.1B). Using the same subset of signals, striatal, depth-related alterations in stimulus-evoked Glu release were also examined (figure A.2). The average Glu release was

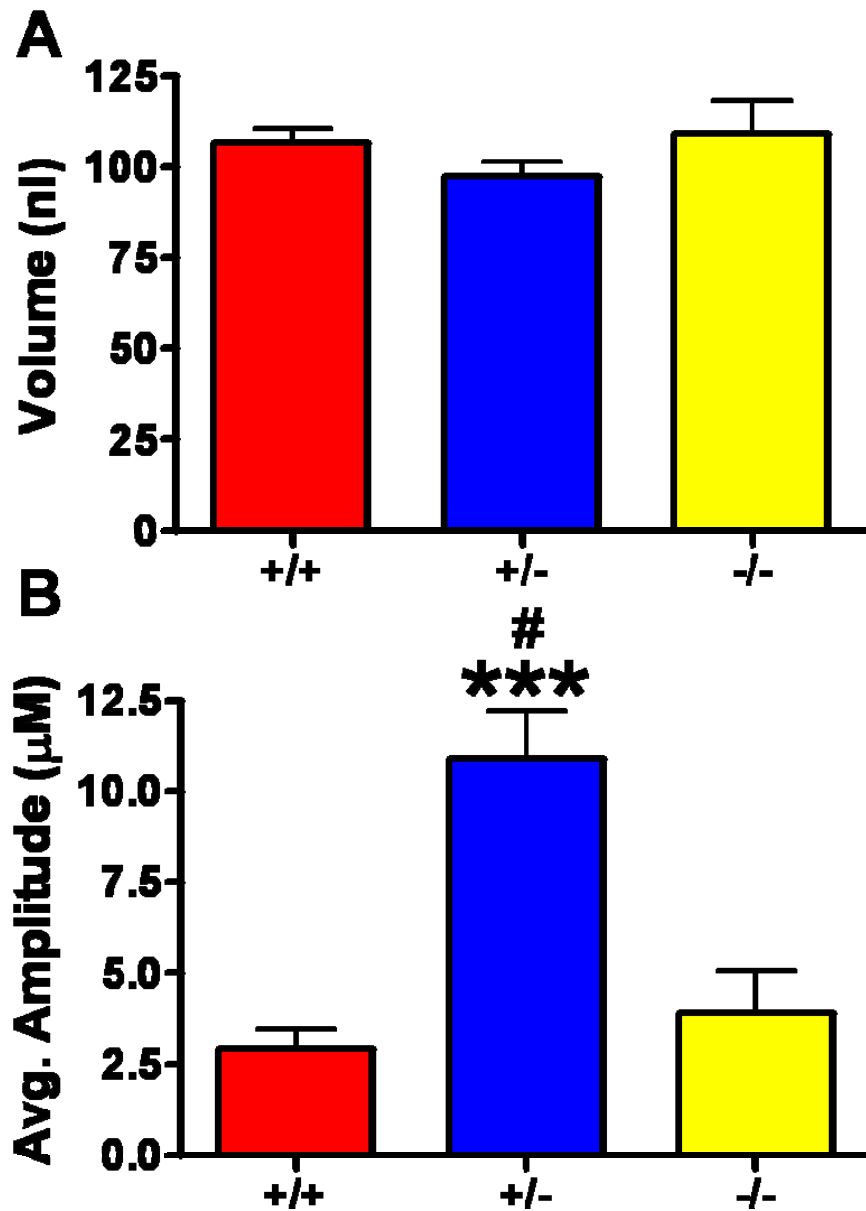


Figure A.1: Stimulus-Evoked Glu Release in the Male GPT KO Mice

A) Only Glu signals that were elicited by 70 mM KCl whose volumes ranged between 50 and 150 nl were analyzed for the GPT WT (n=4; +/+; red), heterozygous (n=7; +/-; blue) and homozygous (n=2; -/-; yellow) mice. Since the volumes were matched, no significant difference in the amount of stimulus locally applied was observed between WT (107 ± 4 nl), heterozygous (97 ± 4 nl), homozygous (109 ± 9 nl) mice. B) The average maximal amplitude of Glu released upon local application of 70 mM KCl was significantly increased (**p < 0.001) in the GPT heterozygous mice (10.9 ± 1.3 µM; blue) compared to WT (2.9 ± 0.5 µM; red) and homozygous (3.9 ± 1.2 µM; yellow) littermates. Male GPT heterozygous mice also released significantly (# p < 0.05) more Glu compared to homozygous mice.

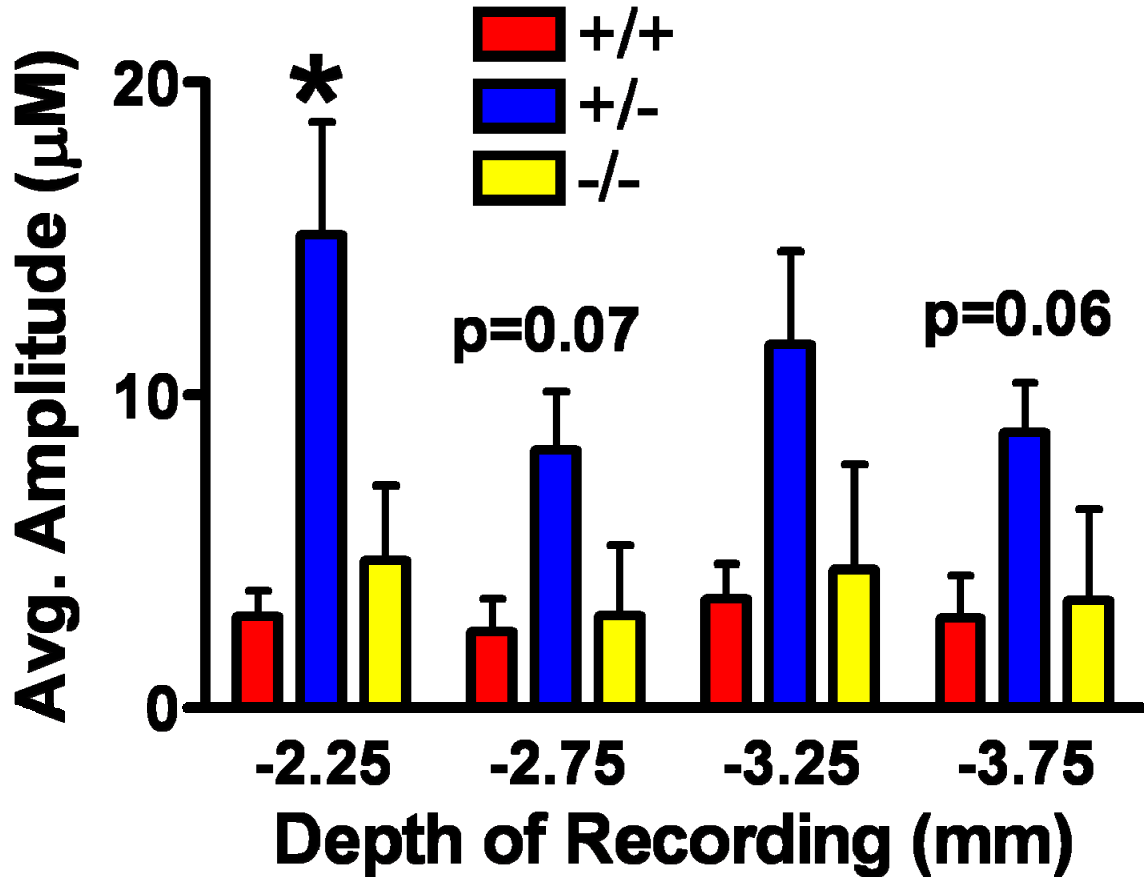


Figure A.2: Stimulus-Evoked Glu Release Depth Profile in the Male GPT KO Mice

Average stimulus-evoked Glu release at different recording depths within the Str of GPT WT (n=4; red; +/+), heterozygous (n=7; blue; +/-), and homozygous (n=2; yellow; -/-) mice. GPT heterozygous ($15.1 \pm 3.6 \mu\text{M}$) mice released significantly ($p < 0.05$) more Glu compared to WT ($2.9 \pm 0.9 \mu\text{M}$) and homozygous ($4.7 \pm 2.4 \mu\text{M}$) mice at recording depth -2.25 mm. A trend was also observed for increased Glu release at recording depth -2.75 and -3.75 mm. A one-way ANOVA with Tukey's post hoc was conducted at each depth for statistical analysis.

calculated at each depth (DV -2.25 to -3.75 mm) and compared amongst the GPT KO mouse groups. GPT KO heterozygous mice released significantly ($p < 0.05$) more Glu at depth -2.25 mm compared to WT and homozygous mice. Also, at recording depths -2.75 mm and -3.75 mm the average maximal Glu released for GPT KO heterozygous mice approached significance ($p = 0.07$ and $p = 0.06$, respectively).

Since neurotransmitter uptake follows classical Michaelis-Menten kinetics (Nicholson, 1995) and was affected by the amount of available substrate, Glu uptake was analyzed by selecting a subset of signals with maximum release values were in the range of 3-13 μM . This range was chosen, because these peak Glu values were easily obtainable in both groups. Within this subset of signals, no significant difference in average maximum release of Glu was observed in WT ($4.8 \pm 0.4 \mu\text{M}$), heterozygous ($5.9 \pm 0.3 \mu\text{M}$) and homozygous ($6.0 \pm 0.4 \mu\text{M}$) mice (figure A.3A). We did observe significantly faster Glu uptake in the GPT KO heterozygous ($p < 0.05$; $1.8 \pm 0.2 \mu\text{M}/\text{sec}$) and homozygous ($p < 0.001$; $2.8 \pm 0.4 \mu\text{M}/\text{sec}$) mice compared to WT ($1.2 \pm 0.1 \mu\text{M}/\text{sec}$). We also observed that the GPT homozygous mice had significantly ($p < 0.05$) faster Glu uptake compared to heterozygous mice (figure A.3B). Examining the same subset of signals, a striatal depth analysis was performed for Glu uptake (figure A.4). At recording depth -3.75 mm, GPT homozygous mice had a significantly ($p < 0.05$) faster Glu uptake rate ($2.6 \pm 0.4 \mu\text{M}/\text{sec}$) compared to WT ($1.0 \pm 0.2 \mu\text{M}/\text{sec}$) mice. Stimulus-evoked Glu uptake in the GPT heterozygous ($3.3 \pm 1.2 \mu\text{M}/\text{sec}$) mice approached significance ($p = 0.0513$) compared to WT ($1.0 \pm 0.1 \mu\text{M}/\text{sec}$) mice at the recording depth -3.25 mm.

Due to the electrogenic nature of Glu transporters (Takahashi *et al.*, 1997; Doble, 1999), we wanted to determine transporter function without membrane depolarization. We locally applied an isotonic solution of 5 mM Glu (pH 7.4) and examined a subset of Glu signals. Unfortunately, the low number of animals studied for the GPT homozygous group limited the number of signals. For this reason, we had to analyze signals that were in the range of 8-13 μM , which was a higher range as those used for our stimulus-evoked Glu uptake analysis.

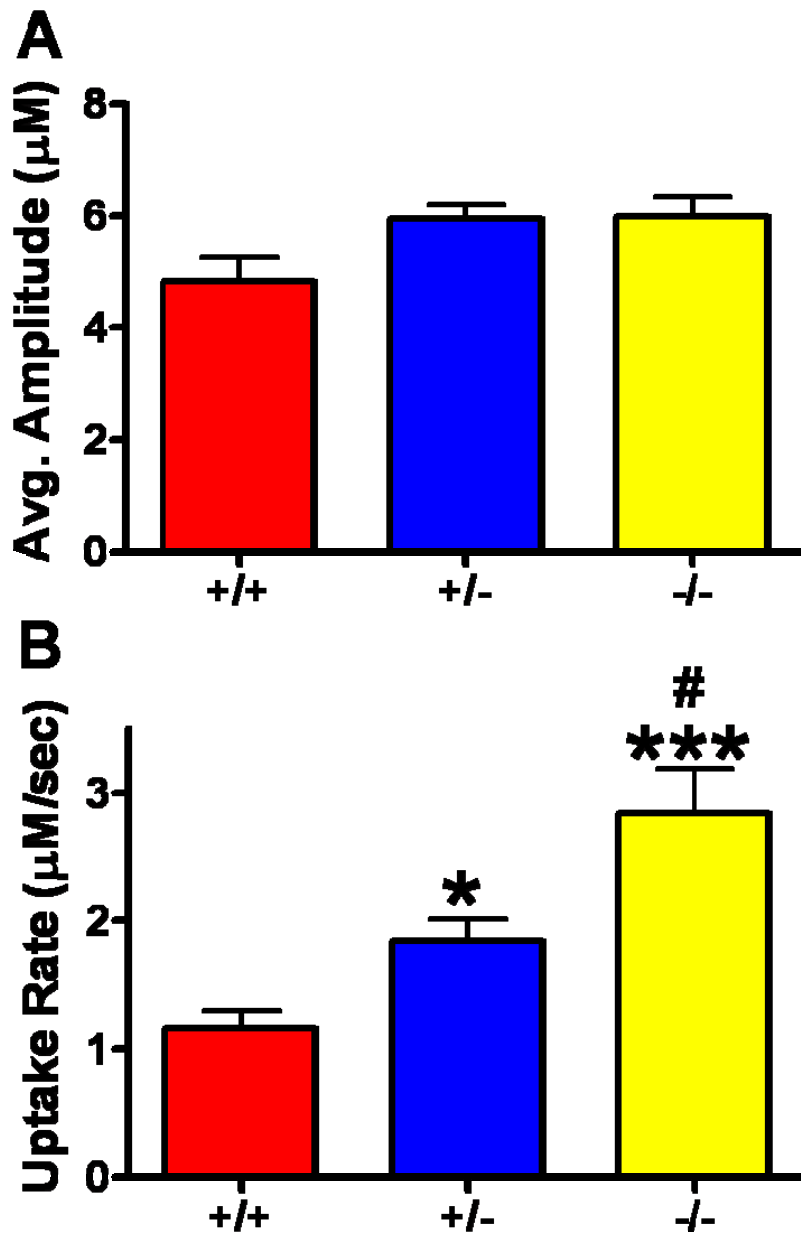


Figure A.3: Stimulus-Evoked Glu Uptake in the Male GPT KO Mouse Groups

A) Subset of Glu signals were examined whose average maximal amplitude fell in a range of 3-13 μM for both the GPT WT (n=4; +/+; red), heterozygous (n=7; +/-; blue), and homozygous (n=2; -/-; yellow) mice. No significant difference was observed between WT ($4.8 \pm 0.3 \mu\text{M}$), heterozygous ($6.0 \pm 0.5 \mu\text{M}$) and homozygous ($6.1 \pm 0.4 \mu\text{M}$) mice. B) When the uptake rate of stimulus-evoked Glu was examined, both heterozygous ($1.8 \pm 0.2 \mu\text{M}/\text{sec}$; blue), and homozygous ($2.8 \pm 0.4 \mu\text{M}/\text{sec}$; yellow) mice had significantly faster Glu uptake (* $p < 0.05$, *** $p < 0.001$; respectively) compared to WT ($1.2 \pm 0.1 \mu\text{M}/\text{sec}$; red) mice. Also, GPT homozygous mice had a significantly ($\#p < 0.05$) faster Glu uptake compared to heterozygous mice.

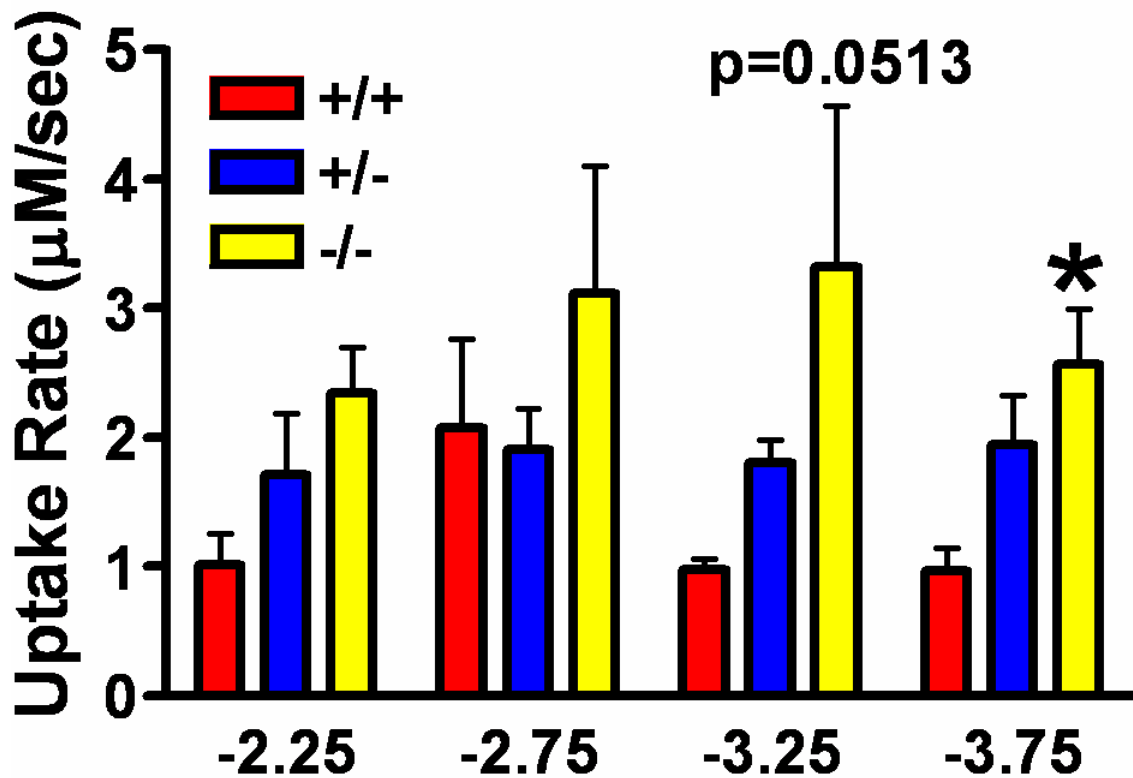


Figure A.4: Stimulus-evoked Glu Uptake Depth Profile in the Male GPT KO Mice

Average stimulus-evoked Glu release at different recording depths within the Str of GPT KO WT (n=4; +/+; red), heterozygous (n=7; +/-; blue), and homozygous (n=2; -/-; yellow) mice. On average, GPT homozygous mice had faster uptake of stimulus-evoked Glu compared to WT and heterozygous mice at all recording depths. This became significant (*p < 0.05) at recording depth -3.75 mm and approached significance at depth -3.25 mm when compared to WT mice. A one-way ANOVA with a Tukey's post hoc was conducted at each depth for statistical analysis.

When examining this range of signals, there was no significant difference in the maximal amplitude of exogenously applied 5 mM Glu in the GPT WT ($9.4 \pm 0.4 \mu\text{M}$), heterozygous ($9.9 \pm 0.4 \mu\text{M}$), and homozygous ($10.5 \pm 0.4 \mu\text{M}$) mice (figure A.5A). Similar to the stimulus-evoked Glu uptake study, we observed significantly ($p < 0.001$) faster uptake in the homozygous ($6.1 \pm 0.3 \mu\text{M}/\text{sec}$) mice compared to the WT ($3.0 \pm 0.4 \mu\text{M}/\text{sec}$) and heterozygous ($3.6 \pm 0.3 \mu\text{M}/\text{sec}$) mice (figure A.5B). Using the same subset of signals, striatal depth-related alterations in clearance of exogenously applied 5 mM Glu was examined (figure A.6). The average clearance rate was calculated at each recording depth (DV -2.25 to -3.75 mm) and compared amongst the GPT KO mouse groups. The clearance of exogenously applied 5 mM Glu was significantly ($p < 0.05$) faster in the GPT homozygous mice compared to controls at recording depths -2.75 mm ($6.0 \pm 0.5 \mu\text{M}/\text{sec}$ and $2.9 \pm 0.8 \mu\text{M}/\text{sec}$, respectively) and -3.75 mm ($6.2 \pm 0.7 \mu\text{M}/\text{sec}$ and $2.3 \pm 0.4 \mu\text{M}/\text{sec}$, respectively). At recording depth -3.25 mm, we observed a nonsignificant increase ($p = 0.1$) in the clearance of exogenously applied 5 mM Glu compared to WT littermates. The limited range of amplitudes chosen for this study made it difficult to obtain enough values to perform statistical analysis at recording depth -2.25 mm.

Since self-referencing MEAs were used to study the GPT KO mice, we were able to determine resting Glu levels in the Str. Thirty second baseline measures were taken prior to local application of 70 mM KCl. Resting Glu levels were only measured when 70 mM KCl was in the barrel of the glass micropipette. Possible diffusion of 5 mM Glu out of the barrel caused unphysiologically elevated levels of resting Glu. Using our self-referencing recording techniques, resting Glu levels showed a nonsignificant ($p=0.09$) decreasing trend in heterozygous ($0.9 \pm 0.1 \mu\text{M}$) and homozygous ($0.4 \pm 0.1 \mu\text{M}$) mice when compared to control ($1.1 \pm 0.3 \mu\text{M}$) mice (figure A.7A). Additionally, a depth analysis profile revealed a similar trend at all recording depths to what was observed when the recording depths were averaged. GPT control mice had elevated resting Glu levels at all recording depths, but this was not significant (figure A.7B).

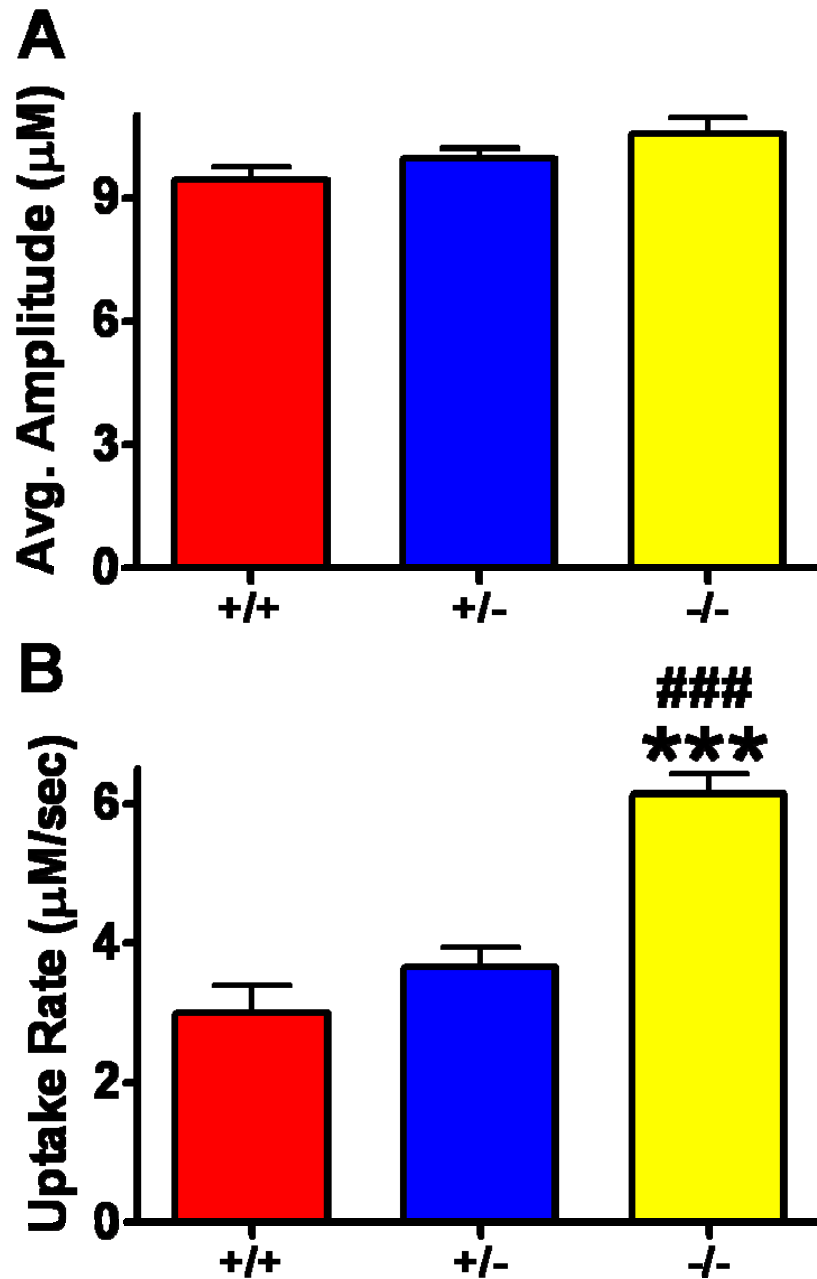


Figure A.5: 5 mM Glu Clearance in the Male GPT KO Mouse Groups

A) A subset of Glu signals were examined whose average maximal amplitude fell in a range of 8-13 μM for the GPT WT (n=3; +/+; red), heterozygous (n=5; +/-; blue), and homozygous (n=2; -/-; yellow) mice. There was no significant difference in the maximal amplitude of exogenously applied 5 mM Glu in the GPT WT (9.4 ± 0.3 μM), heterozygous (9.9 ± 0.3 μM), and homozygous (10.5 ± 0.4 μM) mice. B) We observed significantly (***) faster Glu clearance in the homozygous (6.1 ± 0.3 μM/sec; yellow) mice compared to the WT (3.0 ± 0.4 μM/sec; red) and heterozygous (3.6 ± 0.3 μM/sec; blue) mice.

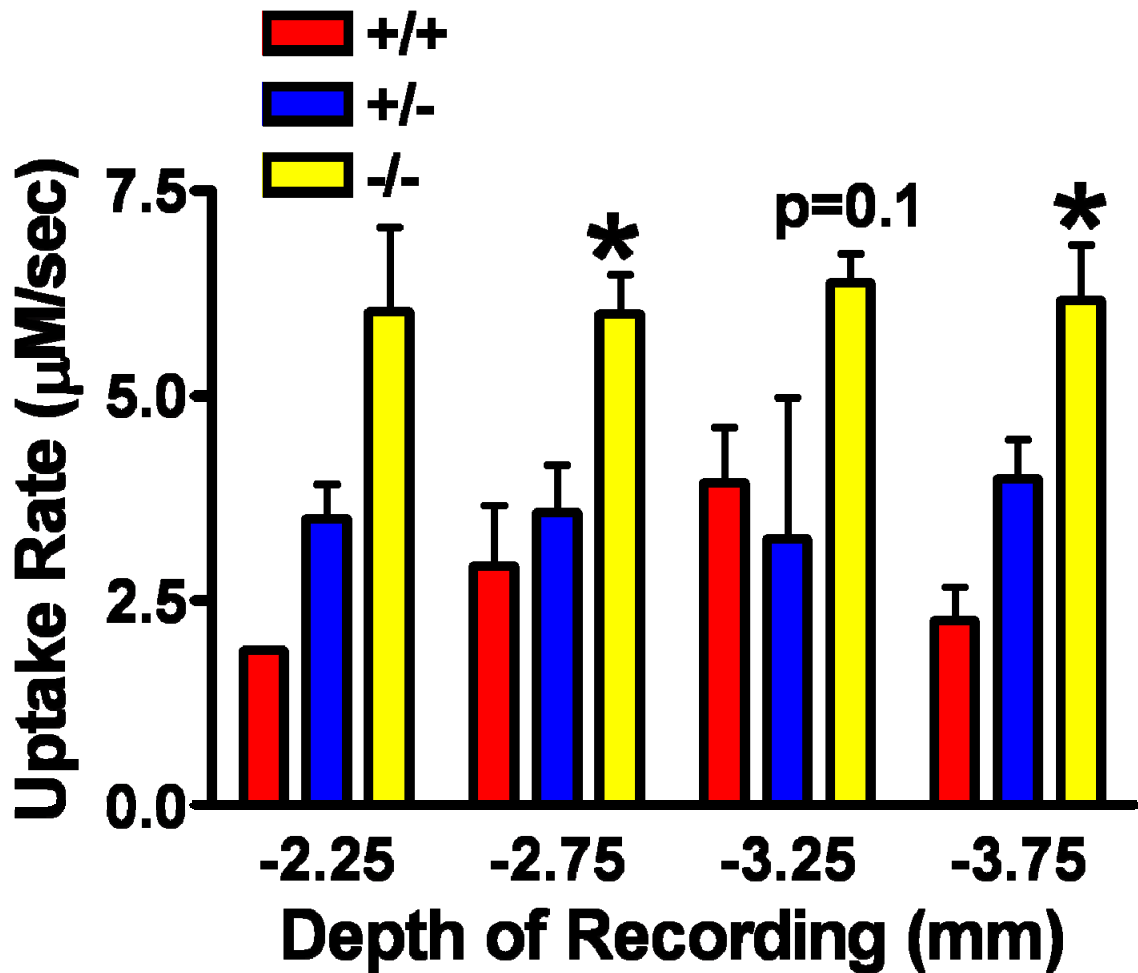


Figure A.6: 5 mM Glu Clearance Depth Profile in the Male GPT KO Mice

Average clearance rates of exogenously applied 5 mM Glu at different recording depths within the Str of GPT WT (n=3; +/+; red), heterozygous (n=5; +/-; blue), and homozygous (n=2; -/-; yellow) mice. On average, Glu clearance was faster in the GPT homozygous mice compared to controls at all recording depths. This was significant (*p < 0.05) at recording depths -2.75 and -3.75 mm and approached significance at recording depth -3.25 mm. A one-way ANOVA with a Tukey's post hoc was conducted at each depth for statistical analysis.

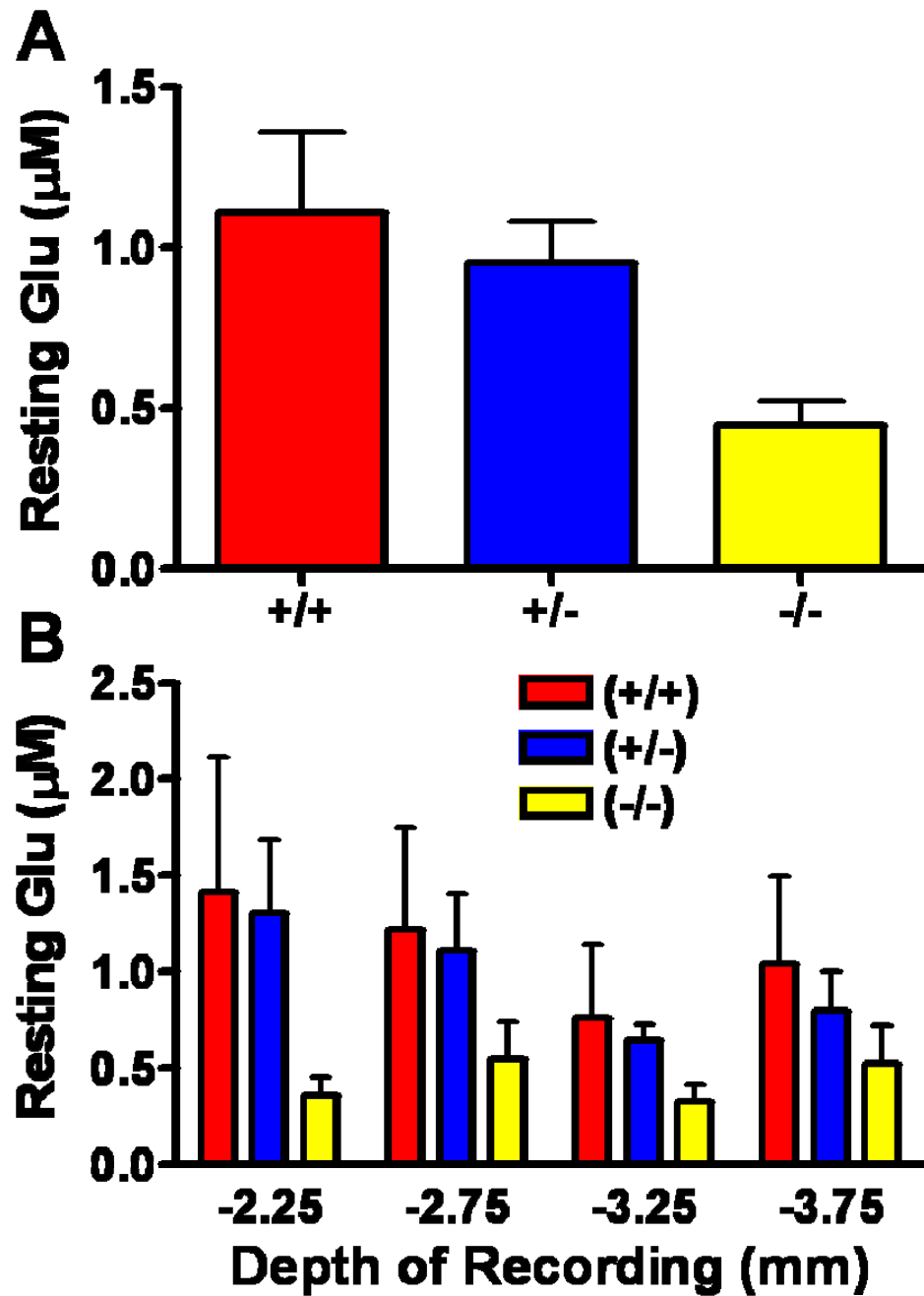


Figure A.7: Resting Glu Levels in the Male GPT KO Mice

A) Resting Glu levels were averaged through the entire Str and no significant ($p=0.09$) differences were found between WT ($1.1 \pm 0.3 \mu\text{M}$; $n=4$; red), heterozygous ($0.9 \pm 0.1 \mu\text{M}$; $n=6$; blue) and homozygous ($0.4 \pm 0.1 \mu\text{M}$; $n=2$; yellow) mice. B) Average resting Glu levels were determined for each depth within the Str of WT (+/+; red), heterozygous (+/-; blue), and homozygous (-/-; yellow) mice. No significant difference was observed within mouse groups over the different recording depths. The slower clearance trend in (A) was observed at each recording depth. A one-way ANOVA with a Tukey's post hoc was conducted at each depth for statistical analysis.

Discussion

The low number of male GPT homozygous mice (n=2) studied made it difficult to statistically compare groups of male mice as well as compare groups of mice across gender. We did, however, observe some drastic differences between the two genders. Stimulus-evoked Glu release was significantly increased in the male GPT heterozygous mice compared to both control and homozygous mice. In the female groups only the GPT homozygous mice showed significantly increased Glu levels compared to WT mice. When the uptake of stimulus-evoked Glu release was examined, both heterozygous and homozygous male mice displayed faster uptake kinetics compared to controls. The female mice exhibited no differences in uptake kinetics across all three groups.

Comparing the clearance rates of exogenously applied 5 mM Glu is difficult. The small number of available homozygous mice studied limited the range of maximal amplitude to 8-13 μ M for analysis. A maximal amplitude range of 3-13 μ M was used to study stimulus-evoked Glu uptake in male and female mice as well as clearance of exogenously applied 5 mM Glu in female mice. Because of the different maximal amplitude ranges examined, direct comparison of uptake or clearance values is skewed. We observed that male GPT homozygous mice cleared exogenously applied Glu significantly faster than WT and heterozygous mice, which was also seen in the uptake analysis of stimulus-evoked Glu release in the male GPT KO mice. When comparing gender, female GPT homozygous mice cleared exogenously applied 5 mM Glu significantly slower compared to controls.

Using our self-referencing recording techniques, we were able to record resting Glu levels in the Str of GPT KO male mice. Resting Glu levels were similar in the WT, heterozygous, and homozygous mouse groups, despite the differences seen in stimulus-evoked Glu release as well as increases in the uptake and clearance rates of Glu in the homozygous mice. We did observe a nonsignificant decrease in resting Glu in the homozygous male mice. The

decrease in resting Glu may be due to the significantly increased Glu clearance in the male homozygous mice. If Glu is cleared from the extracellular space faster, that may indicate an increased transporter density, which would lower resting Glu levels. Further studies are needed to determine the validity of this hypothesis. In the GPT KO female mice, we did not see any significant differences in resting Glu levels, but a nonsignificant increase was observed in the GPT heterozygous female mice. Resting Glu values were similar between male and female GPT KO mouse groups.

Despite the low number of male homozygous mice studied, there are obvious differences in Glu regulation between the male and female GPT KO mice, especially when examining the uptake of stimulus-evoked Glu release and clearance of exogenously applied Glu. These comparisons indicate extreme differences in either the number or function of EAATs in the mouse striatum. By increasing the number of male GPT homozygous mice in our studies, we can make some direct comparisons between genders.

Copyright © Kevin Nicholas Hascup

Appendix B: Understanding L-Glutamate Dynamics in the Awake, Freely Moving BALB/C Mouse Model.

Introduction

The C57BL/6 mouse line was used for feasibility and initial characterization of the freely moving recording because we anticipated studying the GLUD1 motor deficient mice. However, as we progress this technology for behavioral research, it will be important to characterize the BALB/C mouse strain as well in order to provide a comparative assessment of behavior between different inbred strains. Inbred strains of mice differ in their behavioral and neurochemical responses to stimuli. For example, the BALB/C strain exhibits neophobia, especially when compared to other inbred strains, which makes them suitable candidates for anxiety research (Belzung and Griebel, 2001, Belzung *et al.*, 2001). This increased anxiety reduces their social behavior and increases aggressive behaviors, which may indicate that the BALB/C mice are a useful model for identifying gene and neurobiological pathways in autism-related diseases (Brodkin, 2007). Studies have also shown that electric footshock induces a higher increase in dopamine in the PFC of BALB/C mice compared to C57BL/6 mice (Herve *et al.*, 1979). However, predator stressors such as fox urine elicit larger DOPAC increases in the PFC of C57BL/6 mice as compared to BALB/C mice further indicating that neurochemical changes due to stress or behavior may be situation-specific (Hayley, *et al.*, 2001). For these reasons it is useful to compare different strains of inbred mice when conducting behavioral research.

Methods

All materials and methods for freely moving recording were thoroughly outlined in Chapter Two. Male BALB/C mice between the ages of 5 and 6 months at the time of recordings were used in these experiments. Glu recordings were conducted using self-referencing, enzyme-based MEAs with a sampling rate of 1 Hz. A craniotomy was performed over the PFC (AP: +1.54 mm; ML: 0.3 mm; DV: -2.45 mm vs. bregma) and MEAs were implanted using

the coordinates from Paxinos and Franklin (2004). A stainless steel guide cannula was attached to the PCB and positioned so an internal, acute stainless steel cannula was positioned among the 4 Pt recording sites, resting 50-100 μm above the recording surface. Through this internal cannula isotonic solutions of 1 mM Glu (in 0.9% saline; pH 7.4) or 50 μM (S)-4-Carboxyphenylglycine (CPG) were locally applied to the surrounding brain tissue to study glutamatergic neurotransmission. Prior to connecting the mouse pedestal with the mouse hat, mice were allowed to freely roam around the recording chamber for at least 30 minutes to acclimate to their environment. Once connected to the mouse hat, the mice underwent a minimum 60 minute acclimation period to establish a stable baseline recording. Following this acclimation period, the dummy cannula was removed and the internal, acute cannula (connected to a 10 μl Hamilton Syringe) was inserted into the guide cannula on recording sessions when chemicals were locally applied. After the internal cannula was inserted, another acclimation period of 30 minutes was allowed to reestablish baseline. Following this period, resting Glu, and the effects of locally applied Glu or CPG were studied for up to three additional hours. The volumes of locally applied Glu were kept constant at 0.5 μl while the volume for 50 μM CPG was kept at 1.0 μl .

Following completion of all recording sessions (after multiple days of recording), mice were anesthetized with isoflurane and transcardially perfused with 0.9% saline followed by 4% paraformaldehyde. The brain was removed and stored in 4% paraformaldehyde for three days followed by storage in 0.1 M phosphate buffer (10% sucrose) for sectioning and staining to confirm MEA placement.

Data analysis involved a one-way ANOVA with Tukey's post hoc to examine any differences in resting Glu levels and maximal amplitude over multiple days post-implantation. Since only two mice were studied, all data was reported as mean \pm standard deviation and significance was defined as $p < 0.05$.

Results

Similar to our studies in the freely moving C57BL/6 mice, the FAST 16 Mark II recording system along with our modified MEA allowed for reliable second-by-second recordings of Glu in the PFC of awake, freely moving BALB/C mice. We implanted the pedestal assemblies and recorded Glu for one week in the awake BALB/C mice. Local application of an isotonic solution of Glu (1 mM; 0.5 μ l) through the internal cannula was used to verify Glu recordings *in vivo*. Figure B.1 shows representative Glu signals in the PFC of awake, freely moving BALB/C mice. Glu measures were robust and reproducible within and over multiple days. Figure B.2A shows the mean maximal Glu response on days 3, 5 and 7 post-implantation.

Resting Glu measures were studied in the PFC of BALB/C mice on days 3 through 7 post-implantation using the self-referencing technique described in Chapter Two. Briefly, the self-referencing site current was subtracted from the Glu recording site current, and divided by the Glu recording site slope obtained from *in vitro* calibration. We observed no significant difference in resting Glu over days in the PFC (figure B.2B).

Local application of 50 μ M CPG in the PFC of BALB/C mice resulted in a bi-phasic affect on glutamatergic neurotransmission. Immediately following local application there was a rapid, robust spike (\sim 4 μ M) in extracellular Glu that returned to baseline after several seconds (figure B.3). Resting Glu levels then decreased (\sim 0.5 μ M) for approximately 15 minutes. The inset in figure B.3 shows the average change in resting Glu due to administration of 50 μ M CPG.

Discussion

Similar to our freely moving studies in the C57BL/6 mice, we successfully adapted our enzyme-based MEAs to record Glu in the awake, freely moving BALB/C mouse for at least 7 days post-implantation. We locally applied an isotonic solution of Glu (0.5 μ l, 1mM) in the PFC of BALB/C mice on days 3, 5 and 7 post-implantation to determine the longevity of the enzyme-based MEA *in vivo*. We saw no significant change in MEA sensitivity for Glu on days 3 - 7 post-

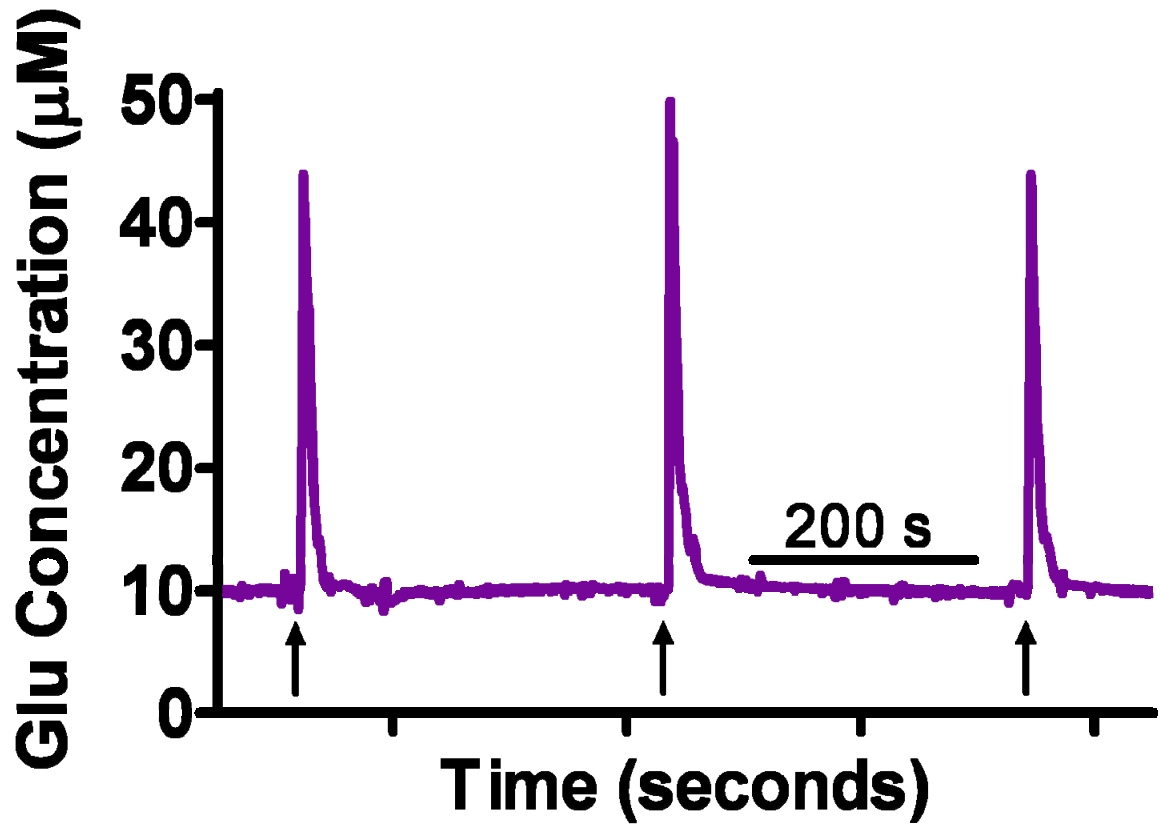


Figure B.1: Representative Glu Traces From Local Application of 1 mM Glu

Representative traces of locally applied Glu (1 mM; 0.5 µl) in the PFC of male BALB/C mice. Glu was locally applied at the time points indicated by the arrows. A rapid, reproducible spike was recorded in the PFC using self-referencing MEAs. Maximal peak height shows *in vivo* Glu signal from local application of Glu (arrows), while baseline measures show resting Glu levels.

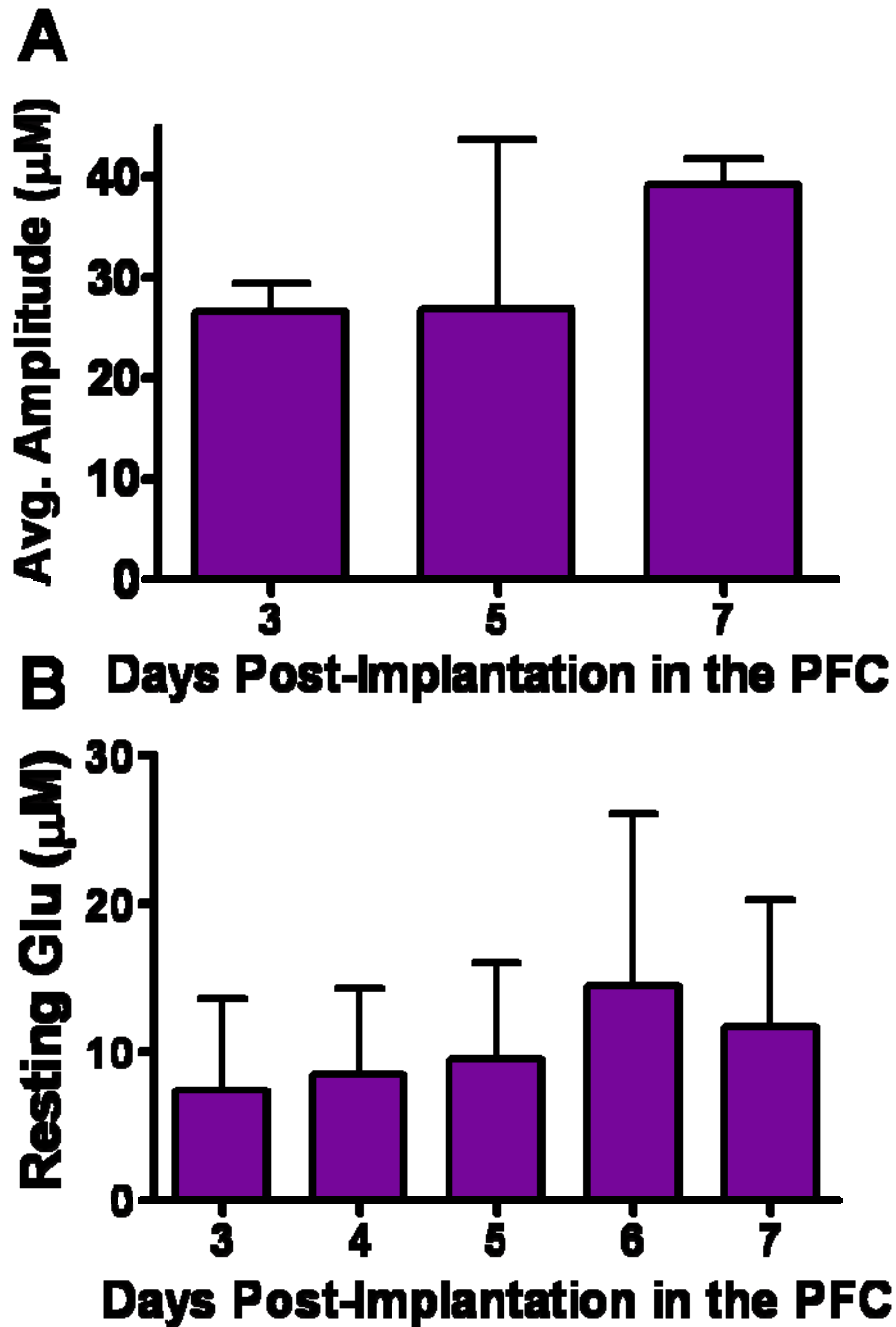


Figure B.2: Local Application and Resting Glu Levels in the PFC of BALB/C Mice

A. Locally applied Glu data for days 3, 5, and 7 post-implantation in the PFC (n=2). Glu (0.5 μl , 1 mM) was locally applied over multiple days and recorded using a self-referencing MEA. Stable Glu recordings were observed over all days measured indicating reliable *in vivo* Glu measurements for at least 7 days post-implantation. B. Resting Glu levels were assessed on days 3 through 7 post-implantation in the PFC (n=2) of BALB/C mice. Self-referencing MEAs were used to determine resting Glu levels.

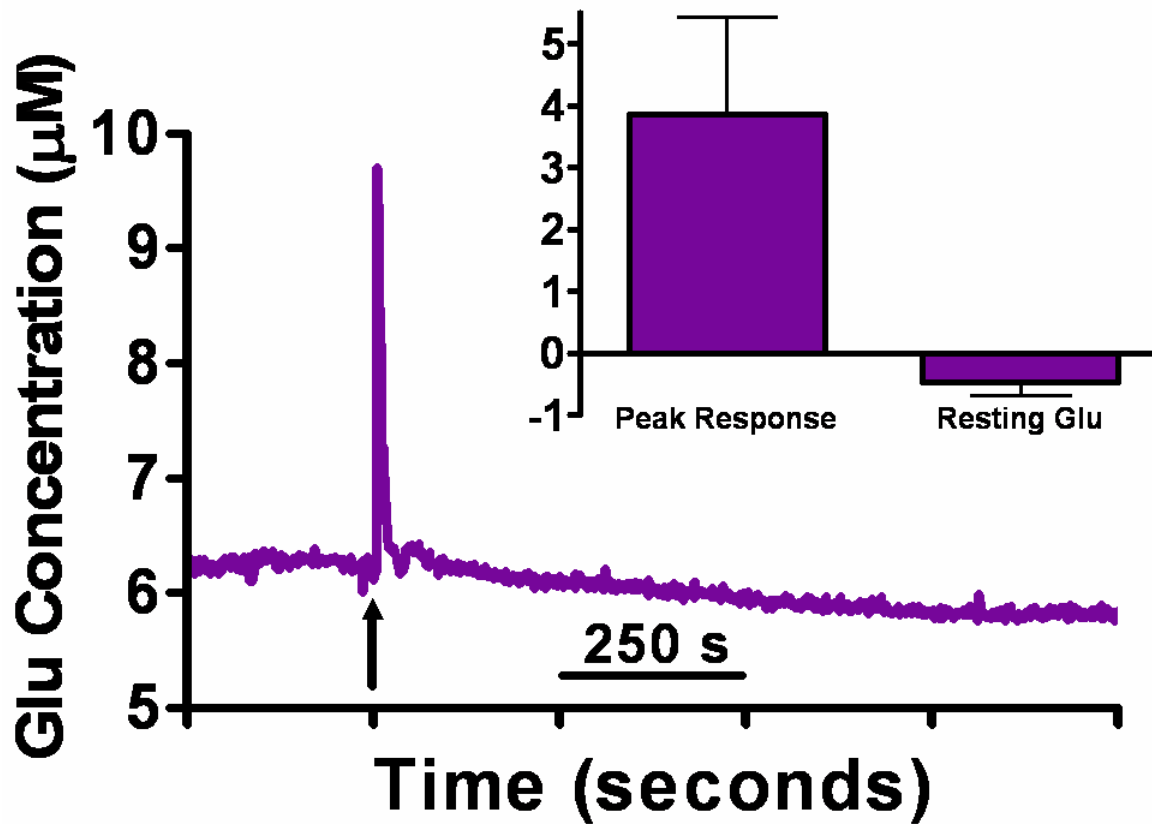


Figure B.3: Local Application of CPG in the PFC of BALB/C Mice

Local application of 50 µM CPG (1.0 µl; pH 7.4) resulted in a rapid increase in Glu followed by a prolonged decrease in resting Glu levels as shown in the trace. The inset shows the average change in Glu from unstimulated resting Glu.

implantation. The average maximum amplitude from local application of 1 mM Glu in the BALB/C mouse strain ($30.8 \pm 7.6 \mu\text{M}$) was similar to what was observed in the PFC of freely moving C57BL/6 mice (30.5 ± 7.8). Also, our self-referencing recording technique allowed us to measure resting Glu levels in the PFC of BALB/C mice on days 3 through 7 post-implantation. We saw a nonsignificant increase in resting Glu levels over days; however, the large variance made it difficult to compare these values to what was observed in the PFC of C57BL/6 mice. Additional studies need to be conducted before definitive comparisons can be determined.

The cystine-Glu exchanger has been a proposed mechanism for regulating resting Glu levels (Baker *et al.*, 2002; Melendez *et al.*, 2005). The cystine-Glu exchanger is located on glia cells (figure 1.1) and acts by uptake of cystine into glia coupled with the export of Glu into the extracellular space. Microdialysis studies examining the cystine-Glu exchanger has shown that blockade of this transporter by CPG results in a decrease in resting Glu levels (Baker *et al.*, 2002; Melendez *et al.*, 2005). In addition, CPG has also been reported as a group I mGluR competitive antagonist (Brabet *et al.*, 1995; Doherty *et al.*, 1999). Group I mGluRs are excitatory autoreceptors located on both pre- and post-synaptic glutamatergic neurons. Blockade of the pre-synaptic group I mGluR should also cause a decrease in resting Glu levels. Unexpectedly, immediately following local application of 50 μM CPG we observed a fast spike in Glu levels, which lasted only seconds. This immediate increase in Glu was reproducible both within and between animals. Following the spike we observed an expected, prolonged decrease in resting Glu levels that lasted approximately 15 minutes. A separate study using 50 μM CPG was conducted in the PFC of the Long Evans rat by our laboratory (manuscript in preparation) and a similar immediate increase followed by a decrease in resting Glu levels was observed. This initial spike in resting Glu levels has not been previously reported and was an unexpected finding. The fact that the initial spike in Glu lasted on the order of seconds makes it difficult for microdialysis to observe this phenomenon due to the low temporal resolution of the technique. Based on current literature, there is

no definitive explanation for this rapid increase in Glu, and may be due to an unknown interaction with a pre-synaptic Glu autoreceptor.

This study demonstrates the ability to successfully use the MEA freely moving technology in more than one strain of mice. The present studies using MEAs configured for second-by-second Glu measurements were viable for at least 7 days post-implantation in the awake, freely moving BALB/C mouse. We observed a nonsignificant increase in resting Glu levels in the PFC of awake, freely moving BALB/C mice over days. Further studies are needed to decrease the variance across days and make comparisons between Glu regulation in the BALB/C PFC and the C57BL/6 PFC. Local application of 50 μ M CPG resulted in a currently unreported rapid spike in Glu followed by an expected decrease in resting Glu levels. These findings provided evidence that the high spatial and low temporal resolution provided by our MEA technology was necessary to better understand the effects CPG has on resting Glu levels. These studies have set the foundation to study behavioral differences in Glu regulation between the BALB/C and C57BL/6 mouse strains.

Copyright © Kevin Nicholas Hascup

Appendix C: Development of a Self-Referencing Microelectrode Array for Detection of Hydrogen Peroxide

Introduction

The first generation of MEAs (despite a multitude of PCB, ceramic tips, and recording site layout designs) all had four or five Pt recording sites (Burmeister and Gerhardt, 2005). While this was revolutionary at the time, our lab prides itself in pushing technology further. We have developed several new MEA designs with 8 and 16 Pt recording sites and eventually one with 32 recording sites. The advantage of additional recording sites allows us to simultaneously measure neurochemicals from multiple brain regions or even measure multiple neurochemicals within a single brain region. With additional recording sites placed in a confined geometrical area, the reporter molecule, H_2O_2 , can diffuse to sites other than those from which it forms leading to false detection of analyte on those sites. Consider a MEA with both GluOx and choline oxidase enzymes placed on neighboring sites. Some of the H_2O_2 generated from a GluOx site may diffuse to the choline oxidase coated site thus falsely contributing to the detection of choline. In an attempt to prevent this, we considered placing a layer of catalase overtop the enzyme and sentinel sites. This would prevent any H_2O_2 from being detected on sites other than those that enzymatically produced the reporter molecule.

Catalase is a tetrameric, diffusion controlled enzyme that catalyzes the decomposition of H_2O_2 into H_2O and $\frac{1}{2}O_2$ (Eventoff *et al.*, 1976; Dringen *et al.*, 2005). We were interested in using catalase for several important reasons. First, catalase is endogenously expressed in peroxisomes that are located in all brain cells *in vivo* (Schad *et al.*, 2003) so introduction of this enzyme would not be foreign to the microenvironment. Second, catalase has a slightly larger molecular weight (250 kilodaltons) compared to that of GluOx (140 kilodaltons) so incorporation of this enzyme into our BSA / Glut mixture is not difficult. Finally, catalase requires no substrates and is considered to be “catalytically perfect”, with reaction rates approaching that of diffusion speeds. This means a

molecule of catalase catalyzes a reaction almost every time it encounters a molecule of H₂O₂, so even large concentrations of this reporter molecule can be decomposed quickly. This makes catalase a great enzyme to prevent H₂O₂ from reaching adjacent recording sites on our MEAs.

The interest in developing a self-referencing catalase MEA for detection of H₂O₂ is two-fold. The first is to advance our MEA technology for measurements of multiple analytes. The second has a more neurochemical basis. Interest in detection of H₂O₂ in living brain tissues is growing. The production of H₂O₂ and other reactive oxygen species is implicated in the etiology of neurodegenerative disorders such as PD (Kulagina and Michael, 2003). Second, the laboratory of Dr. Margaret Rice has demonstrated that H₂O₂, similar to nitric oxide, plays an important role as a diffusible neuromodulator (Avshalumov *et al.*, 2003; Kulagina and Michael, 2003; Avshalumov *et al.*, 2007). Dr. Rice's group contends that complex I of the electron transport chain found on the inner mitochondrial membrane is responsible for the majority of H₂O₂ found in the Str (figure C.1). To determine if it was even possible for H₂O₂ to diffuse out of mitochondria, we enlisted the help of Dr. Patrick G. Sullivan's laboratory to collect mitochondrial preparations for study. Various electron transport chain complex inhibitors were added *in vitro* to determine if H₂O₂ could be generated and subsequently leave the mitochondria where it can be detected by our MEA. These studies would help determine the factors that control the rate and concentration of H₂O₂ that can be produced in the brain.

To conduct these studies, we developed a self-referencing MEA for H₂O₂ determination. The concept of this MEA is similar to that of the GluOx self-referencing MEA. The sites coated with a mixture of BSA/Glut and Catalase was applied on two of the Pt recording sites to act as a sentinel sites while the other pair of recording sites were coated with just the BSA/Glut mixture and subsequently detected H₂O₂. Several feasibility studies were conducted to determine if catalase could block exogenously applied H₂O₂ from being detected by our MEA both *in vitro* and *in vivo*. The following section outlines the development and application of our catalase MEA.

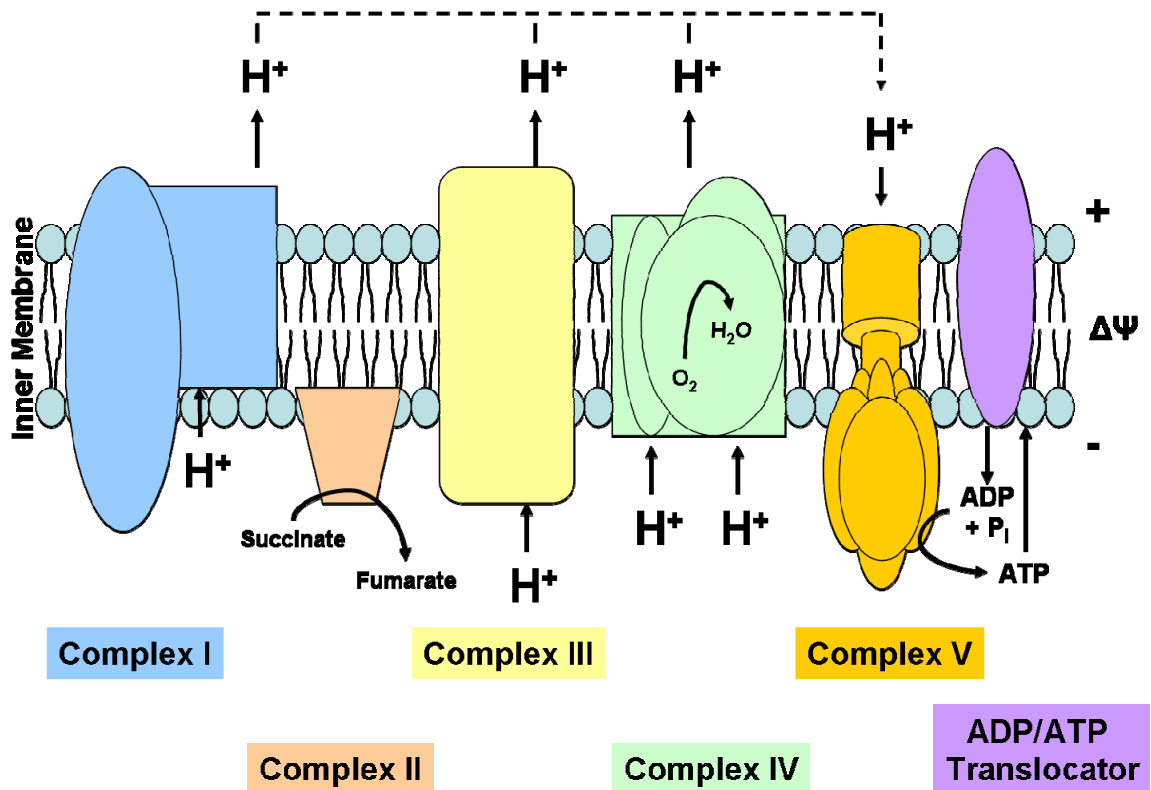


Figure C.1: Mitochondrial Electron Transport Chain

The electron transport chain builds up a proton electrochemical gradient across the inner mitochondrial membrane. For simplicity, electron flow is not shown but is transported between Complexes I, II, and III by the membrane soluble Coenzyme Q and between complexes III and IV by the membrane protein cytochrome c. H^+ is pumped out of the mitochondrion during electron transport (Complexes I, III, and IV) and its exergonic return powers the synthesis of ATP from ADP through the ATP synthase (Complex V). Figure adapted from Mattiasson and Sullivan, 2006).

Materials and Methods

Bovine liver catalase (aqueous solution >40,000 units/mg protein) was obtained from Sigma-Aldrich (Catalog #C3155). Preparation for enzyme coating was similar to that of GluOx. All proteins and enzymes were brought to room temperature and 0.010 g of BSA Fraction V, 99% (Sigma-Aldrich, Catalog #A-3059) was dissolved in a 1.5 mL microcentrifuge tube containing 985 μ l ddH₂O by manual agitation. Once dissolved, 5 μ l of Glut solution, Grade I, 25% (Sigma-Aldrich Catalog #G-6257) was added to the BSA mixture and manually mixed by inversion five times. The solution was then set aside for five minutes until it turned a faint yellow color. Glut crosslinked proteins that adhered to the MEA surface when cured. The BSA served as a matrix to protect catalase activity during immobilization. Next, 9 μ l of the BSA/Glut mixture was removed and added to a 300 μ l microcentrifuge tube. Lastly, 1 μ l of the catalase stock solution was added and mixed by pipette agitation.

All MEAs were tested for their response to H₂O₂ to ensure Pt site functionality prior to enzyme coatings. After testing, MEAs were rinsed with ddH₂O and dried in an oven (105 – 115 °C) for 10 minutes to remove residual H₂O prior to coating. Catalase solutions and the inactive protein matrix of BSA/Glut were applied to the Pt recording sites by hand. Solutions were drawn up into a 10 μ l Gastight[®] Hamilton microsyringe (Hamilton Co. Catalog #80065) and slowly dispensed to form a small droplet of solution at the tip of the microsyringe. Using a dissecting microscope, the droplet was briefly applied to the Pt recording sites. The solution quickly dried, leaving behind a thin, translucent layer of enzyme that was visible underneath a dissecting microscope. Two additional coats of catalase were applied in the same manner with one minute dry times in between each coat. This procedure was complete once a visible film remained following coating. The advantage of using multisite MEAs was that a pair of recording sites was coated with the catalase mixture and the adjacent sites were coated with the inactive protein matrix in the same manner as applying the catalase mixture to create the self-referencing catalase MEA. MEAs were allowed to cure at room temperature for 48-72 hours.

Adult, male Sprague-Dawley rat (~250g) mitochondria were isolated in the laboratory of Dr. Patrick Sullivan using previously published protocols (Nukula *et al.*, 2006). Rats were anesthetized using a carbon dioxide chamber and decapitated. Their brains were quickly removed and the cortices dissected. Cortex tissue was placed in ice cold isolation buffer with 1 mM ethylene glycol tetraacetic acid (EGTA) (75 mM sucrose, 215 mM mannitol, 0.1% BSA, 1 mM EGTA, 20 mM HEPES, pH 7.2). Tissue was put into an all glass dounce homogenizer with 3 mLs of isolation buffer with EGTA, homogenized, split into four 2 mL tubes, topped off with isolation buffer and spun at 1,300 x g for 5 minutes at 4°C. The supernatant was taken off and saved in separate tubes. The pellet was resuspended in isolation buffer and spun at 1,300 x for 5 minutes at 4°C. Supernatant was discarded (by slinging off) and the pellets were resuspended in 500 µl of isolation buffer. A nitrogen bomb was used to rupture the cell membrane in order to release the mitochondria from cells. The samples were placed in a cold nitrogen bomb for 10 minutes at 1000 psi to burst synaptoneuroosomes formed by homogenization. After bombing, the sample was spun on a Percoll gradient, with fresh stocks of 30%, 24%, and 40% Percoll made with isolation buffer. The gradient was made by first adding 3.5 mLs of the 24% stock to the ultracentrifuge tube and then, using a 5 mL syringe, injecting 3.5 mLs of the 40% stock to the bottom of the tube. Using equal amounts of the 30% Percoll stock and sample, a 15% Percoll solution was made and 3 mLs were added to the top of the gradient. The gradient was spun in a high speed Sorval centrifuge for 10 minutes at 30,400 x g. The third fraction containing the purified mitochondria was removed, put into clean tubes, and topped off with isolation buffer without EGTA. The samples were spun at 16,700 x g for 15 minutes. The supernatant was removed and the pellet was resuspended in isolation buffer without EGTA and spun at 13,000 x g for 10 minutes. After the supernatant was removed and discarded, the pellet was resuspended in 500 µl isolation buffer without EGTA and transferred to a microcentrifuge tube, which was then spun at 10,000 x g for 10 minutes. The supernatant was removed and the pellet was resuspended in enough isolation buffer without EGTA to get a

concentration of 10-15 $\mu\text{g}/\mu\text{l}$. A BCA protein assay kit was used to determine protein concentration by measuring absorbance at 560 nm with a BioTek Synergy HT treated plate (Winooskin, Vermont).

Results

The catalase MEA was tested first *in vitro* to determine its ability to block exogenously applied H_2O_2 . Figure C.2 shows a representative tracing of a catalase coated MEA calibration. The MEA tip was placed into a 40 mL solution of 0.05 M PBS. 500 μl of 20 mM AA (final beaker concentration of 250 μM) and 3 additions of 40 μl of 8.8 mM H_2O_2 (final beaker concentration of 8.8, 17.6, and 26.4 μM) were added to the beaker. As seen in figure C.2, the sites coated with catalase showed minimal response to additions of H_2O_2 , while those coated with just BSA and Glut showed a large change in current from baseline.

Next, we wanted to determine if the catalase could decompose H_2O_2 before it was detected on our Pt recording sites *in vivo*. To do this we anesthetized a C57BL/6 mouse with three subcutaneous injections of 12.5% urethane for a final dose of 1.25 g/kg. 100 μM H_2O_2 was added to the glass micropipette and locally applied in 30 second intervals in the mouse Str. Figure C.3A shows a trace of the responses to 100 μM H_2O_2 (25 nl) on the catalase coated and inactive protein matrix coated sites. As shown in figure, local application 100 μM H_2O_2 resulted in robust, reproducible peaks that quickly returned to baseline on the BSA/Glut coated sites. The catalase coated sites showed minimal response to additions of H_2O_2 . Figure C.3B shows the trace after subtracting the concentration on the catalase coated sites from the concentration on the BSA/Glut coated sites. This figure also indicates resting H_2O_2 levels in the extracellular space of the mouse Str, which were approximately 0.3 μM .

Since we observed a small response to H_2O_2 on the catalase coated sites *in vivo* we wanted to determine if this was due to H_2O_2 reaching the Pt recording sites or if this was due to pressure artifact from locally applying a solution close

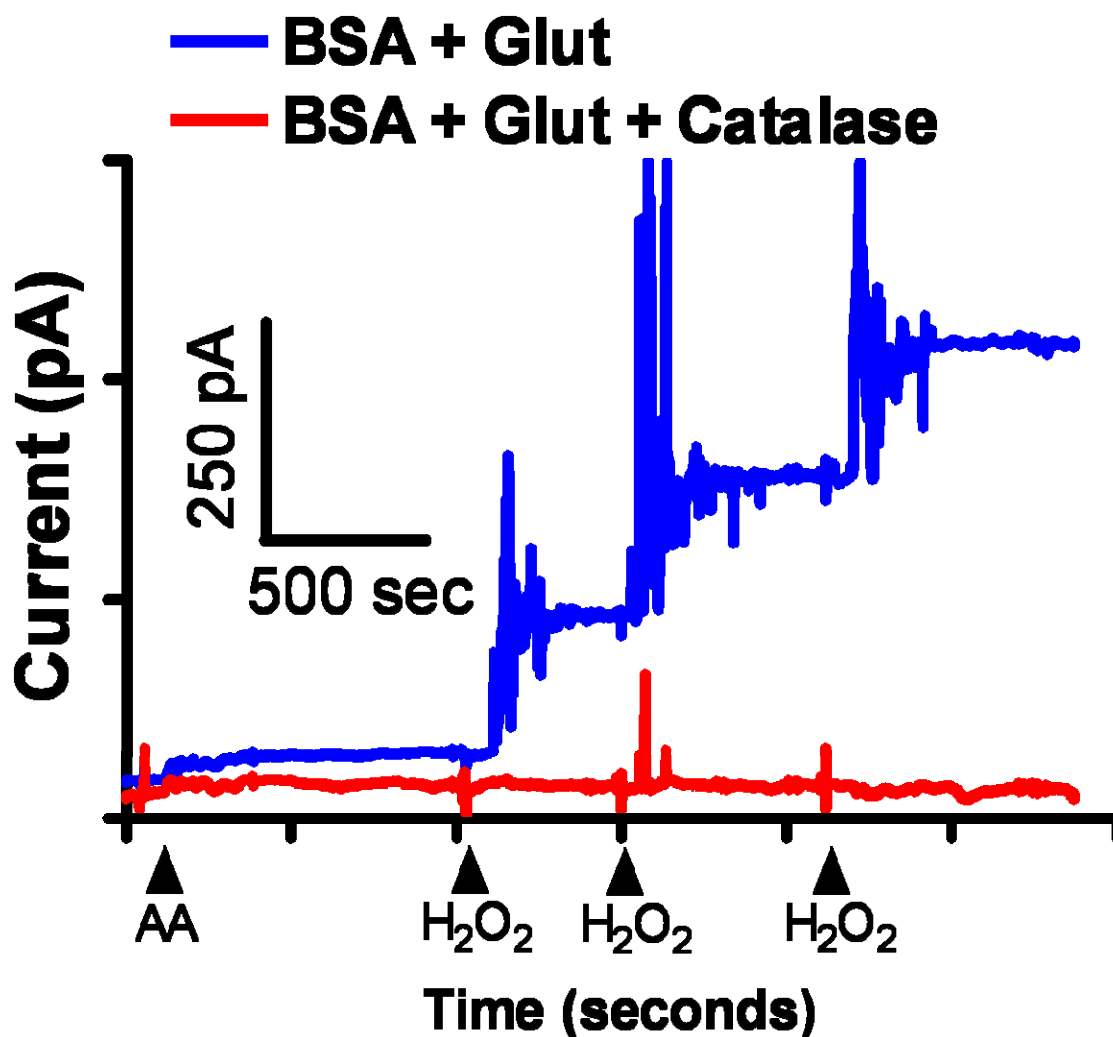


Figure C.2: Calibration Trace of a Catalase MEA

A self-referencing catalase coated MEA for detection of H₂O₂. The red trace represents a site coated with BSA/Glut and catalase while the blue trace represents a site coated with just the inactive protein matrix of BSA and Glut. All four sites of the MEA were electroplated with 5 mM mPD prior to calibration. 500 μ l of 20 mM AA (final beaker concentration of 250 μ M) was first added (arrow head) and allowed to come to baseline. Minimal change in baseline current was observed indicating good selectivity of the MEA. Next, 3 additions of 40 μ l of 8.8 mM (final beaker concentration of 8.8, 17.6, and 26.4 μ M H₂O₂) were added. Only the site coated with the inactive protein matrix showed a measurable response to H₂O₂ indicating the effectiveness of catalase degrading H₂O₂ before it could be detected on the Pt recording sites.

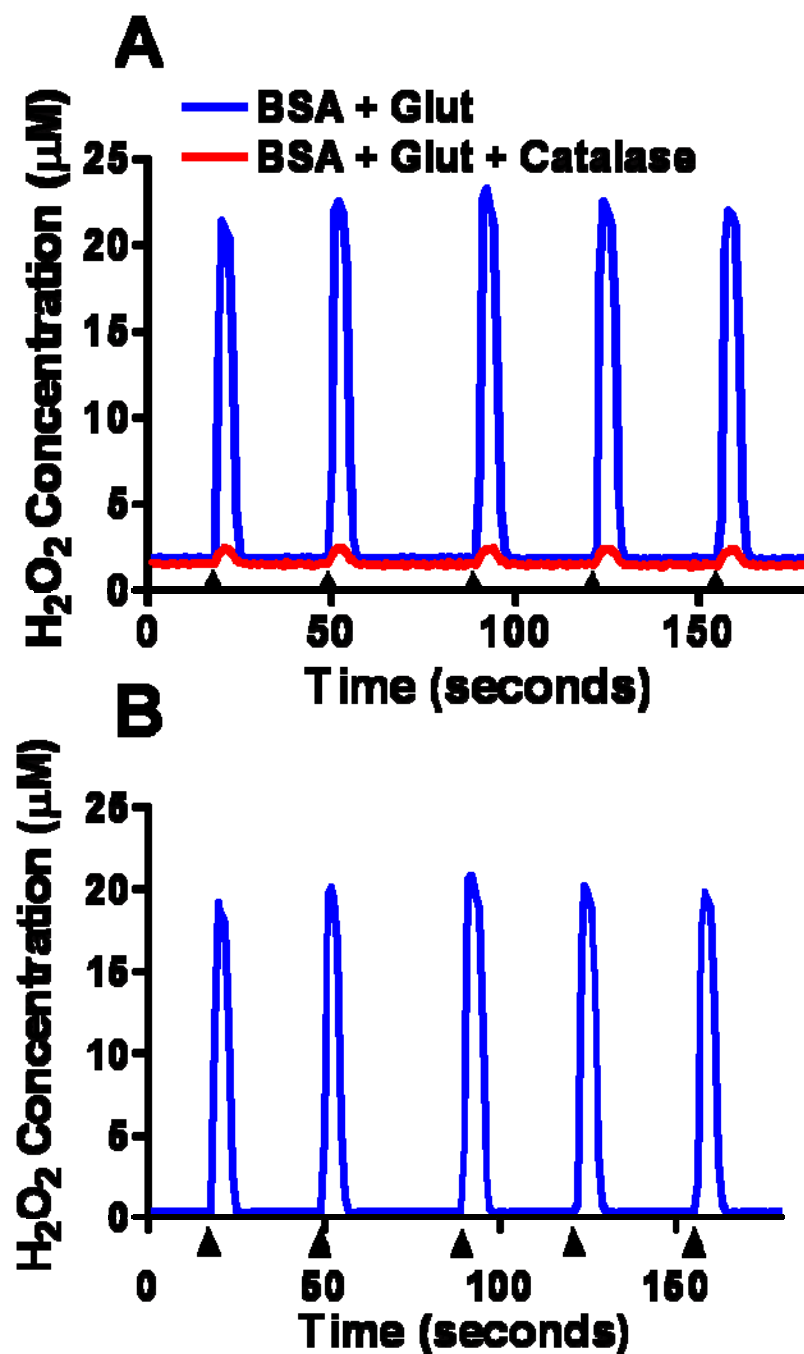


Figure C.3: Local Application of 100 μM H_2O_2

A) Local application of 100 μM H_2O_2 (25 nl, arrow heads) resulted in robust, reproducible peaks compared to baseline on the BSA/Glut (blue) coated sites. A minimal response on the catalase coated site was observed. B) The concentration on the catalase coated site was subtracted from the concentration on the BSA/Glut coated site to obtain the self-referencing trace. Baseline values indicate resting H_2O_2 levels, while peak heights indicate maximal amplitude of response.

to the MEA. To do this we performed a series of recordings at two different potentials in the mouse Str. The first series of recordings was taken at an applied potential of +0.7 V vs. a Ag/AgCl reference electrode; a potential where H₂O₂ was readily oxidizable. Next, we dropped the potential to +0.2 V vs. a Ag/AgCl reference electrode; a potential where H₂O₂ was not as readily oxidized. Figure C.4 shows the responses on the catalase and BSA/Glut coated sites to local application of 100 μM H₂O₂ at an applied potential of +0.7 and +0.2 V vs. a Ag/AgCl reference electrode. As shown by the graphs, the BSA/Glut coated site (figure C.4A) had a robust response to local application of 100 μM H₂O₂ that was attenuated when the potential was dropped to +0.2 V. The catalase coated sites showed a much lower response to local application of 100 μM H₂O₂ at +0.7 V. When the potential was dropped to +0.2 V on the catalase coated sites, there was no longer a response, but rather a dilution artifact. This indicates that the catalase was not completely degrading the locally applied H₂O₂, so a small portion was detected on the Pt recording sites.

Next, we wanted to determine the linearity of the catalase MEAs response to local application of increasing volumes of 100 μM H₂O₂. To do this, a catalase MEA was positioned in the Str of a Fisher 344 rat and a dose response test was performed by increasing the volume of 100 μM H₂O₂ locally applied. Peak responses were determined from three ejections, in thirty second intervals of 25, 50, 75, 125, 175, and 250 nl of 100 μM H₂O₂. Figure C.5A shows the series of self-referenced recordings from increasing the volume of 100 μM H₂O₂ locally applied adjacent to the catalase MEA. As shown by the trace, increasing the volume led to an increase in peak response. To quantitate this, the three ejections at each volume were averaged as shown in figures C.5B and C.5C. Peak responses were reproducible for each volume as indicated by the tight error bars. Also, we reported an $r^2 = 0.85$ for the six series of volumes ejected. Finally, we noticed that resting H₂O₂ levels in the Fisher 344 rat Str were similar (~ 0.3 μM) to what was observed in the C57BL/6 mouse Str.

We wanted to incorporate catalase with our GluOx coated MEAs to determine the feasibility of coating multiple enzymes onto a single MEA. To do

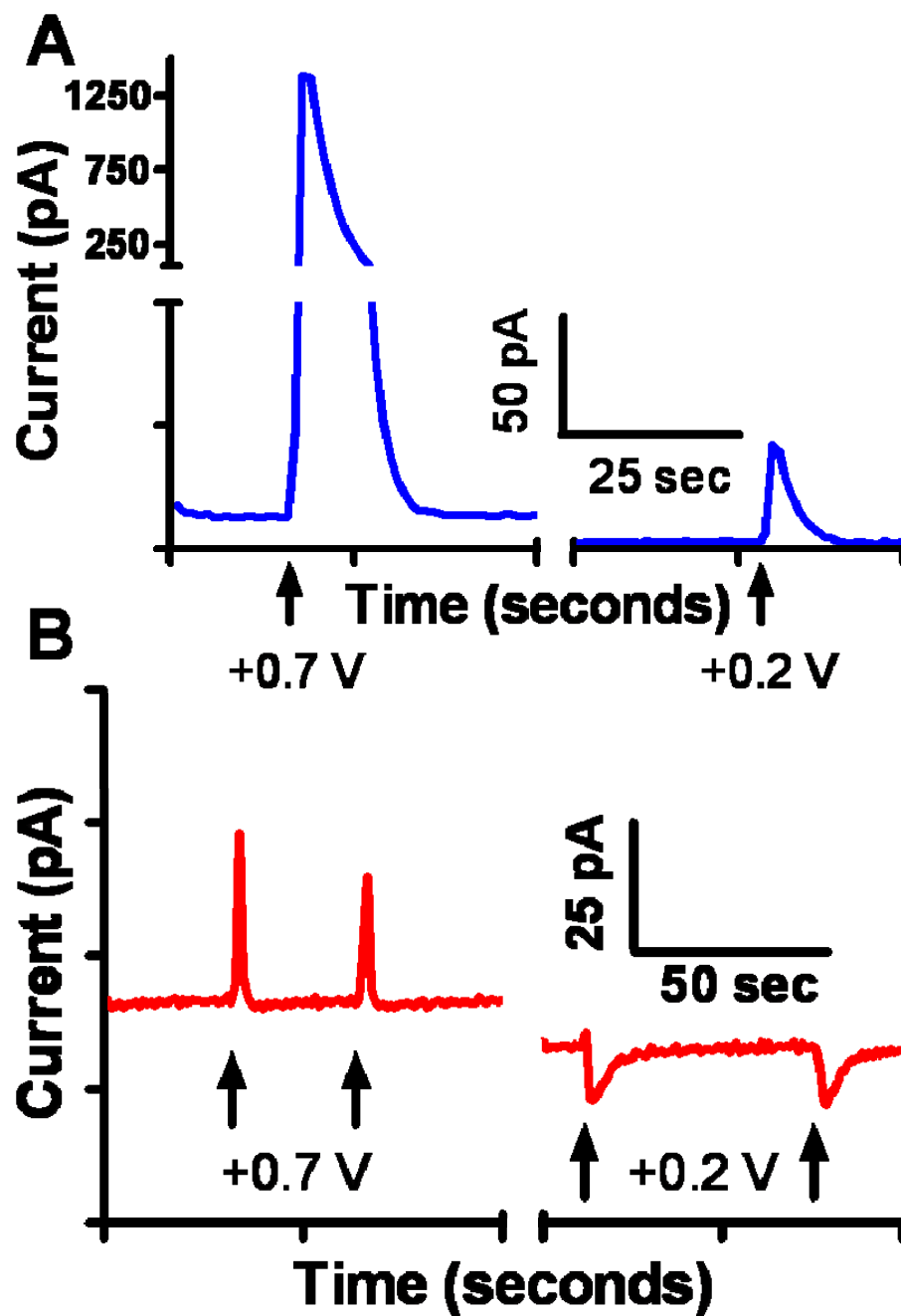


Figure C.4: Potential Change for H₂O₂ Determination

A.) A BSA/Glut coated site showing a large response to local application of 100 μM H₂O₂ (arrows) at an applied potential of +0.7 V vs a Ag/AgCl reference electrode. When the potential was dropped to +0.2 V, much of the H₂O₂ was not oxidized resulting in smaller peaks. The y-axis was split in order to see the peak response at +0.2 V B) A BSA/Glut and catalase coated site showing a small response to local application of 100 μM H₂O₂ at +0.7 V and a dilution effect at +0.2 V. Arrows indicate time points for local application.

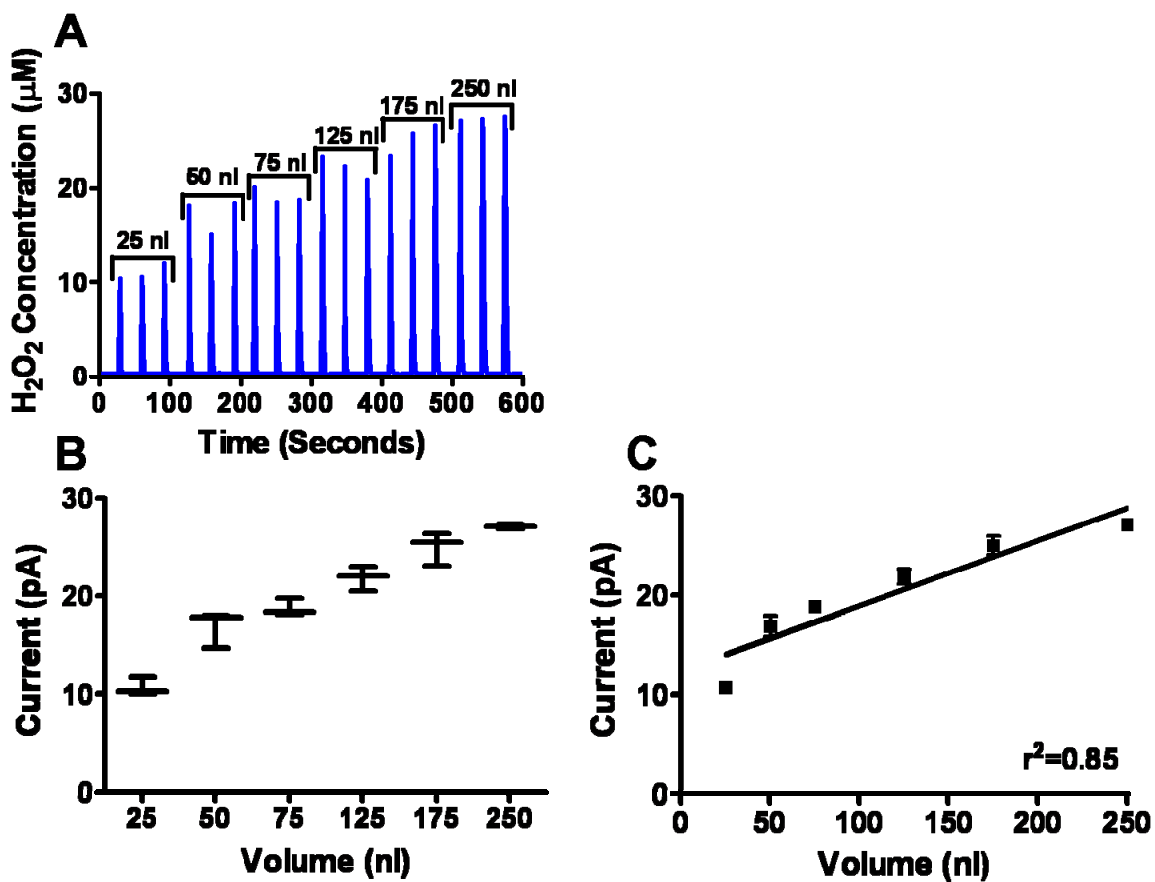


Figure C.5: Increasing Volume of Locally Applied 100 μM H_2O_2

A) A self-referenced trace from local application of 100 μM H_2O_2 in the Str of Fischer 344 rats. A series of three ejections were performed for each volume ejected (25, 50, 75, 125, 175, and 250 nl), which are shown above the peaks. Within each series of volumes, peak heights were robust and reproducible. Baseline values indicate resting H_2O_2 levels. B and C) For each group of similar ejection volumes, peak heights were averaged into a single data set and the linear regression was determined with a fit of $r^2 = 0.85$.

this, we applied 3 layers (as previously described in Chapter 2) of BSA/Glut and GluOx onto recording sites 1 and 2. Next, we applied 3 layers of BSA/Glut and Catalase onto recording sites 3 and 4. This dual enzyme MEA was allowed to cure for 72 hours and then mPD was electropolymerized onto all four recording sites. The MEA was then calibrated as shown in figure C.6 and showed good response to additions of Glu on sites 1 and 2, no response to H₂O₂ on sites 3 and 4, and no response to interferents such as AA and DA.

Our last catalase design included a self-referencing GluOx with a BSA/Glut and Catalase mixture placed over top of this layer. This was an experiment to test whether or not catalase could be used to prevent diffusion of GluOx generated H₂O₂ to additional recording sites. Two different MEAs were tested prior to coating to ensure all four sites responded to H₂O₂. Sites 1 and 2 were coated with 3 layers of BSA/Glut and GluOx while sites 3 and 4 were coated with just the inactive protein matrix of BSA/Glut. This was allowed to cure for 48 hours. Next, 3 layers of a mixture of BSA/Glut and catalase was applied onto all 4 Pt recording sites and cured for 48 hours. A second MEA was prepared in the similar fashion except only 1 layer of the BSA/Glut and catalase mixture was applied on all four sites. No exclusion layer was applied to either MEA. Calibration consisted of final beaker concentrations of 20, 40, and 60 μM Glu and 8.8 and 17.6 μM H₂O₂. Both MEAs showed very small responses to Glu (< 1 pA/ μM). The first MEA with 3 layers of catalase showed a smaller response to Glu than the second MEA with 1 layer of catalase. When examining the response to H₂O₂, the first MEA, with 3 coats of catalase, showed no response, but the second MEA, with 1 coat of catalase, had a small response (Data not shown).

Mitochondria were isolated as described above and 50 μg/250 μl was placed in a sterile 48 well cell culture plate (Corning Incorporated, Corning, NY) filled with 1 mL of respiration buffer. A waterpad connected to a circulating water bath was placed underneath to maintain a 37°C temperature. A miniature stir bar (10 mm X 3 mm) was placed in the well for faster diffusion and was controlled by a battery operated stirrer that was placed underneath the water

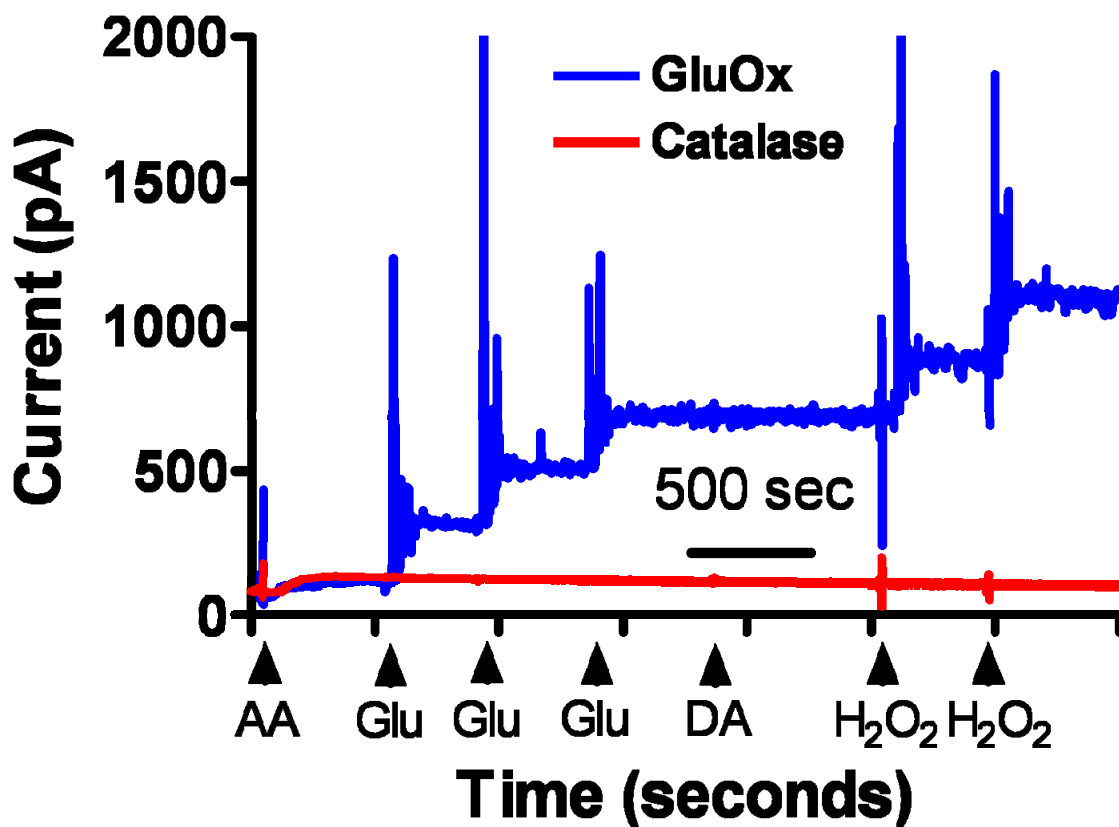


Figure C.6: Calibration of a Glutamate Oxidase and Catalase Coated MEA.

This dual enzyme MEA was coated with BSA/Glut and GluOx on sites 1 and 2 (blue trace) and BSA/Glut and Catalase on sites 3 and 4 (red trace). Final beaker concentrations of 250 μM AA; 20, 40, and 60 μM Glu; 2 μM DA; and 8.8 and 17.6 μM H₂O₂ were added (arrow heads) for the calibration. A trace from site 1 shows the response to both Glu and H₂O₂. A trace from site 3 shows no response to either Glu or H₂O₂. Neither site responded to additions of AA or DA. The MEA was tested prior to enzyme coating to ensure all sites responded to H₂O₂.

pad. A Ag/AgCl reference electrode and a catalase coated MEA was placed into the well and allowed to reach baseline. 10.0 μl of pyruvate malate (PM) was added to start the Krebs' Cycle and buildup the membrane potential. This was allowed to reach baseline for 1 minute and then 5.0 μl of adenosine diphosphate (ADP) was added. This provides the substrate for Complex V and, along with the membrane potential, drives the synthesis of ATP. A byproduct of respiration was superoxide, however, addition of ADP did not result in formation of measurable levels of H_2O_2 as shown in figure C.7. This reaction was allowed to occur for 2 minutes and then 4.0 μl of oligomycin was added, which blocks Complex V thereby stopping respiration. Blocking Complex V allows production of reactive oxygen species. During *in vitro* calibration of the catalase MEA, Oligomycin was added as a test substance and found to be electrochemically active at an applied potential of +0.7 V vs a Ag/AgCl reference electrode. This explains the immediate increase in baseline after its addition rather than the formation of H_2O_2 . After 1 minute a new baseline was reached and, 1 μl of Antimycin-A was added, which is a Complex III inhibitor. This prevents electrons from moving along the electron transport chain, stops oxygen consumption to water, and forms large levels of superoxide. After addition of Antimycin-A, we observed a sustained, elevated increase in H_2O_2 production ($\sim 4 \mu\text{M}$) that reached baseline after ~ 8 minutes as shown in figure C.7. Two separate additions of 4 μl of carbonyl cyanide 4-(trifluoromethoxy) phenylhydrazone (FCCP) were added once H_2O_2 production had baselined. FCCP is a chemical uncoupler that translocates H^+ down its concentration gradient across the inner mitochondrial membrane thus shutting down respiration. Additions of FCCP resulted in a decrease in H_2O_2 concentration that had built up from Antimycin-A (figure C.7).

Discussion

Catalase was successful at blocking H_2O_2 detection both *in vitro* and *in vivo* indicating that this enzyme could be used for self-referencing, amperometric detection of H_2O_2 . A pair or recording sites were coated with the BSA/Glut and catalase while the other pair of recording sites were coated with just the

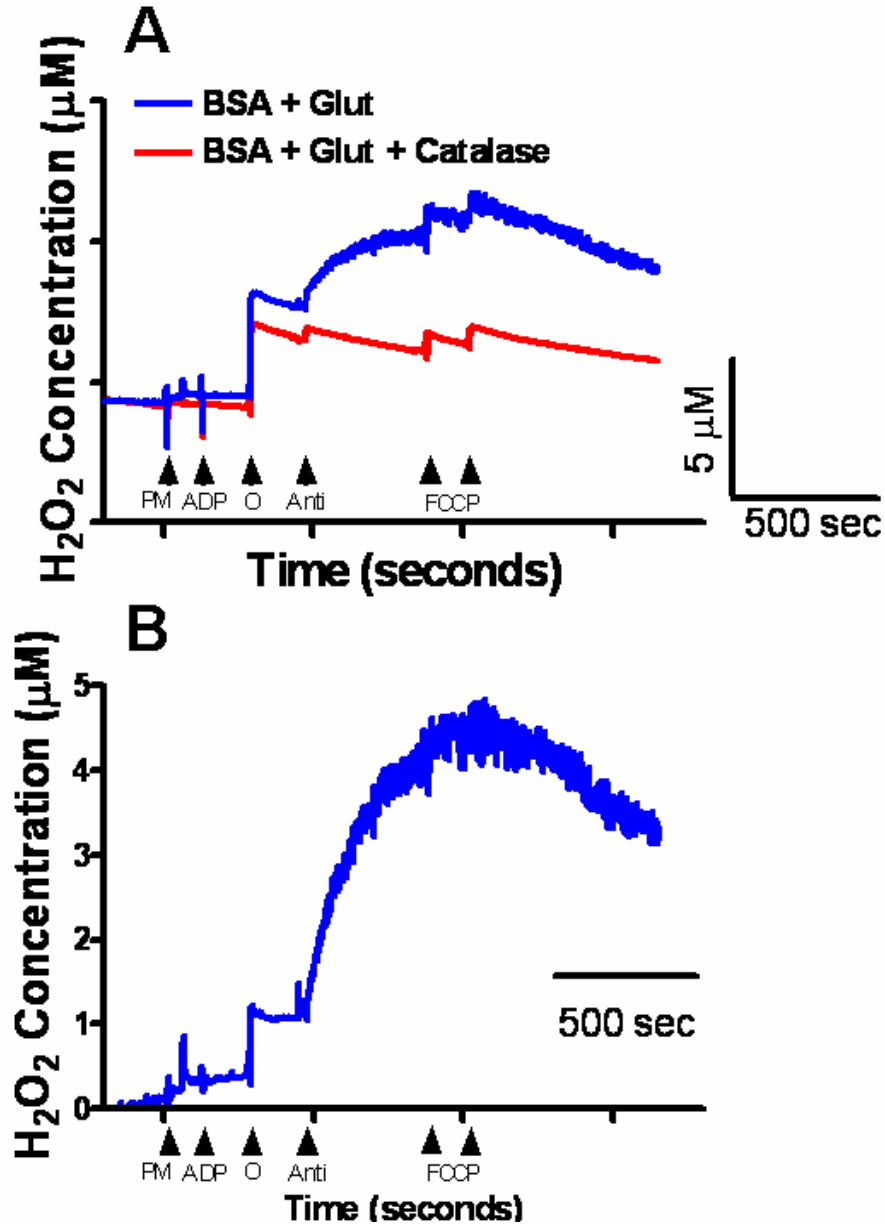


Figure C.7: Amperometric Traces of H₂O₂ Produced from Mitochondria Preparations

A.) A self-referencing catalase MEA was used to measure H₂O₂ formation (blue trace) due to blocking specific complexes of the electron transport chain in mitochondria. B) The self-referenced trace of the data shown in A. ATP synthesis was begun by adding PM and ADP. Respiration results in superoxide formation, but this did not cause measurable H₂O₂ formation. Next, oligomycin (O) was added, which was electrochemically active, resulting in the fast increase in baseline. Antimycin-A (Anti) was added and inhibits Complex III thus driving formation of ~ 4 µM H₂O₂. After ~8 minutes when H₂O₂ production had reached baseline, two additions of FCCP were added and a decrease in H₂O₂ levels were seen.

BSA/Glut mixture. Without this protein coating, the H₂O₂ detecting sites would respond more quickly to analyte. Protein layers are necessary on both recording sites to minimize difference between the recording properties of the different MEA recording sites.

In vivo, local application of 100 μM H₂O₂ (25 nl) resulted in robust, reproducible peaks compared to baseline in both the C57BL/6 mouse and a Fisher 344 rat. Local application of 100 μM H₂O₂ (25 nl) in the mouse Str resulted in responses that were ~ 20 μM in peak height while a small (~ 1 μM) response was observed on the catalase coated sites. To determine if this was due to pressure artifact or incomplete decomposition of H₂O₂ by catalase, the potential was dropped from +0.7 V to +0.2 V vs a Ag/AgCl reference electrode. At an applied potential of +0.2 V, where H₂O₂ is not as readily oxidized, the catalase coated sites showed dilution artifact after local application of 100 μM H₂O₂. This indicates that the responses seen on the catalase coated site was due to incomplete decomposition of H₂O₂ by catalase. It should be noted that the concentration of H₂O₂ locally applied adjacent to the recording site was significantly larger than the concentration of H₂O₂ released from the mitochondrial preparations. This helps to justify that the catalase coated MEA works well at physiologically relevant concentrations of H₂O₂ *in vivo*.

Unfortunately, addition of the BSA/Glut and Catalase coating over top of the already cured GluOx layer resulted in minimal Glu detection during calibration. When only 1 catalase layer was applied rather than 3, we observed a better response to Glu during calibration; however, the catalase was not capable of fully degrading the exogenously applied H₂O₂. This indicates that the layers of GluOx and catalase are too thick thus preventing diffusion of molecules to the Pt recording sites. It should be noted that this experiment was conducted without any exclusion layers. An additional layer of either Nafion[®] or mPD would likely prevent detection of any analyte by the MEA. This test has pushed the laboratory towards other MEA designs with additional Pt recording sites positioned among the analyte detecting sites. These additional sites would be raised above the surface of the MEA to act as a physical barrier to prevent

diffusion of H₂O₂ to other recording sites. Also, a current can be applied to these sites to treat them as a H₂O₂ scrubber, oxidizing the molecule into H₂O and ½ O₂.

With our self-referencing capabilities we were able to examine resting levels of extracellular H₂O₂. The few studies we conducted in the Str of an anesthetized C57BL/6 mouse and Fisher 344 rat indicated that resting H₂O₂ were ~0.3-0.4 μM. This is slightly less than the 1-2 μM resting levels reported using microdialysis in the gerbil hippocampus (Lei *et al.*, 1998) as well as the 1-3 μM levels reported using carbon fiber amperometric microsensors in the Str of Sprague-Dawley rats (Kulagina and Michael, 2003). The levels we reported may be lower for several reasons. First, the damage caused by microdialysis probes has been thoroughly discussed already in this thesis (refer to Chapters 1 and 5). The damage may produce elevated levels of H₂O₂ and other reactive oxygen species which are known to form due to brain injury. Also, the fact that the microdialysis study was conducted in a different rodent model (gerbil) as well as a different brain area may account for the differences. But, this does not explain the differences in resting levels seen with our MEA and a similar dimension carbon fiber microsensor. The carbon fiber microsensor does not have multiple recording sites which prevents the removal of interferents from the analyte signal. If good exclusion layers were not applied, interferents may account for the elevated resting levels of H₂O₂ observed in this study.

Finally, we used the self-referencing catalase MEA to measure H₂O₂ formation from mitochondrial preparations *in vitro*. In order to induce H₂O₂ we needed to provide substrates (PM and ADP) to start respiration. Superoxide formation is a byproduct of respiration and is used to synthesize H₂O₂. Respiration did not result in measurable levels of H₂O₂ formation *in vitro*. Next, we added an inhibitor of Complex V, oligomycin, which stops respiration, thus backing up the electron transport chain creating high levels of reactive oxygen species. Oligomycin is electrochemically active, which causes the response seen on both sets of recording sites. The response is much too quick to be attributed to the formation of H₂O₂, therefore blocking Complex V does not result in detectable levels of H₂O₂ formation. We did observe that blocking

Complex III with Antimycin-A resulted in steady formation of H_2O_2 (~4 μM) over an 8 minute time period. Blocking Complex III prevents consumption of O_2 so none is converted to water. This leads to formation of high levels of superoxide that is shown to be synthesized into H_2O_2 . FCCP is a chemical uncoupler that can carry H^+ across the inner mitochondrial membrane, shutting down the electron transport chain and thus formation of superoxide. Additions of this resulted in a decrease in the H_2O_2 already formed from blocking Complex III. This phenomenon is difficult to explain since FCCP itself should not induce degradation of already formed H_2O_2 , but rather prevent additional formation of H_2O_2 . Prior to additions of FCCP, H_2O_2 production probably reached baseline, because the amount of available substrates may have been fully utilized for respiration. Without available substrates, the electron transport chain would halt. Furthermore, adding FCCP would diminish the proton gradient and prevent respiration. With no more superoxide production to generate H_2O_2 , endogenous catalase present in mitochondria may begin to degrade the H_2O_2 formed. This may explain the decrease in H_2O_2 observed after additions of FCCP.

As mentioned in the introduction, we were interested in determining if H_2O_2 was generated in the mitochondria from blocking certain electron transport complexes. Dr. Margaret Rice's group has data demonstrating that Rotenone, a compound that blocks electron transfer from Complex I to ubiquinone, can lead to H_2O_2 formation and release from the mitochondria. Our laboratory performed several studies *in vitro* with the mitochondrial preparations that were similar to those conducted using Antimycin-A. Substituting Rotenone for Antimycin-A we did not observe any H_2O_2 formation (data not shown). We did however, determine that blocking Complex III causes a large accumulation of H_2O_2 , most likely through the generation of superoxide. We determined that this H_2O_2 is capable of leaving the mitochondria since we detected increased H_2O_2 levels in the respiration buffer using our self-referencing catalase MEA. Additional studies need to be conducted to determine if any of this H_2O_2 can escape the intracellular space *in vivo* prior to degradation by endogenous catalase as well as determine if H_2O_2 can act as a diffusible neuromodulator.

I would like to thank Laurie Davis for providing the mitochondrial preparations as well as her help in understanding the data as to how it relates to the electron transport chain. Also, a special thanks to Thomas Schlierf for his help in performing many of the experiments shown in this appendix.

Copyright © Kevin Nicholas Hascup

References

- Albin, R.L. and Greenamyre, J.T. (1992) Alternative excitotoxic hypotheses. *Neurol.* 42, 733-738.
- Anderson, C.M., Bridges, R.T., Chamberlin, A.R., Shimamoto, K., Yasuda-Kamatani, Y., Swanson, R.A. (2001) Differing effects of substrate and non-substrate transport inhibitors on glutamate uptake reversal. *J. Neurochem.* 79, 1207-1216.
- Antuono, P.G., Jones J.L., Wang, Y., and Li, S.J. (2001) Decreased glutamate + glutamine in Alzheimer's diseases detected *in vivo* with ^1H -MRS at 0.5T. *Neurology* 56: 737-742.
- Avshalumov, M.V., Bao, L., Patel, J.C. and Rice, M.E. (2007) H_2O_2 signaling in the nigrostriatal dopamine pathway via ATP-sensitive potassium channels: issues and answers. *Antioxid. and Redox Signal.* 9 (2), 219-231.
- Avshalumov, M.V., Chen, B.T., Marshall, S.P., Peña, D.M. and Rice, M.E. (2003) Glutamate-dependent inhibition of dopamine release in the striatum is mediated by a new diffusible messenger, H_2O_2 . *J. Neurosci.* 23 (7), 2744-2750.
- Baiping, L., Adachi, N. and Arai, T. (1998) Measurement of the extracellular H_2O_2 in the brain by microdialysis. *Brain Res. Prot.* 3, 33-36.
- Bak, L.K., Schousboe, A., and Waagepetersen, H.S. (2006) The glutamate/GABA-glutamine cycle: aspects of transport, neurotransmitter homeostasis and ammonia transfer. *J. Neurochem.* 98, 641-653.
- Baker, D.A., Xi, Z.X. Shen, H. Swanson, C.J. Kalivas, P.W. (2002) The origin and neuronal function of *in vivo* nonsynaptic glutamate. *J. Neurosci.* 22 (20), 9134-9141.

Balazs, R. and Haslam R.J. (1965) Exchange transamination and the metabolism of glutamate in brain. *Biochem J.* 94, 131-141.

Bartholow, R. (1874) Experimental investigations into the functions of the human brain. *Am. J. Med. Sci.* 67, 305-313.

Beal., M.F. (1992) Does impairment of energy metabolism result in excitotoxic neuronal death in neurodegenerative illness. *Ann. Neurol.* 31, 119-130.

Beart, P.M. and O'Shea, R.D. (2007) Transporters for L-glutamate: an update on their molecular pharmacology and pathological involvement. *British J. of Pharm.* 150, 5-17.

Beck, J.A., Lloyd, S. Hafezparast M., Lennon-Pierce, M., Eppig, J.T., Festing, M.F., Fisher E.M. (2000) Genealogies of mouse inbred strains. *Nat. Genet.* 24, 23-25.

Belzung, C. and Griebel, G. (2001) Measuring Normal and Pathological Anxiety Like Behaviour in Mice: A Review. *Behavioural Brain Research.* 125 (1-2), 141-149.

Belzung, C., El Hage, W., Moindrot, N., and Griebel, G. (2001) Behavioral and Neurochemical Changes Following Predatory Stress in Mice. *Neuropharmacol.* 41 (3), 400-408.

Benabid, A.L., Pollak, P., Gao, D. Hoffmann, D. Limousin, P., et al. (1996) Chronic electrical stimulation of the ventralis intermedius nucleus of the thalamus as a treatment of movement disorders. *J. Neurosurg.* 84, 203-214.

Benabid, A.L., Pollak, P. Gervason, C., Hoffmann, D., Gao, D.M., et al. (1991) Long-term suppression of tremor by chronic stimulation of the ventralis intermediate thalamic nucleus. *Lancet* 337, 403-406.

Benjamin, A. and Quastel, J.H. (1975). Metabolism of amino acids and ammonia in rat brain cortex slices in vitro: a possible role of ammonia in brain function. *J. Neurochem.* 25, 197-206.

Benveniste, H. and Diemer, N.H. (1987) Cellular reaction to implantation of a microdialysis tube in the rat hippocampus. *Acta Neuropath.* 74 (3) 234-238.

Bergeron, R., de Montigny, C., and Debonnel, G. (1996) Potentiation of neuronal NMDA response induced by dehydroepiandrosterone and its suppression by progesterone: effects mediated via sigma receptors. *J. Neurosci.* 16, 1193-1202.

Boksha, I.S. (2004) Coupling between neuronal and glial cells via glutamate metabolism in brain of healthy persons and patients with mental disorders. *Biochemistry* 69, 869-886.

Beschorner, R., Dietz, K., Schauer, N., Mittelbronn, M., Schluesener, H.J., Trautmann, K., Meyermann, R. and Simon, P. (2007) Expression of EAAT1 reflects a possible neuroprotective function of reactive astrocytes and activated microglia following human traumatic brain injury. *Histol. and Histopathol* 22, 515-526.

Borland, L.M., Shi, G., Yang, H., Michael, A.C. (2005) Voltammetric study of extracellular dopamine near microdialysis probes acutely implanted in the striatum of the anesthetized rat. *J. Neurosci. Meth.* 146, 149-158.

Brabet, I., Mary, S., Bockaert, J. Pin, J.-P. (1995) Phenylcyclycine derivatives discriminate between mGluR1- and mGluR5-mediated responses. *Neuropharmacol.* 34 (8), 895-903.

Brodkin, E.S. (2007) BALB/c mice: Low sociability and other phenotypes that may be relevant to autism. *Behavioural Brain Res.* 176, 53-65.

Broman, J., Hassel, B., Rinvik, E., Ottersen, O.P. (2000) Biochemistry and anatomy of transmitter glutamate. In: *Glutamate*. Eds Ottersen, O.P., Storm-Mathisen, J. Elsevier, Amsterdam. 1–44.

Bungay, P.M., Morrison, P.F. and Dedrick, R.L. (1990) Steady-state theory for quantitative microdialysis of solutes and water *in vivo* and *in vitro*. *Life Sci.* 46 (2), 105-119.

Bungay, P.M., Newton-Vinson, P., Isele, W., Garris, P.A., and Justice, J.B. (2003) Microdialysis of Dopamine Interpreted With Quantitative Model Incorporating Probe Implantation Trauma. *Journal of Neurochemistry* 86 (4), 932-946.

Burbaeva, G.S., Boksha, I.S., Tereshkina, E.B., Savushkina, O.K., Starodubtseva, L.I., Turishcheva, M.S., Mukaetova-Ladinska, E. (2007) Systemic neurochemical alterations in schizophrenic brain: glutamate metabolism in focus. *Neurochem. Res.* 32 (9), 1434-1444

Burbaeva, G.S., Boksha, I.S., Tereshkina, E.B., Savushkina, O.K., Starodubtseva, L.I., and Turishcheva, M.S. (2005) Glutamate Metabolizing Enzymes in Prefrontal Cortex of Alzheimer's Disease Patients. *Neurochem. Res.* 30 (11), 1443-1451.

Burbaeva, G.S., Boksha, I.S., Turischeva, M.S., Vorobyeva, E.A., Savushkina, O.K., and Tereshkina, E.B. (2003) Glutamine Synthetase and Glutamate

Dehydrogenase in the Prefrontal Cortex of Patients With Schizophrenia. *Prog. in Neuro-Psychopharmacol. & Biolog. Psychiatry* 27 (4), 675-680.

Burki, F. and Kaessmann, H. (2004) Birth and Adaptive Evolution of a Hominoid Gene That Supports High Neurotransmitter Flux. *Nature Genetics* 36 (10), 1061-1063.

Burmeister, J.J., Moxon, K., Gerhardt, G.A. (2000) Ceramic-Based Multisite Microelectrodes for Electrochemical Recordings. *Anal. Chem.* 72 (1), 187-192.

Burmeister, J.J. and Gerhardt, G.A. (2001) Self-Referencing Ceramic-Based Multisite Microelectrodes for the Detection and Elimination of Interferences from the Measurement of L-Glutamate and Other Analytes. *Anal. Chem.* 73 (5), 1037-1042.

Burmeister, J.J. and Gerhardt, G.A. (2005). Neurochemical Arrays. In: *Encyclopedia of Sensors*. (Eds. Grimes, C.A, Dickey, E.C., Pishko, M.V.) American Scientific Publishers. Valencia, CA.

Burmeister, J.J., Palmer, M. and Gerhardt, G.A. (2003) Ceramic-Based Multisite Microelectrode Array for Rapid Choline Measures in Brain Tissue. *Analytica Chimica Acta* 481 (1), 65-74.

Burmeister J.J., Palmer, M. and Gerhardt, G.A. (2005) L-Lactate Measures in Brain Tissue With Ceramic-Based Multisite Microelectrodes. *Biosensors and Bioelectronics* 20 (9), 1772-1779.

Burmeister, J.J., Pomerleau, F., Palmer, M., Day, B.K., Huettl, P., Gerhardt, G.A. (2002) Improved ceramic-based multisite microelectrode for rapid measurements of L-glutamate in the CNS. *J. Neurosci. Meth.* 119, 163-171.

Burmeister J.J. and Gerhardt, G.A. (2003) Ceramic based-multisite microelectrode arrays for *in vivo* electrochemical recordings of glutamate and other neurochemicals. *Trends in Anal. Chem.* 22 (8), 498-502.

Clapp-Lilly, K. L., Roberts, R.C., Duffy, L.K., Irons, K.P., Hu, Y., Drew, K.L. (1999) An ultrastructural analysis of tissue surrounding a microdialysis probe. *J. Neurosci Meth.* 90, 129-142.

Chatton, J., Shimamoto, K., Magistretti, P.J. (2001) Effects of glial glutamate transporter inhibitors on intracellular Na⁺ in mouse astrocytes. *Brain Res.* 893, 46-52.

Choi, B.H., Kim, R.C., Suzuki, M., and Choe, W. (1992) The ventriculus terminalis and filum terminale of the human spinal cord. *Hum. Pathol.* (23, 916-920.

Choi, D.W. (1987) Ionic dependence of glutamate neurotoxicity in cortical cell culture. *J. Neurosci.* 7, 369-379.

Consortium (Mouse Genome Sequencing Consortium). (2002) *Nature* 420, 520-562.

Cooper, I.S. (1973) Effect of chronic stimulation of anterior cerebellum on neurological disease. *Lancet* 1, 206.

Cooper, J.R., Bloom, F.E., Roth, R.H (2003) *The Biochemical Basis of Neuropharmacology*. Oxford University Press, 8th Edition.

Crabbe, J.C., Metten, P., Gallaher, E.J., Belknap, J.K. (2002) Genetic determinants of sensitivity to pentobarbital in inbred mice. *Psychopharmacol.* 161, 408-416.

Cryan, J.F. and Holmes, A. (2005) The ascent of mouse: advances in modeling human depression and anxiety. *Nat. Rev. Drug Discov.* 4, 775-790.

Day, B.K., Pomerleau, F., Burmeister, J.J., Huettl, P., Gerhardt, G.A. (2006) Microelectrode array studies of basal and potassium-evoked release of L-glutamate in the anesthetized rat brain. *J. Neurochem.* 96, 1626-1635.

DeFelipe, J., Alonso-Nanclares, L. and Arellano, J. I. (2002) Microstructure of the neocortex: Comparative aspects. *J. Neurocytol.* 31, 299-316.

Doble, A. (1999) The role of excitotoxicity in Neurodegenerative disease: implications for therapy. *Pharmacol. Ther.* 81 (3), 163-221.

Di Chiara, G., Tanda, G., Carboni, E. (1996) Estimation of in-vivo neurotransmitter release by brain microdialysis: the issue of validity. *Behavioural Pharmacol.* 7, 640-657.

Doble, A. (1999) The Role of Excitotoxicity in Neurodegenerative Disease: Implications for Therapy. *Pharmacol. & Therapeutics* 81 (3), 163-221.

Doherty, A.J., Collingridge, G.L., Jane, D.E. (1999) Antagonist activity of α -substituted 4-carboxyphenylglycine analogues at group I metabotropic glutamate receptors expressed in CHO cells. *British J. Pharmacol.* 126, 205-210.

Drew, K.L., Pehek, E.A., Rasley, B.T., Ma, Y.L., Green, T.K. (2004) Sampling glutamate and GABA with microdialysis: suggestion on how to get the dialysis membrane closer to the synapse. *J. Neurosci. Meth.* 140, 127-131.

Dringen, R., Pawlowski, P.G., and Hirrlinger, J. (2005) Peroxide detoxification by brain cells. *J. Neurosci. Res.* 79, 157-165.

Engelman, H.S. and MacDermott, A.B. (2004) Presynaptic ionotropic receptors and control of transmitter release. *Nat. Rev. Neurosci.* 5, 135-145.

Erecińska, M., Nelson, D., Nissim, I., Daikhin, Y., Yudkoff, M. (1994) Cerebral alanine transport and alanine aminotransferase reaction: alanine as a source of neuronal glutamate. *J. Neurochem.* 62, 1953-1964.

Eventoff, W. Tanaka, N., and Rossmann, M.G. (1976) Crystalline Bovine Liver Catalase. *J. Mol. Biol.* 103, 799-801.

Fray, A.E., Ince, P.G., Banner, S.J., Milton, L.D., Usher, P.A., Cookson, M.R., and Shaw, P.J. (1998) The Expression of the Glial Glutamate Transporter Protein EAAT2 in Motor Neuron Disease: an Immunohistochemical Study. *Euro. J. of Neurosci.* 10 (8), 2481-2489.

Festing, M.F. (2004) The choice of animal model and reduction. *Altern. Lab. Anim.* 32 (2), 59-64.

Fonnum, F. (1993) Regulation of the synthesis of the transmitter pool of glutamate. *Prog. In Biophys. and Mol. Biol.* 60 (1), 47-57.

Fournier, K.M., González, M.I., Robinson, M.B. (2004) Rapid Trafficking of the Neuronal Glutamate Transporter, EAAC1. *J. Biol. Chem.* 279 (33), 34505-34513.

Friedemann, M.N. and Gerhardt, G.A. (1992) Regional Effects of Aging on Dopaminergic Function in the Fischer-344 Rat. *Neurobiology of Aging* 13 (2), 325-332.

Friedemann, M.N., Robinson, S.W., and Gerhardt, G.A. (1996) O-Phenylenediamine-Modified Carbon Fiber Electrodes for the Detection of Nitric Oxide. *Anal. Chem.* 68 (15), 2621-2628.

Frumberg, D.B., Fernando, M.S., Lee, D.E., Biegon, A., and Schiffer, W.K. (2007) Metabolic and Behavioral Deficits Following a Routine Surgical Procedure in Rats. *Brain Res.* 1144, 209-218.

Furukawa, H., Singh, S.K., Mancusso, R., and Gouaux, E. (2005) Subunit Arrangement and Function in NMDA Receptors. *Nature* 438 (7065), 185-192.

Gaillet, S., Plachez, C., Malaval F., Bézine, M.-F., Récasens, M. (2001) Transient increase in the high affinity [³H]-L-glutamate uptake activity during in vitro development of hippocampal neurons in culture. *Neurochem. Intl.* 38, 293-301.

Galvan, A., Kuwajima, M., Smith, Y. (2006) Glutamate and GABA receptors and transporters in the basal ganglia: What does their subsynaptic localization reveal about their function. *Neurosci.* 143, 351-375.

Gardoni, F. and Di Luca, M. (2006) New targets for pharmacological intervention in the glutamatergic synapse. *Euro. J. of Pharm.* 545, 2-10.

Georgieva, J., Luthman, J., Mohring, B., and Magnusson, O. (1993) Tissue and Microdialysate Changes After Repeated and Permanent Probe Implantation in the Striatum of Freely Moving Rats. *Brain Res. Bulletin* 31 (5), 463-470.

Gerhardt, G.A. and Hoffman, A.F. (2001) Effects of Recording Media Composition on the Responses of Nafion-Coated Carbon Fiber Microelectrodes Measured Using High-Speed Chronoamperometry. *J. of Neurosci. Meth.* 109 (1), 13-21.

Gerhardt, G.A., Oke, A.F., Nagy, G., Moghaddam, B., Adams, R.N. (1984) Nafion-coated electrodes with high selectivity for CNS electrochemistry. *Brain Res.* 290 (2), 390-395.

Gladden, L.B. (2004) Lactate metabolism: a new paradigm for the third millennium. *J. Physiol.* 558 (1), 5-30.

Gordon-Krajcer W., Salinska, E. and Lazarewics, J.W. (2002) N-methyl-D-aspartate receptor-mediated process of beta-amyloid precursor protein in rat hippocampal slice: in vitro – superfusion study. *Folia Neuropathol.* 40: 13-17.

Greene, J.G. and Greenamyre, J.T. (1996) Bioenergetics and glutamate excitotoxicity. *Prog. in Neurobio.* 48, 613-634.

Grewer, C. and Rauen, T. (2005) Electrogenic glutamate transporters in the CNS: Molecular mechanism, Pre-steady-state kinetics, and their impact on synaptic signaling. *J. Membrane Biol.* 203, 1-20.

Gruetter, R., Seaquist, E.R. and Ugurbil, K. (2001) A mathematical model of compartmentalized neurotransmitter metabolism in the human brain. *Am. J. Physiol. Endocrinol. Metab.* 281, E100-E112.

Gylfe, E. (1976) Comparison of the effects of leucine, non-metabolizable leucine analogues and other insulin secretagogues on the activity of glutamate dehydrogenase. *Acta Diabetol. Lat.* 13, 20-24.

Hara, K. and Harris R.A. (2002) The anesthetic mechanism of urethane: the effects on neurotransmitter-gated ion channels. *Anesth. Analg.* 94, 313-318.

Hascup, K.N., Rutherford, E.C., Quintero, J.E., Day, B.K., Nickell J.R., Pomerleau, F., Huettl., Burmeister J.J., Gerhardt, G.A. (2006) Second-by-Second

Measures of L-glutamate and other neurotransmitters using enzyme-based microelectrode arrays. In: *Electrochemical Methods for Neuroscience*. (Ed A.C. Micheal and L.M. Borland) CRC Press, Boca Raton, FL. 407-450.

Hassel, B., and Bråthe, A. (2000) Neuronal pyruvate carboxylation supports formation of transmitter glutamate. *J. Neurosci.* 20 (4), 1342-1347.

Hao, Y., Yank, J.Y., Wu., C.F., Wu., M.F. (2007) Pseudoginsenoside-F11 decreases morphine-induced behavioral sensitization and extracellular glutamate levels in the medial prefrontal cortex in mice. *Pharmacol., Biochem., and Behavior* 86, 660-666.

Hayley, S., Borowski, T., Merali, Z., and Anisman, H. (2001) Central Monoamine Activity in Genetically Distinct Strains of Mice Following a Psychogenic Stressor: Effects of Predator Exposure. *Brain Res.* 892 (2), 293-300.

Heath, P.R. and Shaw P.J. (2002) Update on the glutamatergic neurotransmitter system and the role of excitotoxicity in amyotrophic lateral sclerosis. *Muscle and Nerve* 26 (4), 438-458

Hertz, L. (2004) Intercellular metabolic compartmentation in the brain: past, present and future. *Neurochem. Intl.* 45 (2-3), 285-296.

Herve, D., Tassin, J.P., Barthelemy, C., Blanc, G., Lavielle, S. Glowinski, J. (1979). Difference in the reactivity of the mesocortical dopaminergic neurons to stress in the BALB/C and C57BL/6 mice. *Life Sci.* 25, 1659-1664.

Holmer, H.K., Keyghobadi, M., Moore, C., Menashe, R.A., Meshul, C.K. (2005) Dietary restriction affects striatal glutamate in the MPTP-induced mouse model of nigrostriatal degeneration. *Synapse* 57, 100-112.

Holmer, H.K., Keyghobadi, M., Moore, C., Meshul, C.K. (2005) L-dopa-induced reversal in striatal glutamate following partial depletion of nigrostriatal dopamine with 1-methyl-4-phenyl-1,2,3,6-tetrahydropyridine. *Neurosci.* 136 (1), 333-341

Hosobuchi, Y., Adams, J.E., Rutkin, B. (1973) Chronic thalamic stimulation for the control of facial anesthesia dolorosa. *Arch. Neurol.* 29, 158-161.

Hu, Y., Mitchell, K.M., Albahadily, F.N., Michaelis, E.K., Wilson, G.S. (1994) Direct measurement of glutamate release in the brain using a dual enzyme-based electrochemical sensor. *Brain Res.* 659, 117-125.

Hynd, M.R., Scott, H.L., and Dodd, P.R. (2004) Glutamate-Mediated Excitotoxicity and Neurodegeneration in Alzheimer's Disease. *Neurochem. Intl.* 45 (5), 583-595.

Ishikawa, T., Sahara, Y. and Takahashi, T. (2002) A single packet of transmitter does not saturate postsynaptic glutamate receptors. *Neuron* 34, 613-621.

Jacobson, L.H. and Cryan J.F. (2005) Differential sensitivity to the motor and hypothermic effects of the GABA B receptor agonist baclofen in various mouse strains. *Psychopharmacol.* 179, 688-699.

Joyner, A.L. and Sedivy, L.M. (2000) *Gene targeting: A Practical Approach.* Oxford University Press, Oxford.

Kanai, Y. and Hediger M.A. (2004) The glutamate/neutral amino acid transporter family SLC1: molecular, physiological and pharmacological aspects. *Eur. J. Physiol.* 447, 469-479.

Kanamori, K. and Ross, B.D. (1995) Steady-state *in vivo* glutamate dehydrogenase activity in rat brain measured by ¹⁵N NMR. *J. Biol. Chem.* 270 (42), 24805-24809.

Kanavouras, K., Mastorodemos, V., Borompokas, N., Spanaki, C., and Plaitakis, A. (2007) Properties and Molecular Evolution of Human GLUD2 (Neural and Testicular Tissue-Specific) Glutamate Dehydrogenase. *J. Neurosci Res.* 85 (5), 1101-1109.

Kaneko, T., Akiyama, H., and Mizuno, N. (1987) Immunohistochemical Demonstration of Glutamate-Dehydrogenase in Astrocytes. *Neurosci. Lett.* 77 (2), 171-175.

Katzman, R., and Saitoh, T. (1991) Advances in Alzheimer's disease. *FASEB J.* 5: 278-286.

Kennedy, R.T., Watson, C.J., Haskins, W.E., Powell, D.H., Strecker, R.E. (2002) *In vivo* neurochemical monitoring by microdialysis and capillary separations. *Curr. Opin. in Chem. Biol.* 6, 659-665.

Kew, J.N.C. and Kemp, J.A. (2005) Ionotropic and metabotropic glutamate receptor structure and pharmacology. *Psychopharmacol.* 179, 4-29.

Kinney, G.A., Overstreet, L.S., Slater, N.T. (1997) Prolonged physiological entrapment of glutamate in the synaptic cleft of cerebellar unipolar brush cells. *J. Neurophysiol.* 78 (3), 1320-1333.

Kirwan, S.M., Rocchitta, G., McMahon, C.P., Craig, J.D., Killoran, S.J., O'Brien, K.B., Serra, P.A., Lowrd, J.P., and O'Neill R.D. (2007) Modifications of Poly (o-phenylenediamine) permselective layer on Pt-Ir for Biosensor Application in Neurochemical Monitoring. *Sensors* 7, 420-437.

Kuhr, W.G. and Wightman R.M. (1986) Real-time measurement of dopamine release in rat brain. *Brain Res.* 381 (1), 168-171.

Kulagina, N.V. and Michael, A.C. (2003) Monitoring hydrogen peroxide in the extracellular space of the brain with amperometric microsensors. *Anal. Chem* 75, 4875-4881.

Kulagina, N.V., Shanker, L., and Michael, A.C. (1999) Monitoring glutamate and ascorbate in the extracellular space of brain tissue with electrochemical microsensors. *Anal. Chem.* 71, 5093-5100.

Kusakabe, H., Midorikawa, Y. And Fujishima, T. (1984) Methods for Determining L-Glutamate in Soy Sauce with L-Glutamate Oxidase *Agric. Biol. Chem.* 48 (1), 181-184.

Kusakabe, H., Midorikawa, Y., Fujishima, T., Kuninaka, A., Yoshino, H. (1983) Purification and properties of a new enzyme, L-glutamate oxidase, from *Streptomyces* sp. X-119-6 grown on wheat bread. *Agric. Biol. Chem.* 47 (6), 1323-1328.

Kvamme, E., Roberg B., Torgner, I. A. (2000) Phosphate-activate glutaminase and mitochondrial glutamine transport in the brain. *Neurochem. Res.* 25 (9/10) 1407-1419.

Lada, M.W., Vickroy, T.W., Kennedy, R.T. (1997) High temporal resolution monitoring of glutamate and aspartate in vivo using microdialysis on-line with capillary electrophoresis with laser-induced fluorescence detection. *Anal. Chem.* 69, 4560-4565.

Lajtha, A., Berl, S., Waelsch, H. (1959) Amino acid and protein metabolism of the brain. IV. The metabolism of glutamic acid. *J. Neurochem.* 3 (4), 322-332.

Larsen, M. and Langmoen, I.A. (1998) The Effect of Volatile Anaesthetics on Synaptic Release and Uptake of Glutamate. *Toxicol. Lett.* 101, 59-64.

Lebedev, M. A. and Nicolelis M.A.L. (2006) Brain-machine interfaces: past, present and future. *Trends in Neurosci.* 29 (9), 536-546.

Liachenko, S., Tang, P., Somogyi, G.T., and Xu, Y. (1999) Concentration-Dependent Isoflurane Effects on Depolarization-Evoked Glutamate and GABA Outflows From Mouse Brain Slices. *Brit. J. of Pharmacol.* 127 (1), 131-138.

Lesch, K.P. (2004) Gene-environment interactions and the genetics of depression. *J. Psychiatry Neurosci.* 29, 174-184.

Lipton, S.A. (2005) The molecular basis of memantine action in Alzheimer's disease and other neurologic disorders: low-affinity, uncompetitive antagonism. *Curr Alzheimer Res.* 2 (2), 155-165.

Loschmann, P.A., De Groote, C., Smith, L., Wullner, U., Fischer, G., Kemp, J.A., Jenner, P., and Klockgether, T. (2004) Antiparkinsonian Activity of Ro 25-6981, A NR2B Subunit Specific NMDA Receptor Antagonist, in Animal Models of Parkinson's Disease. *Exp. Neurol.* 187 (1), 86-93.

Lowry J.P., Miele M., O'Neill R.D., Boutelle M.G., Fillenz M., (1998) An amperometric glucose-oxidase/poly(o-phenylenediamine) biosensor for monitoring brain extracellular glucose: *in vivo* characterization in the striatum of freely behaving rats, *J. Neurosci. Meth.* 79 (1), 65-74.

Lu, Y., Peters, J.L., and Michael, A.C. (1998) Direct Comparison of the Response of Voltammetry and Microdialysis to Electrically Evoked Release of Striatal Dopamine. *J. of Neurochem.* 70 (2), 584-593.

Madl, J.E., Clements, J.R., Beitz, A.J., Wenthold, R.J., and Larson, A.A. (1988) Immunocytochemical Localization of Glutamate-Dehydrogenase in Mitochondria of the Cerebellum - An Ultrastructural-Study Using A Monoclonal-Antibody. 452 (1-2), *Brain Res.* 396-402.

Malessa, S., Leigh, P.N., Bertel, O., Sluga, E., and Hornykiewicz, O. (1991) Amyotrophic-Lateral-Sclerosis - Glutamate-Dehydrogenase and Transmitter Amino-Acids in the Spinal-Cord. *J of Neurol. Neurosurgery and Psychiatry* 54 (11), 984-988.

Masliah, E., Alford, M., DeTeresa R., Mallory, M. and Hansen, L. (1996) Deficient glutamate transport is associated with neurodegeneration in Alzheimer's disease. *Ann. Neurol.* 40: 759-766.

Mastorodemos, V., Zaganas, I., Spanaki, C., Bessa, M., and Plaitakis, A. (2005) Molecular Basis of Human Glutamate Dehydrogenase Regulation Under Changing Energy Demands. *J. Neurosci. Res.* 79 (1-2), 65-73.

Matthews, C.C., Zielke, H.R., Parks, D.A., Fishman, P.S. (2003) Glutamate-pyruvate transaminase protects against glutamate toxicity in hippocampal slices. *Brain Res.* 978, 59-64.

Matthews, C.C., Zielke, H.R., Wollack. J.B., Fishman, P.S. (2000) Enzymatic degradation protects neurons from glutamate excitotoxicity. *J. Neurochem.* 75, 1045-1052.

Mattiasson, G and Sullivan, P.G. (2006) The emerging functions of UCP2 in health, disease, and therapeutics. *Antioxid. Redox. Signal.* 8 (1-2), 1-38.

McGeer, E.G. and McGeer, P.L. (2005) Pharmacologic Approaches to the Treatment of Amyotrophic Lateral Sclerosis. *Biodrugs* 19 (1), 31-37.

McKenna, M.C., Stevenson, J.H., Huang, X.L., and Hopkins, I.B. (2000) Differential Distribution of the Enzymes Glutamate Dehydrogenase and Aspartate Aminotransferase in Cortical Synaptic Mitochondria Contributes to Metabolic Compartmentation in Cortical Synaptic Terminals. *Neurochem. Intl.* 37 (2-3), 229-241.

McMahon C.P and O'Neill R.D. (2005) Polymer-enzyme composite biosensor with high glutamate sensitivity and low oxygen dependence, *Anal. Chem.* 77 (4), 1196-99

Melendez, R.I., Vuthiganon, J., Kaliva, P.W. (2005) Regulation of extracellular glutamate in the prefrontal cortex: Focus on the cystine glutamate exchanger and group I metabotropic glutamate receptors. *J. of Pharmacol. and Exp. Therapeutics* 314 (1), 139- 147.

Mellon, R.D., Simone, A.F., and Rappaport, B.A. (2007) Use of Anesthetic Agents in Neonates and Young Children. *Anesthesia and Analgesia* 104 (3), 509-520.

Methods and Materials in Microelectronic Technology (IBM Research Symposia Series) edited J. Bargon Plenum Pub Corp; 1984.

Miguel-Hidalgo, J.J., Alvarez, X.A., Cacabelos, R., and Quack, G. (2002) Neuroprotection by Memantine Against Neurodegeneration Induced by Beta-Amyloid (1-40). *Brain Res.* 958 (1), 210-221.

Murphy, L.J (1998) Reduction of interference response at a hydrogen peroxide detecting electrode using electropolymerized films of substituted naphthalenes. *Anal. Chem.* 70, 2928-2935.

Nash, J.E., Fox, S.H., Henry, B., Hill, M.P., Peggs, D., McGuire, S., Maneuf, Y., Hille, C., Brotchie, J.M., and Crossman, A.R. (2000) Antiparkinsonian Actions of Ifenprodil in the MPTP-Lesioned Marmoset Model of Parkinson's Disease. *Exp. Neuro.* 165 (1), 136-142.

Nicholls D.G. and Budd S.L (2000) Mitochondria and Neuronal Survival. *Physiological Rev.* 80 (1), 315-360.

Nickell, J., Pomerleau, F., Allen, J., Gerhardt, G.A. (2004) Age-related changes in the dynamics of potassium-evoked L-glutamate release in the striatum of Fischer 344 rats. *J. Neural Transm.* 112 (1), 87-96.

Nickell, J., Salvatore, M.F., Pomerleau, F., Apparsundaram, S., Gerhardt, G.A., (2006) Reduced plasma membrane surface expression of GLAST mediates decreased glutamate regulation in the aged striatum. *Neurobiol. Aging* (epub ahead of print).

Norenberg, M.D. and Martinez-Hernandez, A. (1979) Fine structural localization of glutamine synthetase in astrocytes of rat brain. *Brain Res.* 161, 303-310.

Nukula, V.N., Singh, I.N., Davis, L.M., and Sullivan, P.G. (2006) Cryopreservation of brain mitochondria: A novel methodology for functional studies. *J. Neurosci. Meths.* 152 (1-2), 48-54.

Obrenovitch, T.P. and Urenjak, J. (1997) Altered glutamatergic transmission in neurological disorders: from high extracellular glutamate to excessive synaptic efficacy. *Prog. Neurobiol.* 51 (1), 39-87.

Oldenziel, W.H., Dijkstra, G., Cremers, T.I.F.H., Westerink, B.H.C. (2006) In vivo monitoring of extracellular glutamate in the brain with a microsensor. *Brain Res.* 1118, 34-42.

Olive, M.F., Mehmert, K.K., Hodge, C.W. (2000) Microdialysis in the mouse nucleus accumbens: a method for detection of monoamine and amino acid neurotransmitters with simultaneous assessment of locomotor activity. *Brain Res. Protocol* 5, 16-24.

Olney, J.W. (1978) Neurotoxicity of excitatory amino acids. In: *Kainic acid as a Tool in Neurobiology*. Eds. McGreer, E.G., Olney, J.W., and McGreer, P.L. Raven Press, New York. 95-112.

Pajor, A.M. (2006) Molecular properties of the SLC13 family of dicarboxylate and sulfate transporters. *Eur. J. Physiol.* 451 (5), 597-605.

Parikh, V., Pomerleau, F., Huettl, P., Gerhardt, G.A., Sarter, M., and Bruno, J.P. (2004) Rapid Assessment of in Vivo Cholinergic Transmission by Amperometric Detection of Changes in Extracellular Choline Levels. *Eur. J. of Neurosci.* 20 (6), 1545-1554.

Parsons, C.G., Danysz, W., and Quack, G. (1999) Memantine Is a Clinically Well Tolerated N-Methyl-D-Aspartate (NMDA) Receptor Antagonist - a Review of Preclinical Data. *Neuropharmacol.* 38 (6), 735-767.

Paxinos, G. and Franklin, K.B.J. (2004) The mouse brain in stereotaxic coordinates. Academic Press, San Diego, CA.

Peel, A.L., Zolotukhin, S., Schrimsher, G.W., Muzyczka, N., and Reier, P.J. (1997). Efficient transduction of green fluorescent protein in spinal cord neurons using adeno-associated virus vectors containing cell type-specific promoters. *Gene Ther.* 4, 16-24.

Peng, L., Hertz, L., Huang, R., Sonnewald, U., Petersen, S.B., Westergaard, N., Larsson, O., Schousboe, A. (1993). Utilization of glutamine and of TCA cycle constituents as precursors for transmitter glutamate and GABA. *Dev. Neurosci.* 15, 367-377.

Peng, L.A., Schousboe, A., Hertz, L. (1991) Utilization of alpha-ketoglutarate as a precursor for transmitter glutamate in cultured cerebellar granule cells. *Neurochem. Res.* 16 (1), 29-34.

Perlmutter, J.S. And Mink, J.W. (2006) Deep Brain Stimulation. *Annual Rev. of Neurosci.* 29, 229-257.

Perouansky, M., Kirson, E.D., and Yaari, Y. (1998) Mechanism of Action of Volatile Anesthetics: Effects of Halothane on Glutamate Receptors in Vitro. *Toxicol. Lett.* 101, 65-69.

Perry, T.L., Hansen, S., Jones, K. (1987) Brain glutamate deficiency in amyotrophic lateral sclerosis. *Neurol.* 37 (12), 1845-1848.

Peters, J.L., Miner, L.H., Michael, A.C., and Sesack, S.R. (2004) Ultrastructure at Carbon Fiber Microelectrode Implantation Sites After Acute Voltammetric Measurements in the Striatum of Anesthetized Rats. *J. of Neurosci. Meth.* 137 (1), 9-23.

Photolithography, edited Texas Engineering Extension Service; Bryan, TX 2001.

Pierre, K. and Pellerin, L. (2005) Monocarboxylate transporters in the central nervous system: distribution, regulation and function. *J. Neurochem.* 94, 1-14.

Plaitakis, A. and Caroscio, J.T. (1987) Abnormal glutamate metabolism in amyotrophic lateral sclerosis. *Ann. Neurol.* 22 (5), 575-579.

Plaitakis, A. and Zaganas, I. (2001) Regulation of Human Glutamate Dehydrogenases: Implications for Glutamate, Ammonia and Energy Metabolism in Brain. *J. Neurosci. Res.* 66 (5), 899-908.

Pomerleau, F., Day, B.K., Huettl, P., Burmeister, J.J. and Gerhardt, G.A. (2003) Real Time *In Vivo* Measures of L-Glutamate in the Rat Central Nervous System Using Ceramic-Based Multisite Microelectrode Arrays. *Annals of the N.Y. Academy of Sciences* 1003, 454-457.

Rahman, A., Kwon, N.H., Won, M.S., Choe, E.S., Shim, Y.B. (2005) Functionalized conducting polymer as an enzyme-immobilizing substrate: an amperometric glutamate microbiosensor for in vivo measurements. *Anal. Chem.* 77, 4854-4860.

Rao, S.D. and Weiss J.H. (2004) Excitotoxic and oxidative cross-talk between motor neurons and glia in ALS pathogenesis. *Trends in Neurosci.* 27 (1), 17-23.

Rice M.E., Gerhardt G.A., Hierl P.M., Nagy G. and Adams R.N. (1986) Diffusion coefficients of neurotransmitters and their metabolites in brain extracellular fluid space. *Neurosci.* 15 (3), 891-902.

Rose, G.M., Gerhardt, G.A., Strömberg, I., Olson, L. and Hoffer, B.J. (1985) Monoamine release from dopamine-depleted rat caudate nucleus reinverated by substantia nigra transplants: an in vivo electrochemical study. *Brain Res.* 341 (1), 92-100.

Rose, G.M., Gerhardt, G.A., Conboy, G.L. and Hoffer, B.J. (1986) Age-related alterations in monoamine release from rat striatum: an in vivo electrochemical study. *Neurobiol. Aging* 7 (2), 77-82.

Rossell, S., Gonzalez, L.E., and Hernandez, L. (2003) One-Second Time Resolution Brain Microdialysis in Fully Awake Rats - Protocol for the Collection, Separation and Sorting of Nanoliter Dialysate Volumes. *J. of Chromatography B-Analytical Technologies in the Biomedical and Life Sciences* 784 (2), 385-393.

Rothe, F., Wolf, G., and Schunzel, G. (1990) Immunohistochemical Demonstration of Glutamate-Dehydrogenase in the Postnatally Developing Rat Hippocampal-Formation and Cerebellar Cortex - Comparison to Activity Staining. *Neurosci.* 39 (2), 419-429.

Rothstein, J.D., Martin, L.J., Kuncl, R.W. (1992). Decreased glutamate transport by the brain and spinal cord in amyotrophic lateral sclerosis. *N. Engl. J. Med.* 326 (22), 1464-1468.

Rothstein, J.D., Tsai, G., Kuncl, R.W., Clawson, L., Cornblath, D.R., Drachman, D.B., Pestronk, A., Stauch, B.L., Coyle, J.T. (1990) Abnormal excitatory amino acid metabolism in amyotrophic lateral sclerosis. *Ann. Neurol.* 28, 18-25.

Rothstein, J.D., Van Kammen, M., Levey, A.I., Martin, L.J., Kuncl, R.W. (1995). Selective loss of glial glutamate transporter GLT-1 in amyotrophic lateral sclerosis. *Ann. Neurol.* 38 (1), 73-84.

Ruščák, M., Orlický, J., Žúbor, V., Hager, H. (1982) Alanine aminotransferase in bovine brain: purification and properties. *J. Neurochem.* 39, 210-216.

Rutherford, E.C., Pomerleau, F., Huettl, P., I.Strömberg, Gerhardt, G.A., (2007) Chronic second-by-second measures of L-glutamate in the CNS of freely moving rats. *J. Neurochem.* 102 (30), 712-722.

Rossell, S., Gonzalez, L.E., Hernández (2003) One-second time resolution brain microdialysis in fully awake rats: Protocol for the collection, separation and sorting of nanoliter dialysate volumes. *J. Chromatography B* 784, 385-393.

Sabeti, J., Adams, C.E., Burmeister, J., Gerhardt, G.A., and Zahniser, N.R. (2002) Kinetic Analysis of Striatal Clearance of Exogenous Dopamine Recorded by Chronoamperometry in Freely-Moving Rats. *J. of Neurosci. Meth.* 121 (1), 41-52.

Saier Jr., M.H. and Jenkins W.T. (1967) Alanine Aminotransferase I. Purification and properties. *J. Biolog. Chem.* 242 (1), 91-100.

Sasaki, S., Komori, T., and Iwata, M. (2000) Excitatory Amino Acid Transporter 1 and 2 Immunoreactivity in the Spinal Cord in Amyotrophic Lateral Sclerosis. *Acta Neuropathologica* 100 (2), 138-144.

Sattler, R. and Tymianski, M. (2000) Molecular mechanisms of calcium-dependent excitotoxicity. *J. Mol. Med.* 78, 3-13.

Schad, A. Fahimi, H.D., Volkl, A. and Baumgart, E. (2003) Expression of catalase mRNA and protein in adult rat brain: detection by nonradioactive in situ hybridization with signal amplification by catalyzed reporter deposition (ISH-CARD) and immunohistochemistry (IHC)/immunofluorescence (IF). *J. Histochem. Cytochem.* 51, 751-760.

Schiffer, W.K., Mirrione, M.M., Biegon, A., Alexoff, D.L., Patel, V., and Dewey, S.L. (2006) Serial MicroPET Measures of the Metabolic Reaction to a Microdialysis Probe Implant. *J. of Neurosci. Meth.* 155 (2), 272-284

Schousboe, A., Sonnewald, U., Waagepetersen, H.S. (2003) Differential role of alanine in GABAergic and glutamatergic neurons. *Neurochem. Intl.* 43, 311-315.

Shakil, S.S., Holmer, H.K., Moore, C., Abernathy, A.T., Jakowec, M.W., Petzinger, G.M., Meshul, C.K. (2005) High and low responders to novelty show differential effects in striatal glutamate. *Synapse* 58, 200-207.

Shaw, P.J., Forrest, V., Ince, P.G., Richardson, J.P., Wastell, H.J. (1995) CSF and plasma amino acid levels in motor neuron disease: elevation of CSF glutamate in a subset of patients. *Neurodegeneration* 4, 209-216.

Smith, E.L. (1979) The evolution of glutamate dehydrogenases and a hypothesis for the insertion or deletion of multiple residues in the interior of polypeptide chains. *Proc. Am. Phil. Soc.* 123, 73-84.

Stanley, C.A., Lieu, Y.K., Hsu, B.Y., Burlina, A.B., Greenberg, C.R., Hopwood, N.J., Perlman, K., Rich, B.H., Zammarchi, E. Poncz, M. (1998) Hyperinsulinism and hyperammonemia in infants with regulatory mutations of the glutamate dehydrogenase gene. *N. Engl. J. Med.* 338, 1352-1357.

Stein, D.G. (2001) Brain damage, sex hormones and recovery: a new role for progesterone and estrogen? *Trends in Neurosci.* 24 (7), 386-391.

Spiegel, E.A., Wycis, H.T., Marks, M., Lee, A.J. (1947) Stereotaxic apparatus for operations on the human brain. *Science* 106, 349-350.

Spreux-Varoquaux, O., Bensimon, G., Lacomblez, L., Salachas, F., Prada, P.F., Le Forestier, N., Marouan, A., Dib, M., Meininger, V. (2002) Glutamate levels in cerebrospinal fluid in amyotrophic lateral sclerosis: a reappraisal using a new HPLC method with coulometric detection in a large cohort of patients. *J. Neurol. Sci.* 193, 73-78.

Swanson, C.J., Bures, M., Johnson, M.P., Linden A.M., Monn, J.A., Schoepp, D.D. (2005). Metabotropic glutamate receptors as novel targets for anxiety and stress disorders. *Nat. Rev. Drug Discov.* 4 (2), 131-144.

Tahar, A.H., Gregoire, L., Darre, A., Belanger, N., Meltzer, L., and Bedard, P.J. (2004) Effect of a Selective Glutamate Antagonist on L-Dopa-Induced Dyskinesias in Drug-Naive Parkinsonian Monkeys. *Neurobiol. of Disease* 15 (2), 171-176.

Takahashi, M., Billups, B., Rossi, D., Sarantis, M., Hamann, M., Attwell, D. (1997) The role of glutamate transporters in glutamate homeostasis in the brain. *The J. of Exp. Bio.* 200, 401-409.

Takamori, S. (2006) VGLUTs: 'Exciting' times for glutamatergic research? *Neurosci. Res.* 55, 343-351.

Timmerman, W. and Westerink B.H.C. (1997) Brain microdialysis of GABA and glutamate: What does it signify? *Synapse* 27, 242-261.

Toledano, A., Barca, M.A., Perez, C., and Martinezrodriguez, R. (1979) Histochemical Electron-Microscope Study of the Enzyme Glutamate-Dehydrogenase in Cerebellum. *Cellular and Molecular Biol.* 24 (2), 113-125.

Toran-Allerand, C.D. (1996) Mechanisms of estrogen action during neural development: mediation by interactions with the neurotrophins and their receptors? *J. Steroid Biochem. Mol. Biol.* 56, 169-178.

Tsai, G.C., Stauch-Slusher, B., Sim, L., Hedreen, J.C., Rothstein, J.D., Kuncl, R., Coyle, J.T. (1991). Reductions in acidic amino acids and N-acetylaspartylglutamate in amyotrophic lateral sclerosis CNS. *Brain Res.* 556 (1), 151-156.

Tucci, S., Rada, P., Sepúlveda, M.J., Hernandez, L. (1997) Glutamate measured by 6-s resolution brain microdialysis: capillary electrophoretic and laser-induced fluorescence detection application. *J. Chromatography B* 694, 343-349.

Uezono, T., Matsubara, K., Shimizu, K., Mizukami, H., Ogawa, K., Saito, O., Hayase, N., Eto, H. Kimura, K., Shiono, H. (2001) glutamate is not involved in the MPP⁺-induced dopamine overflow in the striatum of freely moving C57BL/6 mice. *J. Neural Transm.* 108, 899-908.

Ungerstedt, U. (1984) Measurement of neurotransmitter release by intracranial dialysis. In: *Measurement of Neurotransmitter Release In Vivo* (Ed. CA Marsden), Wiley, New York, 81-105.

Van den Bosch, L., Van Damme, P., Bogaert, E., and Robberecht, W. (2006) The Role of Excitotoxicity in the Pathogenesis of Amyotrophic Lateral Sclerosis. *Biochimica et Biophysica Acta-Molecular Basis of Disease* 1762 (11-12), 1068-1082.

Van Den Berg, C.J. and Garfinkel, D. (1971) A stimulation study of brain compartments. *Biochem. J.* 123, 211-218.

Waagepetersen, H.S., Qu, H., Sonnewald, U., Shimamoto, K., Schousboe, A. (2005) Role of glutamine and neuronal glutamate uptake in glutamate homeostasis and synthesis during vesicular release in cultured glutamatergic neurons. *Neurochem. Intl.* 47 (1-2), 92-102.

Waagepetersen, H.S., Sonnewald, U., Larsson, O.M., Schousboe, A. (2000) A possible role of alanine for ammonia transfer between astrocytes and glutamatergic neurons. *J. Neurochem* 75 (2), 471-479.

Wang, X., Ai, J., Hampson, D.R., Snead III, O.C. (2005) Altered glutamate and GABA release within thalamocortical circuitry in metabotropic glutamate receptor 4 knockout mice. *Neurosci.* 134 (4), 1195-1203.

Wessell, R.H., Ahmed, S.M., Menniti, F.S., Dunbar, G.L., Chase, T.N., and Oh, J.D. (2004) NR2B Selective NMDA Receptor Antagonist CP-101,606 Prevents Levodopa-Induced Motor Response Alterations in Hemi-Parkinsonian Rats. *Neuropharmacol.* 47 (2), 184-194.

Westergaard, N., Varming, T., Peng, L., Sonnewald, U., Hertz, L., Schousboe, A. (1993) Uptake, release, and metabolism of alanine in neurons and astrocytes in primary cultures. *J. Neurosci. Res.* 35, 540-545.

Westerink, B.H.C. (1995) Brain Microdialysis and Its Application for the Study of Animal Behavior. *Behavioural Brain Res.* 70 (2), 103-124.

Williams, D.B. and Windebank, A.J. (1991) Motor neuron disease (amyotrophic lateral sclerosis) *Mayo Clin. Proc.* 66 (1), 54-82.

Wilson, N.R., Kang, J.S., Hueske, E.V., Leung, T., Varoqui, H., Murnick, J.G., Erickson, J.D., and Liu, G.S. (2005) Presynaptic Regulation of Quantal Size by

the Vesicular Glutamate Transporter VGLUT1. *J. of Neurosci.* 25 (26), 6221-6234.

Win-Shwe, T.T., Misushima, D., Nakajima, D., Ahmed, S., Yamamoto, S., Tsukahara, S., Kakeyama, M., Goto. S., Fujimaki, H. (2007) Toluene induces rapid and reversible rise of hippocampal glutamate and taurine neurotransmitter levels in mice. *Toxicol. Letts.* 198, 75-82.

Winblad, B. and Poritis, N. (1999) Memantine in severe dementia: results of the 9M-Best Study (Benefit and efficacy in severely demented patients during treatment with memantine. *Int. J. Geriatr. Psychiatry* 14, 135-146.

Wire Bond, edited Texas Engineering Extension Service; Bryan, TX 1998.

Wojcik, S.M., Rhee, J.S., Herzog, E., Sigler, A., Jahn, R., Takamori, S., Brose, N., and Rosenmund, C. (2004) An Essential Role for Vesicular Glutamate Transporter 1 (VGLUT1) in Postnatal Development and Control of Quantal Size. *Proceedings of the National Academy of Sciences of the United States of America* 101 (18), 7158-7163.

Wu, X.S., Xue, L., Mohan, R., Paradiso, K., Gillis K.D., and Wu, L.G. (2007) The origin of quantal size variation: vesicular glutamate concentration plays a significant role. *J. Neurosci.* 27 (11), 3046-3056.

Yamakura, T., Bertaccini, E., Trudell, J.R., and Harris, R.A. (2001) Anesthetics and Ion Channels: Molecular Models and Sites of Action. *Annual Review of Pharmacol. and Toxicol.* 41, 23-51.

Yang, H., Peters, J.L., and Michael, A.C. (1998) Coupled Effects of Mass Transfer and Uptake Kinetics on in Vivo Microdialysis of Dopamine. *J. Neurochem.* 71 (2), 684-692.

Yi, J.H. and Hazell, A.S. (2006) Excitotoxic mechanisms and the role of astrocytic glutamate transporters in traumatic brain injury. *Neurochem. Intl.* 48, 394-403.

Yudkoff, M., Nissim, I., Nelson, D., Lin, ZP., Erecińska, M. (1991) Glutamate dehydrogenase reaction as a source of glutamic acid in synaptosomes. *J. Neurochem.* 57, 153-160.

Zuo, D.Y., Zhang, Y.H., Cao, Y., Wu, C.F., Tanaka, M., Wu, Y.L. (2006) Effect of acute and chronic MK-801 administration on extracellular glutamate and ascorbic acid release in the prefrontal cortex of freely moving mice on line with open-field behavior. *Life Sci.* 78, 2172-2178.

Copyright © Kevin Nicholas Hascup

VITA

Name: Kevin Nicholas Hascup

Date of Birth: 05/11/1979

Birthplace: Milford, Delaware

Education

2001 B.S. Biochemistry, University of Delaware
Newark, Delaware 19711

1997 High School Diploma, Milford High School,
Milford, Delaware 19963

Professional Experience

2002-2007 Doctoral candidate, University of Kentucky,
Department of Anatomy and Neurobiology, Greg
Gerhardt, Ph.D., Supervisor

2003-2007 Undergraduate/Graduate Student Mentor, University
of Kentucky, Department of Anatomy and
Neurobiology, Greg Gerhardt, Ph.D., Supervisor

2006 FAST-16 Installation and Training, Karolinska
Institute, Department of Pharmacology, Stockholm,
Sweden

2004, 2005, 2006	Center for Microelectrode Technology Training Course, University of Kentucky, Greg Gerhardt, Ph.D., Supervisor
2006	Teaching assistant, University of Kentucky, Department of Anatomy and Neurobiology, Dr. Douglas Gould Ph.D., Supervisor
2004	Student researcher, University of Kentucky, Department of Anatomy and Neurobiology, Greg Gerhardt, Ph.D., Supervisor
2003	Student researcher, University of Kentucky, Department of Anatomy and Neurobiology, Kurt Hauser, Ph.D., Supervisor
2003	Student researcher, University of Kentucky, Department of Pharmacology, John Littleton, M.D./Ph.D.
2001-2003	Research assistant, Dade Behring, Inc., Research and Development, Gerald, Siefring, Ph.D., Supervisor
1999-2000	Student researcher, University of Delaware, Department Plant and Soil Sciences, Thomas Evans, Ph.D., Supervisor

Scholastic and Professional Honors

- 2007
Invited Speaker
12th Institute of Biological Engineering Meeting
St. Louis, Missouri
Czarena Crofcheck, Ph.D., Chairman
- 2007-2008
Translational Neuroscience Training Grant
“Therapeutic Strategies for Neurodegeneration”
University of Kentucky
Edward Hall, Ph.D., Chairman
- 2006
Graduate Student Outstanding Poster Award
Monitoring Molecules in Neuroscience – 11th
International Congress on *In Vivo* Methods
Sardinia, Italy
Gaetano Di Chiara, Ph.D., Chairman
- 2006
Graduate Student Outstanding Poster Award
Bluegrass Chapter, Society for Neuroscience
University of Kentucky
Joe Springer, Ph.D., Chairman
- 2004-2006
Research Challenge Trust Fund Training Grant
University of Kentucky

Publications

Manuscripts:

Bao, X. Pal, R., Hascup, K.N., McKerchar, T., Hui, D., Agbas, A., Fowler, S., Michaelis, M., Gerhardt, G.A., Michaelis, E.K. (2007) Mice transgenic for glutamate dehydrogenase 1 (*Glud1*) under the control of the neuron-specific enolase promoter: A model of hyperglutamatergic nervous system. Submitted- *Neuron*

Hascup, K.N., Rutherford, E.C., Pomerleau, F., Huettl, P., Gerhardt, G.A. (2007) Second-By-Second measures of L-glutamate in the prefrontal cortex and striatum of freely moving mice. Submitted- *Journal of Pharmacology and Experimental Therapeutics*

Book Chapters

M.L. Stephens, D.D. Spencer, I. Cavus, M.C. Hsiao, D. Song, S.H. Courellis, S.A. Deadwyler, R.E. Hampson, D. Putz, J.E. Quintero, M.K. Bensalem-Owen, K.N. Hascup, E.C. Rutherford, B.K. Day, J.R. Nickell, F. Pomerleau, P. Huettl, J.J. Burmeister, P.M. Talauliker, V.Z. Marmarelis, J.J. Granacki, T. Berger, G.A. Gerhardt. (in press, 2007) Microelectrode-Based Epilepsy Therapy: A Hybrid Neural Prosthesis Incorporating Seizure Prediction and Intervention with Biomimetic Maintenance of Normal Hippocampal Function. Computational Neuroscience in Epilepsy.

Hascup KN, Rutherford EC, Quintero JE, Day BK, Nickell JR, Pomerleau F, Huettl P, Burmeister JJ, Gerhardt GA (2006) Second-by-Second Measures of L-Glutamate and Other Neurotransmitters Using Enzyme-Based Microelectrode Arrays. Chapter 19 of Electrochemical Methods for Neuroscience.

Abstracts

K.N. Hascup, E.C. Rutherford, F. Pomerleau, P. Huettl, G.A. Gerhardt. Second-by-Second Measures of L-glutamate Resting Levels Using Enzyme-Based Microelectrode Arrays in the CNS of Conscious Freely Moving Mice. 12th Institute of Biological Engineering Meeting. St. Louis, Missouri March, 2007.

G. A. Gerhardt, E. Rutherford, K. Hascup, J.E. Quintero, P. Talauliker, T. Currier Thomas, M. L. Stephens, J. Fuqua, T. Coates, J. J. Burmeister, F. Pomerleau, P. Huettl . Second-by-Second Measurements of L -Glutamate and Other Neurochemicals in the CNS of Animal Models and Humans. 12th Institute of Biological Engineering Meeting. St. Louis, Missouri March, 2007.

K.N. Hascup, E.C. Rutherford, F. Pomerleau, P. Huettl, G.A. Gerhardt. Second-By-Second Measures of L-Glutamate Using Enzyme-Based Microelectrodes in the CNS of Conscious, Freely Moving Mice. Monitoring Molecules in Neuroscience: 11th International Conference on *In Vivo* Methods. Villasimius-Cagliari, Italy, May 2006.

Gerhardt GA, Pomerleau F, Huettl P, Nickell J, Rutherford E, Hascup K, Quintero JE, Day BK, Currier Thomas T, Stephens ML, Burmeister JJ. Ceramic Enzyme-Based Microelectrode Arrays for Second-by-Second Measurements of L-Glutamate and Other Neurochemicals in CNS. Monitoring Molecules in Neuroscience: 11th International Conference on *In Vivo* Methods. Villasimius-Cagliari, Italy May, 2006.

- Hascup KN, Rutherford EC, Pomerleau FP, Gerhardt GA. Real time (second-by-second) *in vivo* measures of L-glutamate in the CNS of conscious, freely moving mice. Society for Neuroscience Meeting. Washington D.C. November, 2005.
- X. Bao, K.N. Hascup, R. Pal, X. Wang, G.A. Gerhardt, S.C. Fowler, M.L. Michaelis, E.K. Michaelis. Glutamate Dehydrogenase (GLUD1) Transgenic Mice: A Model of Age-Dependent Endogenous Glutamate Excitotoxicity. Society for Neuroscience Meeting. Washington, D.C. November 2005.
- K.N. Hascup, C.R. Gash, F.P. Pomerleau, X. Bao, D. Hui, E. K. Michaelis, G.A. Gerhardt. Second-By-Second *In Vivo* Electrochemical Analysis of L-Glutamate in the Striatum of GPT and GDH Overexpressing Mice. Society for Neuroscience Meeting. San Diego, CA. October 2004.
- X. Bao, G. Wang, K.N. Hascup, C.R. Gash, F.P. Pomerleau, G.A. Gerhardt, S.C. Fowler, M.L. Michaelis, E.K. Michaelis. Behavioral and Neurochemical Characterization of c57BL/6, BALB/c, and CD1 Mice and generation of Glutamate Dehydrogenase (GDH) Transgenic BALB/c. Society for Neuroscience Meeting. San Diego, CA. October 2004.
- Buch S., V.K. Khurdayan, J. Wang, K. Hascup, N. El-Hage, I.N. Singh, P.E. Knapp, A. Nath, and K.F. Hauser. Vulnerability of glial-restricted precursors (GRPs) to combined opioid and HIV-1 Tat and gp120 *in vitro*. Soc. Neuroimmune Pharmacol. Abstrs. 10:49. Santa Fe, N.M., March 2004.

K.N. Hascup, Y. Yue, M. Staples. Demonstration of a 150 ng/mL Cutoff for the Urine Cocaine Metabolite Assay on the Dimension[®] Clinical Chemistry System. Clinical Chemistry Meeting. Philadelphia, PA, July 2003.

Signed: Kevin Nicholas Hascup